Reliability and scalabity of low power and long range networks.

Ulysse Coutaud

THÈSE

Pour obtenir le grade de

DOCTEUR DE L'UNIVERSITÉ GRENOBLE ALPES

Spécialité : Informatique

Arrêté ministériel : 25 mai 2016

Présentée par

Ulysse COUTAUD

Thèse dirigée par **Bernard TOURANCHEAU**,Professeur, Université Grenoble Alpes
et codirigée par **Martin HEUSSE**,Professeur, Grenoble INP

préparée au sein du **Laboratoire d'Informatique de Grenoble**
dans **l'École Doctorale Mathématiques, Sciences et technologies de l'information, Informatique**

Fiabilité et capacité des réseaux à faible puissance et longue portée

Reliability and scalabity of low power and long range networks.

Thèse soutenue publiquement le **7 décembre 2021**,
devant le jury composé de :

Monsieur BERNARD TOURANCHEAU
PROFESSEUR DES UNIVERSITES, UNIVERSITE GRENOBLE ALPES, Directeur de thèse
Monsieur ANDRE-LUC BEYLOT
PROFESSEUR DES UNIVERSITES, TOULOUSE INP, Rapporteur
Madame NATHALIE MITTON
DIRECTEUR DE RECHERCHE, INRIA CENTRE DE LILLE-NORD EUROPE, Rapporteure
Monsieur MARTIN HEUSSE
PROFESSEUR DES UNIVERSITES, UNIVERSITE GRENOBLE ALPES, Co-directeur de thèse
Monsieur DIDIER DONSEZ
PROFESSEUR DES UNIVERSITES, UNIVERSITE GRENOBLE ALPES, Président
Monsieur PHAM CONGDUC
PROFESSEUR DES UNIVERSITES, UNIVERSITE DE PAU ET PAYS DE L'ADOUR, Examinateur
Monsieur BAOZHU NING
DOCTEUR EN SCIENCES, SEMTECH, Examinateur

Abstract

This thesis focuses on Low Power Wide Area Networks (LPWAN), a new class of wireless networks which aim to provide massive connectivity at a low cost in the context of the Internet of Things (IoT). This thesis focuses more particularly on the LoRaWAN technology, which is an open protocol based on the LoRa proprietary modulation. LoRaWAN knows a significant popularity among both the academic and industry communities. It is now established as one of the major players in LPWAN networks.

A typical LoRaWAN network is composed of a massive number of end devices (ED), i.e. connected objects, a set of gateways (GW) acting as bridges between the LoRa network and the Internet Protocol (IP) network and finally a network server (NS). EDs transmit their data via LoRa modulation with an random channel access method (unslotted Aloha-like), i.e. without any form of coordination. The GWs transmit to the NS via the IP network all the data captured on their LoRa interface. The NS is responsible for processing the received data. LoRaWAN is an uplink oriented network, meaning that the overwhelming majority of the traffic is expected to be from the EDs to the NS. However, LoRaWAN also allows rare downlink transmissions, from the NS to the EDs.

Due to the massive number of EDs, the low transmission power and the random channel access method, data is sometimes lost by the LoRa link.

This thesis proposes solutions to make LoRaWAN communication more reliable, i.e. to deliver more than 99% of the application data. The reliability gain must be achieved in a realistic manner with respect to the capacity of the network, i.e. the number of EDs that can be served by the network in the same area. The consequence of this constraint is twofold: on the one hand the Time On Air (TOA) for the uplink transmissions must be kept as low as possible in order to avoid network congestion as much as possible, and on the other hand the TOA for downlink transmissions must be kept extremely low due to the limited downstream capability of LoRaWAN.

With the goal of a reliable LoRaWAN communication, this thesis firstly proposes an in-depth study of the characteristics of the LoRaWAN link, based on experimental measurements in a public urban network. Our characterization of the LoRaWAN link leads us to conclude that the reliability mechanisms currently existing in the LoRaWAN protocol are unfit to provide a highly reliable link. We therefore propose adaptations to make the LoRaWAN protocol reliable while conserving the technology scalability.

The thesis proposes two types of adaptations: The first adaptation consists in adding an error recovery protocol overlay, transparent for LoRaWAN, based on error correcting codes applied transversely to the packet flow. This approach makes it possible to reconstitute all of the data transmitted despite packet losses. The thesis proposes two distinct algorithms for this error recovery aspect, one based on the Reed-Solomon correcting code, and the other based on a correcting code derived from Low Density Parity Check (LDPC) codes. This thesis evaluates the performance of the two proposed error recovery algorithms.

The second proposed adaptation consists in reviewing the distribution of the transmission parameters of the EDs in the network. It is based both on the characterization of the LoRaWAN channel and on the observation that the proposed error recovery overlay makes it possible to obtain high reliability while making it possible to be tolerant to a certain threshold of packet losses. This thesis therefore proposes to review the LoRaWAN's Adaptive Data Rate (ADR) algorithm. The ADR is an algorithm which supports over-the-air and dynamic configuration of the EDs transmission parameters. We propose in this thesis, to optimize the ADR in order to reduce the TOA of the EDs to the minimum required.

Keywords LoRaWAN; Wireless networks; Internet of Things; Quality of Service; LPWAN; Capacity;

Résumé

Cette thèse concerne les réseaux dit "Faible Puissance et Longue Portée" (Low Power Wide Area Networks LPWAN), une nouvelle classe de réseaux sans fils qui visent à fournir une connectivité massive à un faible coût dans le contexte de l'Internet des Objets (Internet of Things IoT). Cette thèse se focalise sur la technologie LoRaWAN, un protocole ouvert, basé sur la modulation LoRa, qui connait un succès important et s'est imposé comme l'un des acteurs majeurs des réseaux LPWAN.

Un réseau LoRaWAN typique est composé d'un nombre massif de noeuds terminaux (i.e. les objets connectés), d'un ensemble de passerelles entre le réseau LoRa et le réseau IP et enfin d'un serveur central. Les noeuds émettent leurs données via la modulation LoRa avec une méthode d'accès au canal radio de type Aloha non slotée (i.e sans aucune forme de coordination). Les passerelles transmettent au serveur via le réseau IP toutes les données captées sur leur interface du réseau LoRa. Le serveur à la charge de traiter les données reçues. LoRaWAN est un réseau structuré essentiellement pour le sens montant, i.e. des noeuds vers le serveur mais permet également de rares transmissions dans le sens descendant, du serveur vers les noeuds.

Du fait du nombre massif de noeuds, des faibles puissances d'émission et du mode d'accès au canal basé sur Aloha, des données sont parfois perdues sur le lien LoRa.

Cette thèse propose des solutions pour fiabiliser la communication LoRaWAN, i.e. de délivrer plus de 99% des données applicatives. Le gain de fiabilité doit se faire de manière réaliste vis à vis de la capacité du réseau, i.e. le nombre de noeuds pouvants être servis par le réseau dans une même zone. La conséquence de cette contrainte est double: d'une part le temps d'émission dans le sens montant doit être maintenu le plus bas possible afin de repousser au maximum la congestion du réseau, et d'autre part le nombre de transmissions dans le sens descendant doit être maintenu extrêmement bas du fait de la capacité descendante restreinte.

Pour atteindre l'objectif d'une communication LoRaWAN fiabilisée, cette thèse propose dans un premier temps une étude en profondeur des caractéristiques du lien LoRaWAN, basée sur des mesures expérimentales dans un réseau urbain public. Notre caractérisation du lien LoRaWAN nous amène à conclure que les mécanismes de fiabilité existants à l'heure actuelle dans LoRaWAN sont inadaptés pour fournir un lien hautement fiable. Nous proposons donc des adaptations pour fiabiliser LoRaWAN tout en conservant au mieux la capacité de la technologie en terme de nombre de noeuds sur le réseau.

La thèse propose deux types d'adaptations: La première adaptation proposée consiste à ajouter une sur-couche protocolaire de recouvrement d'erreurs, transparente pour LoRaWAN, basée sur des codes correcteurs d'erreurs appliqués de manières transversales sur le flux de paquets. Cette approche permet de reconstituer l'intégralité des données transmises malgré des pertes de paquets. La thèse propose pour cet aspect récupération d'erreurs, deux algorithmes distincts, l'un basé sur le code correcteur Reed-Solomon, et l'autre basé sur un code correcteur dérivé des codes Low Density Parity Check (LDPC). Cette thèse évalue les performances des deux algorithmes de récupération d'erreurs proposés.

La seconde adaptation proposée consiste à revoir la distribution des paramètres de transmission des noeuds du réseau. Elle se base à la fois sur la caractérisation du canal LoRaWAN et sur le constat que la sur-couche de recouvrement d'erreurs proposée permet d'obtenir une haute fiabilité tout en permettant d'être tolérant à un certain seuil de pertes de paquets. Cette thèse propose donc de revoir l'algorithme de LoRaWAN: l'Adaptive Data Rate, qui prend en charge à la volée et de manière dynamique la configuration des paramètres de transmission des noeuds du réseau afin de réduire au minimum requis le temps de transmission des noeuds.

Mots-clefs LoRaWAN; Réseaux sans-fils; Internet des Objets; Qualité de Service; LPWAN; Capacité;

Contents

Introduction

Research issue The growth of the Internet Of Things (IoT) brings legacy wireless networks technologies to their limits. The scalability, energy consumption, deployment cost and operating cost of the legacy conventional cellular technologies make them unsuitable for the massive deployments required by applications for smart city, smart farm, smart factory, wide scale asset tracking, etc. To address these challenges, Low Power Area Networks (LPWAN) promise to provide long range and large scale connectivity for the IoT, at low cost and low power consumption.

LoRaWAN® is one of the leading LPWAN technologies, it is a networking protocol specification developed by the open LoRa Alliance® on top of Semtech's proprietary modulation LoRa®.

Thanks to the robust LoRa modulation and its wide range of physical and MAC parameters, LoRaWAN has the potential to successfully provide low cost connectivity to a wide variety of application, with various, and sometimes contradictory, strongly constrained requirements. Typically, these requirements are in terms of energy consumption, communication range, reliability, throughput or scalability. So, LoRaWAN claims the ability to provide connectivity to thousands of battery-powered autonomous devices into a single cell of up to ten kilometers of radius with throughput up to a kilobyte per second, for a decade.

But versatility comes at the cost that LoRaWAN requires careful and sharp engineering of the network parameters to get the best of the technology, or the performance might quickly falls below expectations.

The typical use case of LoRaWAN is to provide connectivity where "traditional" communications technologies are unable to meet the needs. It is therefore expected that LoRaWAN networks will be confronted with challenging radio conditions: very low transmission power, long range, obstructed radio propagation path, high interference levels due to co-located LoRaWAN networks, or other technologies using the same free-to-use frequency bands, etc. Under these conditions, it is expected that some of the transmissions are not received successfully. It is therefore necessary to provide mechanisms to recover these losses in order to ensure a reliable communication.

Moreover, the radio channel random access (ALOHA type) which is a key feature to lighten the embedded device side of the protocol, open a double challenge to LoRaWAN. On the one hand, an inadequate parameterization of the network will drastically increase the collision rate and cause the data loss rate to explode. On the other hand, a fraction of the transmitted frames will inevitably suffer collisions and risk of being lost, thus reinforcing the need for an adequate reliability mechanism.

Our approach and contributions In this thesis we analyze in depth the characteristics of the LoRaWAN link with a particular attention on the conditions of frame losses, and to losses distribution. We show in particular through a large scale field experiment in an urban environment, that the LoRaWAN link follows a quasi-static Rayleigh channel model.

This in-depth analysis of the LoRaWAN link and the more precise knowledge of the losses pattern, allows us to conclude that the current reliability mechanism of LoRaWAN are inadequate. Thus, we provide a tailored solution to make the LoRaWAN link more reliable. It consists in the use of error recovery protocols based on error correcting codes. We describe two reliability protocols built from this basis. The first, based on the Reed-Solomon correction code, keeps the data loss rate below 1% despite a frame loss rate up to 92%. The second, based on pseudo-random combinations of data fragments, can correct residual frame losses up to a loss rate of 40%, without any downlink acknowledgment (which is a scarce resource in LoRaWAN).

Finally, rooting from the observation our loss recovery protocols modify the transmission parameter adjustment paradigm, we develop a solution to optimize the LoRaWAN dynamic parameterization algorithm. The combination of our dynamic parameterization algorithm and our erasure correction layer provide highly reliable LoRaWAN communication while keeping the network load as low as possible. As a result, our solution can recover the LoRaWAN typical 10% data loss floor while reducing the network load by up to half.

Thesis content The thesis is organized as follow:

In chapter 1 we lay down the scientific basis of the thesis matters with the fundamentals of wireless networks, channel coding, IoT and LPWAN networks.

In chapter 2 we present in detail the LoRaWAN technology. Beyond describing the technology in detail, with its strengths and weaknesses, we highlight the intrinsic trade off of LoRaWAN that must be handle.

In chapter 4 we present the experimental field measurement campaigns that we carried out, and we dissect the results in order to define an accurate and truthful model.

In chapter 5 we describe and analyze the performance of two error recovery algorithms based on error correcting codes applied transversely over the LoRaWAN packets.

In chapter 6 we optimize the LoRaWAN dynamic parameterization algorithm to make the LoRaWAN link reliable while keeping the network load as low as possible.

Finally, in chapter 7, we conclude this thesis by emphasizing the main finding and their consequences. We also sketch the potential follow-up to this work.

Thesis context This thesis was carried out under a Cifre convention in partnership with the Semtech company and the Drakkar research team from the Grenoble Informatics Laboratory (LIG). Semtech owns and develops the physical layer of LoRaWAN: the LoRa modulation. Semtech also plays a major role in the LoRa alliance which develop the LoRaWAN protocol. LIG's DRAKKAR team is a research team that focus on various aspects related to networks, especially wireless networks and IoT, as well as their security. The team is made up of 8 permanent staff and around as many PhD students.

Chapter 1

Context

Contents

Chapter Introduction

In this chapter we lay down the scientific basis of the thesis matter. In section 1.1 we recall the fundamental of the wireless networks which will serve as a basis in the rest of the thesis. In section 1.2 we describe the various coding techniques used in information theory. We make a special focus on the ECC since it is one of the keystones of our solution for reliability in LoRaWAN. In section 1.3 we describe the Internet Of Things (IoT) paradigm and explain why the legacy wireless network technologies are unable to fill these new requirements. In section 1.4 we focus on a sub-category of IoT: the Low Power Area Networkss (LPWANs). First, we define the needs and constraints to which the LPWANs respond. Then we detail the levers used by LPWAN technologies to achieve long ranges despite low transmission power. Finally, we provide an overview of the different LPWAN technologies.

1.1 Wireless Networks

Since the early radio-communication experiments at the end of the 19th century, wireless communication technologies have been widely developed and diversified, whether in scientific, industrial or military fields Thus, the uses of radio-communications are many and varied. We can distinguish some examples of typical technologies:

AM/FM radio and terrestrial television use a model of **unidirectional broadcasting** of audio and/or video data: the relay stations (transmitters) broadcast the data to all user stations (receivers) within reach. Modulations, initially analog as for AM/FM radio or analogue terrestrial television, are now supplemented or replaced by digital modulation technologies (DAB, DTT, DVB-S, ...).

Walkie-talkies and amateur radios carry out the **bidirectional broadcasting** of the users' voices, in analog (PMR446) or digital (dPMR446) modulation in which each station is successively a transmitter and a receiver.

Radio guidance which requires **point-to-point bidirectional ad-hoc** data communication (without architecture) for remote device control.

Mobile telephony (GSM, UMTS, LTE, ...) which allows long-distance bidirectional **point-to-point communication via an architecture** between users. Communication is performed both by the radio communications between each of the terminals and their respective associated relays (terrestrial or satellite antenna), and by the back-end communication between relays via a secondary network.

Wireless Local Area Network (WLAN), such as Wi-Fi 802.11, or Wireless Personal Area Network (WPAN) such as Bluetooth 802.15 allow **point-to-point bidirectional communications over short distances**, either ad-hoc or with infrastructure. The terminals use the radio link to communicate either on the personal/local network, or in interconnection with a long distance network to communicate on the Internet.

Technological and industrial breakthroughs, particularly in the precision of silicon etching and in the transistors size reduction, have made it possible to integrate processors, memories, and radios in many objects: measuring and sensors devices, street furniture, household appliances ... The proliferation of uses, the diversity and novelty of constraints as well as the mass of these newly connected objects gave birth to the concept of the IoT which brings together these new fields of wireless networks development.

This thesis studies an IoT support technology : the LPWAN. I will particularly focus on the LoRaWAN technology: an open standard, supported by the LoRa Alliance, and built on top of the Semtech patented LoRa physical layer.

The different technologies that make up a network are generally broken down and represented by following the *Open Systems Interconnection* (OSI) model shown in the figure 1.1. However, this strict separation of the roles and tasks of each of the layers is sometime fully or partially drop, especially for wireless, cellular or IoT networks. Indeed, a so-called cross-layer approach makes it possible to better optimize and operate the network under severe constraints.

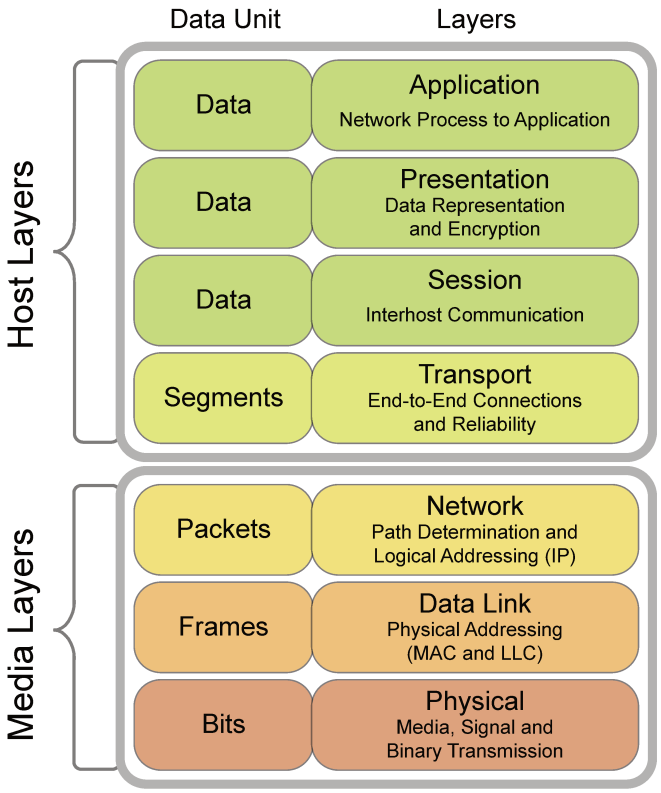

Figure 1.1: Diagram of the OSI model.
From `https://commons.wikimedia.org/wiki/File:OSI_Model_v1.svg` under CC0 1.0 licence.

As detailed in the 2.4 section, the LoRaWAN technology under study here is deeply cross-layer. Therefore in the following we will distinguish only three layers:

- the *physical layer* which tackles the transmission of the radio wave and the modulation;
- the *link layer* which in fact encompasses the roles of all the upper layers up to and except the application layer;
- and finally the application layer which is handled by the third party using the LoRaWAN technology.

In this section we will give already established base fundamentals [12, 13] first on the physical layer for wireless communications, then on some link layer elements, namely the Medium Access Control (MAC) sub-layer and the reliability sub-layer.

1.1.1 Physical Layer of Wireless Networks

1.1.1.1 Radio Transmission of Information

The radio transmission of information consists of transmitting an information signal over an electromagnetic wave. In the case of wired communication, the information signal can be sent directly, i.e. without frequency transposition, to the medium in the form of an electrical signal. This is referred to as baseband transmission. In the case of wireless communication, baseband transmission isn't possible, thus the information signal must be modulated to a higher frequency sinusoidal signal. We then speak respectively of modulating signal and carrier. The result of the modulation of the carrier by the modulating signal is the modulated signal. The information signal is then represented by variations of one - or a combination - of the physical characteristics of the carrier: amplitude, frequency and phase. On reception, the receiver performs the reverse operation - demodulation - to extract the modulated signal, the information, from the received signal.

In analog modulation, the modulating signal, the data, is directly the input signal. In digital modulation, discrete values are assigned to different physical states of the carrier: symbols which then make it possible to represent bits. Each of the distinct states that the signal coding represent is a symbol. The number of symbols is called the signal valence V. The figure 1.2 illustrates the basic digital modulation of valence $V = 2$. This thesis focuses on the performance of digital communications and therefore uses digital modulations and analog modulations are out of scope.

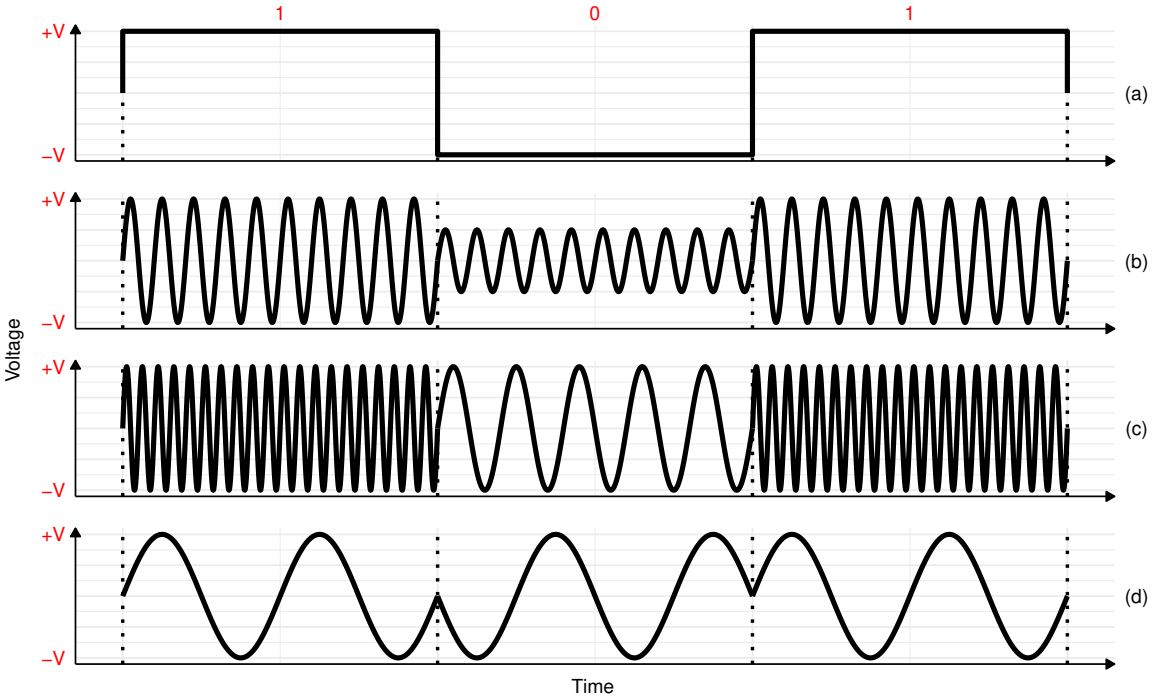

Figure 1.2: Basic digital modulations of valence $V = 2$: The information is encoded by (a) the amplitude of the baseband signal (b) the amplitude of the signal on a carrier, (b) the frequency on a carrier, (c) the phase on a carrier.

The Bandwidth (BW) is the difference between the lowest and highest frequencies used by the signal. The BW limits the rate at which symbols can be modulated onto the signal, thus this limit the modulation data rate (DR_{mod}). Nyquist's theorem thus gives $DR_{mod\text{-Nyquist}}$, the maximum DR_{mod} (in bits/s) of a signal transmitted on a channel according to the BW (in Hz) and the number of distinct symbols V:

$$DR_{mod-Nyquist}(BW) = 2 \times BW \times \log_2(V) \tag{1.1}$$

However, a real channel is noisy, i.e. the signal of interest is mixed with electromagnetic noises which deteriorates the signal transmission. For instance, there is always at least, the *thermal noise*: an Additive White Gaussian Noise (AWGN) noise due to thermal agitation in the radio equipment. The sum of all noise sources is the *noise floor*, with P_{N} its power. In the following, unless stated otherwise, we will refer to the noise floor simply as the noise. For convenience, the noise is often normalized as the noise spectral density N_0: the P_{N} per unit of BW. As it deteriorate the signal, the noise makes it more difficult for the receiver to discriminate between different symbols. Thus the noise limits V the valence of the signal that the receiver is able to distinguish. Therefore over a real channel, thus in presence of noise, DR_{mod} that can be reached over a given BW is bounded. Also, to be successfully demodulated, the received signal power P_{Rx} must be strong enough, both in absolute value and relatively to the P_{N}. We call this minimal P_{Rx} for correct reception the sensitivity. Therefore the ratio $\frac{P_{\mathrm{Rx}}}{P_{\mathrm{N}}}$, called *Signal-to-Noise Ratio (SNR)*, is often used to characterize the strength of a received signal. We define the physical data rate (DR_{phy}) as the rate at which the physical layer transmits, taking into account the overhead from any physical layer error recovery scheme, i.e. the overhead of channel coding at the physical layer (see sec.1.1.1.3). In short, DR_{phy} is the DR_{mod} multiplied by the physical coding rate.

The formulation of the maximal DR_{phy} has been extended from equation 1.1 by Shannon [157] in the case of AWGN noise. This maximal $DR_{phy\text{-Shannon}}$ (in bits/s) is the maximal capacity of a real channel. It is expressed as a function of the BW and *SNR*:

$$DR_{phy-Shannon}(BW, SNR) = BW \times \log_2(1 + SNR) \tag{1.2}$$

DR_{phy} is to be distinguish from the physical net data rate (DR_{net}) that we define as the data rate provided to the upper layer, i.e. the data rate of the effective payload thus excluding both any redundant data and also any protocol overhead. Notice that by definition $DR_{net} \leq DR_{phy} \leq DR_{mod}$.

Figure 1.3 plots the Shannon equation for a signal received with P_{Rx} to N_0 ratio : $\frac{P_{\mathrm{Rx}}}{N_0} = 1$. The core consequence of the Shannon equation is the possibility, for a given P_{Rx}, to trade BW for DR_{phy} and vice versa. The extremities of the curve are particularly interesting: when the BW is narrow, it is the main factor limiting the DR_{phy}. This is called *Bandwidth Limited Regime*. Conversely, when the BW is wide enough, widening it further does not improve achievable DR_{phy} significantly and P_{Rx} is the main limiting factor in this case. This is referred to as *Power Limited Regime*. The Shannon equation can then be approximated when *SNR* is small (≤ 1) and BW is wide: $DR_{phy} \approx 1.44 \times \frac{P_{\mathrm{Rx}}}{N_0}$.

Bandwidth in the radio spectrum is a relatively scarce resource in view of the number of technologies and users who share it. This pressure on the radio spectrum tends to make it particularly expensive for operators and manufacturers. It is therefore essential to be able to scale and for the viability of deployments of radio technologies, to use it effectively. For this, we speak of spectral efficiency η, which we define as the DR_{net} per Hz:

$$\eta = \frac{DR_{net}}{BW} \tag{1.3}$$

Spectral Efficiency can be measured for a single transmitter and receiver -we then speak of link spectral efficiency- in which case it measures the physical layer efficiency. Spectral Efficiency can also be measured for the entire system with multiple transmitters and receivers -we then speak

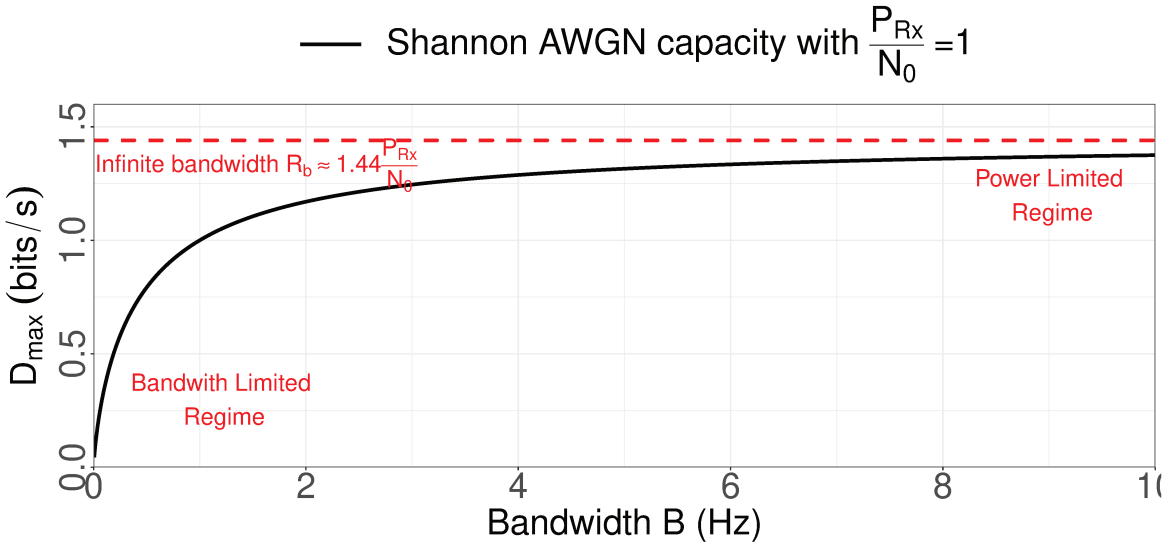

Figure 1.3: Shannon capacity with $\frac{P_{Rx}}{N_0} = 1$.

of system spectral efficiency- in which case it measures the physical layer efficiency alongside the channel multiple access efficiency.

Although BW is a resource to be saved, many technologies use so-called spread spectrum techniques. Spread spectrum consists, for a given throughput, in deliberately using a much larger BW than necessary. The data signal, encoded on a narrow band BW_{narrow}, is modulated a second time on a much wider band signal with BW_{wide} following a *spreading code*. The energy of the narrow-band signal is distributed on the wide-band signal. At reception, the wide-band signal is demodulated by the inverse function of the spreading code. Demodulation has the effect of despreading the received signal to recover the original narrow-band signal. On the contrary, the interfering signals and noise, which are not synchronized and therefore not correlated with the spreading signal, are spread by demodulation. Figure 1.4 illustrates the spread spectrum technique. This improves the signal to noise ratio *SNR*. This *SNR* gain is called Processing gain (P_g) and is equal to the ratio of both BW:

$$P_g = \frac{BW_{\text{narrow}}}{BW_{\text{wide}}} \tag{1.4}$$

By increasing the BW used, spread spectrum improves the robustness and therefore the range of the communication.

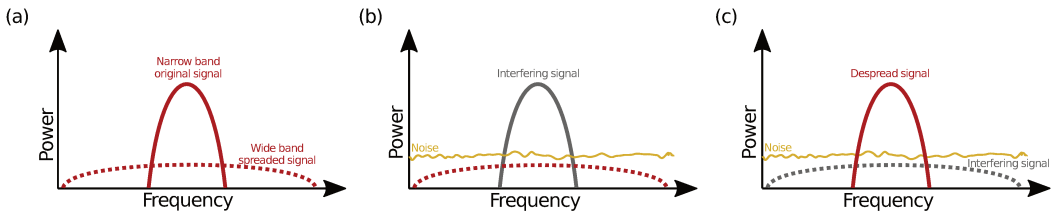

Figure 1.4: Spread spectrum modulation: (a) the original narrowband signal is modulated (spread) over a wider frequency band. (b) the spread signal is received with interference (noise and interfering signal). (c) the signal is demodulated (despread).

Notice that spread spectrum also makes it possible to share the channel between several competing users: several spread signals can be received simultaneously if the correlation of their respective spreading codes is sufficiently low, they appear as mere noise with low power spectral density to each other. Spread spectrum can thus be used as a multiplexing technique: Code Division

Multiple Access (CDMA). This makes it possible to greatly attenuate the additional BW cost of the spreading. However, because spreading codes have usually either low auto-correlation (against interference and multipath) or low cross-correlation properties (against collisions) [13, Chapter 13], and so the design of the spreading codes is subject to a trade off.

1.1.1.2 Radios Waves Propagation

The signal can be transmitted either on a guided medium (on an electric cable or an optical fiber for instance), we then speak of wired communication, or on a non-guided medium in which case we speak of wireless communication. In wireless communication the signal is then diffused through the environment. This thesis focuses on wireless communications, wired communications are out of scope.

Path Loss (PL) Definition
The PL is the attenuation of the signal power between the transmitter and the receiver. I.e. it is the ratio between the transmitted power P_{Tx} and the P_{Rx}. In linear units, the PL is expressed:

$$PL_{\text{linéaire}} = \frac{P_{\text{Tx}}}{P_{\text{Rx}}} \tag{1.5}$$

PL is generally expressed in logarithmic units:

$$PL = 10\log_{10}\frac{P_{\text{Tx}}}{P_{\text{Rx}}}\text{dB} \tag{1.6}$$

The PL is due to various phenomena which degrade an electromagnetic wave during its propagation: absorption, dispersion, diffraction , reflection, refraction ... The PL determines whether the transmitter and receiver are within communication range, as well as the quality of the link: the probability to receive or lose the transmitted data.

Path Loss (PL) Models
The exact calculation of the PL requires the computation of the exhaustive Radar Cross Section of the environment around and between the transmitter and the receiver. Such a calculation is most often impossible because it is too complex and too expensive. Simplified approximations and models are therefore used to estimate the PL.
We break down the PL into 3 components:Large Scale Fading (LSF), Shadow Fading (ShF) and Small Scale Fading (SSF):

1. **Large Scale Fading (LSF)**
   The LSF depends on the distance between the radios, and on the Path Loss Exponent $\gamma$of the propagation medium.

   Because the electromagnetic wave is not guided, it diffuses in space. The energy emitted at the source is therefore distributed over a portion of a sphere. The sphere portion depends on the opening of the transmitting antenna: the energy is distributed over a complete sphere with an isotropic antenna and over a portion of a sphere with a directional antenna. This distribution of the energy radiated at the source in space is S the power density per unit area in W/m^2:

   $$S = G_{Tx} \times \frac{P_{\text{Tx}}}{4 \times \pi \times D^2} \tag{1.7}$$

   with P_{Tx} in W, G_{Tx} the transmitter antenna gain which depends on the antenna technology, and D the distance between the transmitter and the receiver in m.

The ability to receive the signal also depends on the effective area of the antenna, the received power P_{Rx} (in W) is:

$$P_{\text{Rx}} = G_{Rx} \times \frac{S \times \lambda^2}{4 \times \pi} \tag{1.8}$$

with G_{Rx} the receiver antenna gain which depends on the antenna technology, and λ the wavelength.

The combination of the equations 1.7 and 1.8 gives the formula for the Free Space Path Loss (FSPL) for isotropic antennas:

$$LSF_{FSPL} = \frac{P_{\text{Rx}}}{P_{\text{Tx}}} = G_{Tx} \times G_{Rx} \times \left(\frac{\lambda}{4 \times \pi \times D}\right)^2 \tag{1.9}$$

This equation is known as the Friis transmission formula.

In the real world, the electromagnetic wave does not pass through void. It passes through an environment with complex geometry and part of the energy is deflected and lost. The proportion of energy lost per distance traveled depends on the environment (urban, forest, plain, indoor, etc.). The equation to compute the LSF of the Lossy Medium Path Loss (LMPL) can be derived from the equation 1.9:

$$LSF_{LMPL} = G_{Tx} \times G_{Rx} \times \left(\frac{\lambda}{4 \times \pi \times D}\right)^{\gamma} \tag{1.10}$$

with $\gamma > 2$.

Other models exist to compute and predict LSF.

- The deterministic techniques of Ray Tracing which reduce the complexity by considering a limited number of propagation paths. The number of paths taken into account can vary in order to simplify the model as for example the two-ray ground-reflection model, or to improve the precision as for the model ten-ray dielectric canyon. Ray Tracing techniques remain difficult to apply due to the complexity and variability of the environment.
- Models based on empirical measurements in specific environments which allow an estimate of PL for deployments in similar environments. Some can be configured to take into account, for example, the height of the antennas, etc. Among these empirical models, the most commonly used are the Okumura model, the Hata model, the COST231 model or even the linear piece-wise with several slopes models . These models can also be supplemented with additional mitigating factors to account for specific obstacles, such as floors and partitions for indoor propagation.
- Statistical models which can be parameterized and refined as needed from experimental data. A classic and generic model is the log-distance model: $PL(d) = PL_0 + 10\gamma \log_{10} \frac{D}{d_0}$ Where PL_0 is the PL at the reference distance d_0.

2. **Shadow Fading (ShF)**
The ShF corresponds to the potential obstructions on the main wave propagation path, such as the presence of trees, buildings, walls, shutters, etc. The resulting received signal can be destructive or constructive depending on the effects of diffraction and reflection. Also, the phenomenon being dependent on the entire geometry of the environment on the path of the wave, it is widely variable. Especially in the case of mobile radios of course, but it might also

be true for fixed radios if the environment is changing, for instance with the opening and closing of doors, depending on whether a tree has foliage or not depending on the season, if a vehicle parks etc. This phenomenon is therefore generally represented in the PL calculation as a random variable X which varies the attenuation around the average at a given distance. The most common model is log-normal shadowing: $X \sim log\text{-}\mathcal{N}(\mu, \sigma^2)$ with parameters $\mathrm{M}$and σ^2 respectively the average and variance of the variable's natural logarithm.

3. **Small Scale Fading (SSF)**
   The SSF phenomena come from multiple paths propagation. All the various multi-path components of the wave arrive at the receiver and their addition can have a destructive or constructive effect. SSF varies over very short travel distances of radios and moves of the environment, and therefore on a shorter timescale than ShF. Thus, due to SSF, the received power can vary between each successive transmissions. The SSF determines the distribution of the PL of multiple transmissions around the mean for the entire communication. The SSF is a key element in determining on the one hand the proportion of transmissions which reach the receiver with sufficient power for demodulation, but also on the other hand to determine the power differences between several simultaneous transmissions which collide. The SSF is also taken into account in the calculation of the PL as a random variable Y which varies the strength of the received signal. The most common models of multipath channels are the Rayleigh channel and Rice channel model.

1.1.1.3 Error Recovery at the Physical Layer

Since the radio link of wireless networks is therefore by definition subject to attenuation and confronted with an unstable environment, the frames received are largely susceptible to binary errors. The modulation is therefore often supplemented by an ECC at the physical layer in an attempt to repair the erroneous bits. For instance 802.11a, 802.11g or even Bluetooth LE Coded PHY standards use a convolutional ECC, the 802.11ad standard uses an Low Density Parity Check (LDPC) code. The ECC basics are detailed in section 1.2.2.

1.1.2 Link Layer

1.1.2.1 Medium Access Control Sublayer

The Medium Access Control (MAC), is fundamental in shared channel systems such as wireless networks as it handles the multiplexing of over the physical transmission medium. Unlike wired networks, wireless networks cannot carry out the Carrier Sense Multiple Access with Collision Detection (CSMA/CD) algorithm which consists on the one hand in the Carrier Sense Multiple Access (CSMA) part: listen to the channel before beginning and transmit only if the channel is free, and on the other hand the CD part: listen while transmitting and stop if a collision is detected. Indeed, the transmission of a radio frame makes it impossible to listen to the channel simultaneously to detect a third-party transmission.

The MAC sub-layer of wireless networks are either:

- **Methods based on explicit allocation**, i.e. based on coordination and reservation of sub-channels.
  The principle is to split the shared channel into logical sub-channels and to assign one (or more) sub-channel to each transmitters. The division of the channel can be done:

  - in time (Time Division Multiple Access (TDMA)),
  - in frequency (Frequency Division Multiple Access (FDMA)),
  - by spread spectrum with orthogonal codes (CDMA).

  These algorithms require synchronization between the transmitters for the allocation of the subchannels. This preliminary phase of resource reservation must be carried out by an access control algorithm without a priori knowledge, i.e. a contention type algorithm.

- **Methods relying on contention**, i.e. based on randomized competitive access to the shared channel.
  The principle is to let the transmitters have a competitive decentralized access to the channel. A fraction of the transmissions will necessarily undergo collisions. The losses of the collided frames must be repaired by an error recovery mechanism otherwise if reliability is required... and if possible. Two subcategories of contention multiple access algorithms exist: CSMA methods - also called Listen-Befor-Talk (LBT)- and ALOHA methods.
  With CSMA methods: a node communicates on the channel only if it detects the radio channel as currently free from any transmission. This solves the problem only partially due to propagation delay and the hidden terminal problem [2]. The hidden terminal problem arises when terminals within range of the same base station are not in range of each others. As a consequence, each terminal is unable to detect the activity of the other ones and thus is unable to prevent the collision despite the use of CSMA. In LPWAN (described in section1.4), the channel gain between the terminals is often several orders of magnitude worse than between the terminals and the base station. This strongly favors the problem of hidden terminals. Moreover, with the CSMA method, the nodes can spend a significant amount of time listening before getting access to the channel. It might represents unacceptable energy consumption overhead for systems with high energy constraints such as LPWAN networks.
  With the ALOHA access methods, each node can transmit at any time without coordination either with the other nodes or with the base station. This is the preferred method in LPWAN networks and in particular used by LoRaWAN technology because there is no additional work nor any energy consumption.

ALOHA Access Methods Variants

The ALOHA Access Methods [3] variants are based on a simplistic principle: in its most basic version, called Pure-Aloha, each transmitter can transmit at any time without any coordination neither with the other transmitters nor with a base station. Fatally, part of the transmissions may suffer a collision but another part of the transmissions on the other hand may be transmitted successfully. We consider Probability of error (P_e) to be the probability of collision. Thus P_e is the probability that there is a concurrent transmission which overlaps the transmission in time and therefore causes a collision. Under the common assumption that frames are generated independently of each other, P_e depends on the channel load $G = \nu \times D_{\text{frame}}$. ν being the intensity of the Poisson process which represents the frequency of generation of new frames by the transmitters and D_{frame} the duration of a frame:

$$P_{e\text{Pure-Aloha}} = 1 - \exp(-2G)$$

The channel use rate, that is to say the time spent transmitting data successfully, is expressed as a normalized useful rate called normalized goodput.

$$normalized\_goodput_{\text{Pure-Aloha}} = G \times \exp(-2G)$$

P_e and therefore the performance of the access method can be improved by discretizing the time in slots of constant time, the duration of a frame. The transmissions are required to start at a slot beginning. We then speak of Slotted-Aloha [1]. The performance of this access method is then:

$$P_{e\text{Slotted-Aloha}} = 1 - \exp(-G)$$

$$normalized\_goodput_{\text{Slotted-Aloha}} = G \times \exp(-G)$$

However, the slotted Aloha algorithm requires keeping the transmitters' clocks synchronized, which is sometimes too expensive. Indeed, the transmitters' clocks cannot be perfect and drift. Thus periodical re-synchronize, through beacons for instance, is required. The frequency of re-synchronization might be prohibitive when using low-cost transmitters with imprecise oscillators, like in LPWAN networks.

Figure 1.5 plots the performance of the Pure-Aloha and Slotted-Aloha methods.

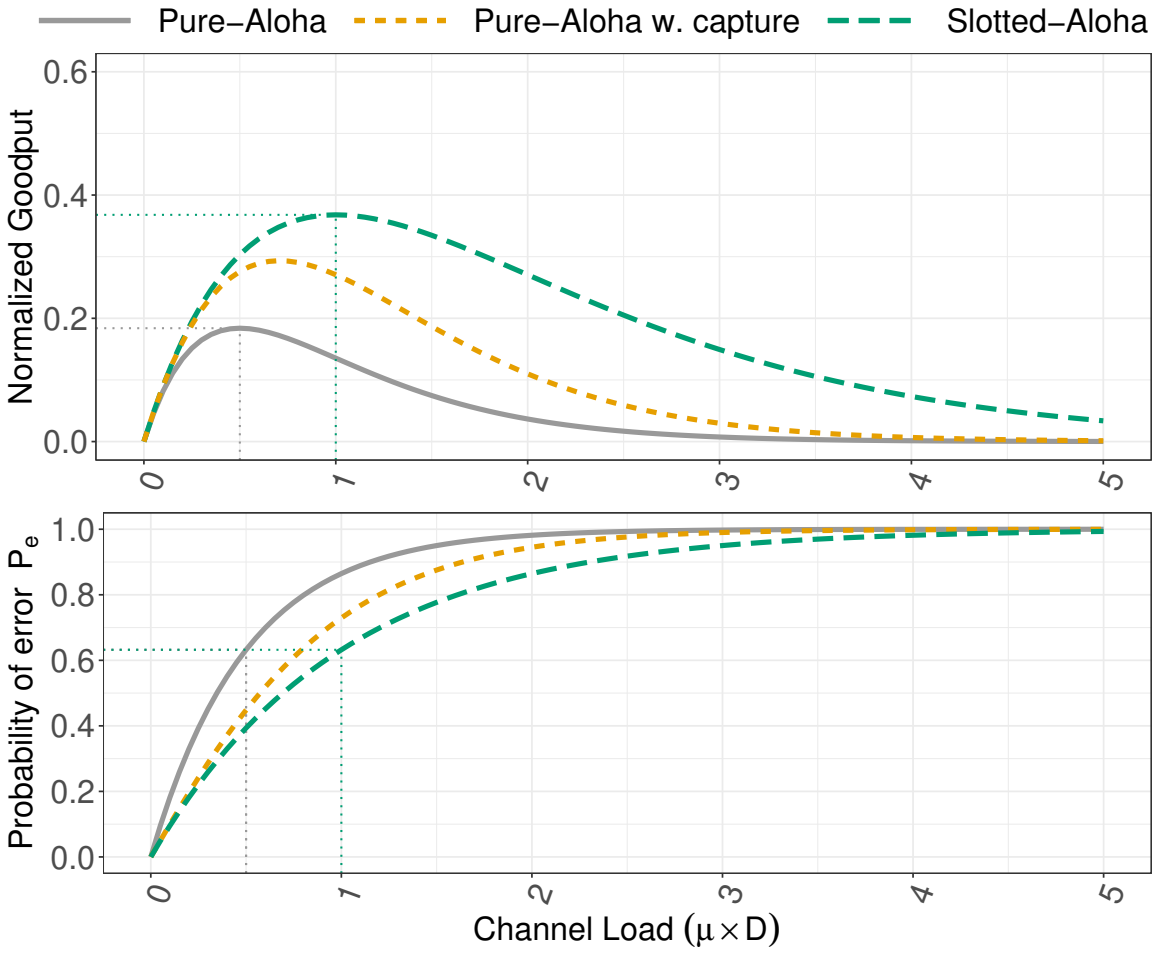

Figure 1.5: Performance of Aloha access methods. Normalized goodput and Probability of error (P_e) as a function of channel load ($G = \mu \times D_{\text{frame}}$). The dotted lines mark the ideal operating point, respectively channel load G of 0.5 and 1 for Pure-Aloha and Slotted-Aloha. The capture effect considered corresponds to a probability = 0.5 of receiving the frame despite a collision.

It is fundamental to denote that under "ideal" channel load conditions, i.e. $G = 0.5$ for Pure-Aloha and $G = 1$ for Slotted-Aloha, the normalized goodput will only be respectively of 18% and 37%. That is, for Pure-Aloha, the channel will be used for correct transmission barely 18% of the time. It is also fundamental to notice the quick P_e fall, almost its collapse, as the channel load increases. Thus, under the optimum load conditions for the useful throughput, only 36% of the frames are transmitted without collisions.

When the receiver is already synchronized on the reception of a frame, the collision by another frame, which is therefore not synchronized with the receiver, may appear as simple noise. This allows good reception despite collisions under the condition of a sufficient power difference [11]. This phenomenon is known as the capture effect. This makes it possible to reduce the impact of collisions and therefore to improve the performance of the Aloha access methods[9]. Figure 1.5 plots the performance of the Pure-Aloha access method with capture effect. The capture effect is here under the assumption that in the event of a collision with a single concurrent frame, the transmission still has half the chances to be received:

$$P_{e\text{Pure-Aloha-with-capture}} = 1 - \exp(-2G) \times \left(1 + \frac{2G}{2}\right)$$

$$normalized\_goodput_{\text{Pure-Aloha-with-capture}} = G \times \exp(-2G) \times \left(1 + \frac{2G}{2}\right)$$

The channel can be divided into independent subchannels if they allow simultaneous transmissions without collisions. The subchannels are then said to be orthogonal and the Aloha access method in such a context is called multi-channel Aloha (MC-ALOHA) [4]. Orthogonal subchannels can be separated in frequency [8] or by spreading code [6]. This sub-channel division enables the benefits of narrower band communication or spread spectrum to be enjoyed while maintaining efficient BW utilization. But it does not change the fundamental performance of the Aloha algorithm which remains defined by the offered load G. Indeed, separating the BW into two subchannels will have the effect of dividing by two μ on each sub-channel but also it multiplies by two the transmission time, to finally have no effect on G.

LoRaWAN uses a multi-channel Pure-Aloha access method with on the one hand a division of the channel by frequency (at least 3 distinct channels of 125kHz in Europe), and on the other hand a division of the channel by spreading code (6 channels by orthogonal codes).

Whatever the version and the improvements adopted, the ALOHA MAC remains subject to losses due to collisions, and the collision rate increases drastically with the channel load. In order to provide a reliable link, the MAC layer must then be supplemented by error recovery mechanisms.

1.1.2.2 Error Recovery at the Link Layer

The radio link of wireless networks is by definition subject to frames losses, because of attenuation, unstable environment as developed in section 1.1.1, or because of collisions in contention channel access methods.

In order to obtain reliability over the radio link, the link layer must be implement an error recovery mechanism:

- The error recovery mechanism can be a retransmission algorithm, typically Automatic Repeat reQuest (ARQ). The lost frames are retransmitted until the reception of an acknowledgment, possibly after a randomized waiting time in order to avoid collisions in series [5].

- The error recovery mechanism can also be an ECC to try to repair lost frames without acknowledgments and retransmissions [19, 7].

These two error recovery mechanisms can be used in a hybrid [10] way.

This thesis focuses on the application to the LoRaWAN technology of ECC, described in section 1.2.2, as an error recovery mechanism for the link layer.

1.2 Channel Coding

1.2.1 Coding Techniques in Networks

In information theory, a data can be transformed according to a reversible function called *code* in order to obtain an encoded data with better characteristics. These techniques are widely exploited in networks:

- **Source Coding** is the application to networks of information compression techniques. It reduces the BW usage and therefore improves the network capacity [159]. The source coding can either be a lossless or sacrifice some of the original information by simplifying it to improve compression performance. Several strategies [158, 26] were proposed that mix source coding of the data with channel coding, data rate adaption and transmit power adaption in order to optimize the data quality while saving the network resources like BW, energy, etc. It is typically used for media live streaming, VOIP,...
- **Channel Coding** is the application to networks of techniques to computing redundancy of information, called ECC. Channel coding allows to recover data corrupted during communication. We develop the techniques and challenges of channel coding in the following section 1.2.2.
- **Network Coding** is an inter-flow coding scheme. The coding is done at relay nodes and combines data flows from multiple sources and to multiple destinations. This way, one can exploit the broadcast nature of wireless communication in multi-hop environment[27, 28]. A simple example is the case when nodes A and B exchange packets through the intermediate node I: by sending the xor of both packet at the intermediate node, the packet exchange can be done in three transmission rounds instead of four. Network coding can improve distributed storage system with a trade-off between storage and repair BW [34]. This trade-off reveals two extreme points: minimum-storage regenerating codes and minimum-BW regenerating codes.

Notice that multiples coding techniques can be used successively and jointly. Figure 1.6 summarize those 3 categories of coding applied to networks with their position and role. This thesis focuses on channel coding to improve reliability of LoRaWAN communication while reducing as much as possible the BW usage.

1.2.2 Error Correction Code (ECC)

1.2.2.1 Fundamentals of ECC

ECC are reversible function that compute redundancy from the original data, called *dataword*, such that corruption of the encoded data, called *codeword*, can be detected and even recovered. ECC has been developed to improve reliability of digital data storage [37], it is used to insure reliability in storage like compact disks (CD) or redundant array of inexpensive disk (RAID) [18]. It is

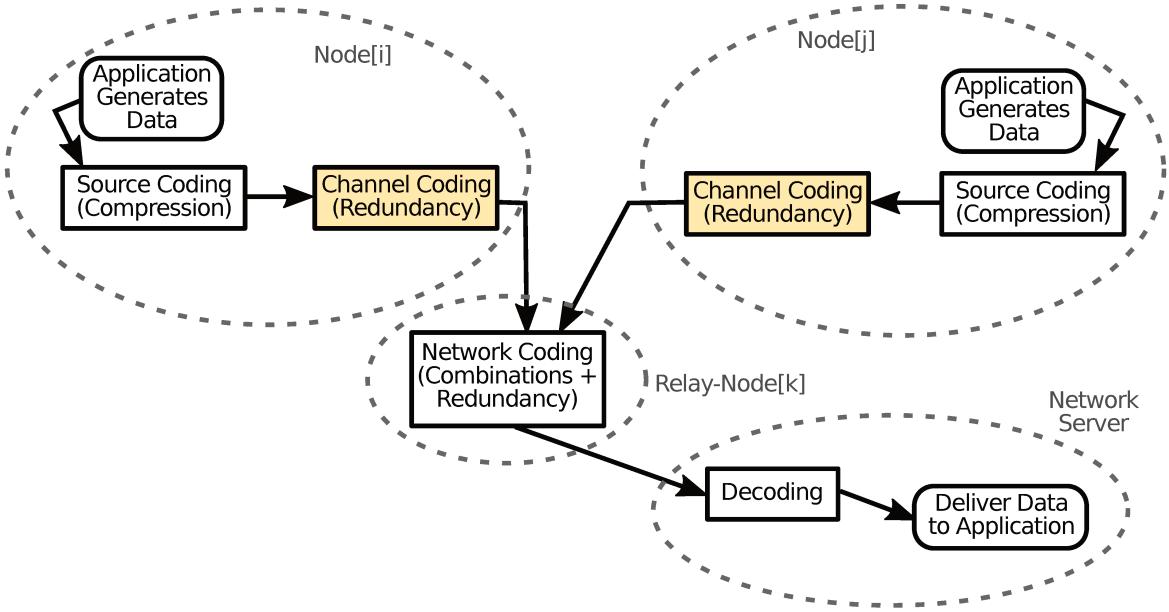

Figure 1.6: Communication diagram for Source Coding, Channel Coding and Network Coding.

also commonly used in networks to improve reliability and throughput of network communications [7, 26, 29, 33].

Intra-Frame ECC and Cross-Packet ECC (CP-ECC)

As mentioned in section 1.1.1.3, ECC can be applied at the physical layer in order to correct misdemodulated symbols. The ECC redundancy is computed from the symbols of a single frame and is carried into this frame. We refer to this technique as *intra-frame* ECC. Intra-frame ECC is used in LoRa with a variable code rate Hamming code, more details are in section 2.4.

ECC can also be applied at the upper layers. The ECC redundancy is computed from the symbols of multiples frames and carried into multiple frames. We refer to this technique as Cross-Packet ECC (CP-ECC). CP-ECC can benefit from more time diversity and smooth the channel variations, also it can reduce latency compared to ARQ in case of high Round-Trip Time. It is widely used in telephony over the internet [23], wireless video streaming [21], wireless broadcast[35] or adaptive reliability mechanism in wireless networks [25, 26].

Types of ECC encoders.

In order to respond to the various requirements of the applications: error or erasure correction capacity, complexity or space constraints, latency, etc and to match the nature of the channel model (gaussian noise, burst errors, packet loss, etc) various ECC have been developed. ECC can be categorized into four categories following two characteristics:

- **ECC can be systematic or non-systematic**, respectively if the dataword appears in clear as a subpart of the codeword or not.
- **ECC can be a block code or convolutional code**.
  - A block ECC encodes a M symbols long finite dataword into a longer codeword. The dataword can be retrieved if the number of corrupted or erased symbols are less than a given threshold which is specific of the ECC used. Classic ECC are fixed-rate codes, the codeword has a fixed length of N+M symbols. The ratio $\frac{N}{(N+M)}$ is the coding rate (CR) of the ECC. Rateless codes, also called fountain codes, were introduced later [22].

They encode the dataword in an infinitely long *codestream*, the dataword can be retrieved from unordered subsets of the codestream, as long as the amount of received data reaches a given threshold [29].

– A convolutional ECC encodes an arbitrary long, and potentially infinite, data stream into an encoded stream with additional redundancy.

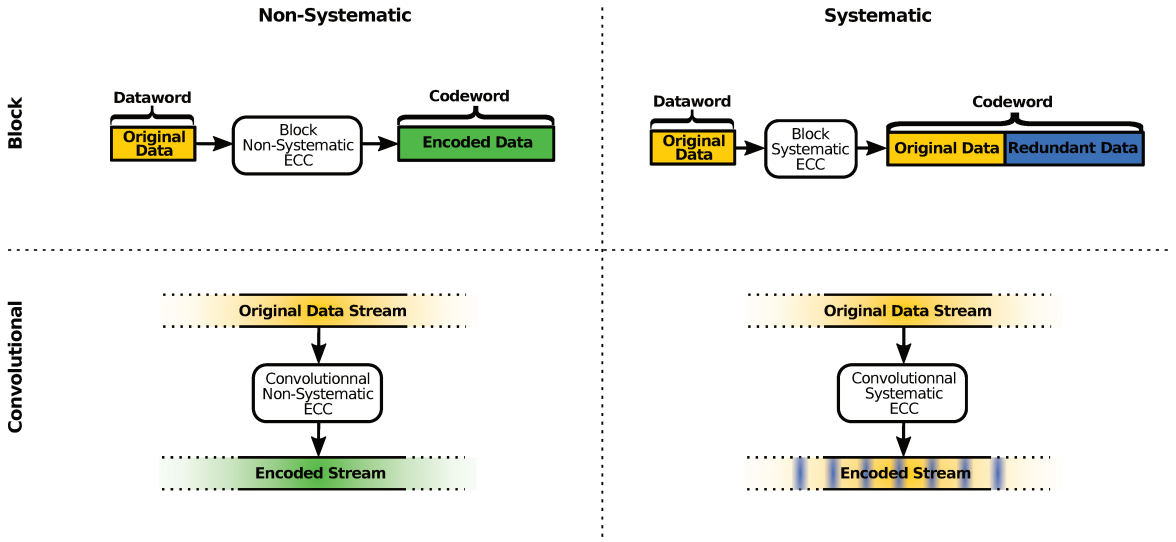

Figure 1.7: The main categories of Systematic Block Error Correction Code.

Figure 1.7 illustrates these main categories of ECC.

ECC correction capacity

The correction capacity of an ECC is the threshold - or the proportion - of correct symbols in the codeword that are necessary in order to correctly decode and recover the dataword. A code is said to be Maximum Distance Separable (MDS) or "perfect", that is to say optimal, if it does not contain any unnecessary redundancy and in the sense that it maximizes the correction capacity with regard to the amount of redundancy introduced. A perfect code which adds N parity symbols in the codeword is able to recalculate N deleted symbols or to correct $\frac{N}{2}$ symbols in errors. .

Hard-Decision and Soft-Decision Decoding

The decoding methods can be categorized into 2 parts: hard decision decoders and soft decision decoders. Unlike hard decision decoders, soft decision decoders use as input a weighting on the error probability associated with each symbol received. It is a kind of reliability index on each symbol received. This additional information helps improve the correction capability, as shown in figure 1.8. The additional information on the reliability of the symbols received is generally measured by the physical layer at demodulation, but can also be the feedback of a first decoder in the case of interlaced code.

Erasure Correction Codes

A particular case of soft-decision decoders is the case of the Binary Erasure Channel (BEC) as defined in the figure 1.9 where the symbols are either received correctly or erased. An erasure is an already detected error - meaning the code is aware of it existence and position - but without any clue on the symbol value. This is sometimes referred to as the Erasure Corrector Code. This is specifically the case this thesis deals with as error detection and rejection is already performed by

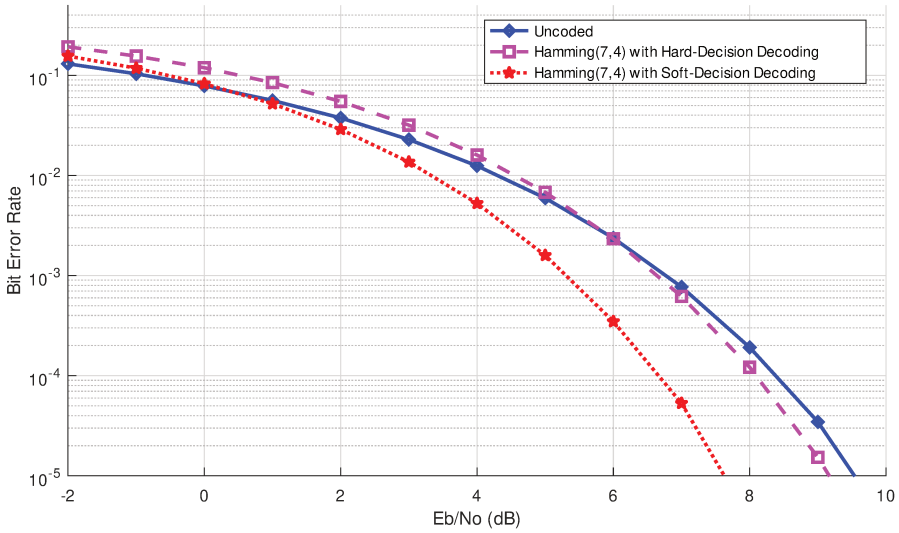

Figure 1.8: Performances comparison of Binary Phase Shift Keying (BPSK) with AWGN with a 0dB variance for no coding, Hamming(7,4) with Hard-Decoding and Soft-Decoding. Each point is a 3×10^7 bits simulation.

the lower layers of LoRaWAN. The frames are either received correctly, i.e. the cycling redundancy check (CRC) is correct, or lost and detected missing thanks to the sequence number. In the following we will use the terms of *errors* or *erasures* indiscriminately to refer to the symbols in errors on the erasure channel that we are dealing with.

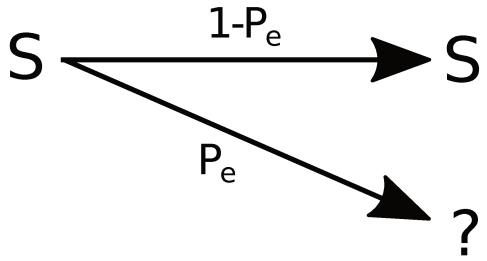

Figure 1.9: Model of the Binary Erasure Channel (BEC). The symbol S is either received correctly with a probability (1-P_e), or deleted with a probability P_e.

This thesis investigates the use of systematic block CP-ECC as an erasure correction mechanism in order to improve the reliability and capacity in LoRaWAN networks.

1.2.2.2 Reed-Solomon and Low-Density Parity Codes

Specifically we will use a Reed-Solomon (RS) code and a LDPC like code as ECC to improve our LoRaWAN target.

Reed-Solomon (RS) codes

RS codes [14] are systematic block MDS codes with fixed data-rate that append an arbitrary long sequence of parity symbols, called *syndrome*, to the *dataword*. We note RS (M,N) a RS-code that encode an M symbols long word into a (M+N) long codeword. The encoding and decoding of RS-codes can be implemented with complexity of respectively $O((N+M) \times \log_2(N))$ and $O((N+M) \times \log_2((N+M)))$ [36, 38]. With N additional parity bits, a RS (M,N) is able to correct $\frac{N}{2}$ corrupted bits or N erased bits. Notice that for the erasure channel case, the outcome is binary: either M

out of the (N+M) symbols are received and the full data can be correctly recovered, or less than M symbols are received and not a single correction can be made. So, RS-codes are weak against burst errors longer than N. Although this problem can be handled by interleaving the data. This way the channel is smoothed: the erasures are spread and independently and identically distributed.

Low Density Parity Check (LDPC) codes

LDPC codes [30, 32] are systematic block codes with fixed data-rate that append an arbitrary long sequence of parity symbols. The principle is to combine, i.e xoring, a subset of the data symbols in each redundant symbols. We note LDPC (M,N) a LDPC-code that encode an M symbols long word into a (M+N) long codeword. The encoding and decoding of LDPC-codes can be implemented with complexity of respectively $O(N+M)$ and $O((N+M)\ln(\frac{1}{\epsilon}))$ with $0<\epsilon<1$ [24, 31] . Although they are not MDS, they provides near-optimum erasure correction performances. The codeword can be recovered from any $N\times(1+\epsilon)$ with probability $1-O((N+M)^{\frac{-3}{4}})$. If less correct symbols are received, some erased symbols might be recovered anyway.

Cliff Effect

Figure 1.10 shows the performances of RS and LDPC codes over the BEC. Both RS and LDPC maintain high Data Delivery Rate (DDR) until the Symbol Erasure Rate (SER) degrades and reaches a tipping point where the DDR drops. Because the ECC is systematic, the DDR drops until it reaches the native SER of the channel. We call this the cliff effect. Notice that the more the ECC operates over large word, the more the cliff effect is pronounced, i.e. steep. This is because large codewords induce more diversity and thus average the local and temporal variation of the PDR (around its mean value).

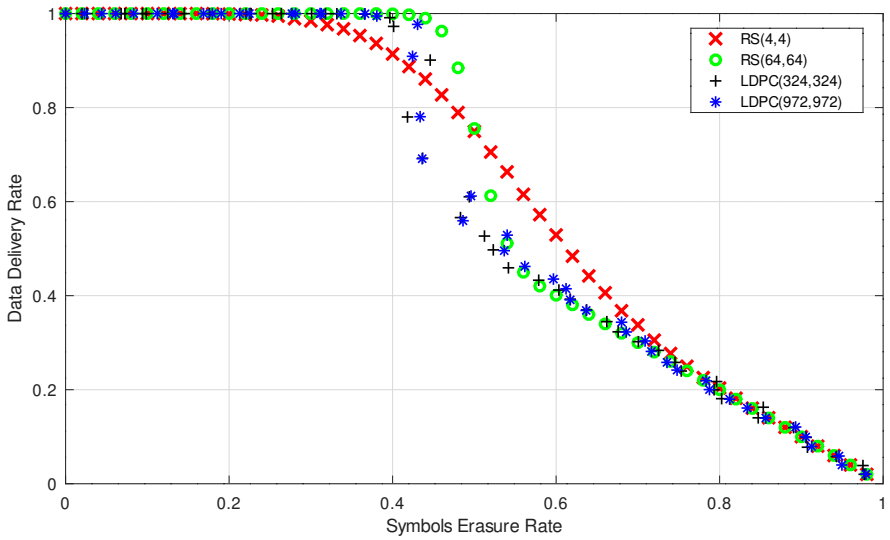

Figure 1.10: Performances comparison of various ECC with coding rate (CR) $\frac{1}{2}$, RS (8,8), RS (128,128), LDPC (324,324) and LDPC (972,972), over the binary erasure channel with independently and identically distributed erasures. Each point is a 2×10^6 symbols simulation.

1.3 Internet Of Things (IoT)

The development of networks, and especially wireless and cellular networks, is based on human-centered use. Web browsing, voice exchange, video streaming generate large amounts of data and have pushed the development of technologies towards increasing throughput and reducing

latency [162]. These improvements have been made on increasingly powerful and expensive devices (smart-phones, laptops, drones).

In recent years, the integration of computing and radio capacity, as auxiliary functions on various devices, has opened up a new field in the development of wireless networks. The data is generated - or even processed - autonomously by these objects without human intervention. The communication pattern, as the type of terminals, is different and has opened up a new field of development of wireless networks. We speak of IoT and Machine-Type Communication (MTC). The IoT paradigm is one of the strong tendencies in the network evolution of the past decade [42, 45].

Two sub-categories are to be distinguish:

- **Critical MTC (cMTC)** also referred to as Ultra-Reliable and Low Latency Communications (URLLC) requires ultra reliability, ultra low latency and availability for applications such as self-driving cars and factory autonomous automaton [161]. cMTC and URLLC are out of scope of this thesis.
- **Massive MTC (mMTC)**, on which this thesis focuses, aims at providing massive and very low cost connectivity to any objects.

1.3.1 Massive MTC (mMTC)

Indeed, the possibilities and industrial applications are numerous: sensors networks, actuators networks, smart city applications, smart-grid, smart-metering, industrial assets monitoring, logistic, infrastructure monitoring, agriculture, home automation, wildlife monitoring, etc. These IoT applications have specific requirements :

- low energy consumption for long battery-based autonomy;
- wide and deep coverage to connect devices throughout the country, including remote areas and adverse environments;
- device mobility handling;
- and capacity to connect up to thousands or even millions of devices per cell of typical surface of a few square kilometers.

These requirements must be met under a strong economic constraint for the deployment of the systems to be economically viable. The capital expenditure (CAPEX) must be low, the infrastructure cost must be reasonable and terminal devices must be very cheap. The operational expenditure (OPEX) must be low, i.e the network operation and maintenance must be low cost.

1.3.2 Legacy Wireless Technologies

Legacy wireless technologies such as Wireless Wide Area Network (WWAN) or WLAN do not meet these requirements for the vast majority of IoT applications.

Conventional WLAN, like 802.11, provides short range which is not suitable for many IoT usages as range is too short and power consumption too high [40]. Range can be extended by increased transmit power and directional antenna which is impractical for mobile and battery powered IoT devices, not to mention radio spectrum regulation problems.

Conventional cellular WWAN cellular networks (EDGE, GPRS, GSM, LTE, NR, UMTS) provide long range connectivity and a quite good global coverage due to the already deployed infrastructure of

Mobile Network Operator (MNO). This has positioned these technologies as first-to-the-market. However, the capacity of cellular networks, the cost of connectivity, the price of radio chipsets and their power consumption are a glass ceiling for scaling up and make cellular technologies inadequate for mMTC.

Satellite WWAN can provide global and cross-country coverage which make the IoT over satellite a promising approach. However, transposing terrestrial wireless technologies to satellite systems is challenging [63, 70] and these technologies have yet to mature .

WPAN networks which can have low energy consumption such as BLE or RFID suits some IoT close range applications, however most of the applications require a much wider range.

An early solution has been to extend WPAN coverage by multi-hop mesh networking. It is the approach for instance of the 802.15.4 protocols[44] such as Zigbee . This is not satisfactory for several reasons: the mesh network requires the deployment and maintenance of a dense network which cost is prohibitive for the targeted application. Also, mobility of the nodes is very difficult under these conditions, the movement of a node might break the connectivity, and it requires regular and expensive routing recalculations. Moreover, even with a mesh network, satisfactory coverage can hardly be achieved in remote areas. Also, the multi-hop nature of mesh networks reduces battery life. And as a result, depending on the topology, some nodes will be more stressed and will deplete their battery sooner, causing a premature collapse of the network [160, 41, 43].

The solution to overcome these limitations is provided by Low Power Wide Area Networks (LPWAN) which fill this gap between short range networks and legacy cellular networks as illustrated in figure 1.11.

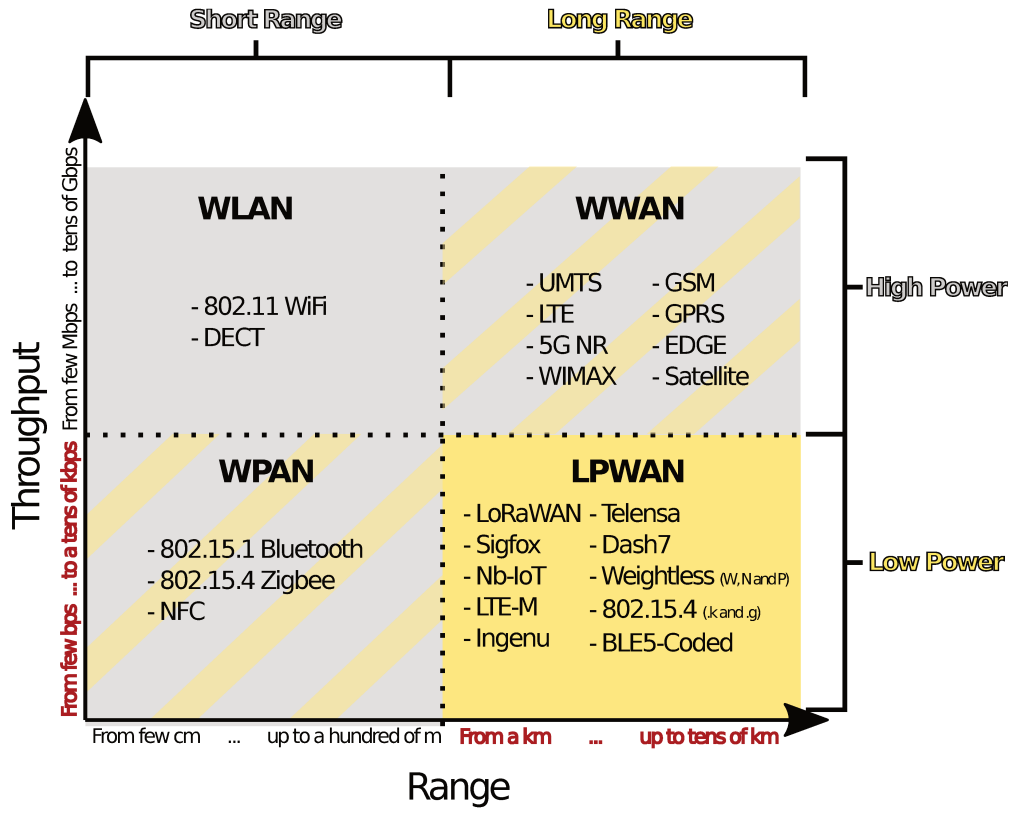

Figure 1.11: Wwireless networks categorization by size and throughput. The long range and low power category is highlighted.

1.4 Low Power Area Networks (LPWAN)

LPWAN is a class of wireless networks that provide massive and very low cost connectivity for the IoT. The LPWAN paradigm has strongly gained momentum in the past few years. Many academic studies present the constraints, challenges and future tracks for the LPWAN, while describing and comparing existing technologies [47, 49, 52, 56, 59, 65, 66]. We give here an overview of these issues based on these studies.

1.4.1 LPWAN Requirements

Following the mMTC requirements, LPWAN must be:

- Low power with battery-based autonomy in the order of a decade.
- Long range connectivity, at least in the order of a kilometer.
- Low cost with radio chips less than 5€ and connectivity less than 1€ by device and by year.
- Able to connect thousands of devices over area from "small" area of only few square kilometers to "large" area up to a hundred of kilometers square, with a single gateway.

To achieve such performance, LPWANs unleash other aspects:

- Low-throughput from few hundred kilobytes per seconds (kbps) and down to to few bytes per seconds.
- Delay tolerant with acceptable latency of a few seconds up to several hours.
- Strongly asymmetric with uplink oriented[1] connectivity or even uplink only connectivity.

Such LPWAN fulfill the requirements for IoT applications with massive number objects that produce non-critical, sparse and sporadic data. This matches many IoT applications including smart-metering, smart-city, public or industrial asset monitoring, smart-farming, livestock or wild life monitoring, etc.

1.4.2 Levers For Long Range Low Power Communications

For a given digital modulation the Bit Error Rate (*BER*) at reception depends on the received energy per bit (E_b) to noise power spectral density (N_0) ratio: $\frac{E_\mathrm{b}}{N_0} = SNR \times \frac{BW}{R_b}$. Therefore, the *BER* of a digital modulation follows a characteristic function P_b:

$$P_\mathrm{b}\left(\frac{E_\mathrm{b}}{N_0}\right) = BER$$

We give in table1.1 P_b functions of widely used modulations.

Table 1.1: *BER* for Binary Frequency Shift Keying (BFSK), BPSK, Multiple Phase Shift Keying (MPSK), Quadrature Amplitude Modulation (QAM) [13]. The approximations are consistent for modulation using grey mapping and with relatively high *SNR*.

Modulation	BFSK	BPSK	MPSK	QAM
P_b	$Q(\sqrt{\frac{E_\mathrm{b}}{N_0}})$	$Q(\sqrt{2\frac{E_\mathrm{b}}{N_0}})$	$\approx \frac{2}{\log_2 M} Q(\sqrt{2\frac{E_\mathrm{b}}{N_0}\log_2 M}\sin(\frac{\pi}{M}))$	$\approx Q(\sqrt{2\frac{E_\mathrm{b}}{N_0}})$

[1] from the devices to the gateways

We define the range of a wireless transmission as the maximal distance $d_{\max}$ at which the link P_b is good enough for correct demodulation, i.e. the *BER* is below BER_{max}:

$$P_b\left(\left(\frac{E_b}{N_0}\right)_{d_{\max}}\right) = BER_{\max} \tag{1.11}$$

With $\left(\frac{E_b}{N_0}\right)_{d_{\max}}$ being the $\frac{E_b}{N_0}$ ratio at distance $d_{\max}$. $\frac{E_b}{N_0}$ is the measure of *SNR* normalized to the amount of bits transported:

$$\frac{E_b}{N_0} = SNR \times \frac{BW}{DR_{net}}$$

Therefore:

$$\frac{E_b}{N_0} = \frac{P_{Rx}}{N_0 \times DR_{net}}$$

It is fundamental to notice here that $N_0$is a given of the system resulting from the electromagnetic environment, thus we cannot control it. This leaves the received power P_{Rx} and the data rate DR_{net} has the only controllable factors to change $\frac{E_b}{N_0}$.

This brings up the 2 fundamental possibilities to increase the communication range: increase the P_{Rx} or reduce DR_{net}.

1.4.2.1 Increase P_{Rx}

As detailed in section 1.1.1, P_{Rx} is the transmitted output power P_{Tx} amputated by the PL, expressed in dB:

$$P_{Rx} = P_{Tx} - PL$$

Thus, P_{Rx} can be increased, either by increasing P_{Tx} or by reducing PL.

Increasing P_{Tx}
Increasing P_{Tx} implies 2 problems: First it requires expensive high quality Power Amplifier (PA) to transmit with higher P_{Tx} without distortion of the output signal. Thereby constant envelope modulation are favored to repel the distortion phenomenon as well as to reduce power consumption. Secondly, in practice the P_{Tx} is restricted, if not by the PA quality, then either by the battery or by regulation.

Reducing Path Loss (PL)
The other way to increase P_{Rx} is to reduce the PL. As detailed in section 1.1.1.2 the PL is dependent on the environment and its geometry on which we do not have control. The use for the terminal devices of high gain directional antennas as well as antenna offset for improved radio waves dissemination is impractical as it implies prohibitive deployment cost and excludes mobility. These techniques are however often used for gateways. The only parameter under control that affects the PL left is the wavelength of the carrier: using lower frequency improve the signal propagation. So, LPWANs using license free bands favor sub-GHz bands for this reason. However, the space in the low frequency bands is reduced and these bands with favorable properties are all the more popular and overused. Finally, the regulations restrict the use of these bands.

1.4.2.2 Reduce the Data Rate

The main other way to increase the communication range is therefore to reduce the data rate. This trade-off stems from the Shannon Equation (sec.1.1.1.1 eq.1.2).

$$DR_{net} = BW \times \log_2(1 + SNR)$$

However, the concern of LPWANs being to optimize not the DR_{net} but the range, we must take the Shannon equation from another angle. First the minimal required $\frac{E_b}{N_0}$ can be expressed as a function of BW and DR_{net}:

$$\frac{E_b}{N_0} = (2^{\frac{DR_{net}}{BW}} - 1) \times \frac{BW}{DR_{net}}$$

Thus, another trade off appears clearly, the lower-bound for minimal required $\frac{E_b}{N_0}$ depends on the

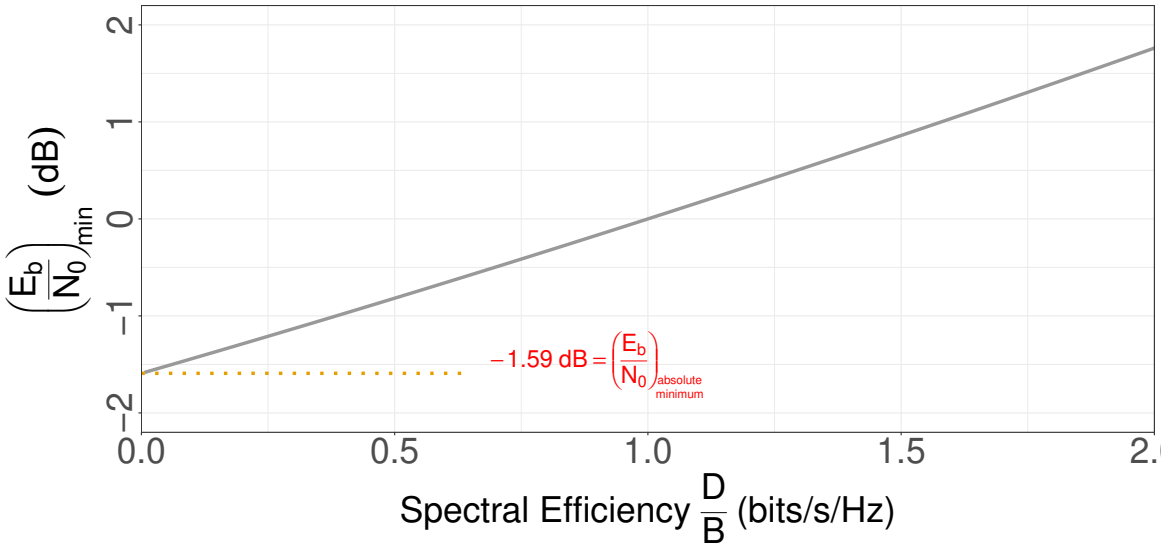

Figure 1.12: Minimal $\frac{E_b}{N_0}$ as a function of the spectral efficiency ($\frac{DR_{net}}{BW}$) following the Shannon Equation.

ratio $\frac{DR_{net}}{BW}$, i.e. the spectral efficiency. Therefore, as illustrated in figure 1.12, this lower bound for achievable minimal $\frac{E_b}{N_0}$ can be reduced at the expense of a reduced spectral efficiency.

Finally, relying on the $\frac{E_b}{N_0}$ definition, the Shannon equation can be re-written to express the lower bound on minimal required received power as a function of BW and DR_{net}:

$$(P_{Rx})_{req} = (2^{\frac{DR_{net}}{BW}} - 1) \times BW \times N_0$$

Figure 1.13 plots the minimal required P_{Rx} as a function of DR_{net} for various BW between 10Hz and 10kHz. This emphasizes the core trade off for long range, yet low power, transmissions: data rate must be sacrificed in favor of sensitivity.

Every LPWAN technologies rely on this trade off, and employ various techniques that trade data rate for sensitivity [46, 54, 55]. These techniques are mainly the use of a combination of:

- *Narrow Band:* The data rate is reduced with the BW, therefore reducing the noise and improving communication range. A subcategory is the Ultra Narrow Band (UNB) category. UNB defined either by a $BW <$ 1kHz or by a BW narrower than the uncertainty of the transmitter oscillator. It allows for long range communication with efficient spectral efficiency at very low data rate.

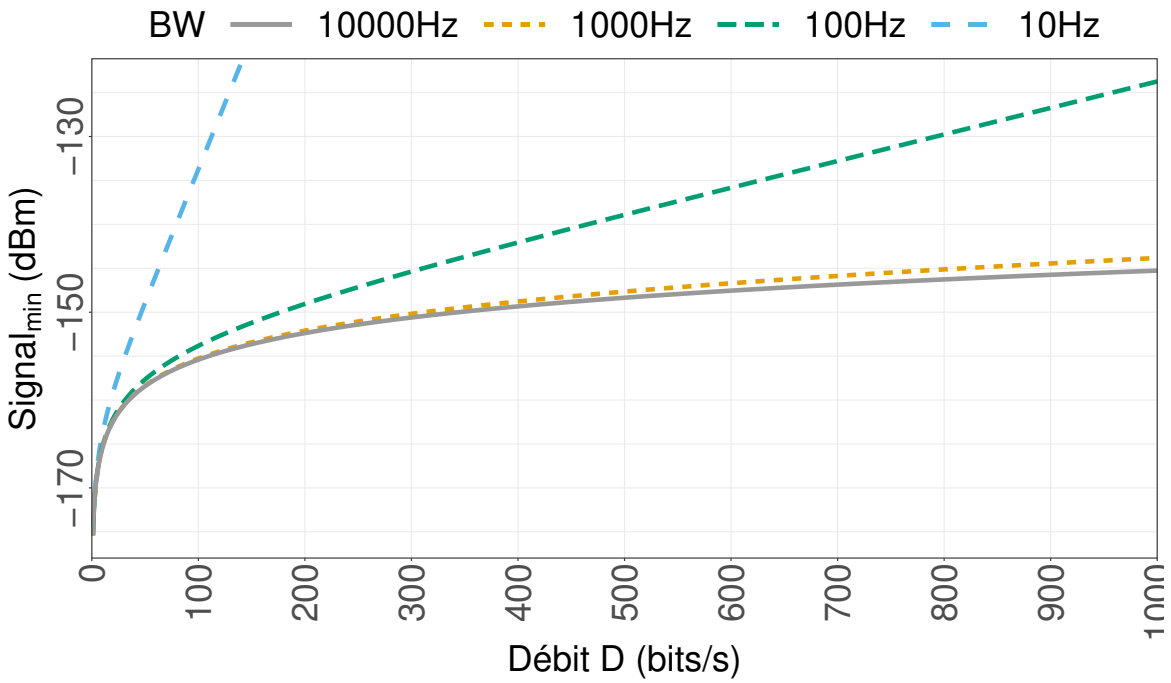

Figure 1.13: Shannon AWGN capacity.

- *Spread Spectrum:* The DR_{net} and spectral efficiency are reduced by spreading the narrow band signal over a larger BW which improves the received $\frac{E_b}{N_0}$ and thus reduces the required P_{Rx}. The low spectral efficiency can be compensated by the use of codes that are orthogonal to each other, thus creating virtual subchannels, or with low auto-correlation coefficients to increase the capture effect.

- *Transmission Redundancy:* By introducing redundancy in the communication the acceptable BER_{max} from equation 1.11 is lowered. Indeed, the error rate will be lowered by the redundancy. For instance, with the most straightforward simple blind systematic repetition, from a Packet Error Rate (PER) being $PER = 1 - (1 - BER)^{packet\_length}$, the effective Data Error Rate (DER) falls to $DER = PER^{number\_of\_repetitions}$. Since the multiple transmissions are spread out over time, and can in addition be on different carriers. This benefits from diversity gain which improve the robustness against temporal and selective fading. Of course, for a fixed time on air the amount of application data is reduced, thus reducing the Applicative Data Rate (DR_{app}), the data rate available and usable at the application layer: $DR_{app} = \frac{DR_{net}}{number\_of\_repetitions}$. Repetition can be seen as a way of increasing the overall energy to transmit each effective bit of data.

1.4.3 Majors LPWAN Technologies

The success of LPWANs is far from being confined to the academic world and industrial developments are also numerous. So much that the market is now fragmented between various technologies with technical and commercial choices, performances and compromises that sometimes vary and sometimes are quite similar. We provide in table 1.2 a technical overview of the main LPWAN technologies.
However the overwhelming majority of the market, around 90% [62], is shared between 4 main players: NBIoT, LTE-M in the mobile operator licensed bands and SigFox and LoRaWAN in the sub-GHz industrial scientific and medical (ISM) bands.

Table 1.2: Technical overview of the main LPWANs technologies.

Technology	Frequency Band	Modulation	Long Range Methods	Multiplexing	BW	Uplink Data Rate	Experimental Range
LoRaWAN [45, 46, 73, 48, 49, 52, 53, 55, 56, 59, 65]	Sub-1GHz ISM	LoRa (CSS) | FSK	SS (CSS) + ECC (Hamming) + Repetitions (up to x15)	Pure-Aloha + CDMA	$\in \{125, 250\}$kHz	183bps-50kbps	30km LOS [74] 14km Urban [153]
Sigfox [45, 46, 48, 49, 53, 55, 56, 59, 65]	Sub-1GHz ISM	DBPSK	UNB + Repetitions (x3)	Pure-Aloha	100Hz	100bps	15km Urban [68]
Dash7 [49, 52, 53, 56, 65]	Sub-1GHz ISM	GFSK	NB + ECC (Convolutional)	CSMA/CA	$\in \{25, 200\}$kHz	9.6kbps-166.67kbps	1500m LOS [51]
802.11ah [56]	Sub-1GHz ISM	(B|Q)PSK | (16|64|256)QAM	ECC (Convolutional + LDPC)	CSMA/CA	$\in [1, 16]$MHz	150kbps-86Mbps	500m LOS [64]
NB-Fi (WAVIoT) [53, 56, 71]	Sub-1GHz ISM	D-BPSK	UNB	TDMA+FDMA	$\in$ [50Hz, 25.6kHz]	50bps-25.6kbps	*NA*
802.15.4k [49, 55, 65]	Sub-1GHz | 2.4GHz ISM	DSSS (B|Q)PSK | (G-)FSK	SS (DSSS) + NB + ECC (Convolutional)	CSMA/CA | Pure-Aloha	$\in [12.5$kHz, 1MHz]	3bps-128kbps	3800m LOS 2100 NLOS [50]
802.15.4g [49, 65]	Sub-1GHz | 2.4GHz ISM	FSK | PSK | OFDM	SS (DSSS) + NB + ECC (Convolutional)	CSMA/CA	$\in [12.5$kHz, 1.2MHz]	2.4kbps-800kbps	800m Rural 250m Semi-Rural 150m Urban [60]
Weightless-N [46, 49, 56, 65]	Sub-1GHz | 2.4GHz ISM	DBPSK	UNB + ECC + Repetitions (up to x8)	Slotted-Aloha	200Hz	30kbps-100kbps	*NA*
Weightless-P [46, 49, 53, 56, 65]	Sub-1GHz | 2.4GHz ISM	GMSK | O-QPSK	NB + ECC	TDMA+FDMA	12.5kHz	150kbps-86Mbps	*NA*
Telensa [49, 53, 65]	Sub-1GHz ISM |TVWS	BFSK	UNB	*NA*	*NA*	62.5bps	*NA*
Ingenu (RPMA-OnRamp)[45, 46, 49, 53, 56, 65]	2.4GHz ISM	D-BPSK+DSSS +RPMA	SS (DSSS) + ECC	TDMA+CDMA	1MHz	30bps-78kbps	*NA*
BLE5-Coded [57]	2.4GHz ISM	GFSK	SS (FHSS) + ECC	TDMA | RTS/CTS	1MHz	112kbps-382kbps	1km LOS 150m NLOS [57]
Weightless-W [49, 56, 65]	470-790MHz TVWS	16-QAM, OBPSK, QPSK, DBPSK	SS (DSSS) + ECC (convolutional)	TDMA+FDMA	5MHz	1kbps-10Mbps	*NA*
Nb-IoT (LTE CatNB1) [48, 52, 53, 55, 56, 59, 65, 67]	700-900MHz Licensed (LTE or GSM bands)	BPSK|QPSK	SS (FHSS) + ECC + Repetitions (up to 2048 DL and 128 UL)	OFDMA|SC-FDMA	180 kHz	20kbps-50kbps	700m Urban [58] 1km Idoor [69] Open Field 16km [61]
LTE-M (LTE CatM1 | eMTC) [56, 65]	700-900MHz Licensed (LTE or GSM bands)	16QAM	SS + ECC	OFDMA|SC-FDMA	1.08MHz	up to 1Mbps	*NA*
EC-GSM-IoT [53, 56, 65]	800-900MHz Licensed (GSM bands)	GMSK|8PSK	SS + ECC	CDMA	200kHz	70kbps-240kbps	*NA*

Among them, LoRaWAN also knows the stronger academic success. LoRaWAN open-source model, hardware availability, large open networks existence and private network ease of deployment were further catalysts for its success in the research world. We compare in Table 1.3, the number of matching articles found via the IEEE Xplore search engine [2].

Table 1.3: Number of keywords occurence in article titles in IEEE Xplore search engine.

Keyword(s)	"NBIoT" OR "NB-IoT"	"LTE-M"	"Sigfox"	"LoRa " OR "LoRaWAN "
Occurrences	406	26	33	1239[3]

1.5 Chapter Conclusion

In this chapter we described the scientific foundation which will be the framework and the tools with which we will develop this thesis. In particular, this thesis focuses on the reliability of LoRaWAN networks, a LPWAN wireless network technology for IoT. The foundations laid down in this chapter give us both the levers and theoretical limits to achieve our goal of a reliable and scalable LoRaWAN link. In particular, the trade-off between throughput and robustness is the keystone of LPWAN technologies and we will use channel coding to further enhance LoRaWAN's robustness.

[2] Search for keyword occurrence in title from https://ieeexplore.ieee.org on the 24/06/21.

[3] Few off-topic results prior to 2010 where filtered out.

Chapter 2

LoRaWAN

Contents

Chapter Introduction

LoRaWAN is a LPWAN open standard supported by the LoRa Alliance, a non-profit organization regrouping around 500 industrialists, academics and institutions of the field. It benefits from detailed documentation [172, 173] and its industrial and academic success have favored its description in numerous technical reports [165] and scientific overviews [45, 46, 73, 48, 49, 52, 53, 55, 56, 59, 65].

LoRaWAN defines a communication protocol on top of the LoRa physical layer, a patented low power and long range modulation developed by Semtech [163, 168].

LoRaWAN defines the network architecture: as shown in Fig. 2.1, LoRaWAN lays out a star-of-stars topology in which few gateways (GWs) relay secured messages between numerous battery powered end-devices (EDs) and a back-end central Network Server (NS). The NS then routes the messages to the application servers (ASs).

LoRaWAN also defines the communication protocol stack as illustrated in figure 2.2. The LoRaWAN protocol stack can be split in two main layers:

- **The physical layer** which is basically the patented LoRa modulation and provides the long range communication capabilities.
- **The data link layer** (sometimes referred to as the "LoRa MAC" in the documentation) which is neither a stricto sensu MAC sublayer or Link Layer from the OSI model rather a wide layer that implements a large set of functionality from layers 2 to 6 of the OSI model such as data encryption, commissioning, network access authorization, applications multiplexing, error control, routing, logical addressing, shared channel access ...

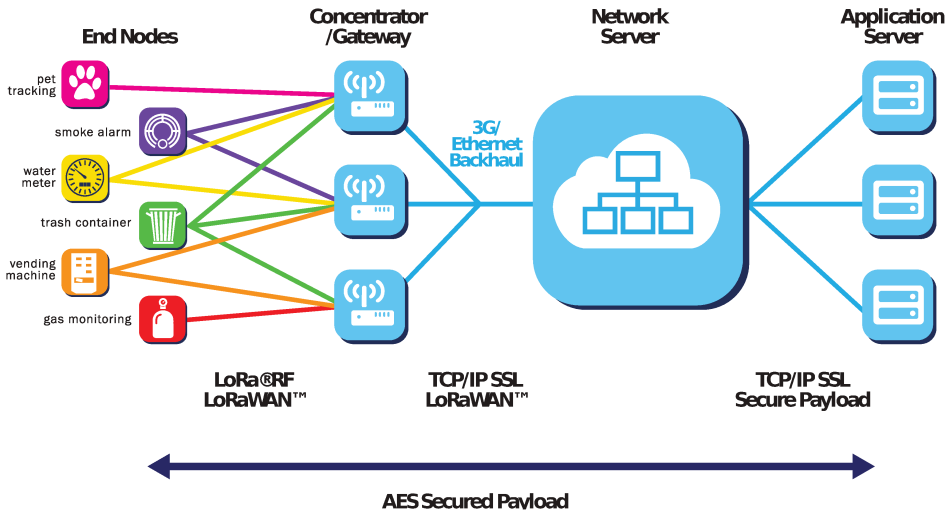

Figure 2.1: LoRaWAN networking architecture.
From "A technical overview of LoRa and LoRaWAN" `https://lora-alliance.org/resource_hub/what-is-lorawan/` [165].

In this chapter we describe the LoRaWAN technology in its essential aspects, starting from the LoRaWAN network architecture, then the LoRa physical layer and then the LoRaWAN data link layer.

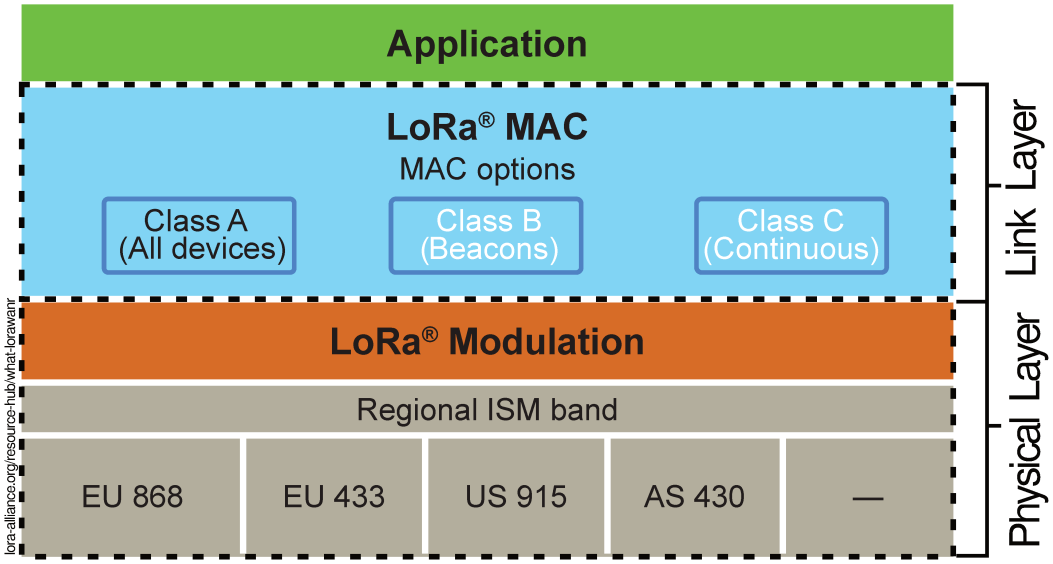

Figure 2.2: The LoRaWAN protocol stack.
From "A technical overview of LoRa and LoRaWAN" `https://lora-alliance.org/resource_hub/what-is-lorawan/` [165].

2.1 Network Architecture

A typical LoRaWAN network topology is cellular-like with several GWs using the same frequency plan and covering the areas of interest. Because of the heterogeneity of hardware, antennas, and placements (indoor/outdoor, on top of building, mountain, etc), the areas covered by each GW is highly variable. Also, there is often large overlapping coverage zones.

The typical network topology is illustrated in Fig.2.3.

The link from EDs to GWs is provided by LoRa single-hop transmissions which can be received by GWs in range. EDs are not associated to a particular GW and GWs forward every received frames to the NS through a backhaul network (wired or cellular). The uplink traffic thus benefits from an inherent macro-diversity which is a strong asset of LoRaWAN as it improves the reliability and allows for geo-localization. Also even if an ED is mobile, there is no need for handover mechanism from GW to GW[1]. The NS server handles frames de-duplication, authentication and decryption, downlink scheduling and routing of uplink data to the ASs. The philosophy is to push the complexity to the NS to lighten the EDs and allows for low cost device and low power operations.

[1] This is a critical feature to enable asset tracking applications, a major target application for IoT [166].

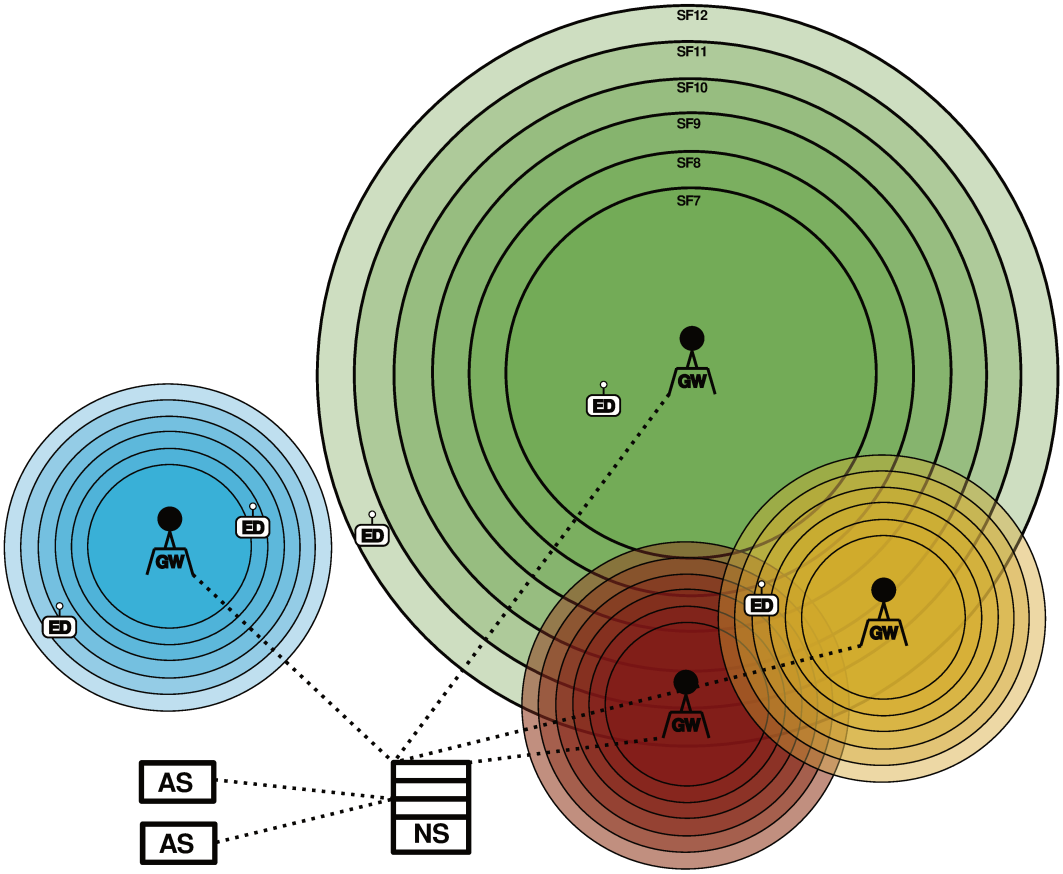

Figure 2.3: Typical LoRaWAN network topology. end-devices (EDs) communicates with a single hop LoRa transmission to gateways (GWs). GWs forward every received LoRa frames via a backhaul connection to the Network Server (NS). NS de-duplicates and multiplexes the data to the application servers (ASs).

2.2 LoRa Physical Layer

2.2.1 Modulation

Even though the LoRa physical layer is a proprietary modulation and all its details are not publicly available, the patent [163], the documentation [168] and academic works to reverse engineer [132, 152], assess its performances [81, 107, 113, 131, 135], or improve them [137] outline a good description of modulation. We describe here the LoRa physical layer from these documents.

Symbols

The LoRa modulation is based on compressed high intensity radar pulse (chirp) Spread Spectrum (CSS). Each symbol is a linearly increasing frequency ramp centered on the carrier frequency (*CF*) as illustrated in Fig. 2.4. The chirp is mapped cyclically over the radio channel BW and the information is encoded by the chirp initial frequency offset as illustrated in Fig.2.5. CSS provides high coding gains and makes the transmissions robust against noise and interference.

The spreading factor (*SF*) determines the speed at which the rising ramp sweeps through the frequency band. The *SF* also determines the valence of the modulation as a LoRa symbol conveys *SF* bits. Therefore the combination of *SF* and BW defines the symbol duration T_{symbol}:

$$T_{\text{symbol}} \frac{2^{SF}}{BW}$$

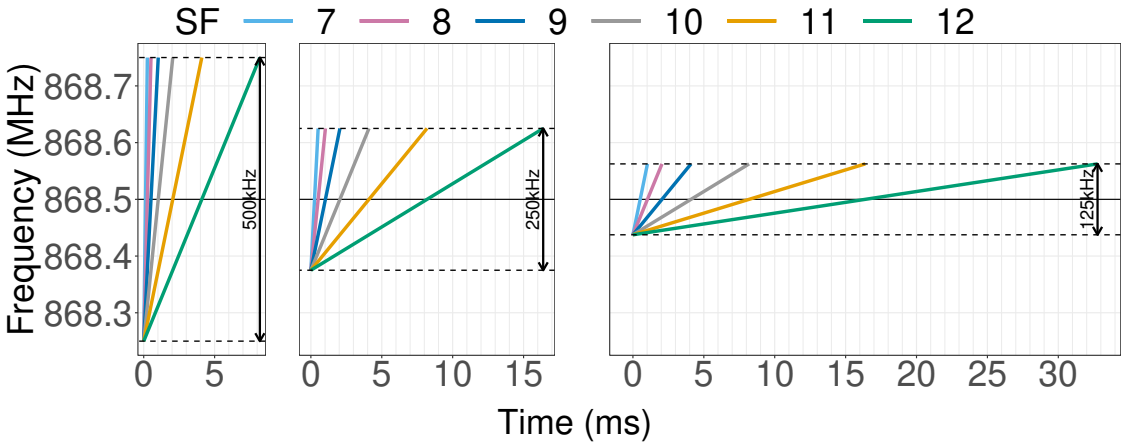

Figure 2.4: LoRa chirps for $spreadingfactor(SF) \in [7..12]$ and $BW \in \{125,250,500\}kHz$ on the CF =868.5MHz channel.

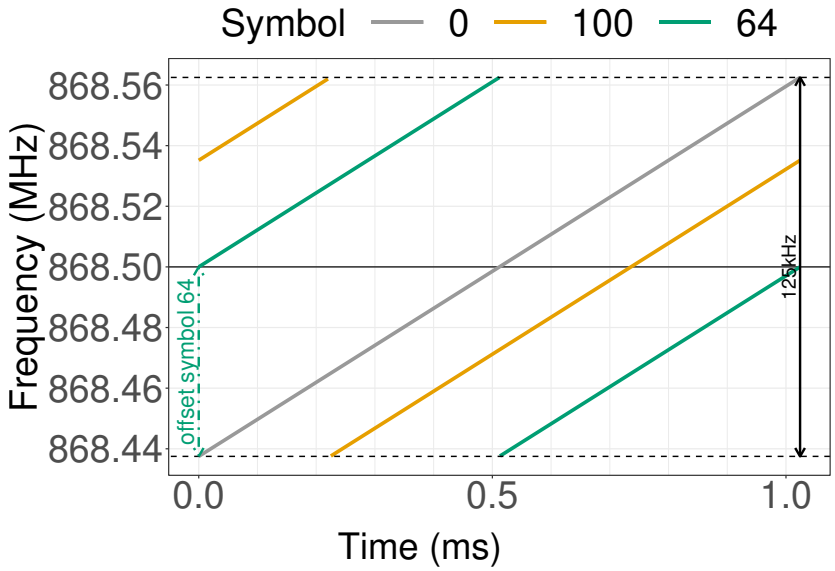

Figure 2.5: LoRa chirps of various values for $SF = 7$ and BW = 125kHz on the CF =868.5MHz channel.

And thus the DR_{mod} is:

$$DR_{mod} = \frac{SF \times BW}{2^{SF}}$$

In the current LoRa implementations, *SF* 5 to 12 are available [167]. Over the same BW, SFs are quasi-orthogonal to each others. So, a GW can simultaneously receive multiple LoRa frames with different *SF*, which greatly improve the network capacity.

Synchronization

However, chirp symbol demodulation is sensible to frequency offset between the transceivers [137]. LoRa modulation tackles this by starting the frames with both a preamble an a synchronization word (SyncWord).

The preamble is a series of unmodulated up-chirps (typically 8). It triggers the receiver demodulation.

The SyncWord is composed of two modulated identical up-chirps and two and a quarter down-chirps. The SyncWord is used to identify the network, to mark the frame start and more importantly to synchronize the clocks of the transceivers. This allows to correct the frequency offset the transceiver. However, the frequency references of the transceivers may drift, causing synchronization loose. LoRa compensate with the *low data rate optimization*, an undocumented feature, which slightly reduce the data rate and is mandatory for $SF \geq 10$. LoRa initial synchronization compensates the use of low precision cheap hardware by making the modulation robust against Doppler effect and frequency drift.

LoRa intra-frame Error Correction Code (ECC)

The inherently robust CSS modulation scheme is complemented by an intra-frame ECC with $CR \in \{\frac{4}{5}, \frac{4}{6}, \frac{4}{7}, \frac{4}{8}\}$ based on Hamming coding. The extra redundancy improves the robustness of the transmission at the expense of the DR_{phy}. The data rate delivered by the physical layer depends on the *SF*, the BW and the *CR*[2]:

$$DR_{phy} \approx \frac{CR \times SF \times BW}{2^{SF}}$$

Based on this modulation, LoRa provides very high link budget of up to 153.5 dB[3].

2.2.2 Frame Structure

A LoRa frame is composed as follow: First the preamble and the Syncword detailed previously, then an optional physical LoRa header with its own CRC, followed by the physical LoRa payload and its CRC.

The LoRa header and its CRC are encoded respectively over 15 and 5 bits and are protected by ECC with $CR = \frac{4}{8}$. The content of the LoRa header is not precisely described publicly and contains information such as the payload size, the frame *CR* or the presence or not of a payload CRC. This explicit header can be removed if theses parameters are fixed.

The physical payload size is restricted to 256 bytes, and its data integrity might be protected by a 2

[2]The equation is an approximation because the *CR* is fixed to $\frac{4}{8}$ over the preamble and lower *CR* are applied only over the payload and its CRC.

[3]With Semtech SX1301[171] chip and 14dBm transmission power (P_{Tx}).

bytes CRC. Both the payload and its CRC benefit from the ECC with configurable *CR*. The overview of the LoRa physical frame structure is given is Fig.2.6.

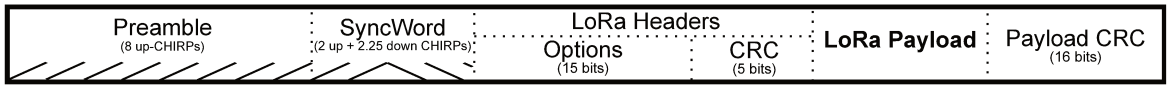

Figure 2.6: LoRa uplink frame structure.

In this thesis we call the data unit of the LoRa physical layer a frame and thus will refer to the loss rate at this layer (i.e. the physical loss rate between an ED and a GW) either as the *BER* or as the Frame Error Rate (*FER*).

2.2.3 Sub-1GHz ISM Bands

A typical LoRaWAN network operates in the sub-1GHz ISM band. Although benefiting from favorable propagation conditions and being license free, theses frequency bands are subject to regulation, and specifically they are strongly duty cycled. We give for instance in table 2.1 the regulation in Europe for the 863-870MHz ISM frequency band [170].

It must be kept in mind that the duty cycle regulations also apply to the GWs, thus the downlink capacity is therefore severely impacted. For instance with a single GW in the area and a 1% duty cycle, as all the EDs has to share the GW downlink capacity, each GW to ED downlink is finally only a fraction of 1% of the channel.

Hence, the frequency plan of a LoRaWAN network, the used CF and BWs, depends on the network operator choice and the regional regulation. Thus for instance, the standard EU868 LoRaWAN frequency plan includes for the uplink 3 mandatory channels with BW =125kHz ($CF \in$ (868.1, 868.3(868.5)MHz), which can be completed by 13 additional channels from the **g** and **g'** bands. A downlink specific channel is also defined in band **g3** as it allows for higher P_{Tx} and duty cycle, which help compensate the low downlink capacity.

Band	Frequency (MHz)	P_{Tx} Max (dBm)	Duty Cycle
g	863-870	14 (-4.5/100kHz)	0.1%
g'	865-868	14 (6.2/100kHz)	1%
g1	868-868.6	14	1%
g2	868.7-869.2	14	0.1%
g3	869.4-869.65	27	10%
g4	869.7-870	7	∞
g4'	869.7-870	14	1%

Table 2.1: European regulation for LoRaWAN in the 863-870MHz ISM band (EU868) for non-specific use with DSSS modulation.

Those regulations limit the maximal frame duration, and as a consequence the maximal payload size. The maximal payload size depends on the local regulation and the others physical parameters, i.e. the DR_{phy}. In table 2.2 we list the minimal and maximal payload allowed by the protocol and the regulation [172].

Table 2.2: Maximal LoRa payload according to protocol documentation and regulation for various regional ISM bands.

Band	Maximal LoRa payload size (bytes)	
	DR_{phy} min	DR_{phy} max
EU863-870	64	255
US902-928	**24**	255
CN779-787	64	255
EU433	64	242
AU915-928	**24**	255
CN470-510	64	255
AS923	32	**263**
KR920-923	64	255
IN865-867	64	255
RU864-870	641	255

2.3 LoRaWAN Data Link Layer

LoRaWAN is a strongly uplink oriented protocol. The traffic pattern is expected to be typically sparse and sporadic data from the EDs to the ASs. It is the mass of connected objects that will make the data flow massive at the GWs. However, LoRaWAN also provides downlink capabilities which is a fundamental feature, not only to allow the sending of application data to the EDs, but also allows firmware update over-the-air, uplink traffic acknowledgement (ACK) and sending service commands in order to administer the network and tune its parameters.

2.3.1 Channel Access Algorithm

As LoRaWAN is strongly uplink oriented, different channel access algorithms are defined for the uplink and downlink channels.

2.3.1.1 Channel Access for the Uplink Channel

LoRaWAN channel access algorithm to transmit uplink frames is Pure-Aloha: every ED transmits at any time whenever data is available without any kind of coordination in a totally asynchronous manner [3]. Limitations of LoRaWAN in terms of capacity and effective throughput are inherent to ALOHA access [83, 89].
A typical LoRaWAN network operates with multiple CFs: a new *CF* is randomly chosen for every uplink frame, which mitigates the effect of selective fading. An uplink frame can be sent with various DR_{mod} which is defined jointly by the BW and the *SF*. Even though more BW and *SF* might be available depending on the hardware, three BW are available $BW \in \{125, 250, 500\}$kHz and the *SF* is restricted to *SF* 7 to *SF* 12.

2.3.1.2 Channel Access for the Downlink Channel

LoRaWAN defines three classes of device with different downlink capabilities: class A (*All end-devices*), class B (*Beacon*) and class C (*Continuously listening*).

Class A: EDs listen for a potential incoming downlink frame solely after sending an uplink frame. Each uplink is followed by two short receive window (Rx1 and Rx2) slightly shifted in time as illustrated in figure 2.7. Rx1 is on the same channel (*CF* and BW) as the uplink frame and with a *SF* that

is a function of the uplink frame's *SF* (same *SF* by default). Rx2 is on a fixed configurable channel (*CF* +BW) and a fixed configurable *SF*.

Apart from the uplink frame and its subsequent receive windows, the ED's radio is turned off all the time which saves substantial energy. Class A EDs are the most energy efficient class at the expense of downlink latency and capabilities.

It is widely the most common class in LoRaWAN deployment. In this thesis we focus solely on class A exclusive LoRaWAN networks.

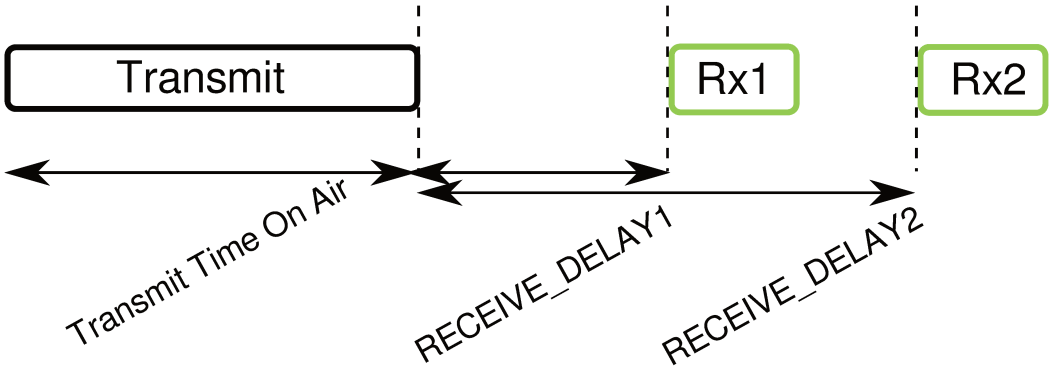

Figure 2.7: LoRaWAN class A receive windows Rx1 and Rx2. Figure from [173].

Class B: Class B is an addition to the class A mode of operation. EDs open additional receive windows, called PING SLOTS, at regular and fixed intervals. In order to allow and maintain sufficient synchronization, the GWs also emit additional beacons at regular intervals. Figure 2.8 illustrate the class B operations.

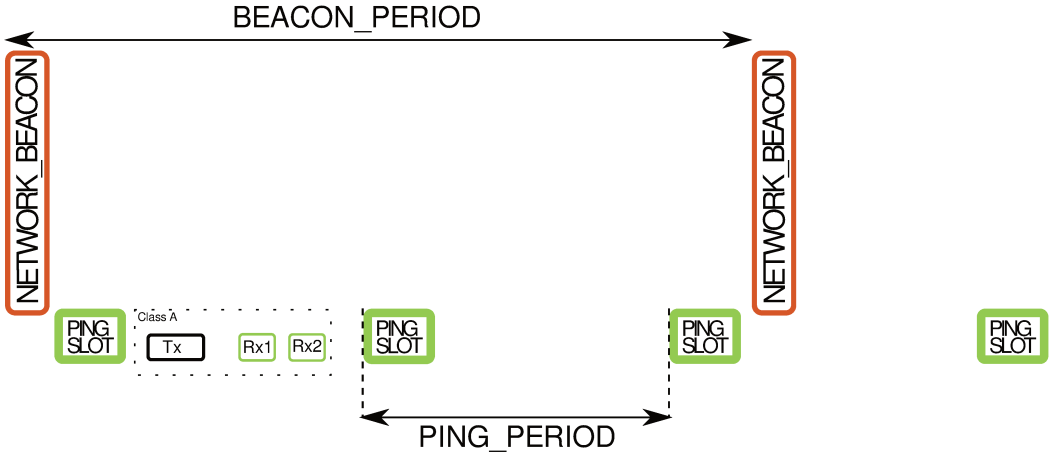

Figure 2.8: LoRaWAN class B network beaconing and additional ED receive windows (PING SLOT).

Class C: Class C is another addition to the class A mode of operation. Class C ED also implements the basic operation mode from class A (thus with same Rx windows and channels) but instead of turning off its radio the rest of the time, it stays in Rx mode continuously. Figure 2.9 illustrate the class C operations. Class C EDs have the lowest downlink latency but the highest energy consumption.

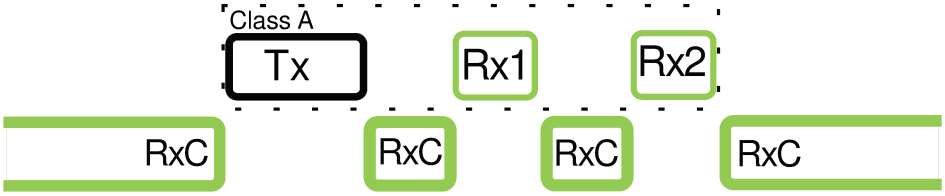

Figure 2.9: LoRaWAN class C network operation: ED stays continuously listening for Rx.

Figure 2.10: LoRaWAN packet structure.

2.3.2 Packet Structure

The LoRaWAN uplink packet structure is given in Fig. 2.10. The packet starts with a header of variable length between 9 and 24 bytes which contains :

- the message type (one of the 6 LoRaWAN message types: join request, join accept, unconfirmed data up, unconfirmed data down, confirmed data up and confirmed data down),
- the protocol major version (LoRaWAN v1 only at time of writing),
- the ED address (over 4 bytes),
- a port number (over 1 byte),
- a packet counter for duplicate detection (over 2 bytes),
- control information (to indicate whether the ED uses ADR described below in sec.2.3.5, to ask or send ADR commands, to request ACK, to signal the ED that more downlink traffic if pending and to indicate whether MAC commands are piggybacked in the current LoRaWAN header),
- and optionally (over 0 to 15 bytes), one or more MAC commands which are control orders between the ED and the NS (for instance to check the connectivity, to change transmission parameter settings, to add or remove channels, to change receive windows settings, etc).

This LoRaWAN header is followed by the application payload which is encrypted by an Advanced Encryption Standard (AES) based algorithm using a 128 bits key. Finally the LoRaWAN packet is sealed by a 4 bytes message integrity code (MIC) computed over both the LoRaWAN header and the application payload with the AEScypher-based message authentification code (CMAC) algorithm using a 128 bits key[4].

In table 2.3 we list the maximal application payload allowed by the protocol and the regulation [172] for the minimal and maximal DR_{phy}. Notice that the presence of the optional MAC command might reduce this available payload by up to 15 bytes.

In this thesis we call the data unit of the LoRa data link layer a packet and thus will refer to the loss rate at this layer as the *PER*. It is the loss rate between an ED and the NS. Thus the *PER* benefits from both the gain of GWs macro-diversity in the network and of LoRaWAN native error recovery mechanisms described in sec.2.3.3.

Notice that we will refer to the loss rate at the application layer as the *DER*. The *DER* is the loss rate

[4] RFC4493.

Table 2.3: Maximal application payload size for packet without any optional fields in the header (i.e. MAC commands) for the minimal and maximal DR_{phy} in various regions.

Band	Maximal application payload size (bytes)	
	DR_{phy} min	DR_{phy} max
EU863-870	51	242
US902-928	**11**	242
CN779-787	51	242
EU433	51	242
AU915-928	11	242
CN470-510	51	242
AS923	19	**250**
KR920-923	51	242
IN865-867	51	242
RU864-870	51	242

between an ED and the AS and thus benefits from any additional error recovery mechanisms that are non-native to LoRaWAN.

2.3.3 Error Recovery Mechanisms

LoRaWAN implements two basics mechanisms at the data link layer to provide reliability for the uplink:

- **Blind Systematic Repetition (BSR)** Uplink frames are systematically repeated a given number of times, which mechanically increases the probability that at least one of the transmissions is received. The number of transmissions parameter being $Nb_{\text{Trans}} \in [1:15]$, from a given *FER*, the *PER* drops to $PER = (FER)^{Nb_{\text{Trans}}}$. However it is obvious that as BSR multiplies the Time-On-Air (TOA) and thus the uplink channel load. It must be used sparingly and with care to avoid network congestion. Overuse of BSR could cause collision rate to increases drastically, undermining the reliability goal.

- **Confirmed Uplink:** Uplink frames are marked as requesting an ACK from the NS and are retransmitted until either an ACK is received or the maximal number of attempt is reached. Each retransmission is done over a new *CF*, and can be done with another DR_{mod}. Indeed, in case of successive failures, it is recommended that the EDs reduce the DR_{mod} to increase the communication robustness and range. The default strategy recommended by the LoRaWAN specification consists in reducing the DR_{mod} by one notch (i.e. generally increment the *SF* of 1) every 2 consecutive failures. However, because of the limited downlink traffic capacity detailed further in 2.3.1.2 and 2.2.3, ensuring reliable uplink traffic handling by means of Automatic Repeat reQuest (ARQ) or any kind of feedback is challenging due to the very restricted downlink capabilities [83, 99], even though improvements are possible [124].

In the following of the thesis, as we are going to manipulate a lot the notions of data loss at different levels of the communication, we define here the units will use:

- The Frame Erasure Rate (*FER*) is the physical loss ratio between an ED and a given GW (i.e. without duplicate transmission from LoRaWAN BSR).

- The Packet Error Rate (*PER*) is the loss ratio between an ED and the NS. *PER* benefits from multiple GWs reception and frame duplicated transmissions from BSR.

- The Data Error Rate (*DER*) is the loss ratio between an ED and the AS, thus benefiting from the presence of any additional erasure recovery mechanism.

Notice depending on the layout, they might be equivalent. For instance in the case of a mono-GW cell and with Nb_{Trans} =1, *FER* is equal to *PER*. Also, if no additional erasure recovery mechanism is used, *PER* is equal to *DER*.

2.3.4 LoRaWAN Fundamental Trade-off: Range for Time-On-Air (TOA)

The LoRaWAN parameters BW, *SF*, *CR* and Nb_{Trans} can be tuned to increase the link robustness at the expense of the DR_{app}. Or in others words the range can be improved at the expense of increased TOA. For instance, each *SF* increments roughly divide the DR_{phy} by half but reduce the required *SNR* by 2.5dB. DR_{phy} ranges from 183bps to 62.5kbps for *SF*, BW, *CR* respectively 12, 125kHz and $\frac{4}{8}$, and respectively 5, 500kHz and $\frac{4}{5}$. Similarly, the minimal required *SNR* range from approximately -2.5dB to -20dB for respectively $SF = 5$ and $SF = 12$. Also, Nb_{Trans} reduces the *DER* at the expense of a TOA multiplied by Nb_{Trans}.

This trade-off is fundamental in LoRaWAN as it offers a wide panel of performances in terms of TOA and range. And, as detailed in sec.3.2.1, both the network reliability and capacity depends on the channel load, thus on the TOA of each ED. Notice that as it is also the main energy consumption of the LoRaWAN algorithm, and thus reducing the TOA is also a gain for ED battery lifetime.

We define the *ToA* per application bit, *ToA/b*, to be the overall time spend for the transmission of one application bit: $ToA/b = \frac{Time\text{-}On\text{-}Air}{Number\ of\ bits\ in\ the\ application\ payload}$.

In Fig. 2.11 we show the *ToA/b* cost to transmit a 25 bytes application PL with $SF \in [7..12]$, $CR \in \{\frac{4}{5}, \frac{4}{8}\}$ and $Nb_{\text{Trans}} \in [1..3]$ with BW =125 kHz. The *ToA/b* cost smoothly increases as we move toward more robust transmission parameters. The transmission with the most robust configuration is two orders of magnitude more costly in TOA than the least robust one.

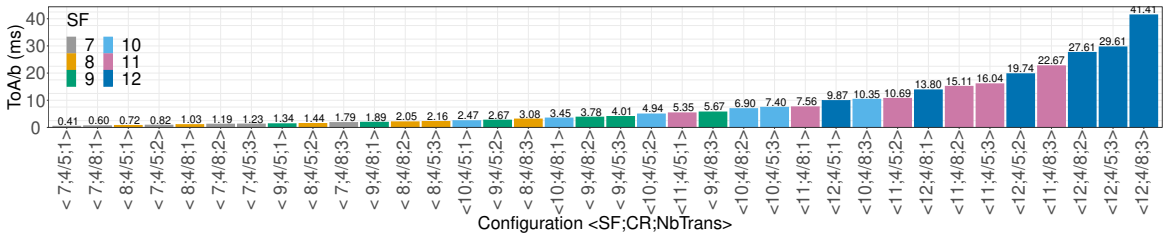

Figure 2.11: Time-On-Air by applicative bit (*ToA/b*) cost for 25 bytes applicative payload over a 125kHz bandwidth for selected transmissions parameters.

2.3.5 MAC Commands

MAC commands are standardized commands that are piggybacked in the LoRaWAN headers and transparent for the application. MAC commands exist in both uplink and downlink frames and are used for fundamental network administration operations such as adapt the uplink transmission parameters (P_{Tx}, *SF*, Nb_{Trans}), check connectivity, add or delete additional channels, modify Rx receive delay or configuration, ping period for class B devices, etc.

The MAC commands allow LoRaWAN to implement one of its key features: the adaptive data rate (ADR). The ADR is an automatic and dynamic tuning of the uplink transmission parameters to adapt to the network and link conditions. The ADR is detailed below in section 2.3.6.

2.3.6 Adaptive Data Rate (ADR)

The ADR is a mechanism part of LoRaWAN to adapt the EDs transmission parameters over-the-air. As described in sec.3.2, the ADR is key in LoRaWAN due to the wide TOA for range tradeoff described in 2.3.4.

With the ADR, the NS estimates the link quality by monitoring the uplink frames metadata and it adapts periodically the ED transmission parameters via MAC commands sent in its rare downlink communication opportunities with the ED. If no downlink frame is received for too long, the ED decreases its DR_{phy} (increases its P_{Tx} and its SF) to try to regain connectivity. No ADR algorithm is strictly defined in the standard, however some indications and recommended behavior are described. The ADR-ED and ADR-NS algorithms appear respectively in algorithm 1 with Semtech's implementation[5] for the ED side and Algorithm 2 from The Things Network[6] (TTN) for the NS side.

Algorithm 1 ADR-ED algorithm.

```
1:  ACK_LIMIT=64;
2:  ACK_DELAY=32;
3:  ACK_CNT=ACK_LIMIT;
4:  ACK_Req=false;
5:  Nb_Trans =3;
6:  P_Tx = P_Tx^max;
7:  SF = 12;
8:  while (true) do
9:      if (ACK_CNT >= ACK_LIMIT) then
10:         ACK_Req=true;
11:     end if
12:     if (ACK_CNT==ACK_LIMIT+ACK_DELAY) then
13:         P_Tx = P_Tx^max ;
14:         increaseSF();
15:         ACK_CNT = ACK_LIMIT;
16:     end if
17:     waitTxRequest();
18:     TxSend(ACK_Req);
19:     if (RxReceived()) then
20:         applyRxADRCommand();
21:         ACK_Req=false;
22:         ACK_CNT = 0;
23:     else
24:         ACK_CNT++;
25:     end if
26: end while
```

This protocol addresses the following three questions by adjusting its internal parameters:

- **How frequently does the ED require a downlink from the NS?** ACK_LIMIT and ACK_DELAY bound the acceptable number of consecutive uplinks without an ACK reception. The default recommended values are ACK_LIMIT=64 and ACK_DELAY=32 transmissions.
- **How does the NS estimate link quality?** ADR_{TTN} takes the SNR maximal value from the last twenty received packets. Even if this maximal value tends to over-evaluate the channel SNR,

[5] Version 1.0.3 github.com/Lora-net/LoRaMac-node [172].

[6] `github.com/TheThingsNetwork/lorawan-stack`

it is less dependent on the *PER* than the average, because one expects that the transmissions facing more attenuation are more likely to be missed. Note that this estimation does not take into account the reception by multiple GWs, and neither BSR[7], both of which tend to increase the estimated *SNR*.

- **How conservative should the transmissions parameters selection by the NS be?** The *MARGIN* parameter biases the algorithm towards more robust transmission, at the expense of channel occupancy. The default value is 15dB.

Algorithm 2 ADR-NS algorithm.

```
1:  MARGIN =15;
2:  PER_Low = 5%;
3:  PER_Med = 10%;
4:  PER_High = 30%;
5:  while true do
6:      ACK_Req=waitRx();
7:      if (ACK_Req) then
8:          SNR_measured = History_20packets.getSNRMax();
9:          SNR_floor = −(7.5 + (SF − 7) × 2.5) + MARGIN;
10:         SNR_margin = SNR_measured − SNR_floor
11:         if (nbPacketsReceived < 20) then
12:             SNR_margin − = 2.5;
13:         end if
14:         while (SNR_margin > 2.5 && SF > 7) do
15:             SNR_margin − = 2.5;
16:             P_Tx = P_Tx^max;
17:             SF − −;
18:         end while
19:         while (SNR_margin > 2.5 && SF == 7) do
20:             SNR_margin − = 2.5;
21:             P_Tx − −;
22:         end while
23:     end if
24:     PER = History_20packets.getPER();
25:     if (PER ≤ PER_Low) then
26:         Nb_Trans = max(1,Nb_Trans -1)
27:     else if (PER_Med ≤ PER < PER_High) then
28:         Nb_Trans = min(3,Nb_Trans +1)
29:     else if (PER_High ≤ PER) then
30:         Nb_Trans = 3;
31:     end if
32: end while
```

2.4 Chapter Conclusion

In this chapter we have seen how the LoRaWAN technology works.

LoRaWAN shared channel access method based on non-slotted Aloha is the lightest for the EDs. But with such an access method the frame collision rate increases quickly with the channel load. This can jeopardize the scalability of the network if poorly taken into account.

[7] For a given received LoRaWAN packet only the best *SNR* value is kept.

LoRaWAN provides two reliability mechanisms to handle packet losses, confirmed traffic and BSR. Both are very basic and particularly expensive for the network. None of them can actually provide reliability in LoRaWAN without heavily impacting the network's scalability.

LoRaWAN provides a very wide range of throughput through its *SF*, *CR* and Nb_{Trans} parameters. The highest data rate setting is about two orders of magnitude higher than the lowest data rate setting (even before touching the BW parameter). This wide range of available data rates gives amplitude to set the best data rate versus robustness trade-off.

LoRaWAN's ADR algorithm is a keystone of this technology. Its role is to automate the adjustment of the data rate versus robustness trade off in order to use the full potential of LoRaWAN. The optimization of the ADR is therefore fundamental to improve LoRaWAN, especially its reliability and scalability.

Chapter 3

State of the Art

Contents

Chapter Introduction

In this chapter we lay down the state of the art on LoRaWAN. Although the technology is only a decade old, LoRaWAN has draw the attention of the scientific community and publications about it number in the thousands. It is not possible for us to make a complete and exhaustive review of all of this work and this is not the point of the chapter of this thesis. We strive to do a commented review of the main works as well as the works that have influenced us and on which we have taken support.

In section 3.1 we review the state of the art of the LoRaWAN link characterization with on the one hand the analytical studies on LoRa modulation and on the other hand the studies based on experimental measurements. In section 3.2 we review studies on the scalability and reliability of LoRaWAN networks. In section 3.3 we present and discuss the few works proposing and testing CP-ECC in LoRaWAN.

3.1 LoRaWAN Link Characterization

Driven by academic and industrial success, many studies have been carried out to understand the performance of LoRaWAN networks. To characterize LoRaWAN performances, especially in terms of range, it is first necessary to precisely characterize its physical layer LoRa. Then, to finish characterizing the performance of the network, with reliability and scaling up, it is necessary to understand the link layer, in particular with its channel access algorithm (upstream and downstream) and its link layer reliability mechanisms. In this section we proceed in this order to present the state of the art of the LoRaWAN link characterization.

Two approaches are possible to characterize the performance of a network physical layer. The first option is to study analytically the modulation performance then potentially simulate the result over a given channel model to estimate the performance of the real link. The other option is to directly test and measure the link into a real deployment.

3.1.1 LoRa Modulation Analytical and Simulation Studies

Based on result of MATLAB simulation with an implementation of a CSS-decoder and on the MATLAB curve fitting tool, an analytical closed form of the CSS modulation Bit Error Rate (BER) under AWGN has been proposed[81]:

$$BER_{\text{Reynders\&Al.}} = Q\left(\frac{\log_{12}(SF)}{\sqrt{2}} \times \frac{E_b}{N_0}\right) \tag{3.1}$$

Through the simulations, the robustness of LoRa symbols against other types of interference such as continuous wave or a concurrent LoRa symbol is also studied.

From the mathematical description of the LoRa modulation and simulation another projection of the BER CSS modulation as a function of the *SNR* has been computed[102]. Through simulation the LoRa modulation is compared with FSK modulation with equivalent cardinal under AWGN or frequency selective channel.

From this mathematical description of the LoRa modulation[102], another analytical study derived closed-forms approximation of LoRa BER performance in AWGN[127]. In particular this ex-

pression is given:

$$BER_{\text{Elshabrawy\&Al.}} = 0.5 \times Q\left(\frac{\sqrt{SNR \times 2^{SF}} - \left((H_{2^{SF}-1})^2 - \frac{\pi^2}{12}\right)^{\frac{1}{4}}}{\sqrt{H_{2^{SF}-1} - \left((H_{2^{SF}-1})^2 - \frac{\pi^2}{12}\right)^{\frac{1}{2}} + 0.5}}\right) \tag{3.2}$$

In figure 3.1 we compare the result from these three studies. We plot both the results for the *BER* and for the *FER* with 10 bytes long frames. The earliest study (Reynders & Al. [81]) is more pessimist than the following two (Vangelist [102] and Elshabrawy & Al. [127]). However these studies do not take into account neither frame imperfect synchronization at demodulation nor LoRa ECC at physical layer.

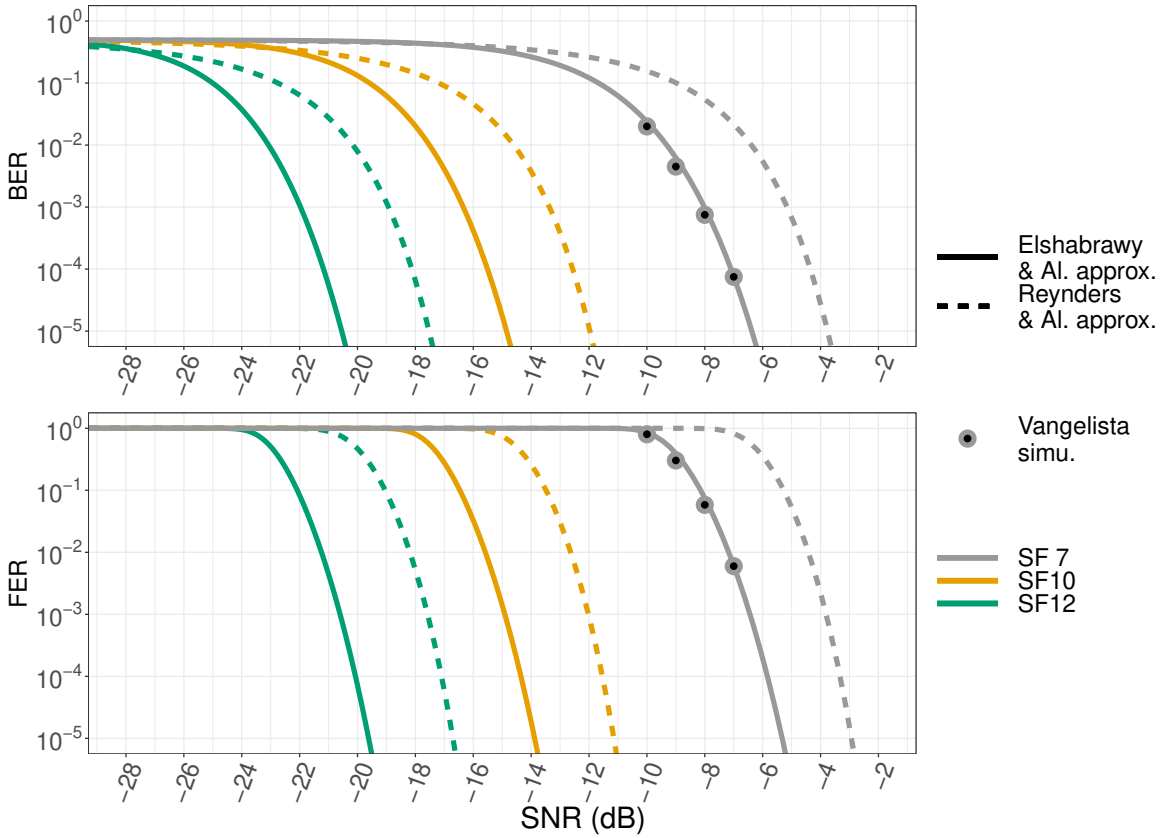

Figure 3.1: Simulated BER (top figure) and FER for a 10 bytes payload (bottom figure) of uncoded LoRa modulation at $SF \in \{7, 10, 12\}$ following closed-form approximations [81, 102, 127].

A study based on the approximation of equation 3.2 proposes a formulation of the coded LoRa BER thus taking into account LoRa*CR* [135]. However, the full correction capacity of LoRa physical layer ECC is not taken into account as it is considered that only $CR \in \{\frac{4}{7}, \frac{4}{8}$ correct an error. It is true for hard-decoding but not with soft-decoding. Not to profit from the inherent information available at demodulation to improve error correction with soft decoding would be a kind of waste. Our experimental results exposed in section 4.3 show that there is a gain between each *CR*, advocating that soft-decoding is used in LoRa demodulation. Therefore, the BER of coded LoRa might be over estimated in this study.

Another study based on the approximation of equation 3.1 proposes a formulation of the coded LoRa BER[149]. However, two fundamental errors are made, although they might partially compensate each other. First, the correction capability of the LoRa physical ECC is once again con-

sidered for hard-decoding only with no correction capability for $CR \in \{\frac{4}{5}, \frac{4}{6}\}$ and a single bit in error correction capability for $CR \in \{\frac{4}{7}, \frac{4}{8}\}$. This underestimates the correction capability of LoRa ECC. Secondly, the ECC gain from LoRa physical layer ECC is already taken into account in the $\frac{E_b}{N_0}$ computation, and thus in the computation of the *BER*. Thus LoRa physical layer ECC gains are accounted twice, which over estimate the correction capability of LoRa ECC. One should either approximate the redundant bits as extra energy injected into the transmission, or count them as bits of the payload, which in a second time are used for error correction by the next sub-layer.

The impact of imperfect synchronization has been demonstrated and as a consequence the role of the frame synchronization algorithm [137]. The LoRa synchronization algorithm being based on the reception of SyncWord, the number of preamble symbols which prepares its detection is therefore also important. It has been shown by simulation and measurements that the number of preamble symbols should be ≥ 6 and beyond this point the gain is marginal.

3.1.2 LoRa Experimental Measurements

However, frame receptions on the field is widely impacted by many environmental factors which can hardly be modeled and taken into account without studying and measuring the LoRa link deployed in real conditions. Thanks to the academic success and ease of deployment of a LoRaWAN network, many experimental measurements are reported in the literature and provides a wide panel of insight on the LoRa channel characterization.

Interference and usage of the 868 ISM band:
The monitoring of the 868MHz ISM radio band in a medium sized city in Denmark at street level [94] gives insight into the interference LoRa may face. It shows that a LoRa channel may experience highly heterogeneous interference patterns, both in periodicity and strength of the colliding signals, even within close distances.

Also, we know from an early extensive study of the meta-data of the public TTN network [85] that the network usage might be highly unbalanced: an overwhelming majority of devices uses SF7 whereas SF12 is the second most used, the 868.1 MHz sub-channel is over-used compared to the others two standards sub-channels (868.3 and 868.5 MHz) and the non-standard sub-channels are almost unused.

The highly heterogeneous interference patterns and the unbalanced network usage emphasize the need for an automatic, dynamic and efficient parameter selection mechanism in LoRaWAN.

LoRa frames collisions:
The results of an analytical study [107] corroborated both by simulation and by experimentation showed on the one hand that the capture effect in case of co-SF collision is underestimated - indeed a Signal-to-Interferer (SIR) of 1dB is sufficient for correct reception if the reference signal is correctly synchronized - and in the other hand that the capture effect in case of inter-SF collision is overestimated compared to previous study [46]. These worse SIR thresholds for correct reception in case of inter-SF collision question the approximation of orthogonality between differents *SF* in LoRa. However, it should be noted that the collisions conditions are rather unfavorable compared to the probable real cases: it is considered equal emission times whatever the SF. It is improbable that different SF frames will have the same broadcast time. For instance, there is a 24 factor between the emission times of an equivalent payload with SF 7 and 12. Finally, this study underlines the strength of LoRa's ECC associated with interleaving and Gray coding which is efficient to correct errors due to mis-synchronization or narrow-band interference.

Another experimental study of LoRa collisions [113] shows the impact of arrival time offset between co-SF colliding frames received by a single channel and single demodulation path receiver (LoRa SX1276 module). The receiver is locked on the incoming frame after 4 preamble symbols. Once the receiver is locked, the colliding signal appear as noise. Also the receiver might release the lock if the header CRC is invalid, thus allowing for immediate reception of another frame without waiting for the end of the failed transmission. As the reception is more vulnerable at these times, a stronger colliding frame is likely to benefit from the capture effect if its preamble arrive a these moments.

LoRa range and PL characterization:
It is to be noticed that thanks to its long range and to its adaptability (i.e. the data rate versus range trade-off), LoRa can fit a wide panel of applications and might be deployed in a large variety of environment. It is reflected in the literature, LoRa has been experimented in different outdoor contexts : over sea[74], in rural areas[72], in forests[75, 123], in farms [116], in various cities[79, 101, 103, 105, 121, 126, 128, 143] and even in Antarctica[88]. Experimental measurements of LoRa can also be found for indoor deployment, for instance in universities[78, 87], office[119], residential[134] or industrial[91] buildings and even historic underground monuments [117].

As expected with such heterogeneous deployments, the LoRa channel characterizations are also heterogeneous. For instance, empirical path loss exponent reported in the literature range from 0.79 in a empty hallway which gives a wave-guiding effect [119], up to 8.4 in a car park with no line of sight [134].

Tables 3.1, 3.2 and 3.3 provide an overview of the experimental characterization of LoRa found in the literature.

The heterogeneity of LoRa channel characterization emphasizes the need for an automatic, dynamic and efficient parameter selection mechanism in LoRaWAN. Also, as pointed in Sec.3.1.3, the LoRa channel characterization is still an ongoing work.

Table 3.1: Survey of the experimental LoRa performance measurements.[1/3]

	Environment	**Maximal Experimented Range** (Config. <*SF*;*CR*;BW (kHz);PL(B);P_{Tx} (dBm)>)	**Characterization**
[72]	Outdoor (rural)	<10;$\frac{4}{6}$;250;10;*NA*> • 8.15km	RSSI std. dev. $\in [0.3, 5.6]$ dB
[74]	Outdoor (urban and over sea)	<12;*NA*;125;*NA*;14> • 15km (ground) • 30km (over sea)	Log-distance path loss model with log-normal shadowing: • $\gamma_{\text{ground}} = 2.32$ • $\sigma_{\text{ground}} = 7.8$dB • $\gamma_{\text{sea}} = 1.762$ • $\sigma_{\text{sea}} = 8$dB
[75]	Outdoor (open, straight road and wooden areas)	<7;$\frac{4}{5}$;125;*NA*;P_{Tx} > • 1.21km	Log-distance path loss model: • $\gamma_{\text{open area}} = 2.8$ • $\gamma_{\text{moderately wooded}} = 5.9$ • $\gamma_{\text{straight road}} = 3.2$ • $\gamma_{\text{heavily wooded}} = 3.5$
[79]	Outdoor (urban and rural)	<12;$\frac{4}{5}$;125;25(including MAC);14> • 6km	RSSI std. dev. $\in [1.12, 5.89]$ dB
[76]	Outdoor (urban)	<7;$\frac{4}{5}$;125;*NA*;14> • 2.3km <12;$\frac{4}{5}$;125;*NA*;14> • 3.5km	-
[78]	Indoor (multi-floor university/office building)	<12;*NA*;125;*NA*;14> • 390m	RSSI std. dev. $\in [4.95, 10.51]$ dB
[92]	Indoor	<12;$\frac{4}{5}$;125;*NA*;14> • $\approx 30m$	3 models fitted with MMSE: • Log-distance path loss model with log-normal shadowing: – $\gamma_{\text{ground}} = 2.75$ – $\sigma_{\text{ground}} = 1.3$dB – $\gamma_{1^{\text{st}}\text{floor}} = 2.5$ – $\sigma_{1^{\text{st}}\text{floor}} = 1$dB • ITU : $N_{\text{ground}} = 27.8$ $N_{1^{\text{st}}\text{floor}} = 25.5$ • Multi-wall COST231: $\alpha_{\text{glass}} = 1.53$ $\alpha_{\text{concrete}} = 4$ $\alpha_{\text{brick}} = 3.2$ $\alpha_{\text{glass}} = 3$
[91]	Indoor (industrial environment) + hybrid (indoor GW with outdoor ED)	<7;$\frac{4}{5}$;125;15;14> • $\approx 200m$ (indoor) <12;$\frac{4}{5}$;125;15;14> • $\approx 400m$ (hybrid)	$\Delta_{(RSSI_{\max} - RSSI_{\min})} \in [10, 40]$dBm
[87]	Outdoor (suburban) + indoor + underground	<7;$\frac{4}{5}$;125;5;20dBm> • 135m (indoor) • 130m (outdoor) • 80m (underground)	Transceivers temperature impacts RSSI: 6dBm are lost from 0°C to 60°
[98]	Outdoor (with mobility, urban and over sea) + indoor (with mobility)	*Same as [74]. See above.*	Doppler effect starts to degrade LoRa reception around : • 38km/h for SF12 • 76km/h for SF11 • 155km/h for SF10
[96]	Outdoor (flat rural and urban)	<12;*NA*;125;*NA*;14> • 7.5km	• Log-distance path loss model with log-normal shadowing: $\gamma = 2.71$, $\sigma = 7.11$dB . • Biased experimental data set: Logger reports only the three best receiving GWs for each transmission.
[84]	Indoor (barn with cows)	<*NA*;*NA*;*NA*;*NA*;14> • 40m	• Log-distance path loss model with log-normal shadowing: $\gamma \approx 2$, $\sigma \in [2.2, 3.7]$dB • Temporal fading: Rician distribution with K-factor $\in [6.4, 10.2]$dB (thus fade margin $\in [6.0, 10.8]$dB) (*Erroneous, see 3.1.3.*)

Table 3.2: Survey of the experimental LoRa performance measurements. [2/3]

	Environment	**Maximal Experimented Range** (Config. <*SF*;*CR*;BW (kHz);PL(B);P_{Tx} (dBm)>)	**Characterization**
[85]	*NA* (Public TTN network)	*NA*	• $\Delta_{(SNR_{max}-SNR_{min})} \approx 14$dB Analysis of network meta-data: • Many EDs send less than 50 packets in their lifetime. • Very few EDs send more than 1000 packets in their lifetime. • A majority of devices are close to GWs. • Most payloads are small (93.7% are <50bytes, 50% <19bytes). • CF=868.1MHz sub-channel is highly overused. • Most devices use SF7 BW=125kHz. Notice that it is an early study (data-set from 2015-2016), the network usage was not necessarily mature yet.
[103]	Outdoor + indoor	<*NA*;*NA*;*NA*;*NA*;*NA*> (433MHz ISM band) • 2km (outdoor) • 120m (indoor)	• $\Delta_{(SNR_{max}-SNR_{min})_{outdoor}} \approx 5$dB • $\Delta_{(SNR_{max}-SNR_{min})_{indoor}} \approx 10$dB
[93]	Outdoor (LOS and NLOS with dense vegetation)	<6;$\frac{4}{5}$;500;9;7> • 450m (LOS) <6;$\frac{4}{5}$;500;9; 20> • 90m (NLOS with dense vegetation) <8;$\frac{4}{8}$;125;9;7> • 900m (LOS)	• High temperature has severe impact on the communication range. • Vegetation has severe impact on the communication range. • P_{Tx} is not key to range.
[101]	Outdoor (urban)	<12;$\frac{4}{5}$;125;*NA*;14> • 8km	-
[88]	Outdoor (antartic LOS and NLOS)	<12;$\frac{4}{5}$;125;3;14> (868 and 433 MHz bands) • ≈ 30km	• Log-distance path loss model: $\gamma \in [1.5, 2.3]$ • $\Delta_{(SNR_{max-SNR_{min}})_{indoor}} \approx 3.5$dB
[116]	Outdoor (tree farm LOS)	<7;$\frac{4}{5}$;250;9;13> • 200m	• Fresnel zone clearance, and thus antenna height, has severe impact on reliability: PDR increases from 25% to 100% for antenna height increasing from 0m to 2m.
[111]	Outdoor (urban over public network)	<11;$\frac{4}{5}$;125;*NA*;14> • 13.2km	• Increasing P_{Tx} and/or *SF* might not decrease PER. • Good level of SNR might result in average PDR. • Variation in PDR are important over a day.
[105]	Outdoor (suburban) + indoor (office) (434MHz and 868MHz ISM bands)	<12;*NA*;*NA*;2;*NA*;> • 2.4km (NLOS) • 4km (LOS)	• Std. dev. of the average P_{Rx} 1.29dB and 2.09dB (Outdoor). • Rainfall has negative impact: up to 10dBm are lost (might be due to humidity on outdoor antenna). • Presence of people in the building increases P_{Rx} std. dev. (from 0.8 to 3.5 dBm).
[133]	Outdoor (suburban LOS body-to-body)	<12;$\frac{4}{5}$;125;*NA*;14> • 1.44km	• Log-distance path loss model: $\gamma_{toward} = 3.9$ $\gamma_{away} = 5.2$ • Signal fluctuations become more apparent for larger distances because of increasing influence of ground and surrounding buildings reflections.
[120]	Outdoor (urban + suburban)	<12;*NA*;*NA*;16;10> • 2.1km (LOS 434MHz and 868MHz) • 10.6km (NLOS only 434MHz)	• Received power fluctuates periodically: it drops by more than 20dBm for approximately an hour twice a day. • Cause of these received power drops is not fully determined. It might be due to daily changes in the troposphere's index of refractivity.
[118]	Outdoor/Indoor (high density urban area NLOS + suburban/rural)	<12;$\frac{4}{5}$;125;*NA*;14> • 200m (urban) • 2km (suburban/rural)	• LoRa ED to ED has lower range than ED to GW. • Signal in rural environment is more stable than in urban environment.

Table 3.3: Survey of the experimental LoRa performance measurements. [3/3]

	Environment	**Maximal Experimented Range** (Config. <*SF*;*CR*;BW (kHz);PL(B);P_{Tx} (dBm)>)	**Characterization**
[119]	Indoor (office)	<7;*NA*;125;*NA*;10> • 40m	• Log-distance path loss model: $\gamma \in \{1.87, 0.79\}$ • Propagation through an empty hallway might be subject to a wave-guiding effect. • $\Delta_{(P_{Rx\max} - P_{Rx\min})\text{same_floor}} \approx 18$dBm
[128]	Outdoor (urban: LOS + NLOS)	<8;*NA*;125;10;*NA*> • 9km (LOS) • 3km (NLOS)	-
[134]	Indoor. LOS (same floor), OBS (same floor obstructed) and NLOS (different floor/level). Office buiding (Off), residential building (Res), car park (Car) and warehouse (War).	<7;*NA*;500;*NA*;20> • 30m (LOS same floor) • 35m (NLOS different floors)	Log-distance path loss model with log-normal shadowing: • Off-LOS $\gamma = 2.2$, $\sigma = 5$. • Off-OBS $\gamma = 2.4$, $\sigma = 5.2$. • Off-NLOS $\gamma = 6.0$, $\sigma = 5.9$. • Res-LOS $\gamma = 2.3$, $\sigma = 4.9$. • Res-OBS $\gamma = 2.0$, $\sigma = 4.6$. • Res-NLOS $\gamma = 5.6$, $\sigma = 5.0$. • Car-LOS $\gamma = 1.5$, $\sigma = 4.7$. • Car-OBS $\gamma = 1.9$, $\sigma = 4.6$. • Car-NLOS $\gamma = 8.4$, $\sigma = 5.3$. • War-LOS $\gamma = 1.7$, $\sigma = 5.2$. • War-OBS $\gamma = 1.7$, $\sigma = 5.1$. • War-NLOS $\gamma = 3.8$, $\sigma = 5.5$. Attenuation factor (dB): 1 floor=21.7, 2 floors=25.9, 3 floors=27.2, 4 floors=50.8, Concrete wall=2.2, glass=2.0, wooden door=2.1, soft partition board=2.5. Temporal Fading (TF): • TF dynamic range is typically about 8dB and occasionally up to 17dB in LOS scenario, and typically 20dB in OBS scenario. • Presence of people in the building highly increases TF. • TF follows Rician distribution with *K-factor* (Kf): – $Kf_{\text{Off-LOS}} = 18.9$ – $Kf_{\text{Off-OBS}} = 12.1$ – $Kf_{\text{Res-LOS}} = 18.6$ – $Kf_{\text{Res-OBS}} = 23.1$ – $Kf_{\text{Car-LOS}} = 22.6$ – $Kf_{\text{Car-OBS}} = 11.1$ – $Kf_{\text{War-LOS}} = 17.6$ – $Kf_{\text{War-OBS}} = 21.4$ • *Notice that this P_{Rx} distribution fit is erroneous. See Sec.3.1.3.*
[123]	Outdoor (urban + forest + coastal)	<12;*NA*;*NA*;*NA*;20> • 1km (urban) • 4km (coastal) • 800m (forest)	Log-distance path loss model with log-normal shadowing: • Urban: $\gamma = 2.7$, $\sigma = 11.2$ • Coastal: $\gamma = 3.6$, $\sigma = 27.5$ • Forest: $\gamma = 2.0$, $\sigma = 6.9$ The coastal experimental data set is likely to be corrupted by handheld device-based experimental campaign. *Model fitting of the experimental data take into account censored data. The distribution is assumed to be a censored normal distribution.*
[121]	Outdoor GWs with indoor ED (urban)	<11;$\frac{4}{5}$;125;*NA*;14> • 18.3km	• Slow Rayleigh channel. • Only slight impact of payload length on reception rate.
[126]	Indoor (multi-floors) + outdoor (rural + suburban + urban)	<12;$\frac{4}{5}$;125;50;14> • 9km (urban) • 47km (rural)	Log-distance path loss model with log-normal shadowing : • Indoor: $\gamma = 2.9$, $\sigma = 8$ (with walls and floors attenuation factors). • Outdoor: $\gamma = 3.1$, $\sigma = 9.7$ (with ED height factor $H_f = -4.7 \times \log_{10}(H_{\text{ED}})$). • Urban: $\gamma = 4.2$, $\sigma = 7.2$ (with $H_f = -6.3 \times \log_{10}(H_{\text{ED}})$) • Rural: $\gamma = 3.0$, $\sigma = 6.4$ (with $H_f = -6.65 \times \log_{10}(H_{\text{ED}})$)
[143]	Outdoor (urban + suburban)	<*NA*;*NA*;*NA*;*NA*;14> • 1km (urban) • 4km (suburban)	HataLoRa model (derived from Hata model) for Large Scale Fading: • $\text{PL}(d) = 122 + 16\log_{10}(\frac{d}{d_0})$ (It is equivalent to log-distance path loss model with $\gamma = 1.6$ and $PL_0 = 122$). RSSI (moving average) variation at fixed distance $\approx$ 25dBm.
[144]	Outdoor (rainforest)	<12;$\frac{4}{5}$;500;*NA*;14> • 250m	• Dense forest is a very challenging environment for LoRa communication. • Signal is subject to strong variations even in a static experiment, which produce link disruptions. • Small variations of speed at low speed ($\leq 12km/h$) do not impact

3.1.3 Discussion

The wide availability of LoRa hardware (EDs and GWs) have allowed many researchers and network operators to assess the benefits brought by the technology. One of the focus point of LPWAN is coverage, so a large fraction of the reports look into the *PER* and P_{Rx} at various distances.

In many cases, though, the authors neglect the fact that the collected data is inherently distorted. In other cases, authors either simply disregard the specifics of their data collection process or expect the wrong distribution for their data.

3.1.3.1 Problems of biased experimental data-sets

Losses when P_{Rx} is low

Many studies propose to model large-scale LoRa propagation by fitting well-known models on newly gathered experimental data (the models are typically the log-distance path loss with log-normal shadowing). Unfortunately, in many papers, the authors do not take into account the bias which stems from the fact that only successfully received frames provide a channel gain measure [72, 74, 75, 79, 88, 96, 126, 143]. Indeed, a frame loss is at least partially dependent on the P_{Rx} for that frame. So, lost frames tend to be the ones arriving at the GW with the lowest P_{Rx} when it is variable, which is often the case in the studies and most probably due to SSF. Consequently, any experimental data-set featuring a significant *PER* is likely to be truncated, with an under-representation of low P_{Rx} values. This effect becomes more salient for the measurements at the coverage edge, where only a fraction of the frames are received. In this case the data-set is not representative of the full P_{Rx} distribution, but only of the upper fraction of the distribution. We illustrate the phenomenon with figures extracted from various studies in Fig.3.2.

Not taking into account the partial nature of the data potentially biases the model fit for the LSF (i.e. the path loss exponent estimation) by underestimating it. Potentially, it also biases ShF and SSF by making the P_{Rx} distribution look different from what it is (for instance log-normal instead of exponential) and under-estimating the associated variability (i.e. the standard deviation).

Nevertheless, not all real-world studies disregard this bias [121, 123, 140, 142, 153].

Also some studies do not provides enough information about the *PER* in their experimental data-set and it is not possible to evaluate whether their conclusions are biased or not [84, 92, 105, 133, 134].

High P_{Rx} corruption:

The opposite phenomenon might happen. As measured and characterized in a experimental work [105], the LoRa receiver can saturate, and the reported P_{Rx} has also a ceiling. For instance, the SX1276 chipset *SNR* measurement saturates slightly above 5dB. Thus measurements from deployment with EDs and GWs close to each other would require measurement equipment with a specific dynamic range[105] to be accurate.

Thus many conclusions or reports on LoRa channel characterization must be considered with caution. Also, only a few experimental studies propose a model for LoRa channel characterization and moreover most mainly focus on LoRa LSF for maximal range estimation. Thus ShF and SSF are often poorly described and analyzed. So, the extensive understanding and accurate modeling of the LoRa channel is still an ongoing work.

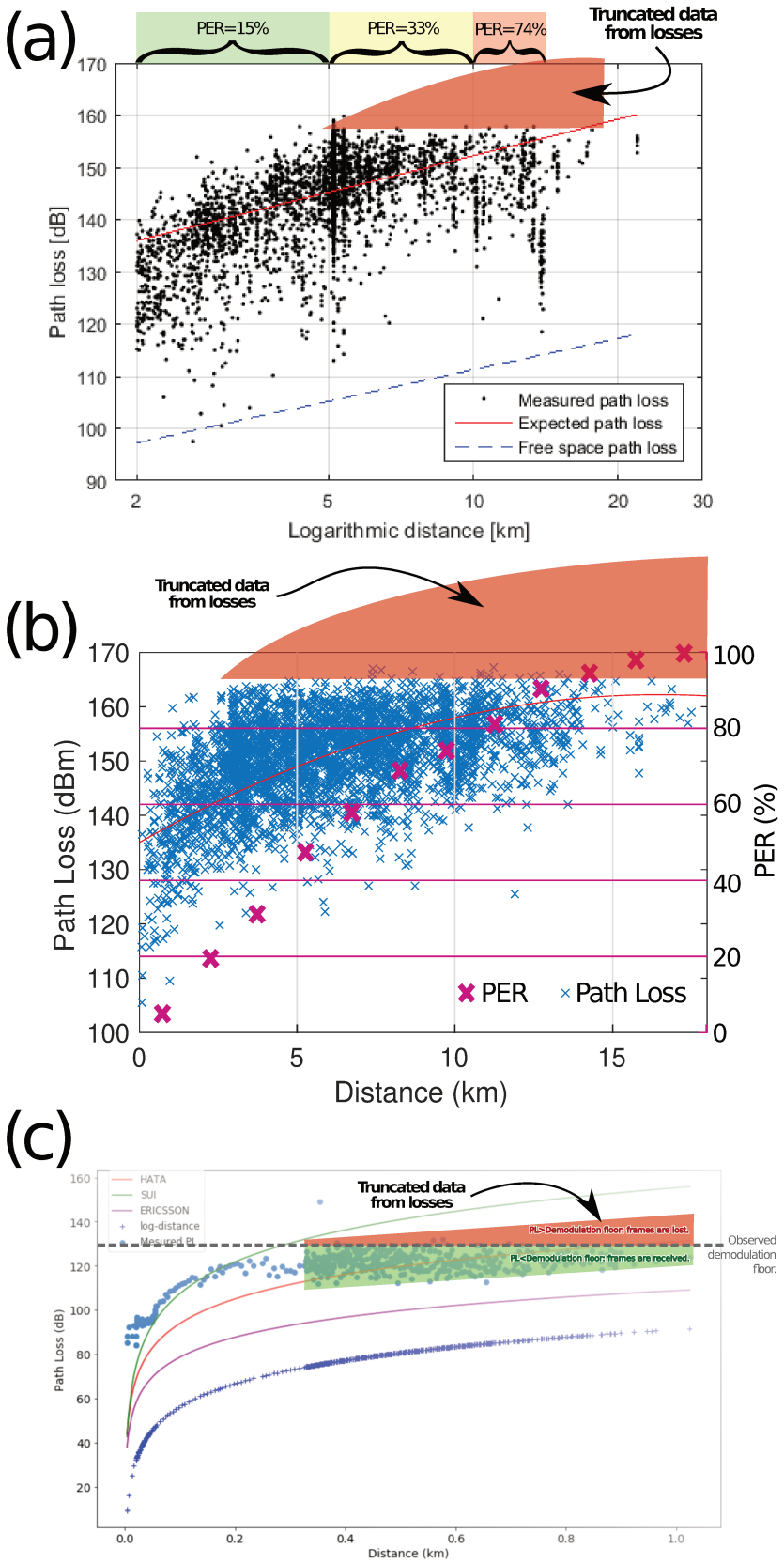

Figure 3.2: Annoted figures from (a) [74], (b) [96] and (c) [143]. Red areas show where the missing PL measurements probably are, thus biasing the model fitting.

3.1.3.2 Other mistakes

Experimental measurements collection with a filtering NS

Some NS do not provide the full meta-data of the transmission. Specifically, some NS do not give the full list of GWs that received a specific frame, but only a subset of the GWs. It is a case in an experimental study where the NS only provide the list of the 3 GWs with the best Received Signal Strength Indication (RSSI) for each received frame [96]. This completely skews the data-set, it is impossible to distinguish the real losses due to too low P_{Rx} from the false negatives produced by NS filtering. The filtering introduces a major bias: with just 4 GWs up to 25% of the data can be false negatives, with 6 GWs potentially half of the data set can be censored. No information on the number of GWs in the experiment is given and it is therefore not possible to estimate the bias order of magnitude. We are convinced that attempting to mitigate this bias is ineffective. Indeed, the displayed PL standard deviation is high ($\sigma = 7.1$) which implies the subset of the "best 3 GWs " is likely to be highly unstable. This study is, to the extent of our knowledge, the only one in which this specific bias is clearly apparent, but its conclusions on the characterization of the channel are nevertheless widely cited in the literature.

It cannot be ruled out that similar biases exist imperceptibly in the rest of the literature. For instance, we identified a risk during our experiments via the The Things Network (TTN) network: whenever a frame is received by multiple GWs, if one of them has a high latency on the backbone network, the packet might be filtered out by the NS. Indeed it might appear as a BSR duplicate to be filtered out because of its sequence number. This phenomenon can easily go unnoticed but ultimately might represents a significant number of false negatives. To avoid this, it is necessary to deactivate the frame counter check.

Signal envelope is not P_{Rx}

Several studies conclude that their experimental LoRa channel is Rician because the distribution of P_{Rx} seems to correspond to a Rician distribution [84, 134]. But it is not the distribution of the P_{Rx} which is supposed to follow a Rician distribution with such a channel: it is the signal envelope. Likewise, the distribution of the powers received on a Rayleigh channel does not follow a Rayleigh distribution but rather an exponential distribution. Which remotely looks Rayleigh when the power is expressed in dB. The difference is fundamental and is particularly well explained in the literature [13] (*Sec.3.2.2 Envelope and Power Distributions*). Consequently, these characterizations should no be considered.

3.2 Capacity, Quality of Service and Configuration of LoRaWAN

Network "performance" may cover different meanings. Capacity, that is roughly defined as the maximum number of EDs connected and served by the network, is the most common assessed and optimized performance in the literature on LoRaWAN, then comes reliability and to a lesser extent energy consumption.

Whatever the performance metric of interest, it is trivial to say that it depends on the physical layer, the protocol stack built on top of it, i.e. the channel access algorithm, the use of reliability mechanisms at the Data Link Layer such as confirmed traffic, channel coding... It is also trivial to say that it depends the deployment characteristics, i.e. the channel load (number of nodes, frames TOA, and transmission frequency), the span of the cell, etc. In addition, for LoRaWAN which benefits from a physical layer offering a wide robustness against TOA trade off, the choice of network parameterization is of major importance for the performance.

First in sec. 3.2.1 we describe and comment the state of the art on LoRaWAN capacity, i.e. the performance achievable by a network configured optimally apriori and therefore statically. Then in sec.3.2.2 we describe and comment the state of the art of dynamic configuration of the LoRaWAN transmission parameters, i.e. the LoRaWAN ADR algorithm.

3.2.1 Capacity

The LoRaWAN capacity has been a subject of interest and discussion since its early emergence. Many studies, analytical or by simulations, evaluate the number of EDs that can fit in a LoRaWAN network, and the consequent *DER*. Some works suggest to modify the LoRaWAN channel access algorithm[80, 115, 130, 148], or the network topology [97], but it does push more complexity to the EDs. In this thesis we focus on the capacity and optimization of the existing LoRaWAN protocol, with its Aloha based channel access algorithm.

The fundamental of the LoRaWAN capacity is the Aloha based channel access algorithm: as the traffic on the network (the channel load) intensifies, each transmission has higher collision probability and faces more interference. Thus the network reliability decreases as the channel load increases and the network tends to saturate. As a consequence, the discussion on the LoRaWAN capacity is about how fast the reliability decreases or at which point the network will saturate and how can this point be pushed further to handle more device with the same infrastructure.

Impact of external factors on LoRaWAN capacity

We call external factors elements not controlled by the network but rather the ones it has to deal with, for instance the span of the cell, the traffic intensity (number of nodes, frames TOA, and transmission frequency), the link properties (PL, ShF, SSF), the duty cycle, GWs hardware, number of GWs, etc... Even though these factors are not controlled by the protocol, they do impact the capacity of the network. Various studies with highly different models result in quite different conclusions about the LoRaWAN capacity. We think this is a reflection of the heterogeneity of the possible deployments of LoRaWAN networks. Also, this variety of studies allows to sketch some elements of understanding about the impact of theses external factors on the LoRaWAN capacity. So, the discussion on capacity with regard to the external factors is mainly how a given external factor impact LoRaWAN capacity and if the model is relevant and corresponds to a credible situation.

An early simulation study [77] of the *FER* as a function of the number of EDs found with its "default" configuration - which consists in using only the most robust configuration and therefore the most TOA expensive - that a LoRaWAN cell with a single GW can only handle 120 EDs with $FER \leq 10\%$, which is far from the expected and required capacity. This study also highlights the major importance of the capture effect as the simulation with capture effect shows a *FER* reduction up to 40 point of percent. It also assesses the importance of macro-diversity as their results shows a *PER* reduction of almost 20 points of percent when switching from 1 to 2 GWs. However the channel model of this study considers no ShF, and moreover no SSF. The later being of primer importance for capture effect performance, especially with macro-diversity.

An analytical and simulation study [89] proposed an improved model of the LoRaWAN capacity which takes into account the temporal variability of the channel, i.e. the SSF via a Rayleigh channel model. Thus EDs status is no binary with EDs either in or out range with a solid frontier, but rather each transmission can reach the GW with a P_{Rx} above the threshold following the probability of the channel model. However, the traffic model considers that each ED saturates its duty cycle, i.e. each ED transmits 1% of the time on whatever *SF* it is set. Therefore, each ED does not transmit

the same amount of data. For instance, an ED set with *SF* =7 transmits 18.8 times more data than an ED set with *SF* =12. This choice is not innocuous when it comes to network capacity measured as an absolute number of ED served rather than an network overall throughput. Indeed, with a fixed application data rate, more EDs could be connected with lower SFs.

Notice that both these studies [77, 89] consider single-channel networks, i.e. a single *CF*, which mechanically increases the channel load and collision rate compared to a standard LoRaWAN network which has at least three distinct channels. Thus the absolute values given as results underestimate the LoRaWAN capacity of LoRaWAN and might be multiplied by 3 for fair capacity estimation.

Another study [83] which also considers a rather pessimistic model as each node saturates its duty-cycle whatever is the used *SF*, and also considers no capture effect, has shown that the number of received packets per hour and per ED decays exponentially with the number of ED in the network.

Interference from overlapping networks can severely damage the reliability of the network, and thus its capacity [82]. It has been shown in simulation that 4 interfering networks can increase the *FER* of the network of interest by about 30 percentage points.

A study which chose a less disadvantageous parameters [95] analyzes the throughput and reliability as a function of the number of EDs but also the coverage of a LoRaWAN network deployed in an urban environment model and obtained through simulation a capacity per GW of about 10000 EDs. Interestingly, the simulation model takes into account the hardware limitations of LoRa GWs with the number of demodulation path limiting the number of frames received simultaneously, independently of the distinct CFs or the orthogonal *SF*. However, due to the large ShF for indoor nodes, up to 20% of EDs are out of range in their simulation with a single GW cell. Their simulation with multiple GWs shows that this problem of deep indoor coverage is not insoluble, although as underlined by the authors, the GWs densification requires the use of an efficient ADR: indeed, the deployed GWs densification pushes an increasing number of EDs towards the lowest *SF* which at a certain point will saturate the channel.

A study specifically analyzed the impact of the limited number of demodulation path in GWs equipment, i.e. a standard GW based on the SX1301 chip can detect 48 preambles at once but only demodulate 8 frames simultaneously, and has shown that the probability to drop a frame by lack of available demodulation path can become significant as the load on the network increases [131].

The macro-diversity, i.e. the multiplication of the number of GWs increases the capacity of the network [122]. Switching from a mono-GW cell to a dual-GW cell increases the capacity by 30% in number of EDs served. However, it is to be noticed that the model of this study has a flaw: although the model considers the SSF with a Rayleigh channel model, the capture effect is calculated with the average of P_{Rx} for each ED. This means that for two given EDs, the collision of their frames will systematically have the same outcome (destruction of both both or capture of the "strongest" ED), and thus it does not take account of the P_{Rx} variability between successive transmissions. However we think it does not invalidate the general dynamic being the capacity improvement with macro-diversity.

It has been shown [147] that the geometry of the cell is of primary importance when assessing the network capacity: a sparse cell $5EDskm^2$ can only serve 550 EDs in a 5.9km cell radius while a dense cell ($90EDskm^2$ can serve more than 3600 EDs in a 3.6km radius cell. In the same vein, an inhomogeneous distribution of EDs within the cell impacts the cell capacity [125]. In particular, a distribution where the density of the EDs closer to the GW is high and decreases with the distance

(which is common for the EDs of cellular networks and also for the density of population or the building in urban centers) increases the capacity of the LoRaWAN cell. Indeed with a homogeneous distribution in a large cell, the higher SFs (thus low data rate) start being saturated before the lower SFs (thus high data rate), so the network is saturated, even thought there is still "room" in the low SFs.

Impact of network configuration on LoRaWAN capacity

Even though fundamentally the network tends to saturate as the channel load increases, as LoRa, the physical layer, offers this robustness against throughput trade off (or equivalently range against TOA), the parameterization is key to reach high capacity. Moreover, as this trade-off is done through the use of various orthogonal *SF*, LoRaWAN benefits from a set of independent virtual channels. Thus a relevant configuration of the network can have huge impact on its capacity. For instance, a basic optimization consists in affecting the lowest *SF* with regard to the PL and thus minimize the TOA. This multiplies by 13.3 (from 120 to 1600 EDs) the number of EDs served when compared to the dummy affection the highest *SF* (the most robust and most TOA expensive configuration) to every EDs [77].

SNR-based optimizations of the network configuration (or equivalently P_{Rx}-based or distance-based) are sub-optimal: each ED is set the lowest *SF* possible. That is to say the lowest *SF* such that it is in range of the GW.Indeed, it has been shown that by balancing the *SF* assignment not only according to the *SNR* but also according to the contention on each *SF*, allows to serve more EDs with the required *FER* on a single-GW cell [147].

The optimization is more complex for multi-GWs networks, but studies proposed solution with Integer Liner Programming for models without capture effet [150] and with capture effect [122].

It is important to notice that increasing the tolerable *FER* required improves the capacity of the cell [147]. Thus "relaxing" the maximum tolerable *FER* constraint from 10% to 40% makes it possible to multiply the number of EDs served by 2.8 for a sparse cell and by 4 for a dense cell. This is of first major importance because the use of an error recovery mechanism at the data link layer level might thus benefits from both the maximized capacity and from a high reliability with a low *PER*.

Downlink capacity

LoRaWAN is intrinsically uplink oriented and most of the traffic is expected to be from the EDs to the NS. Thus even if LoRaWAN provides downlink connectivity, its downlink capacity is low. The downlink capability is highly limited. The first main reason being that GWs are submitted to the duty-cycle. But also, it has been shown that downlink traffic is severely harmfull for the uplink capacity. First because many GWs are half-duplex, i.e. uplink traffic is drop while transmitting a downlink frame, thus mechanically increasing the *FER*. But moreover, because EDs will retransmit confirmed frames that GWs where unable to acknowledge, saturation of the downlink might increases drastically the uplink channel load [99]. Moreover, the default retransmission strategy of confirmed traffic is to drift to higher *SF* every two missed acknowledgements, thus accentuating the channel load increase. As a consequence the network capacity drops in presence of uplink traffic: just 5% of confirmed traffic might reduce the uplink goodput of up to 10%; if 100% of uplink is confirmed traffic, the network capacity drops to 15% of its capacity.

So, even though downlink traffic is a key feature of LoRaWAN as it allows over-the-air activation, administration, dynamic configuration over even sporadic applicative downlink traffic, it must be minimized to the strict necessary. For instance the use of systematic confirmed traffic (ARQ) as a

reliability mechanism cannot scale [83].

This low downlink capacity can be mitigated by smart scheduling of the downlinks in multi-GWs networks and by combining multiples downlink frames in a single transmission[124].

3.2.2 Adaptive Data Rate (ADR)

Various studies evaluate and improve the ADR's performances. But because the algorithm is not strictly defined by the LoRaWAN specification, various implementations exist and variations of their interpretation appear in the literature.

A solution based on machine learning improve the ADR by detecting network congestion and thus decides either to wait longer for a downlink or switching to a more robust configuration. Notice that this solution push more complexity to the EDs as it requires them to compute the decision metric, also the NS must periodically broadcast additional data (the learning function weights) to the EDs, thus adding load over the dowlink channel.

Some studies [90, 114, 136] suggest that the ADR_{TTN} (as described in algorithm 2) tends to overestimate the link quality because of the MAX operator used for the *SNR* estimation. As a consequence, they suggest to replace it by a MEAN operator or a MIN operator. But because the frames with lowest *SNR* are likely to be more censored, the current PL estimation might be biased by MIN, MEAN and MAX. Moreover, the *SNR* variance has a major influence on the ADR's operation [114]. We think that the real matter is to understand how the used metric will be biased to take informed decision on the best configuration. In that sense, the *SNR* distribution pattern and parameters estimation as described in chapter 4 and chapter 6 are key for optimized ADR decisions.

The ADR can be slow to converge, especially decreasing to more robust and lower data rate, because it relies on EDs to drift toward more robust configuration until a downlink is received [110, 145]. For the same reason, the ADR does not converge to the same final configuration depending on its starting configuration. Thus we think the ADR should not be based solely on this drift to switch to a more robust configuration.

In a previous work [142], we improved the ADR protocol by relying on the characterization of the channel as a Rayleigh channel and the use of an application layer ECC algorithm. This solution is only tailored for a single cell LoRaWAN network, which is a major weakness for dense deployments composed of few to many gateways.

The ADR algorithm can be extended as a load-balancing algorithm to maximize the overall throughput on a single cell LoRaWAN network [109]. However, this may come at the cost of decreasing the network's reliability. A load-balancing algorithm in the ADR can also aim to minimize the overall energy consumption [149]. A load-balancing algorithm can balances the channel load in each *SF* virtual sub-channel which reduces the overall collisions in a single cell network [104], and can be extended to P_{Tx} allocation to reduce near-far problems in the network [100].

A study proposed a simple way to extend the solution to multiple GWs by virtually associating each ED to the GWs with best P_{Rx}, thus reducing the problem to the single GW case [129]. However this solution do not fully exploit gains from macro-diversity. Also, variations of the P_{Rx} due to SSF might cause excessive re-calculation of both GW-ED pairing and *SF* affectations. Another multi-GWs solutions consists in mitigating the TOA pressure globally over the network [108]. In a nutshell, the idea is to change the *SF* of the "stressing" EDs, i.e. EDs that cause congestion to the most GW while they could maintain connectivity using another *SF*.

Notice that these solutions come at the expense of an increased TOA, and thus energy consumption, for some nodes that are set to use higher *SF* than required in order to reduce the collision rate. The ADR algorithm can be set to balance this energy consumption overhead and maximize the network lifetime [146].

An algorithm to select adequate LoRa transmissions parameters to achieve a given reliability between one transmitter and one receiver while reducing energy consumption has been proposed [86]. It starts from the most robust setting and evolves towards a satisfactory setting after the transmission of a few hundreds probes while temporal dynamics is handled by regular restarts. All of this makes it impractically slow.

3.3 Error Correction Code (ECC) in LoRaWAN

Digital communications and especially wireless communications have been using ECC for decades, either at the physical layer (intra-frame) or at the data link layer (cross-packet). In order to match the various requirements of the applications (error/erasure correction capacity, computation/memory constraints), or to match the nature of the channel model (Gaussian noise, burst error, frame loss, byte error,...) various ECC have been developed and deployed, as listed for instance in Table 3.4.

As detailed in sec.2.2.1, LoRa uses intra-frame ECC which improves the demodulation performance. However, in this thesis we focus on CP-ECC to improve the quality of service of LoRaWAN network and intra-frame ECC is out of the scope.

Cross-frame ECC has been used for instance by Y.Birk et al. in satellite communication: a Reed-Solomon code [15] with feedback is used to sharply increase the attainable throughput of a multi-channel ALOHA network under delay and reliability constraints[7].

However, there are seldom works related to CP-ECC for LPWAN.

The Channel Coding Adaptive Redundancy Rate (CCARR) scheme is an example of CP-ECC [106]. CCARR uses Reed-Solomon coding to implement CP-ECC at the application layer of LoRaWAN. CCARR sharply boosts the acceptable *PER* while reducing the channel load by dynamically tuning the effective coding rate. But CCARR relies on periodic downlinks which should be kept as rare as possible in the LoRa context, as discussed in sec.3.2.1. Chen et al. proposed a similar approach but based on fountain code [139]. Notice that as the code used is not a systematic code, and so *DER* might exceed the *PER* if no enough packets are delivered (highly congested network for instance).

Marcelis et al. proposed a scheme, called DaRe, to reduce the *PER* through CP-ECC [96]. DaRe computes redundancy over the application data with an LDPC-like code (linear combination of a pseudo-random subset of previous frames) and it doesn't require any additional downlinks. Even though their result shows a reliability improvement, but the gain is unclear as there are inconsistencies between their analytic and simulation results. However it is expected to achieve low *DER* with rather low overload if the coding rate matches well the channel state, i.e. the *PER*. Thus, such channel coding should be included in the ADR in order to run in favorable conditions. Similarly to them, our solution *LoRa Fragmentation and FEC (LoRaFFEC)* uses LDPC-like encoding, without downlink communication [141]. It combines error correcting with a fragmentation mechanism, thus addressing the varying payload length issues of LoRaWAN. This allows to solve two issues while offering a solution which is appropriate given the diversity of transmission parameters of LoRaWAN.

Table 3.4: ECC usage in various networking technologies.

Technology	ECC description
UMTS 3G	Turbo code [20]
GSM 2G	Convolutional code [17]
DVB-S2	Low-Density Parity-Check (LDPC) [16]

Montejo-Sanchez et al. proposed a scheme with linear combination of previous frames with less timing diversity (frames are XORed two by two) and thus lower delay for data delivery [112]. They compare the performances of piggybacked redundant messages against performances of redundant messages included in independent frames and show that with their coding scheme independent redundancy perform better as long as protocol overhead is not prohibitive. Souza Sant'Ana et al. extended the solution use both coded and uncoded replicas which both increase the network capacity and battery lifetime [151].

Borkotoky et al. use a similar LDPC-like encoding along side piggybacked repetition and propose a protocol which uses periodic feedback to adapt dynamically the data to be included in the redundant symbols [138]. However, the proposed protocol requires many additive downlink which make it impractical with regard to the LoRaWAN downlink capacity.

3.4 Chapter Conclusion

Several lessons can be learned from this chapter:

First of all, we must underline the relevance of carrying out studies based on experimental measurement campaigns in the field. Indeed, using the same hardware that will be used by the deployed networks, in the real environment and context is of major importance. The variety of deployment and experimental context, and the variety of obtained results attest of this. For instance, the maximum range obtained varies from a few hundred meters to several tens of kilometers, but also the dispersion of the measured received powers is not at all the same from one study to another, from one environment to another, etc ... Thus carrying out experiential field measurement campaigns over real LoRaWAN deployments makes it possible to be as close as possible to the real mode of operation and therefore to the performances. In addition, this experimental approach with real LoRaWAN hardware which is inexpensive and easy to deploy, allows massive amounts of experimental data to be gathered.

But the consequences of measuring performance in this way must be considered. The equipment used is therefore designed as communication devices and not measurement devices. The difference which may at first seem trivial is in fact determinant here Indeed, the measurements must be taken with a critical viewpoint: the hardware is not necessarily calibrated to provide precise measurements, the hardware does not necessarily have a sufficient measurement dynamic allowing them to correctly record the real values especially the "extreme" values. The analytical processing of the collected data must take into account these potential biases to avoid drawing unfounded conclusions.

The capacity of a LoRaWAN network cannot be dissociated from the transmission configuration of the EDs. Improper use and distribution of EDs' transmission parameters causes network capacity to collapse. Indeed with the most pessimistic assumptions and with the worst parameterization of the EDs, the capacity of the network is reduced to only a few hundred EDs per cell. However, with a more relevant setting - even basic - especially a balanced distribution of *SF* used, increases

the capacity to thousands of EDs per cell. This observation underlines the need for an efficient automatic parameterization mechanism in LoRaWAN, i.e? an optimized and efficient ADR.

Chapter 4

LoRaWAN Link Characterization

Contents

Chapter Introduction

In this chapter we characterize the LoRaWAN link, i.e. the raw LoRa channel and the performance of BSR which is the repetition mechanism of the LoRaWAN MAC layer. To this intent, we carried out campaigns to collect experimental measurements described in sec.4.1. Then we analyze them, in the light on what we have learned and commented in the state of the art chapter, and also with in mind our objective which is to optimize LoRaWAN for high reliability.

4.1 Setup and Experiments

We have gathered an experimental dataset by recording LoRaWAN transmissions collected by several GWs in an urban area.

The test-bench consists of one ED[1], placed indoors on the third floor of a residential building, sending traffic to the TTN community network through a set of GWs. The ED transmits series of LoRaWAN frames and randomly varies the transmission parameters from one frame to the next. The transmission parameters are randomized in order to avoid shadow correlations and moderate the effect of possibly congested CFs.

We present in this thesis the results from two measurements sessions. In both cases, we used three *CF* centered on 868.1, 868.3 and 868.5 MHz, with *BW*=125kHz.

In the first session, we considered 48 combinations of (P_{Tx}, *SF*) value pairs. We set the LoRaWAN intra-frame ECC*CR* to the default *CR*=$\frac{4}{5}$. The PL was 15 Bytes resulting in LoRa frames with a number of symbols per frame (N_s) from 38 to 53. The experiment ran for a whole week and there were on average 4300 frames transmission attempts per series, i.e. one frame every ≈ 2.4 minutes.

In the second experiment we extended the possible configurations to many more (P_{Tx}, *SF*, *CR*) combinations with a payload such that $48 \leq N_s \leq 50$. We also extended the possible configurations for *SF* =7 with $CR \in \{\frac{4}{5}; \frac{4}{6}; \frac{4}{7}; \frac{4}{8}\}$ and with 10 different frame sizes: $48 \leq N_s \leq 298$ [2]. 336 transmission parameters configurations are thus tested. The experiment ran for twelves days and the dataset includes on average 940 frames transmissions attempts per series, i.e. one frame every ≈ 20 minutes.

Table 4.1 summarizes the choice of experimental configurations.

Table 4.1: Transmissions configurations used in the experiments

	P_{Tx} (dBm)	*SF*	*CR*	N_s
XP1	{0;2;4;6;8;10;12;14}	[7..12]	$\frac{4}{5}$	{38;43;48;53} (15 Bytes PL)
XP2	{0;2;4;6;8;10;12;14}	7	$\{\frac{4}{5}; \frac{4}{6}; \frac{4}{7}; \frac{4}{8}\}$	50
		7	$\{\frac{4}{5}; \frac{4}{8}\}$	{80;98;128;178;200;224;248;280;298}
		[8..12]	$\frac{4}{5}$	50

Twelve and thirteen TTN GWs showed up within the transmission range of the ED during respectively the first and the second experiment. Among them, 8 were up for both experiments. Fifteen are GWs deployed in the Grenoble urban area within 5 km of the ED. Two GWs are outside the city

[1] B-L072Z-LRWAN1 LoRa®/Sigfox™ Discovery kit.

[2] Notice that because each *SF* does not encode the same amount of bits and because the intra-frame ECC add redundant Bytes to the payload in a non continuous manner, some value of N_s might not be feasible with some transmissions parameters combination. Frame with up to 2 less symbols are then used.

at 6km and 14km from the ED with respectively 1000m and 2000m higher elevation from the city. We could not retrieve the position of one of the GWs.

Fig. 4.1 shows the position of the GWs in red and their distance from the ED (in yellow).

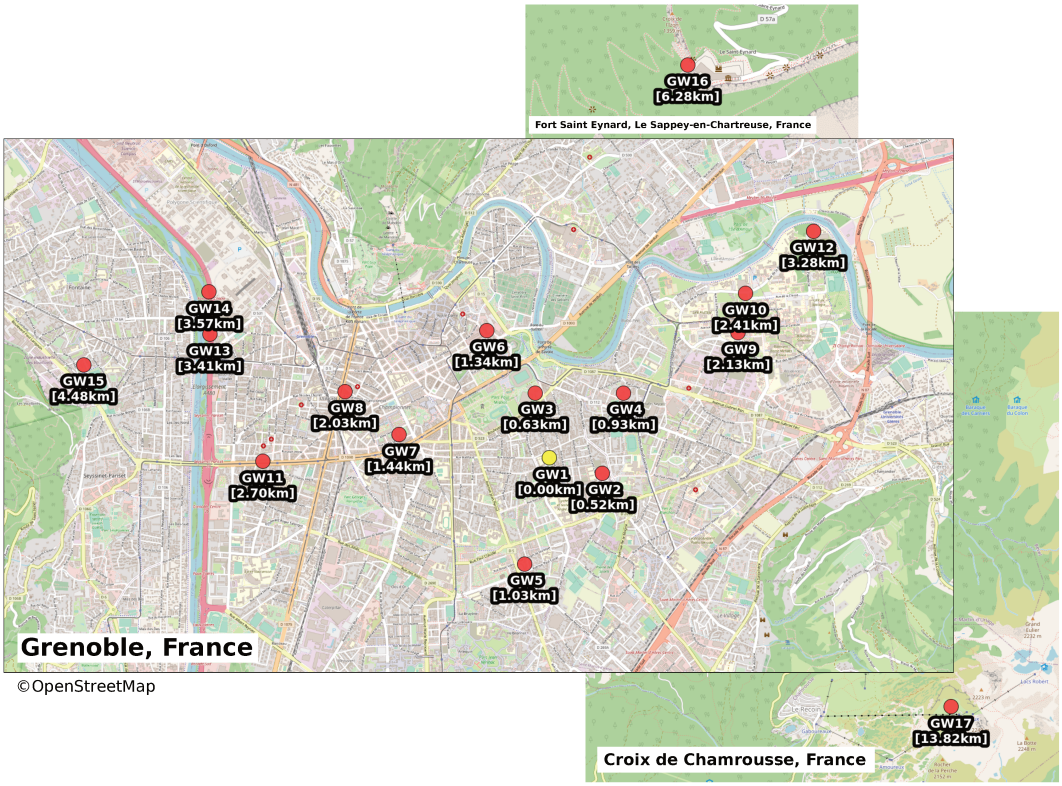

Figure 4.1: Experimental Setup

We reject from the data set the series with *FER* >0.99. In these cases, the transmission is not robust enough and only residual frames are received. The valid data represents a total of 2319 independent LoRaWAN series of frames.

This set of measures captures the frame erasure patterns over a typical LoRaWAN urban network, and it is publicly available[3].

4.2 Rayleigh Channel Behavior

For all GWs, our experiments show that the *SNR* distribution roughly follows a quasi-static Rayleigh channel exponential distribution. This distribution is expected in our setup in which there is no Line-of-Sight (LoS) and thus the propagation is likely to be highly multi-path, with no dominant path. The *SNR* over a Rayleigh channel follows an exponential distribution with cumulative distribution function $CDF_{\exp}(x) = 1 - e^{-x}$ (and its reciprocal $CDF^{-1}_{\exp}(x) = -\log(1-x)$), multiplied by a factor $\overline{SNR}$ corresponding to the *SNR* mean, i.e. the gain factor from the unit mean exponential distribution. Fig. 4.2 shows the *SNR* distribution for several GWs and several P_{Tx}. Theoretical *SNR* distributions over a Rayleigh channel appears in red in Fig. 4.2, with manually fitted gain shifts. The histogram does not follow perfectly the exponential distribution, more precisely it is truncated of its left tail (the lower values). It is because as we reduce P_{Tx}, the *SNR* distribution translates to the left, towards lower values. Thus, more and more frames fail to meet the GW sensitivity, i.e. more frames have *SNR* below demodulation floor (*Df*). The typical

[3] `https://gricad-gitlab.univ-grenoble-alpes.fr/coutaudu/lora-measurements`.

sensitivity for each considered *SF* according to the documentation [168] is marked by an arrow in Fig. 4.2. Below this point, most of the frames are lost, resulting in a progressively more and more censored sample as P_{Tx} decreases. It is important to note that because of this censoring of the lower *SNR* frames, the $\overline{SNR}$ is biased compared to the one which would include the lost frames and their below *Df* SNRs.

Besides, notice that there is an artifact at 0 dB due to a bad interpretation of some frames by the hardware monitoring system, which wrongly marks them with a 0 value and it is not possible to distinguish them from the frames received with an actual 0 dB *SNR*.

Assuming that the channel is quasi-static Rayleigh, and that meeting *Df* is necessary and sufficient for successful reception (thus in absence of collision) *FER* is:

$$FER = CDF_{\mathrm{exp}}(10^{\left(\frac{Df-\overline{SNR}}{10}\right)}) \tag{4.1}$$

with $\overline{SNR}$ and *Df* both in dB. Obviously, any of these three parameters can be obtained from the two others:

$$Df - \overline{SNR} = (10 \times \log_{10}(-\ln(1-FER))) \tag{4.2}$$

Theses relations capture the erasures from fading. However, notice that collisions in a loaded network would introduce an additional bias.

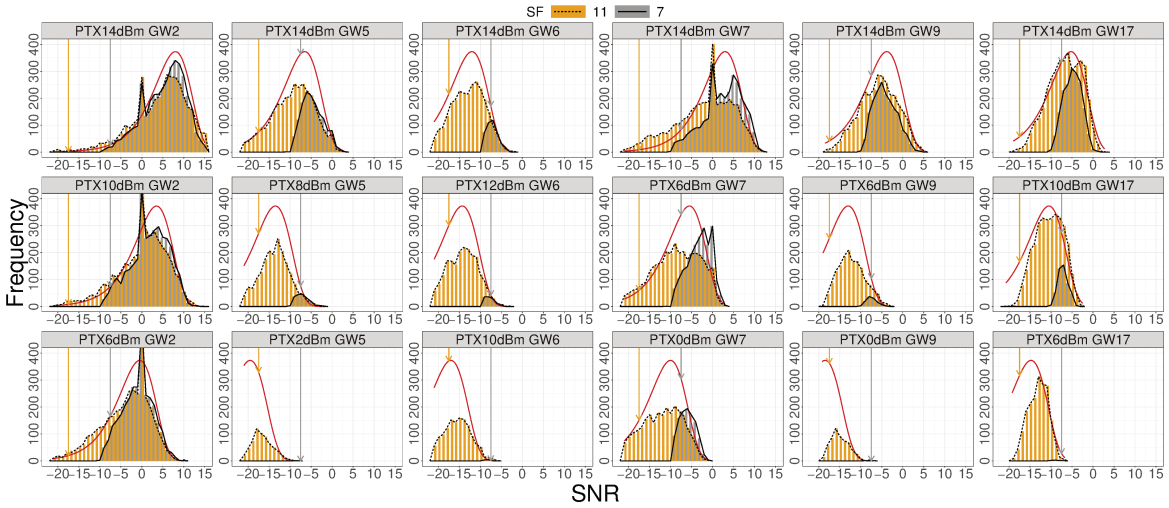

Figure 4.2: Distribution of the measured *SNR* of several LoRaWAN series of frames with *SF* 11 and 7, compared to an exponential distribution curve in red (manually centered), for several P_{Tx}. Yellow and black arrows mark each *SF* 11 and 7 *Df*[4].

4.3 Impact of LoRa Intra-Frame ECC

LoRaWAN uses an intra-frame ECC derived from the Hamming code. A couple of studies using reverse engineering and analysis offer a glimpse of the algorithm and its performance[135, 152]. These studies predict error detection only capabilities for $CR \in \{\frac{4}{5}, \frac{4}{6}\}$ and then more and more error correction for $CR \in \{\frac{4}{7}, \frac{4}{8}\}$. As shown in Fig. 4.3 for relevant series of frames, our measurements do not corroborate these findings as we do observe a reliability gain for $CR = \frac{4}{6}$ compared to $CR = \frac{4}{5}$.

[4] Typical values from the documentation [168].

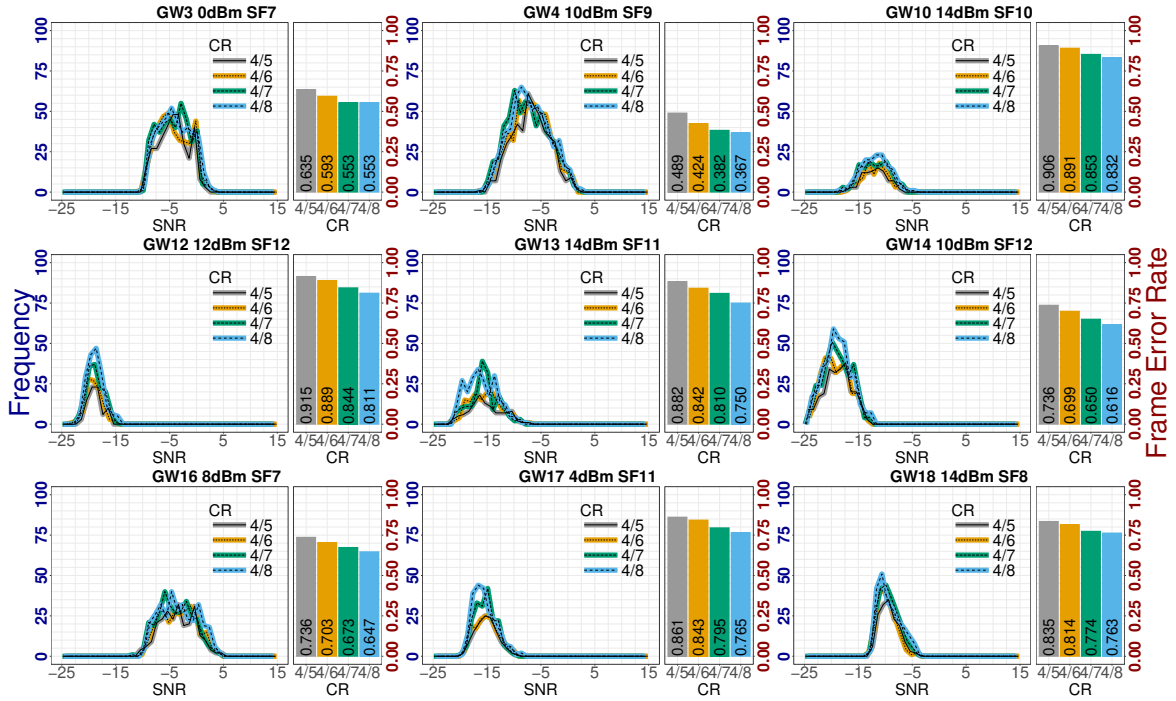

Figure 4.3: Distribution of the measured *SNR* and *FER* as a function of the *CR* for selected series of frames.

To quantify this reliability gain, we find the *Df* difference ΔDf between a reference configuration ($CR = \frac{4}{5}$) and other configurations ($CR \in \{\frac{4}{6}, \frac{4}{7}, \frac{4}{8}\}$), all other transmissions parameters (*SF*, P_{Tx}, N_s) being equal. Assuming that all losses are due to a received *SNR* below D_{frame}, and thus due to the *SNR* variations around its mean value, we estimate $\left(Df - \overline{SNR}\right)_{\text{ref}}$ the margin between *Df* and $\overline{SNR}$ for the reference configuration by applying Eq.4.2 to FER_{ref}.

$$\left(Df - \overline{SNR}\right)_{\text{ref}} = (10 \times \log_{10}(-\ln(1 - FER_{\text{ref}}))) \tag{4.3}$$

Using Eq.4.1 we can calculate the estimated $\widehat{FER}$ obtained by considering that *Df* is improved (i.e., shifted to the left) by ΔDf (in dB).

$$\widehat{FER} = CDF_{\text{exp}}(10^{\left(\frac{\left(Df - \overline{SNR}\right)_{\text{ref}} + \Delta Df}{10}\right)}) \tag{4.4}$$

Finally, we find the ΔDf value for which $\widehat{FER}$ fits the experimental *FER*, FER_{XP} . We find the adequate ΔDf value using the Ordinary Least Square (OLS) method which consists in minimizing $\chi^2(\Delta Df) = \sum (\widehat{FER} - FER_{\text{XP}})^2$.

Fig. 4.4 shows FER_{ref} and FER_{XP} for each *CR*. The black curves show the fitted reliability gain $\Delta\widehat{FER} = FER_{\text{ref}} - FER_{\text{XP}}$ for the fitted ΔDf. The experimental *FER* gain ΔFER_{XP} distributions matches the shape of the theoretical *FER* gain distributions induced by sensitivity gains -0.40 dB, -0.88 dB, -1.21 dB for respectively *CR* $\frac{4}{6}$, $\frac{4}{7}$ and $\frac{4}{8}$.

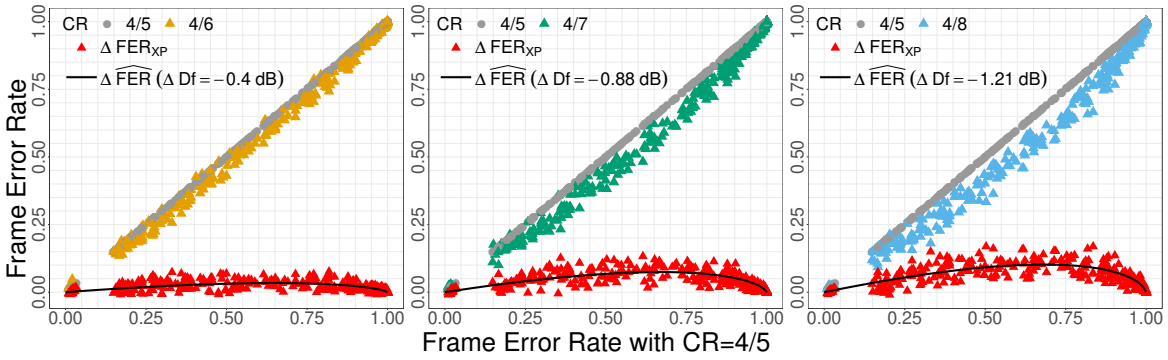

Figure 4.4: Comparison of the *FER* with $CR = \frac{4}{5}$ against $CR = \frac{4}{6}$, $CR = \frac{4}{7}$ and $CR = \frac{4}{8}$. The black curve is the computed *FER* gain expected for sensitivity gain over a Rayleigh channel.

4.4 Impact of the Frame Length

Frame length is expected to have a minor impact on successful reception because the latter depends on successful initial synchronization [121]. Still, our experimental measurements show a noticeable impact of frame length on the *FER*. To assess the magnitude of this effect, we gather measurements for diverse frame lengths using $SF = 7$, in Fig. 4.5. It shows the *SNR* distribution for frames of various lengths $N_s \in \{48, 128, 298\}$ and the *FER* for various[5] values of $N_s \in [48..298]$.

Reliability clearly decreases as N_s increases. Up to 20 percentage points of *FER* can be lost between the shortest and longest frames.

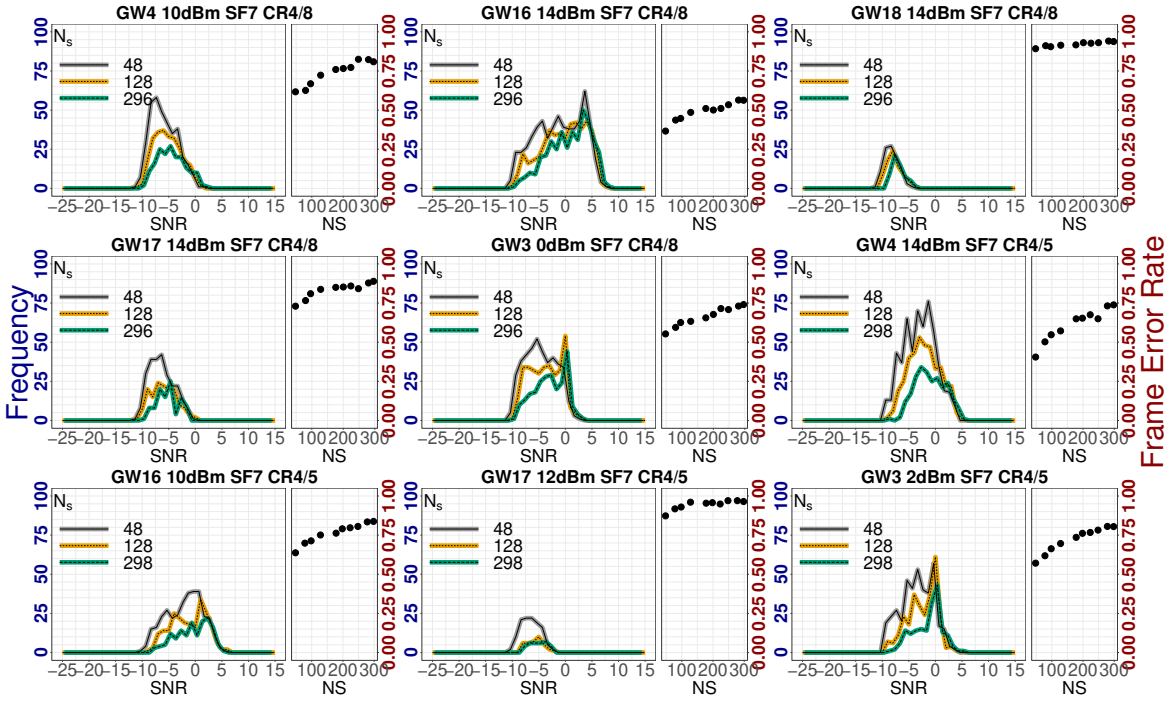

Figure 4.5: Distribution of the measured *SNR* and *FER* as a function of the number of symbols per frame (N_s) for selected series of frames.

In Fig. 4.6, we compare again the experimental *FER* difference ΔFER_{Exp} and the expected *FER* difference $\Delta\widehat{FER}(\Delta Df)$. using the same methodology as in Sec. 4.3, using the configuration with N_s =298 as reference. The OLS fit results are given in Tab.4.2. With our experimental setup, reducing

[5] In particular 48 and 298 that are key values to compare precisely between different *SF* and *CR*.

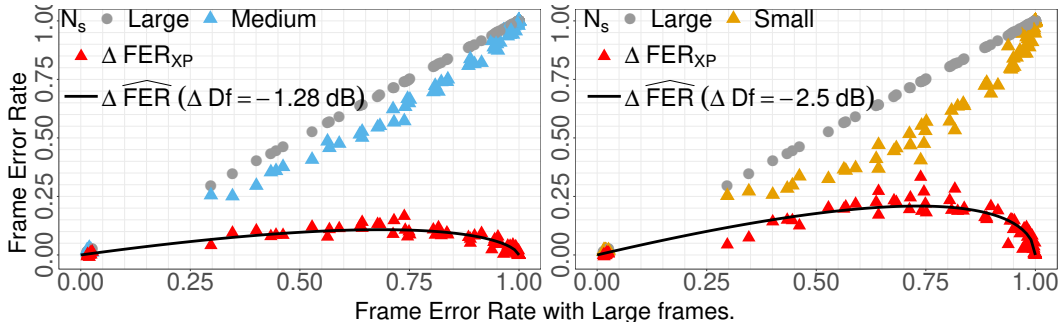

Figure 4.6: Comparison of the *FER* with $N_s = 48$ (Small) and $N_s = 128$ (Medium) against $N_s \in [296..298]$ (Large). The black curve is the computed *FER* gain expected for sensitivity gain over a Rayleigh channel.

N_s	48	[78..80]	[96..98]	128	[17..178]	200	[223..224]	248	[278..280]	[296..298]
ΔDf (dB)	-2.50	-1.93	-1.74	-1.28	-0.85	-0.70	-0.48	-0.39	-0.11	0
χ^2 ($\times 10^{-4}$)	8.844	4.903	3.673	2.366	2.018	1.693	1.393	2.056	0.949	0
Frame Length Ratio	0.16	0.27	0.33	0.43	0.6	0.96	0.75	0.83	0.94	1

Table 4.2: Ordinary Least Square (OLS) values of the ΔDf gains for various frame lengths compared to $N_s \in [296..298]$.

frame length from $N_s \in [296..298]$ to $N_s = 128$ and $N_s = 48$ produces a sensitivity gain of respectively -1.28 dB and -2.5 dB.

However, one must keep in mind that the sensitivity gain from a reduced physical frame length comes at the expense of an increased protocol overhead. Indeed the preamble and protocol header lengths are fixed and only the application payload is reduced. Thus, with a "small" application payload, most of the TOA is spent in the physical preamble and protocol header. For instance, with $SF = 7$, $CR = \frac{4}{5}$ and $BW = 125$kHz, a frame with $N_s = 50$ encapsulates a 13 bytes applicative payload with $TOA/b = 0.59$ ms, whereas with $N_s = 298$ it encapsulates a 188 bytes applicative payload with $TOA/b = 0.21$ ms, i.e. 2.8 times lower. We illustrate this in Fig. 4.7 which plots the *ToA/b* against the applicative payload from 1 to 250 bytes. Notice that the effective *ToA/b* for a 30 bytes applicative payload with $SF = 7$ is equivalent to the one for a 250 bytes applicative payload with $SF = 8$.

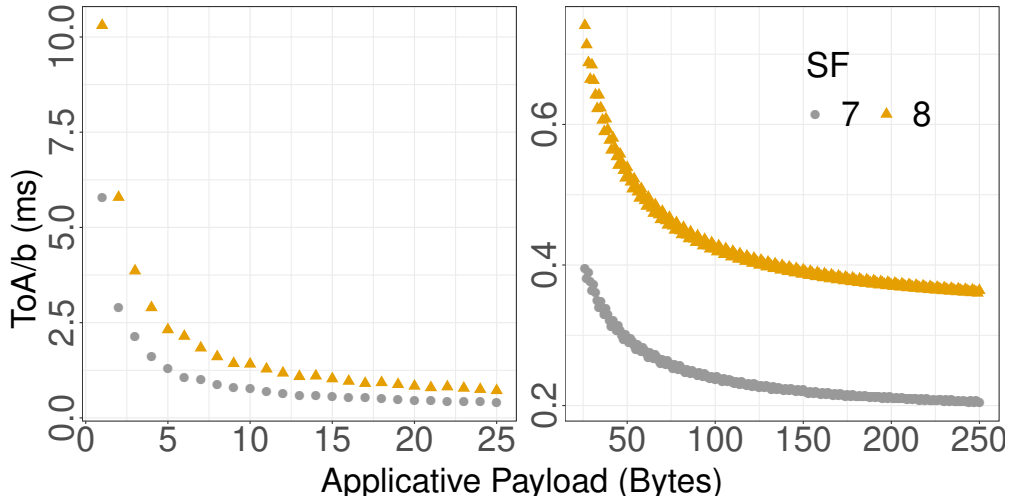

Figure 4.7: *ToA/b* as a function of the application data payload length for *SF* 7 and 8 with *BW*=125kHz and *CR*=$\frac{4}{5}$

4.5 Channel Burstiness Behavior

Another crucial point from the perspective of providing reliable communication is erasures burstiness. We compare in Fig. 4.8 the proportion of frames lost in erasure bursts in a simulated channel with independent and identically distributed (iid) losses vs. in our experimental data. The experimental data erasure patterns are close enough to be approximated in the following as an iid erasure channel.

However, even though the erasure distribution is iid, it does not prevent the loss of multiple frames in a row, as illustrated by the length of erasure bursts plotted in Fig. 4.9. Moreover, this length increases with the *FER*. Even over a channel with reasonable *FER* (< 0.3), a significant proportion of the lost frames comes from erasures bursts (length ≥ 2).

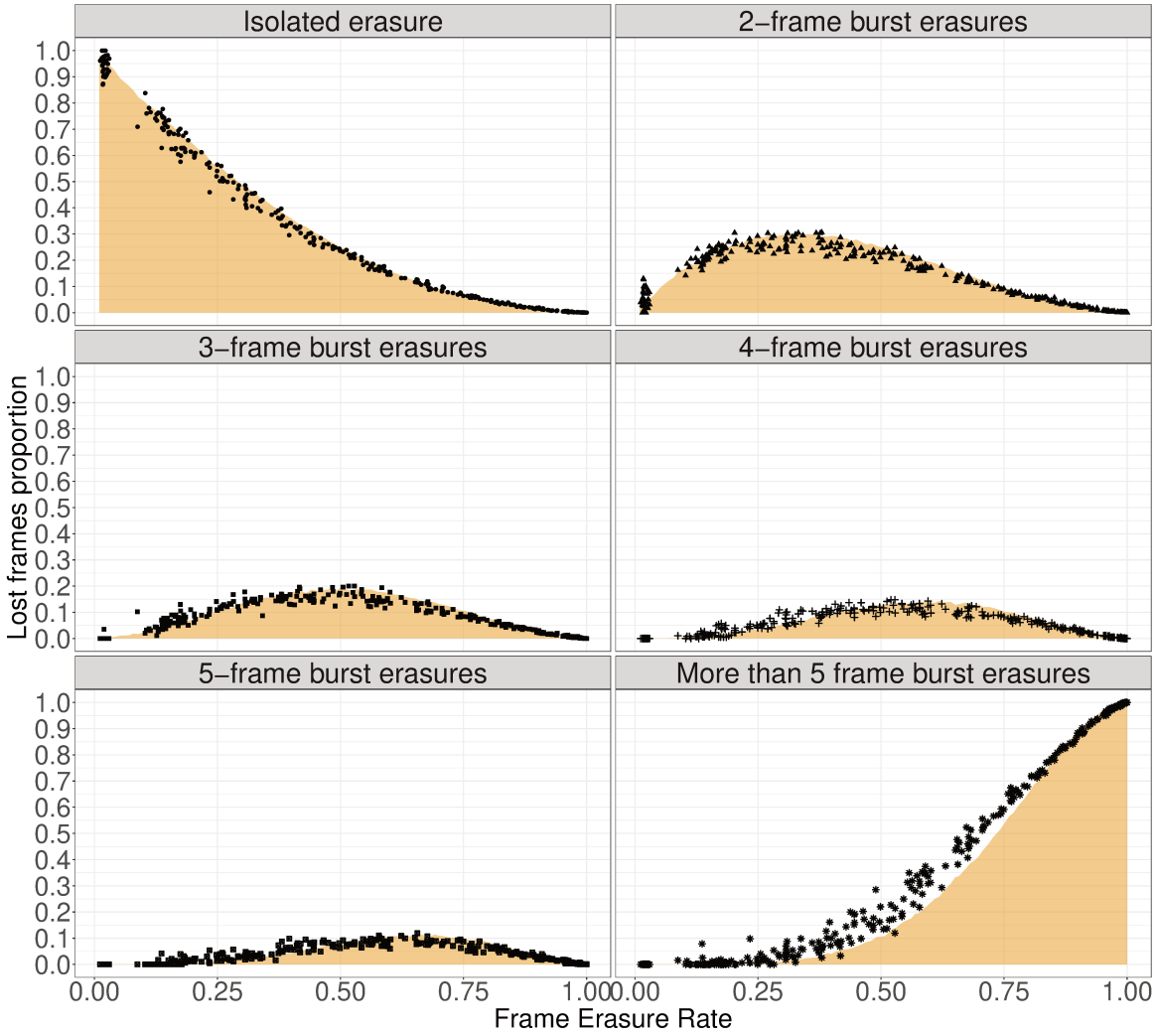

Figure 4.8: Dots marks the experimental proportion of frames lost in bursts of various sizes. The colored areas correspond to a simulated independent and identically distributed (iid) channel.

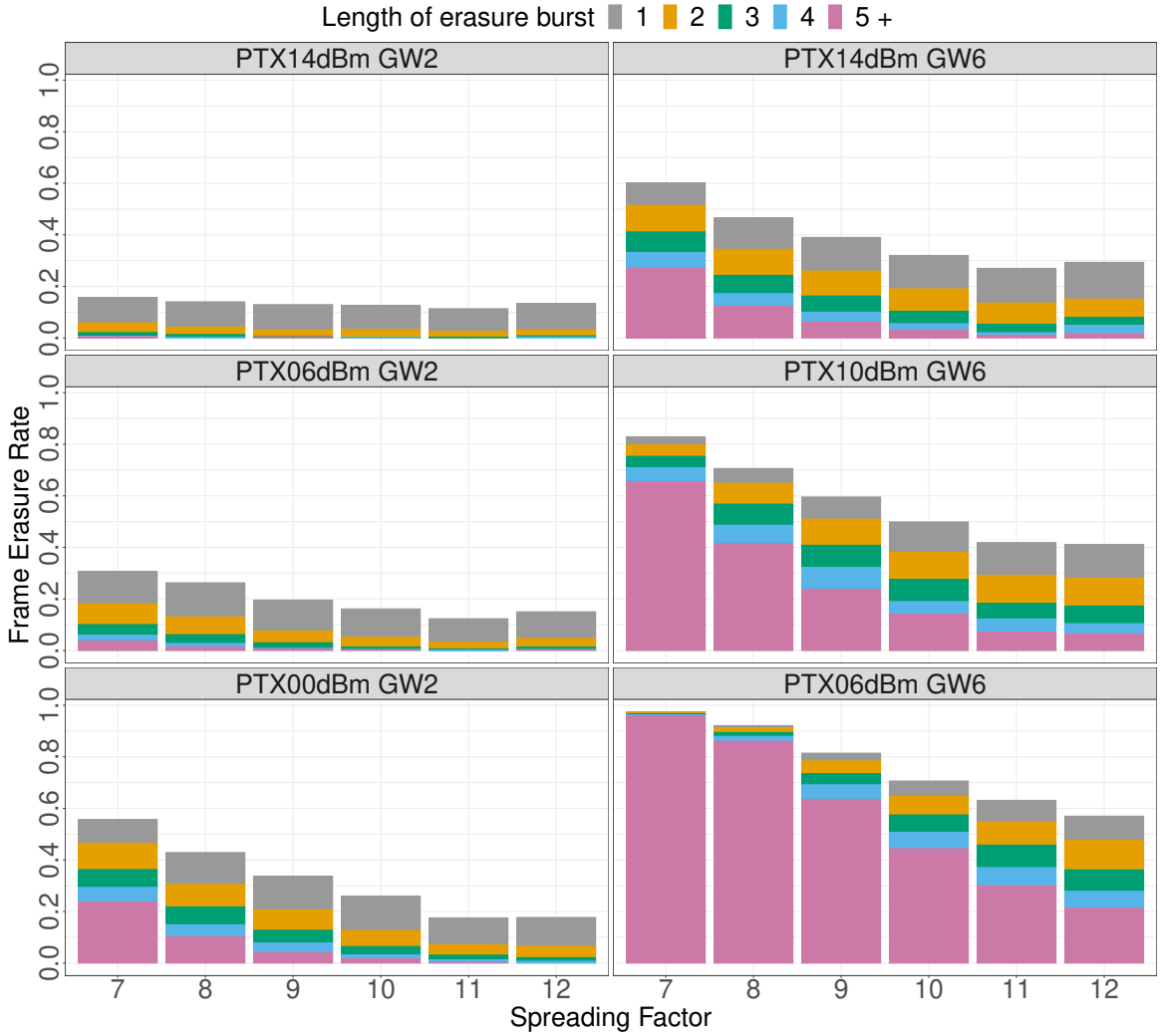

Figure 4.9: FER against SF showing the distribution of erasure burst lengths for several LoRaWAN series of frames with two GWs and several P_{Tx}.

4.6 Performance of LoRaWAN BSR

The BSR mechanism implemented by the LoRaWAN MAC layer parameter Nb_{Trans}, can be seen as the simplest kind of CP-ECC. The redundancy is a duplicate of the original frame, transmitted successively, thus it is weak against burst losses. However, although the channel erasures are close to iid, the probability to loose multiple frames in a row mechanically increases with the *FER*. For instance, over a *FER* =0.25 iid erasures channel around 15% of the lost frames are lost in burst of length≥ 3.

We use our real-world experimental measurement series to emulate BSR in order to better understand its limits and assess its performance. By replaying our experimental data set, we emulated the MAC layer parameter Nb_{Trans} over our experimental data and the results are illustrated in Fig. 4.10 with the *PER* as a function of the *FER* for various Nb_{Trans}. LoRaWAN BSR indeed provides important reliability improvement: $Nb_{\text{Trans}} = 2$ reduces *PER* by more than 20 percentage points over a channel with *FER* =0.5. Increasing Nb_{Trans} from 2 to 4 reduces *PER* by around 20 percentage points over a channel with *FER* =0.65. Nb_{Trans} can be increased to reduce the *PER* without changing the *SF* and with no decoding latency. However, even with Nb_{Trans} as high as 32, residual erasures appear over a channel with $FER > 0.7$. As expected, with the *FER* increase, BSR quickly fails to provide high reliability as it is weak against burst erasures and residual erasures are left uncovered. Moreover it becomes impractical due to its tremendous channel occupation overhead.

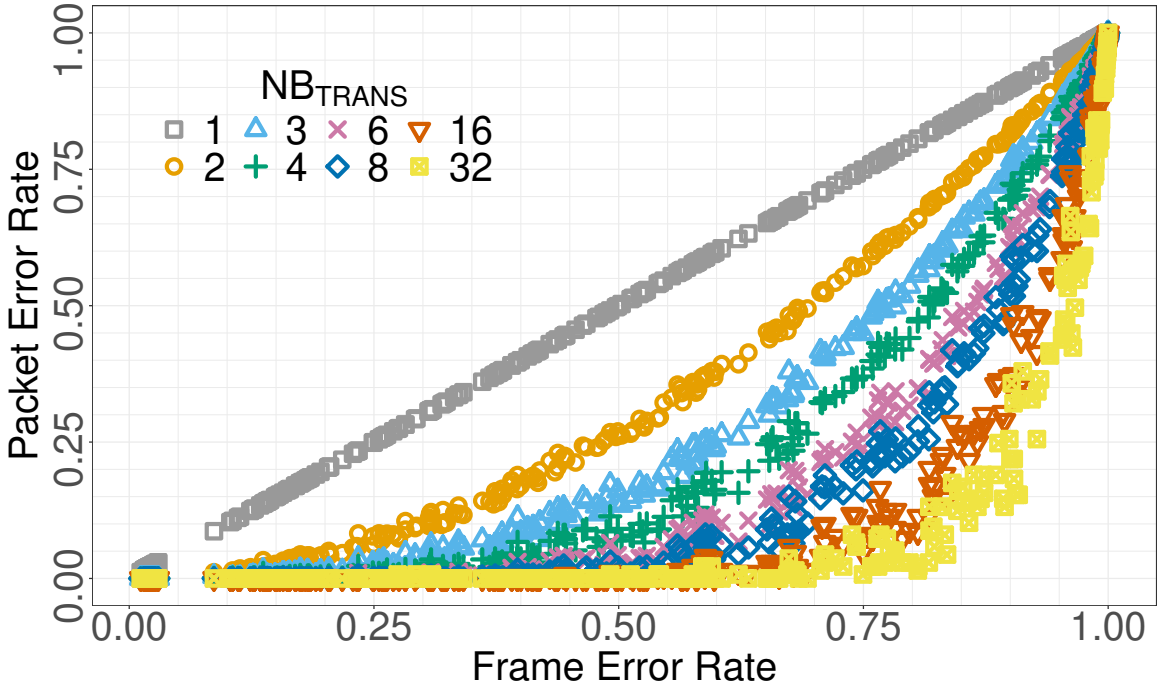

Figure 4.10: Experimental *PER* as a function of *FER* using BSR with various Nb_{Trans} values.

4.7 Additional Remarks

LoRaWAN communication is often confronted to a *FER* floor

In our experimental measurements, the $\overline{SNR}$ increases as we increase the P_{Tx} and this in turn reduce the *FER*. Such behavior is expected. However, for many of our experimental series, the *FER* decreases until it reaches a floor which depends on the GW. For instance this ceiling is $FER \approx 0.15$ for GW $\{2,5\}$ and is apparent for instance for GW2 in Fig.4.11. Hence, the reception has typically a

floor around $FER = 0.12$ for most GWs.

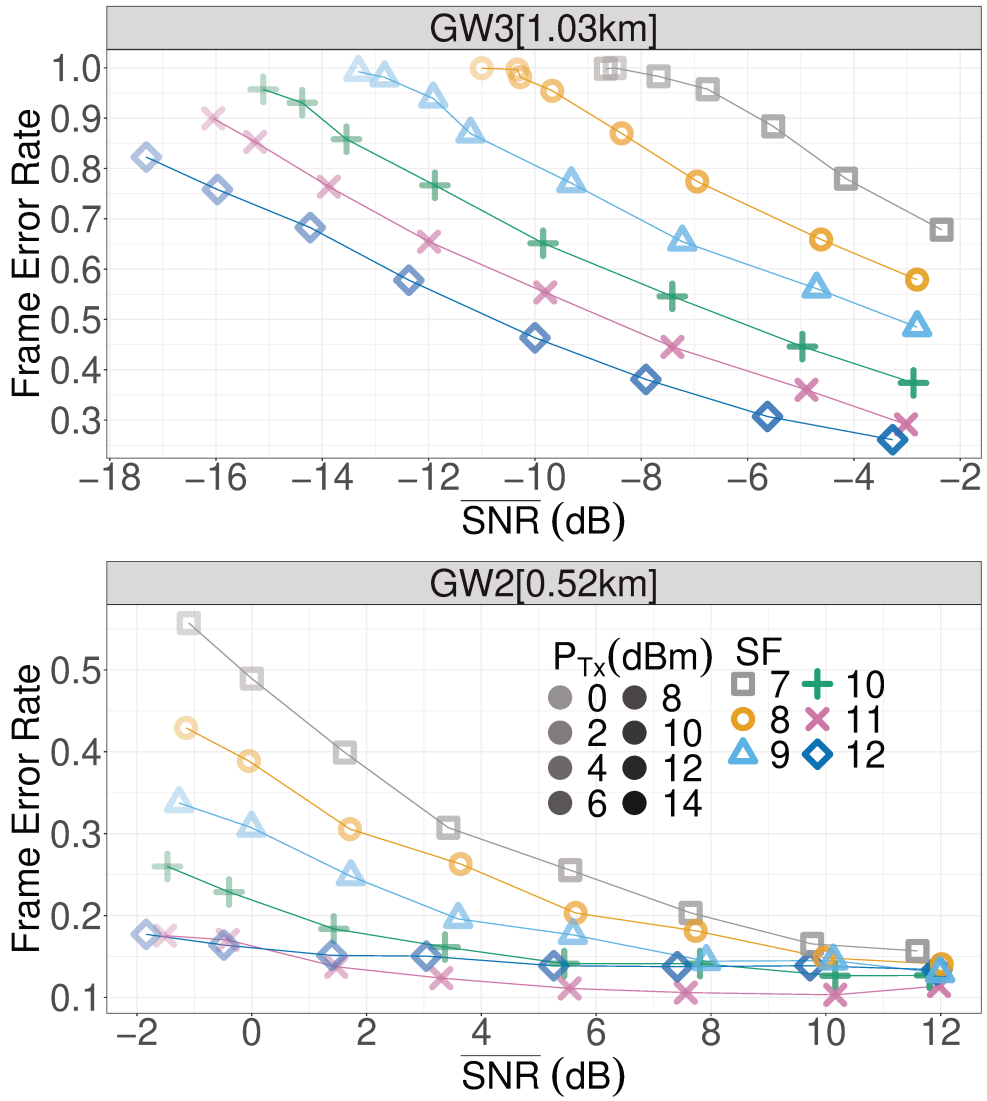

Figure 4.11: Experimental *FER* as a function of $\overline{SNR}$ for GW2 and GW3 in XP1.

Such phenomenon is coherent with a slow Rayleigh channel model. This model is coherent with our test-bench without any LoS between the ED and the GWs resulting in highly multipath propagation. Following this model, P_{Rx} is exponentially distributed [13] with a probability distribution function: $\text{PDF}(P_{\text{Rx}}) = \frac{e^{(-\frac{P_{\text{Rx}}}{B})}}{B}$ where B is the average P_{Rx}. As a consequence, over such a Rayleigh fading channel, a significant fraction of transmission faces very challenging conditions.

Higher *SF* does not always reduce *FER*

Most of the time, an higher *SF* results in lower *FER*. This *FER* improvement is the more pronounced when $\overline{SNR}$ is relatively "low" ($\overline{SNR} \leq -2$dB). For instance, in Fig. 4.11, the *FER* of GW3 with P_{Tx} =14 dBm reduces from 0.68 to 26 when switching from *SF* 7 to 12. However, when the P_{Rx} is strong enough, a higher *SF* may not provide a better *FER* and a significant fraction of the frames is lost even when the $\overline{SNR}$ is high. See for instance GW2 in Fig. 4.11 with $\overline{SNR}$ between -2.5 and 12 dB, all *FER* series converge to similar values. We also point the fact that for GW{2}, *SF* 10 and 11 lead to a better *FER* than *SF* 12 for high $\overline{SNR}$. We believe this comes from congestion due to an over-usage of *SF* =12 with frames having a large TOA footprint. Also, GW1, only a few meters from the device, still presents a few percents of residual frame losses even with a very high $\overline{SNR}$.

4.8 Chapter Conclusion

From extensive experimental measurements and analysis with consideration for bias from censored experimental data, we found that the LoRaWAN channel in an urban environment follows a quasi-static Rayleigh channel model. This corresponds to the multi-path propagation of the signal. Thus, the received power corresponds to the LSF multiplied by the ShF (therefore the average received power), then multiplied for each transmission by a new drawing of the SSF which therefore follows a random variable of unit mean exponential distribution.

We also found that frame losses are mutually independents. However, notice that - obviously - this does not prevent multiple frames to be lost in a row when the *FER* is high. Thus LoRaWAN BSR is poorly designed to provide high reliability.

Our experimental data shows that - unlike to what can sometimes be suggested in the literature [135, 149] - each LoRaWAN intra-frame ECC*CR* reduction does improve the modulation robustness.

Chapter 5

Cross-Packet Error Correction Code in LoRaWAN

Contents

Chapter Introduction

The finding that the channel can be modeled as a Rayleigh channel as detailed in Sec. 4.2 is key to understand the challenge to efficiently provide high reliability (DER <0.01) in LoRaWAN. The fact that the distribution of the frames SNR follows an exponential distribution, implies that a fraction of the frames faces a significantly higher path loss than the average. For instance, 10% of the transmissions will face a -9.8 dB SNR from the $\overline{SNR}$. Likewise, respectively 5% and 2% of the frames will face a -12.9 dB and -16.9 dB SNR from the $\overline{SNR}$. As a consequence, either an extremely robust transmission configuration, therefore over-robust most of the time, is used to received those few "very low SNR" frames, either the communication protocol faces this "erasure floor". The solutions based on acknowledgement frames, such as ARQ, are strongly limited by the asymmetry of LoRaWAN networks where downlink transmission opportunities are scarce [99]. As expressed in sec.4.6, the LoRaWAN BSR mechanism is weak to provide high reliability and has a tremendous channel occupation cost. In this chapter we present two CP-ECC protocols for high reliability in LoRaWAN. By introducing more time diversity in the communication, more elaborate CP-ECC can provide high reliability at a lower cost [96, 106]. In this chapter we propose two overlay protocols using CP-ECC which ,transparently for both the application and the LoRaWAN protocol, recover the losses and provide high reliability in LoRaWAN.

5.1 Channel Coding Adaptive Redundancy Rate (CCARR)

With the aim of providing high reliability ($PER < 0.01$)) while maintaining the ED TOA as low as possible, we propose in the following CCARR, a protocol that uses Reed-Solomon based CP-ECC and scarse completion acknowledgments.

5.1.1 CCARR Algorithm

With CCARR (n,m), the information to be sent is gathered in a $(n+m)$ frames long segment where each frame has l bytes length. The first n frames contain application data and the following m frames contain redundant data. The redundant frames are build from a RS-code computed vertically over the preceding frames as shown in Fig. 5.1. Notice that n, the maximal amount of redundant frames, is adjustable, for instance to the application requirement, the physical payload needs and also to adjust downlink channel load. The ratio $\frac{n}{n+m}$ is the maximal coding rate of the CCARR instance. We call it CR_{CCARR} to make the distinction with CR from the LoRa native intra-frame ECC.

Algorithm.3 defines the ED side of the CCARR protocol: the CCARR (n,m) protocol sends the frames of the segment one by one. It only starts listening for acknowledgement in the downlink at the n^{th} frame transmission. If no such acknowledgement is received, it then continues sending the following frames of the segment one by one in a sequential manner, until the reception of the segment completion acknowledgement.

Thanks to RS-code properties, the NS will be able to retrieve the whole application data from any n received frames. As described in algorithm 4, CCARR (n,m) only triggers the downlink acknowledgement(s) emission to the ED when it received n frames, i.e. enough to reconstruct the entire segment. Notice that the NS keeps acknowledging when it receives new uplink frames for an already retrieved segment because this means that the previous acknowledgement(s) was(were) lost. In the best case of a loss-free channel, CCARR (n,m) transmits only n uplink data frames and one downlink acknowledgement. And if some frames are lost, CCARR (n,m) keeps transmitting

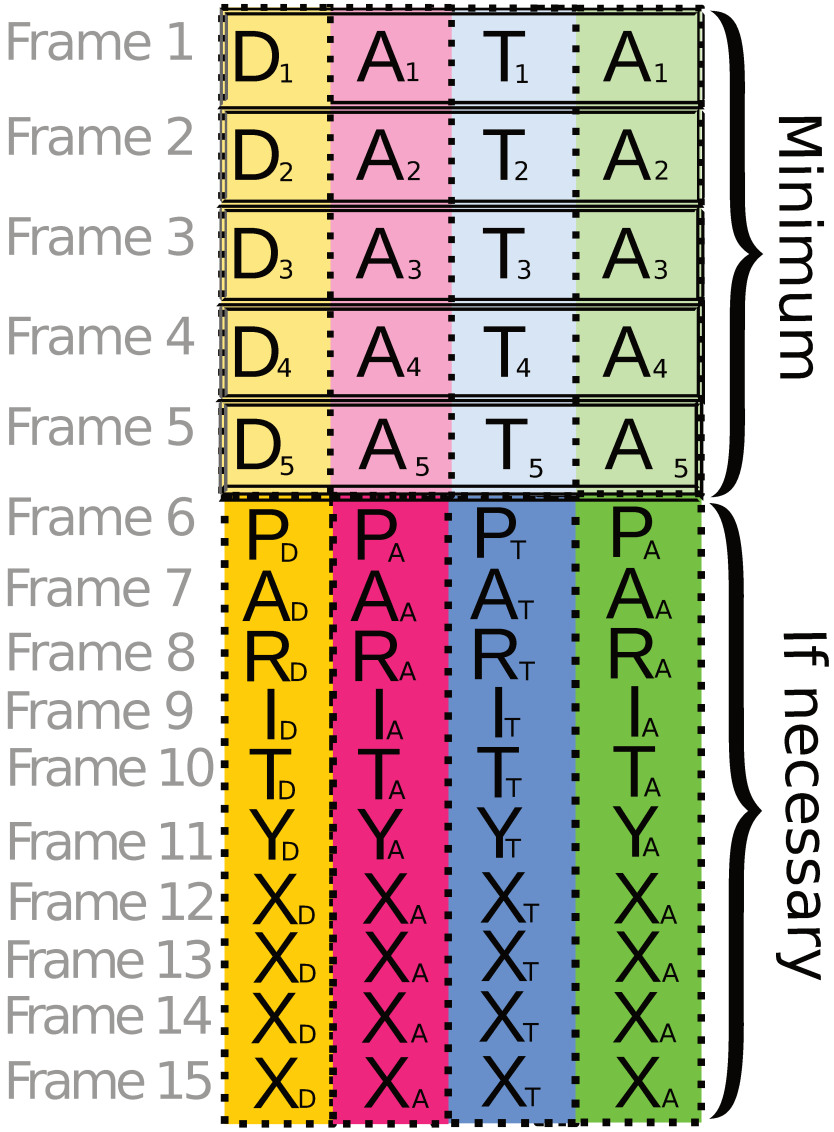

Figure 5.1: Layout of a CCARR ($n = 5; m = 10$) segment with $l = 4$.

frames of the segment until the successful reception of n frames. Thus, the acknowledgement "covers" at least n frames, and more than n successful frames transmissions only happen if acknowledgments are lost. Thus, the number of acknowledgments is divided by up to n compared to the ARQ protocol. This dynamic acknowledgment procedure results in a effective CR_{CCARR} dynamically adapted to the *PER* over the segment.

Compared to ARQ, CCARR reduces the downlink overload: with only segment completion acknowledgments, the downlink need is divided by n the minimum number of frames for successful decoding of the segment.

CCARR does not need estimation or extra feedback of the current channel condition: by design, it continuously adapts its ECC overload until it reaches the decoding floor, intrinsically adapting to the current channel *PER*. Hence, CCARR has a TOA overload inversely proportional to the channel's *PER*. However, the price to pay in CCARR is regular but sparse downlink acknowledgments and extra computing for the encoding by EDs and decoding by the NS. CCARR increases application communication delivery delay which is not a strong requirement for many LPWAN applications, such as metering, while high *PER* is a major concern.

Algorithm 3 CCARR (n, m) segment uplink emission on ED side.

```
f←0;
ack←FALSE;
while (f< n + m) AND (!ack) do
    sendFrame(CurrentFrame);
    f++;
    if (f≥ n) then
        ack ← listenForAck();
    end if
end while
if (f == n + m) AND (!ack) then
    lostSegmentError();
end if
```

Algorithm 4 CCARR (n, m) segment reception treatment on NS side.

```
f← 0;
receiveFrame(currentFrame);
while (currentFrame DIV (n + m)) == currentSegment do
    f++;
    if (f ≥ n) then
        sendAck();
    end if
    receiveFrame(currentFrame);
end while
if (f < n) then
    lostSegmentError();
end if
```

5.1.2 CCARR Probabilistic Analysis

5.1.2.1 Reliability

One can notice that the segment completion acknowledgement is triggered by any n frames receptions over $(n+m)$ sent. Thus, in the analysis with i.i.d. frame losses, this results in a cumulative binomial law for the probability of successfully receiving the full data of the segment[156].

For CCARR (n,m) over channel with $PER = P_e$, we can write more formally the segment transmission failure probability $P_{\text{fail}_{\text{CCARR(n,m)}}}$:

$$P_{\text{fail}_{\text{CCARR(n,m)}}} = \mathscr{B}_c(n-1, n+m, (1-P_e) = \sum_{i=0}^{n-1} \binom{n+m}{i} (1-P_e)^i (P_e)^{n+m-i} \tag{5.1}$$

with $\mathscr{B}_c$ the cumulative value of the binomial law $\mathscr{B}(i, 1-P_e)$ when i varies from 0 to $n+m$, and $1-P_e$ is the probability of success.

We plot in fig.5.2 the probability to fail the reception of a single segment as a function of the channel *FER*, for various CCARR configurations having the same $CR_{\text{CCARR}} = \frac{1}{5}$, namely CCARR (10,40), CCARR (5,20) and CCARR (1,4), the latter being equivalent to the failure probability of LoRaWAN BSR with $Nb_{\text{Trans}} = 5$. The failure probability remains low until P_e approaches a given tipping point which depends the maximal available CR_{CCARR}. After this point, the probability of failure takes off quickly. We call this a waterfall effect. The waterfall effect is all the more pronounced the longer the segment length of CCARR is. This is an advantage and then a disadvantage before and after

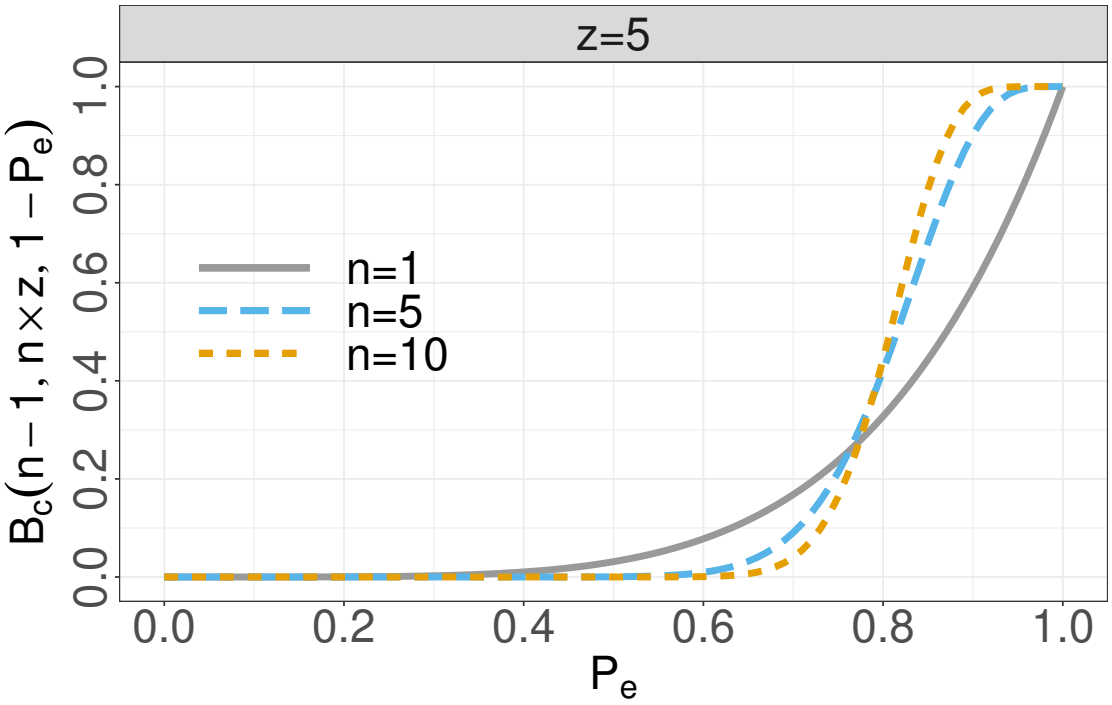

Figure 5.2: Probability to get less than n successes over a Bernouilli process with $n \times z$ trials and a $(1-P_e)$ success probability. This is the probability to fail at receiving a segment $(n, n\times z-k)$ ($z=5$ which correspond to $CR_{\text{CCARR}} = \frac{1}{5}$) over a channel with $PER = P_e$. Notice that n=1 is equivalent to LoRaWAN BSR.

the tipping point, respectively. With the objective being high reliability and not just a reliability improvement, it is therefore better to use long segments.

In fig.5.2 the erasure probability is computed for a single segment for each configuration, meaning that the amount of application data is not equivalent. Thus for fair comparison we plot in fig.5.3 the probability to fail at receiving 1 segment of CCARR (10,40), 2 segments of CCARR (5,20) and 10 segments of CCARR (1,4). It shows that CCARR is way better than LoRaWAN BSR (n=1) to provide an highly reliable connection. It also emphasizes even more the fact that CCARR with a longer segment makes is better to provide highly reliable channel.

5.1.2.2 Time-On-Air (TOA)

As stated in sec.3.2, the capacity is a key element of LoRaWAN and it must be preserved. Thus, any reliability mechanism must use as few TOA as possible. We define R_{TOA}, a comparison metric, that represents the channel over-usage ratio (including uplink and downlink), i.e. TOA_{useless}, the redundant transmissions duration that occurs while the data have already been recovered, over TOA_{useful}, the transmissions duration that was necessary to complete these data reception:

$$R_{TOA} = \frac{TOA_{\text{useless}}}{TOA_{\text{useful}}}$$

Thus, the "perfect" channel usage would result in $R_{TOA} = 0$, which means that all the transmissions that happened, including the redundant ones, were strictly necessary to recover the data. Consequently, $R_{TOA} > 0$ reflects the "wasted" network capacity normalized relatively to the useful transmissions necessary in order to successfully transmit the data with the given protocol. For instance $R_{TOA} = 1$ arises when the data is re-transmitted once while it was already recovered by the

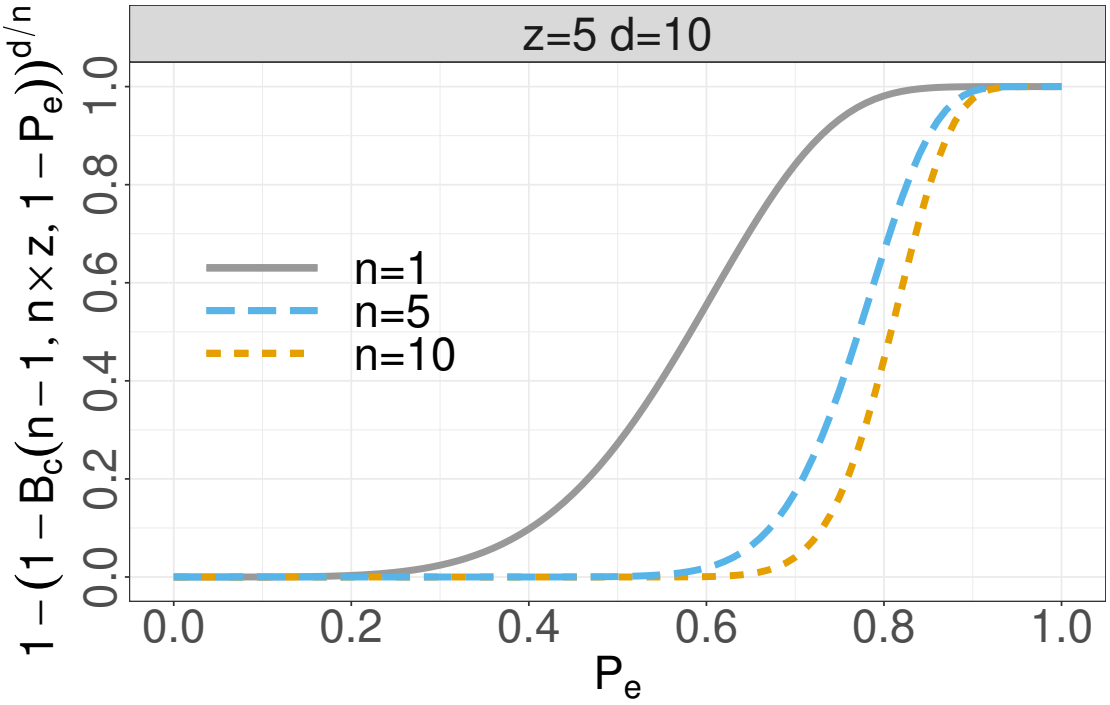

Figure 5.3: Probability to get less than n successes in a least one of $\frac{d}{n}$ a Bernouilli process with $n \times z$ trials and a $(1-P_e)$ success probability. This is the probability to fail at fully receiving 10 application data frames with $CR_{\text{CCARR}} = \frac{1}{5}$ with CCARR (10,40), (5,20) or (1,4).

NS.

Considering symmetric behavior of the channel, thus equal i.i.d $PER = P_e$ for both uplink and downlink, the cost of sending an uplink frame with CCARR depends on:

- a_i which the TOA generated by the i^{th} frame transmission attempt (with regard to T and T' the TOA of respectively an uplink data frame a downlink acknowledgement).
- b_i which is the probability to reach this i^{th} transmission attempt.
- c_i the probability that not enough successes occurred (i.e. less than n frames) to retrieve the whole data at this i^{th} attempt.

Formally:

$$\begin{aligned} a_i &= T + \left((1-c_i) \times (1-P_e) \times T'\right) \\ b_i &= \prod_{k=1}^{i-1} \left((1-c_k) \times (1-P_e)^2\right) \\ c_i &= B_c(n-1, i, 1-P_e) \end{aligned}$$

And, as a result:

$$R_{\text{TOA-CCARR}} = \frac{\sum_{i=1}^{n+m} (a_i \times b_i)}{\sum_{i=1}^{n+m} (a_i \times b_i \times (1-c_i))} \tag{5.2}$$

Fig. 5.4 shows the computed $R_{\text{TOA-CCARR}}$, the overload ratio to send uplink frames with CCARR, as a function of the channel's PER and $z = \frac{1}{CR_{\text{CCARR}}} \in \{1..15\}$ [1] , with T and T' being typical LoRaWAN

[1] $z = 15$ matches the redundancy of the LoRaWAN BSR maximal Nb_{Trans}.

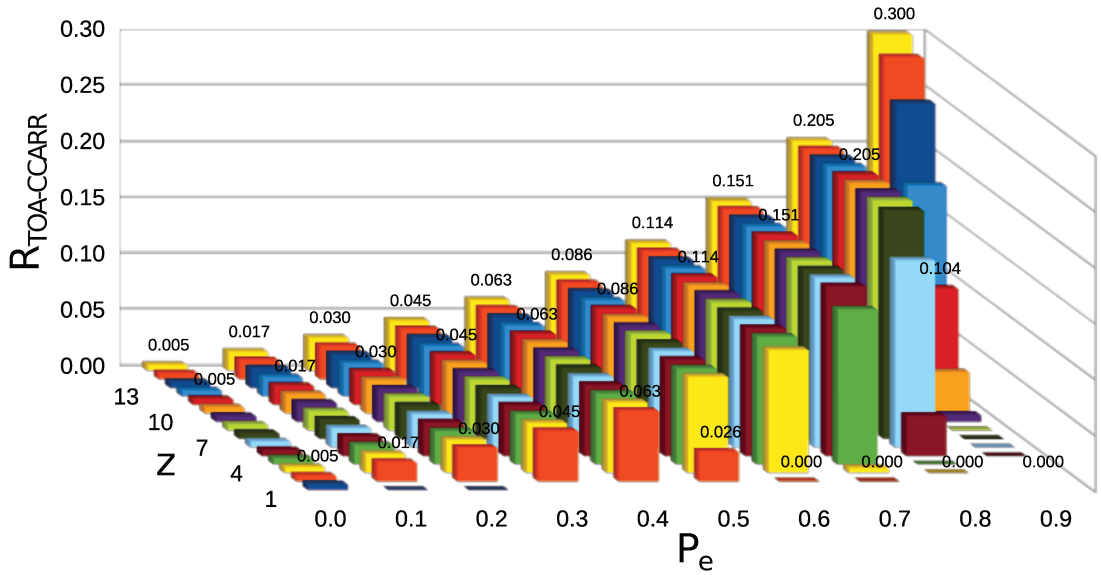

Figure 5.4: Probabilistic $R_{\text{TOA-CCARR}}$ for CCARR (100,100×(z-1)), T=66.8ms and T'=46.3ms, as a function of $z = \frac{1}{CR_{\text{CCARR}}}$ and P_e the error probability.

values [2]. $R_{\text{TOA-CCARR}}$ increases with the channel *PER* until a maximum, depending on CR_{CCARR}. This overload happens when the CCARR server does not succeed to acknowledge the segment soon enough, i.e. acknowledgments are lost. Then the cost decreases as the *PER* increases beyond the tipping point, showing that more and more of the redundant frames are necessary to recover the full segment.

5.1.2.3 Comparison with LoRaWAN BSR

As described in sec.2.3.3 has a very trivial packet loss recovery mechanism: the BSR. LoRaWAN proposes to set its parameter $Nb_{\text{Trans}} \in [1..15]$ that determines the number of duplicated transmission for each uplink frame. We refer to this mechanism as BSR.

Considering a channel with iid frame loss and $PER = P_e$, the probability P_{useful} for a transmission attempt to be useful is the probability that every previous frame transmission attempts were failures. Thus

$$P_{\text{useful}}(i) = P_e^{i-1}$$

with $i \in \{1..Nb_{\text{Trans}}\}$ the index of the transmission attempt. As a consequence :

$$TOA_{\text{Useful-BSR}} = \sum_{i=1}^{Nb_{\text{Trans}}} (P_{\text{useful}}(i) \times T)$$

and

$$TOA_{\text{Useless-BSR}} = (T \times Nb_{\text{Trans}}) - TOA_{\text{Useful-BSR}}$$

With T the TOA of an uplink frame.

[2] T and T' respectively 66.8ms and 46.3ms. These values matches payloads of 16 and 2 bytes for respectively the uplinks and downlinks, with transmission configuration: $SF = 7$, $BW = 125$kHz, $CR = \frac{4}{5}$. It matches the experimental values used in sec.5.1.4

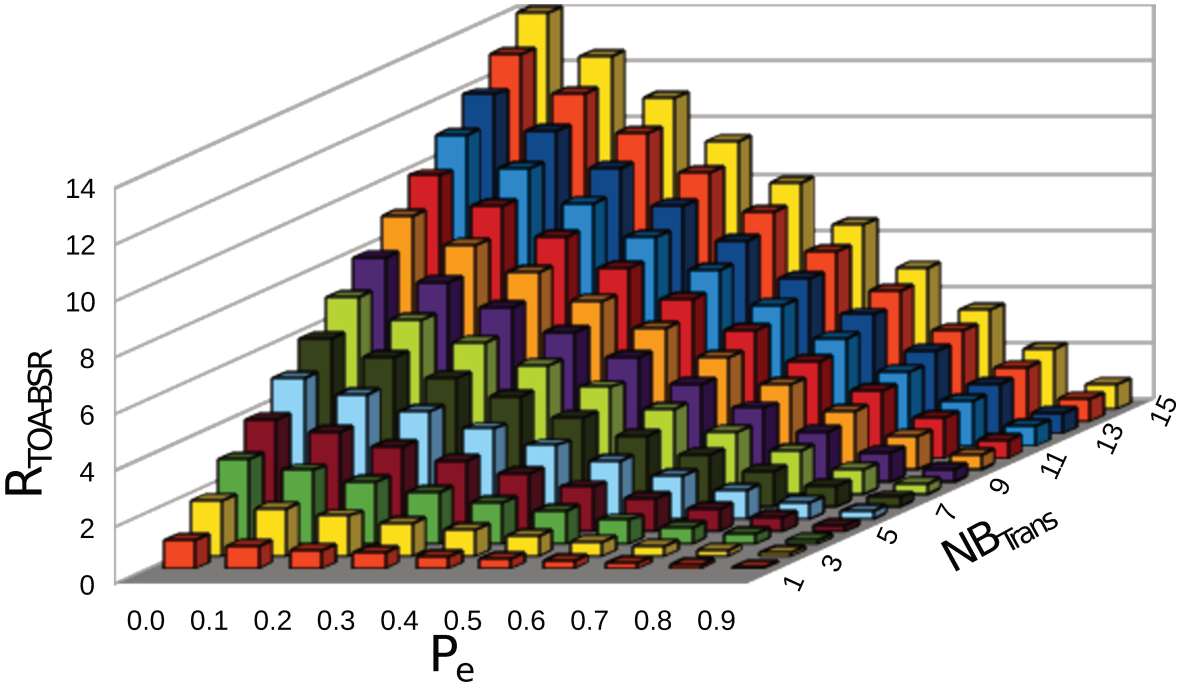

Figure 5.5: $R_{\text{TOA -BSR}}$ as a function of P_e the failure probability and $z = Nb_{\text{Trans}}$.

From this we can express $R_{\text{TOA -BSR}}$:

$$\begin{aligned} R_{\text{TOA -BSR}} &= \frac{TOA_{\text{Useless-BSR}}}{TOA_{\text{Useful-BSR}}} \\ &= \frac{Nb_{\text{Trans}} - \sum_{i=1}^{Nb_{\text{Trans}}} \left(P_e^{i-1}\right)}{\sum_{i=1}^{Nb_{\text{Trans}}} \left(P_e^{i-1}\right)} \end{aligned} \tag{5.3}$$

Fig. 5.5 shows $R_{\text{TOA -BSR}}$ as a function of the erasure probability P_e and Nb_{Trans}. This shows that BSR with a too high Nb_{Trans} introduces a lot of unnecessary network overload, when the channel's *PER* is low. However, $R_{\text{TOA -BSR}}$ stays low when the *PER* is very high. Thus, this protocol is only efficient for very high *PER*.

Fig. 5.6 displays the difference between the $R_{TOA-BSR}$ and $R_{\text{TOA-CCARR}}$ with equivalent amount of redundancy, respectively $Nb_{\text{Trans}} = z$ and CCARR (100,100×(z-1)). Thus in the worst CCARR case, the exact same number of uplink frames are sent. A positive value for this difference implies that CCARR has lower TOA , which implies network capacity gain. Clearly, in this analysis context, CCARR sends much less frames for the same overall successful data transmission[3]. The gain increases as the maximal amount of redundancy (parameter z) increases. It reflects the fact that CCARR emits only the required amount of redundancy while LoRaWAN BSR emits lot of useless extra repeated frames. The gain decreases as the error probability P_e increases because a large amount of redundant frames has to be sent to recover the data, thus reducing the margin for TOA gain.

[3]The very small negative values correspond to CCARR acknowledgement penalty when exactly the same number of frames occurs for very low *PER*.

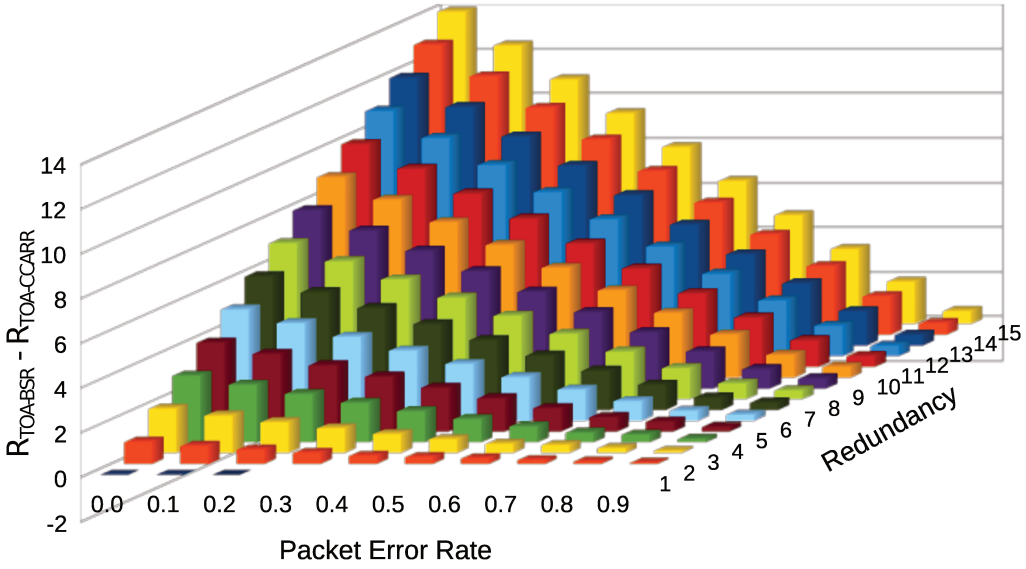

Figure 5.6: ($R_{TOA-BSR}$ - $R_{\text{TOA-CCARR}}$) with respectively $Nb_{\text{Trans}} = z$ and CCARR (100,100×(z-1)) as a function of the ratio of redundant frames z and P_e the error probability.

5.1.3 CCARR Simulation

In order to see the limits of the CCARR analytic trends, we implemented a simulator in C to observe its behavior in various situations. In the following, all the simulation experiments represent the transmission of at least 400000 uplink frames in order to get a 95% confidence interval.

The simulator runs three unix processes working together to emulate the ED, the LoRa channel and the NS. The ED process reads data from a file, computes the *segment* and emits it using the CCARR protocol. The LoRa channel process drops or transmits the frames from the ED process to the NS following the propagation model implemented. The channel follows the i.i.d. frame erasure channel model discussed in sec.1.2.2.1. Its *PER* is configurable. The NS process receives the frames and recovers the data through RS-decoding if necessary. All the simulator processes write their meta-data in a log-file to allow post-mortem analysis.

For the sake of simplicity, we assume a static channel, i.e. the *FER* of the physical channel does not fluctuate in time, nor frame's parameters (length, preamble length), nor uplink/downlink parameters. Similarly, the simulator implements only one receive window after each transmission where the device listens over the emission channel. For consistency with sec.5.1.4 constraints, the physical PL are set to 29 bytes frames and 15 bytes acknowledgments.

CCARR is evaluated against LoRaWAN BSR with its best robustness $Nb_{\text{Trans}} = 15$. The three evaluated configurations CCARR (a,a×(15-1) with $a = 1, 10, 100$ have a CR_{CCARR} which is equivalent to the redundancy ratio of LoRaWAN BSR with Nb_{Trans} =15. The simulation results of Fig.5.7 compare the *DER* reached by CCARR with the different segment sizes and the *DER* obtained with LoRaWAN BSR with $Nb_{\text{Trans}} = 15$ as a function of the LoRa channel *FER*. For CCARR (1,14), which is equivalent to the ARQ protocol, the *DER* is as expected similar to BSR with $Nb_{\text{Trans}} = 15$. It is consistent with analytical results from sec.5.1.2, CCARR reliability performance increases with the segment sizes. We distinguish three trends from the curves :

- **For *FER* < 0.74** all the tested strategies offer enough redundancy to recover the data with *DER* < 0.01.

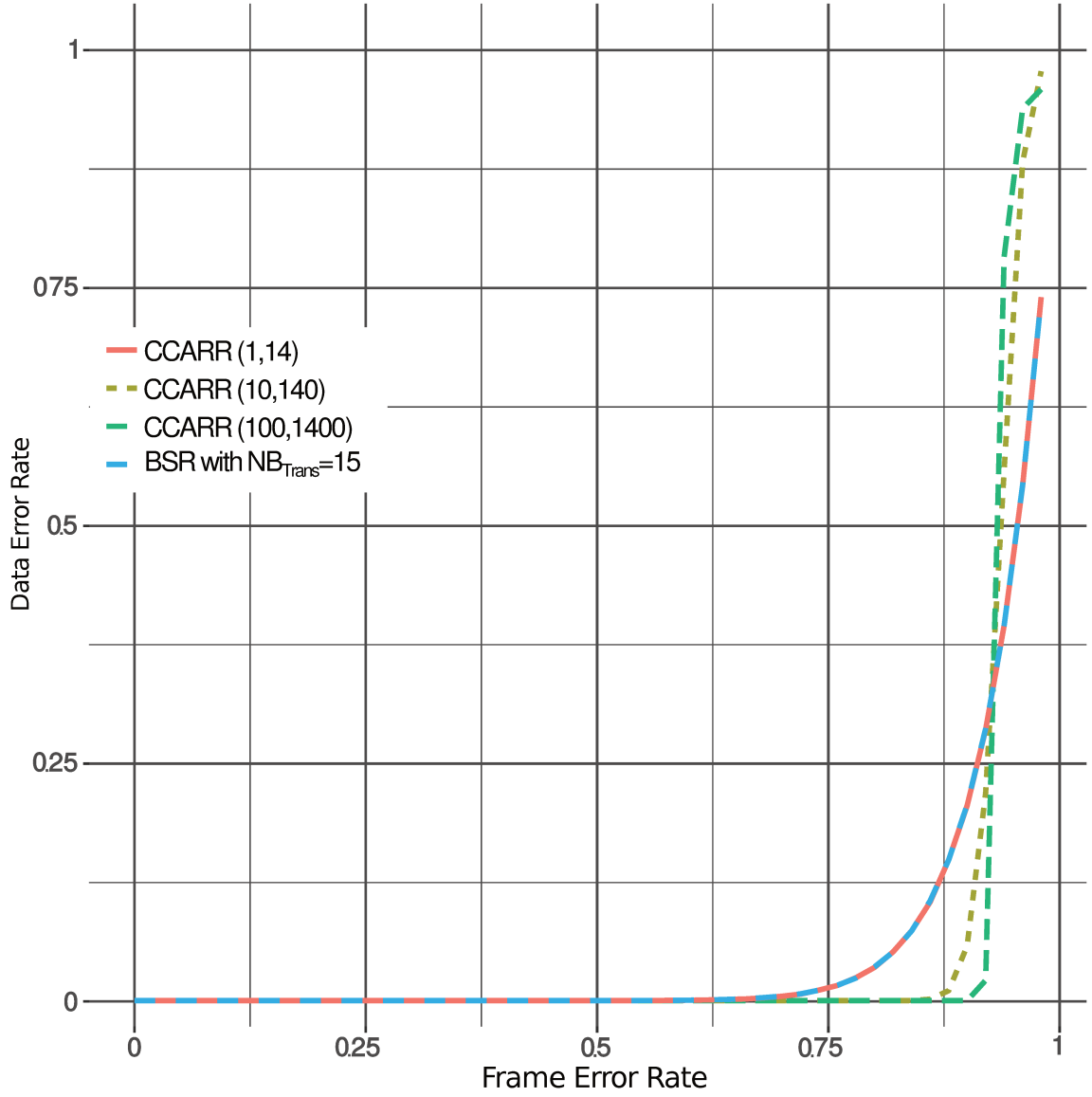

Figure 5.7: *DER* as a function of the *FER* for LoRaWAN BSR with $Nb_{\text{Trans}} = 15$, CCARR (1,14), CCARR (10,140) and CCARR (100,1400).

- **For 0.74 ≤ *FER* ≤ 0.92**, CCARR gives a progressively better robustness than BSR with $Nb_{\text{Trans}} = 15$. Around *FER* = 0.9, CCARR (100,1400), obtains a 26 points of percentage better *DER* than BSR $Nb_{\text{Trans}} = 15$.
- **For *FER* > 0.92**, CCARR (10,140) and CCARR (100,1400) *DER* increases quickly as the error recovery scheme fails and the whole data cannot be recovered anymore; Thus so the *DER* is equal to *FER*.

Fig. 5.8 shows the TOA of CCARR and LoRaWAN BSR as a function of the LoRa channel *FER*. For the sake of clarity, the results are normalized such that 1 uplink frame is 1 time unit. As expected, LoRaWAN BSR shows a constant TOA that only depends on Nb_{Trans}. For most cases, the CCARR protocol largely reduces the necessary TOA as it stops transmitting as soon as the data is successfully received. For instance, CCARR (10,140)'s TOA is half BSR with $Nb_{\text{Trans}} = 15$ over a *FER* =0.8 channel. When the channel *FER* increases, the TOA to emit a frame with CCARR tends to the TOA of transmitting with BSR with $Nb_{\text{Trans}} = 15$. This corresponds to the cases when all the available redundant frames have to be emitted to try recover the data. Notice that, as expected, the CCARR

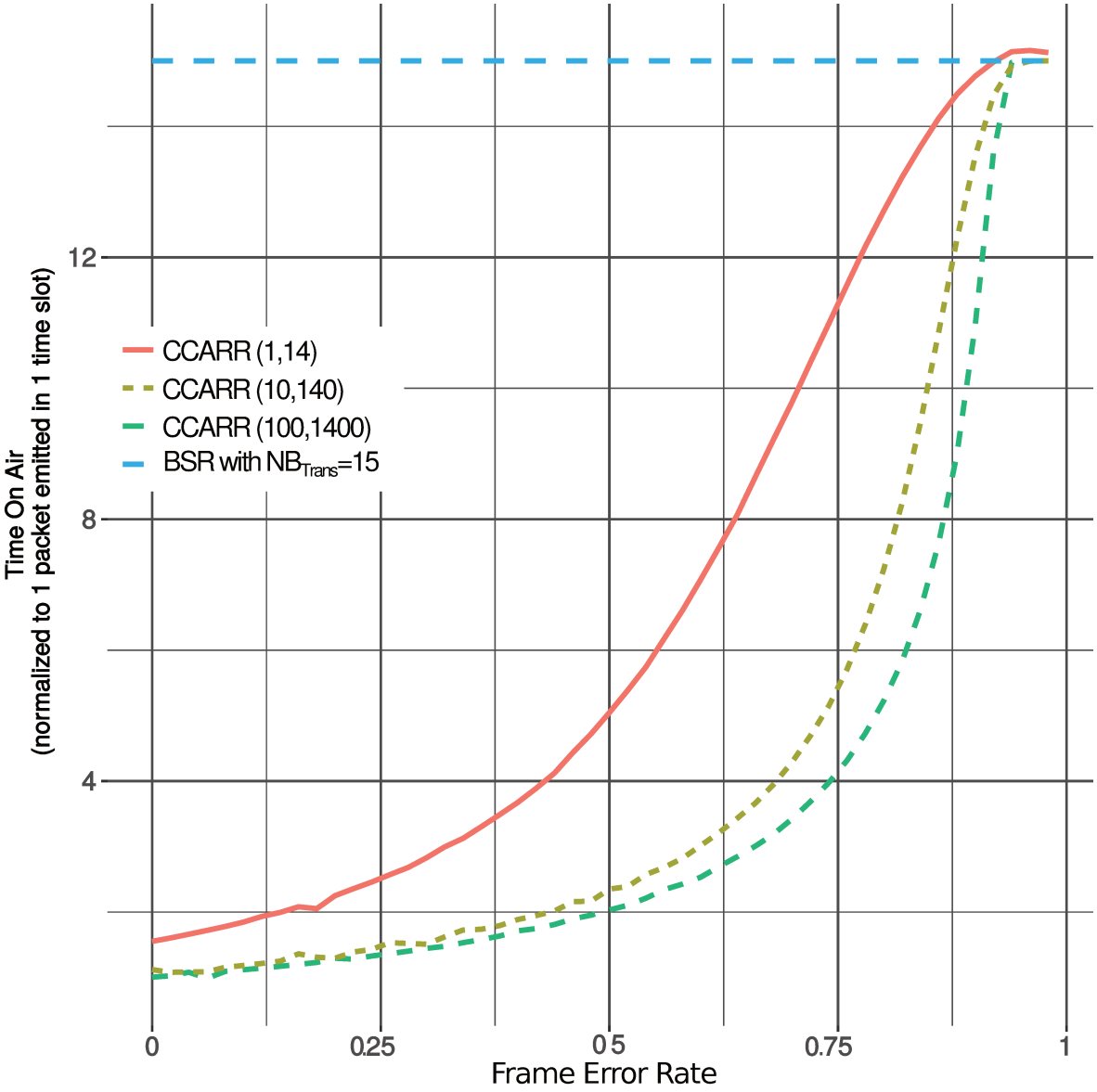

Figure 5.8: Average normalized TOA of LoRaWAN BSR with $Nb_{\text{Trans}} = 15$, CCARR (1,14), CCARR (10,140) and CCARR (100,1400).

average overload on the channel tends to be close to the minimal overhead that has to be introduced to successfully achieve the communication over a lossy channel. For instance, in order to achieve $DER = 0$ over a channel with $FER = 0.5$, the TOA of CCARR (10,140) and CCARR (100,1400) is only respectively around 2.3 and 2 times the raw single frame transmission TOA . Within the simulation assumptions, the CCARR protocol demonstrates its hability to provide high reliability with $DER < 0.1$ with a low TOA .

5.1.4 CCARR Experimental Results

Our experimental platform consisted in a single GW[4] and three EDs[5] placed in a large room. The GW was connected to the Internet through wired Ethernet. This Internet connection allowed the access to a NS, TTN[6], which implements LoRaWAN specifications. We did not control the behavior

[4] Kerlink Wirnet Station 868 [169].
[5] LoRaMOTE ARM-based EDs from ISMT[164].
[6] Provided by The Things Networks (TTN)[154].

Table 5.1: Frames TOA during experiments.

Link	SF	TOA (ms)	Payload (Bytes)
Up	12	1646.6	16
Down	9	164.9	2

Table 5.2: CCARR implementation extra code sizes[12]

Segment	Text (flash)	BSS(RAM)
Size (Bytes)	6320	5160

of this cloud NS. Especially its internal policy where it implements downlink transmissions using a lower *SF* and the maximum downlink allowed P_{Tx}[7]. Hence, this acknowledgement channel was lossless during the experiments. Notice that, compared with the simulation context, it is advantageous for the CCARR protocol to get 100% of its completion acknowledgments. With our testbed experimental setup, the acknowledgement's TOA was a tenth of the uplink frame's TOA, as detailed in Table 5.1. We used the maximal $SF = 12$ to generate contentions easily.

The ED LoRaMac firmware from [155] was modified to implement the CCARR protocol and its RS-coded CP-ECC. In particular, we modified an open-source[8] RS code library software [39] in order to fit our embedded software needs in terms of memory management, computation complexity, maximum size of dataword and codeword. The resulting CCARRCP-ECC computation does not constrain the communication system because it takes less time to compute than the frame TOA on our end-device MCU[9]. However, even optimized, the RS-code memory footprint is still relatively expensive on our typical MCU[10]. So we limited the segment dimension in order to adjust CP-ECC to typical LoRa frames and metering application demand. This resulted in a CCARR (10,140) protocol implantation with twenty-nine bytes frame for uplinks and 15 Bytes frames for downlinks[11] and a code size fitted to our ED as described in Table 5.2.

In order to variate the channel *FER*, we created various contention levels, by using 1, 2 or 3 ED within a single uplink *CF* =868.1MHz, at $SF = 12$. The uplink P_{Tx} is set to 2dBm, the minimum allowed by the ED. Then the desired channel *FER* was adjusted by tuning the intensity of the frame generation process of the EDs interfering on the contention-based ALOHA channel while respecting the LoRaWAN protocol and especially its active listening on receive slots. As a result each ED emitted at around 0.25Hz. We monitored the channel *FER*, the *DER* and the TOA on both the uplink and downlink. Each experiment was conducted until 150 packets were delivered to the application.

Fig. 5.9 displays the *DER* reached by LoRaWAN BSR with $Nb_{\text{Trans}} = 5$ and our CCARR (10,140) implementation as a function of the *FER*. LoRaWAN BSR with $Nb_{\text{Trans}} = 5$ measurements have $DER = 0$ up to $FER \approx 0.25$, $DER = 0.02$ with $FER = 0.43$, and $DER = 0.13$ for $FER = 0.6$. This corresponds to the probabilistic behavior described in sec.5.1.2, as $(0.43)^5 < 0.02$ and $(0.60)^5 < 0.09$. Interestingly, CCARR (10,140) protocol provides $DER = 0$ for all tests up to $FER = 0.67$ which is the highest stable *FER* that we were able to reach with our experimental platform.

Fig.5.10 displays the measured TOA consumed by LoRaWAN BSR with $Nb_{\text{Trans}} = 5$ and our CCARR

[7] SF9 and an effective radiated power (ERP) of 27dBm over the 125kHz wide channel centered on 869.525MHz.
[8] Under GPL license.
[9] 32 MHz STM32L151C8U6
[10] 10kBytes RAM and 64kBytes flash
[11] Respectively 16 and 2 Bytes of data with 13 control Bytes.
[12] Compiled with arm-none-eabi-gcc version 5.4.1.

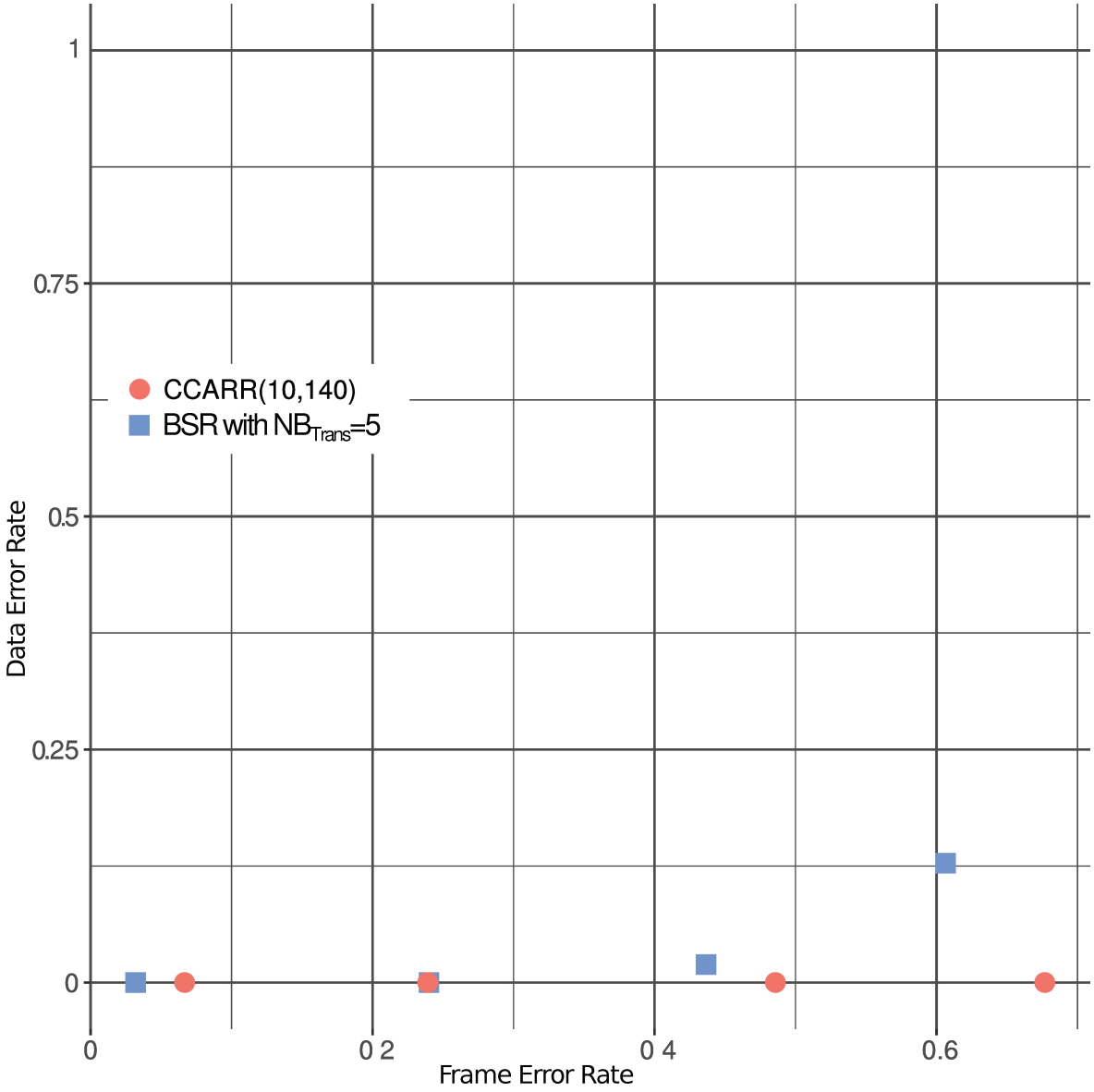

Figure 5.9: Experimental *DER* of CCARR (10,140) and LoRaWAN BSR with $Nb_{\text{Trans}} = 5$ as a function of the *FER*.

(10,140) implementation as a function of the *FER*. As in sec.5.1.3, the TOA is normalized such that a single frame is transmitted in 1 unit of time. As expected, LoRaWAN BSR with $Nb_{\text{Trans}} = 5$ emits a constant number of frames and is TOA is exactly 5 times higher than transmission without any error recovery mechanism. CCARR (10,140)'s TOA increases smoothly with the *FER* as the protocol compensates the channel degradation. Finally, CCARR gives $DER = 0$ over a channel with $FER = 0.67$ an average normalized TOA of 3.3, which is much less than BSR with $Nb_{\text{Trans}} = 5$.

The experimental conditions with no loss over the downlink were favorable for CCARR relatively to the model of sec.5.1.3 where the uplink and the downlink had the same *FER*. Thus in our experiments, CCARR emits exactly the number of frame needed to successfully recover the full the data because of the lossless downlink acknowledgement channel.

CCARR presents very good practical performance results which corroborate our probabilistic estimations and simulations trends.

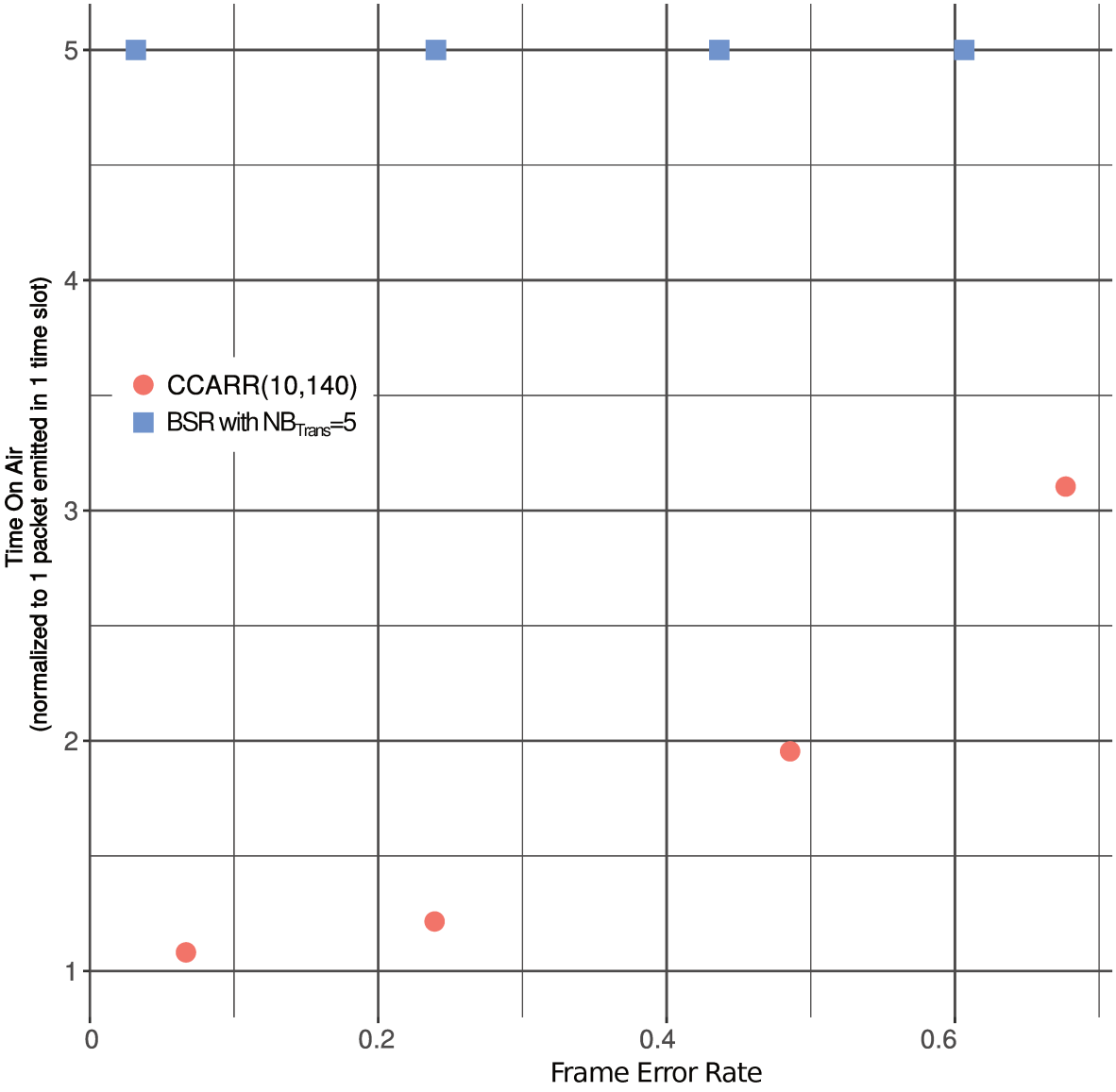

Figure 5.10: Average experimental TOA, in frame TOA, for the different protocols against channel PER.

5.2 LoRaFFEC

This section describes the LoRaFFEC protocol, an alternative to CCARR. LoRaFFEC addresses two LoRaWAN problems.

- First, because of the very low downlink capacity, any protocol which relies on acknowledgment might overload the downlink of the network, and in a second times overload the uplink of the network as more uplink frames are emitted until an acknowledgement is received. CCARR is weak against this phenomenon as even though the downlink requirement is reduced compared to confirmed traffic, it still heavily relies on the periodic acknowledgment. LoRaFFEC uses another CP-ECC and also provides highly reliable communication over LoRaWAN ($DER < 0.01$) but without the need for any downlink communication which is a major asset compared to CCARR.
- Secondly, as LoRaWAN operates in the ISM bands which are subject to legal restrictions, the maximal payload is function of both the region of deployment and the Data Rate (DR) resulting from the transmission parameters. As a consequence the available application payloads varies from 11 bytes to a maximum of 250 bytes. Fragmentation, as provided by

LoRaFFEC, is thus needed to ensure application compatibility with any legislation and any link quality.

5.2.1 LoRaFFEC Protocol

LoRaFFEC considers uplink communications between an ED and the NS as a stream of packets which need to abide by the regulation of the considered frequency band. The stream implements LDPC-like CP-ECC by computing redundancy packets on the fly using pseudo-random linear combinations of already sent data. On top of that mechanism, application data is fragmented to fulfill the stream packet size.

Thus LoRaFFEC implements the fragmentation of the application payload, called Application Data Unit (ADU) and thanks to the CP-ECC, it allows the recovery of lost data. On the one hand, fragmentation has a strong negative impact on the *DER*: every single fragment of the ADU needs to be received for reconstructing the full original ADU:

$$DER = 1 - (Fragment\_Reception\_Rate)^{\#\text{fragments}}$$

So it is natural to supplement a fragmentation scheme with an erasure recovery such as CP-ECC to regain a satisfactory *DER*. On the other hand, CP-ECC implies more payload overhead to carry the additional redundancy control information. This reinforces the need for fragmentation, in order to be able to transmit any payload size, by splitting if necessary the data over multiple packets while optimizing the use of each packet transmission with the aggregation of many fragments when possible. This interdependence affirms the need for a protocol ensuring both fragmentation and reliability.

LoRaFFEC is realized through three sub-layers performing respectively: integrity check, fragmentation and erasure recovery. A LoRaFFEC ED first sends data fragments, followed by a number of redundancy fragments as shown in fig.5.14. Thus, the ED has to store a window of previous fragments. On the NS side, when a data fragment is missing, the previously received data and redundancy fragments form a linear system of equations which enables to attempt to rebuild the data. This involves storage and relatively heavy computation. The corresponding ED and NSLoRaFFEC algorithms are presented in sec.5.2.1.7 and 5.2.1.8 with a precise evaluation of the memory and computational complexity costs.

To precisely assess LoRaFFEC, several parameters have to be discussed: the Window Length (*WL*) on which the CP-ECC is computed, the Redundancy Density (*RD*) which is the number of data fragments combined in each redundancy one, and the Decoding Depth (*DD*) that the NS considers when building the system of equations.

5.2.1.1 Integrity Sub-layer

The integrity sub-layer guarantees that no false positive is delivered to the upper layer, i.e. it guarantees that the output of LoRaFFEC (at NS side) is effectively an ADU produced by the application (at ED side). As shown in fig.5.11, each ADU is identified in the implementation by a 4-bytes Application Counter (Cnt_{App}) and a 2-bytes hash computed on the ADU and its Cnt_{App}. The concatenation of the Cnt_{App}, the ADU and the hash forms the Integrity Data Unit (IDU) .

In order to reduce protocol overhead, the three Most Significants Bytes (MSB) of the Cnt_{App} are truncated after computing the hash and before fragmentation, only the Least Significants Bytes (LSB) are sent along the data.

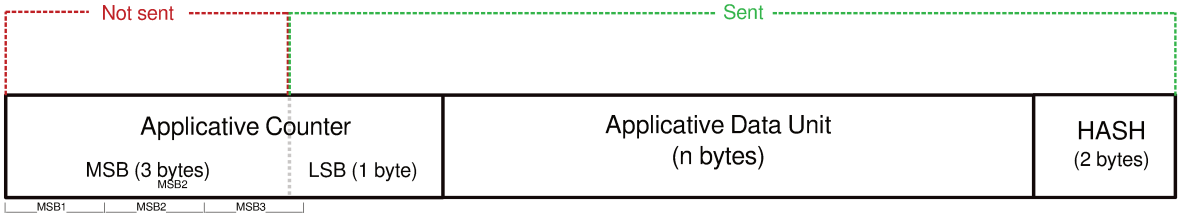

Figure 5.11: IDU structure.

5.2.1.2 Fragmentation Sub-layer

The fragmentation sub-layer splits the IDU in data fragments (strictly smaller than 11 bytes) as shown in fig.5.12. This guarantees that communication can respect the most restricting conditions and regulations.

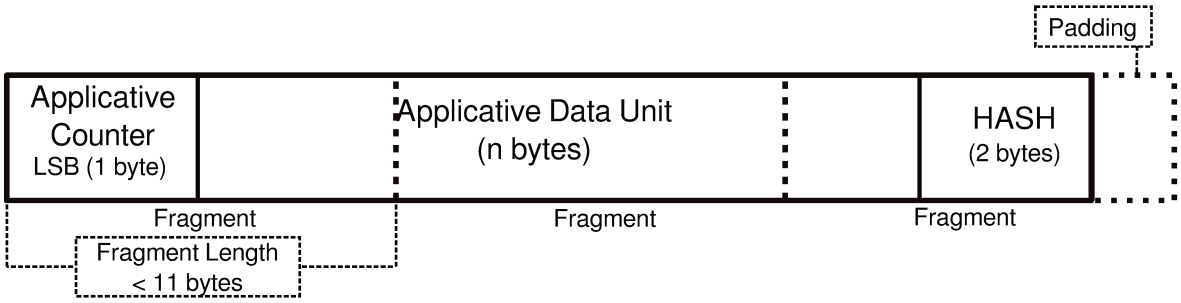

Figure 5.12: IDU fragments splitting.

The data fragments are numbered from 0 to 127. Data fragment 0 is always the first data fragment of a splitted IDU .

Figure 5.13: Fragment structure.

5.2.1.3 Erasure Correction Sub-layer

The erasure correction sub-layer implements the CP-ECC algorithm to recover the data lost during communication. The correction code is a derivative of LDPC [16] and we call it Multiple Parity Check (MPC) . MPC coding consists in sending, in addition to the data fragments, pseudo-random linear combinations of the data fragments written in redundancy fragments. Eventually, lost data fragments might be recovered from solving the linear system formed of the successfully received data and redundancy fragments.

5.2.1.4 Window Length (*WL*)

The data fragments included in the combinations are pseudo-randomly chosen among a window of the previous data fragments. This window spans between $fragment[i]$ (the current ADU last data fragment) and $fragment[i-w+1]$, where WL is the window length. Redundancy fragments are sent after the data ones, i.e. the data fragments of a single ADU are sent consecutively and cannot be interleaved with redundancy fragments.

In our implementation the fragments are numbered on one byte. These redundancy fragments are numbered with an offset of 128, relatively to their matching data fragments numbered from 0 to 127. Fig.5.14 illustrates the computation windows used for consecutive redundancy fragments. The maximal WL is limited by the fragment numbering, here $WL \leq 128$. However, ED memory requirement grows linearly with WL as the ED buffer size is $WL \times$ fragment_length. Depending on

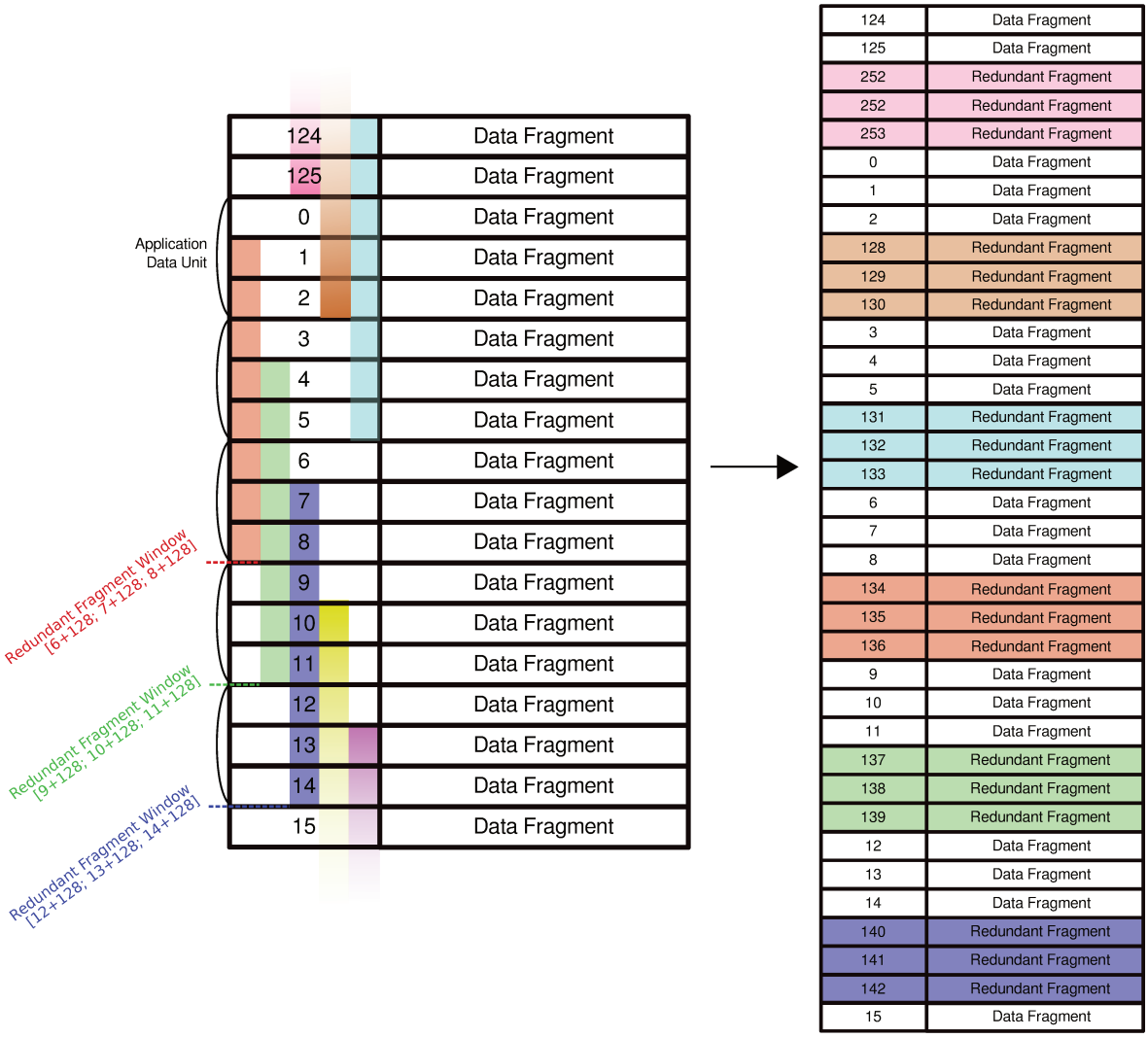

Figure 5.14: Fragment computation window and numbering, $WL = 8$ and each ADU contains 3 fragments.

the maximum frame size, each fragment can either be transmitted alone as a LoRaWAN payload, or aggregated with other fragments into a multi-fragments LoRaWAN payload as illustrated respectively in fig.5.15 and fig.5.16. In the second case, so as to reduce overhead, only one fragment counter is transmitted over the air, the others ones are deduced from the first one by the NS.

Figure 5.15: A LoRaWAN payload with a single fragment.

Data fragments and redundancy fragments can either be sent separately or together into a LoRaWAN packet. In order to allow puncturing of the redundancy and still being able to retrieve

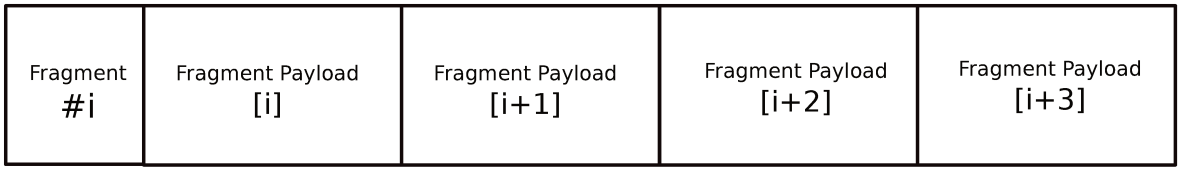

Figure 5.16: A LoRaWAN payload with multiple fragments.

correctly each fragment number, data fragments are always sent in front. I.e. data fragments of a new ADU cannot be piggybacked after the redundancy fragments of the next ADU . Fig. 5.17 illustrates the aggregations possibilities.

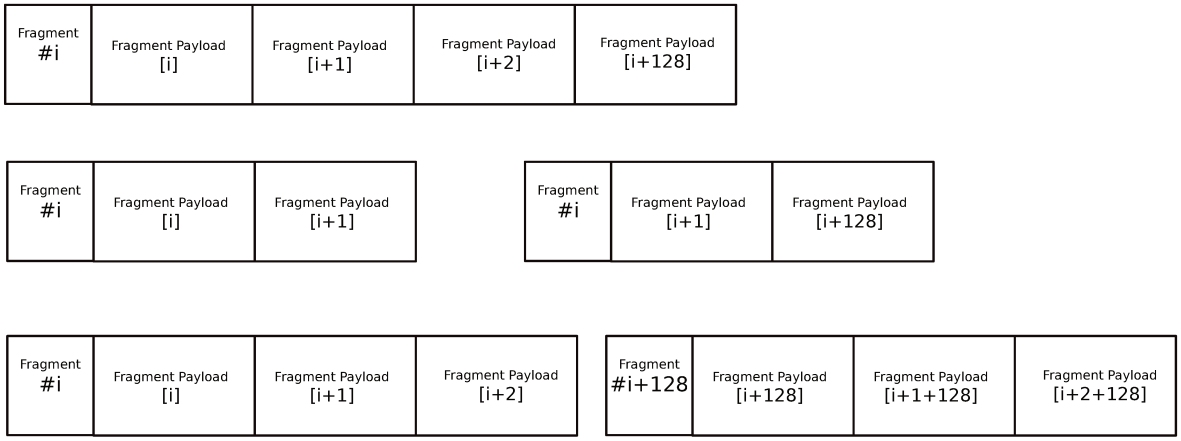

Figure 5.17: Aggregation of data and redundancy fragments into LoRaWAN frames.

5.2.1.5 Redundancy Density (*RD*)

The *RD* represents the number of data fragments combined to constitute a redundancy fragment as a proportion of the *WL*. Thus, with $RD = 0$ no redundancy fragment is computable, whereas with $RD = 1$ all data fragments in the window are always combined in each redundant fragment. For instance, in LoRaFFEC with $WL = 128$ and $RD = 0.5$, 64 pseudo-randomly chosen data fragments are combined into each redundancy fragment. Hence, *RD* influences the amount of computation on the EDs. Notice that the NS and the EDs share the same pseudo-random generator (with the same seed) for use in the CP-ECC coding and decoding processes.

5.2.1.6 Decoding Depth (*DD*)

The decoding of LoRaFFEC consists in progressively diagonalizing a binary index matrix in which each fragment corresponds to a line. In this index line, each "1" corresponds to a data fragment combined into the fragment. Thus, a data fragment is a line comprising a single "1", whereas a redundancy fragment is a line with multiple "1"s. Each new line in the index matrix can, by linear combination gear effect, resolve a data fragment from the past. There is no bound to this effect, so a missing data fragment could, in theory, be unlocked infinitely long after its reception as part of a redundancy fragment. However, the practical bound is the storage and the computation available. In order to make the decoding sustainable, we bounded the backtracking *DD*. For simplicity we arbitrarily set *DD* as a multiple of *WL*.

5.2.1.7 Encoding on the ED

On the ED, following the algorithm described in algo.5, the encoding process computation complexity for each redundancy fragment is $WL \times RD$. The real bottleneck is the memory footprint: the ED needs a buffer of $WL \times f$ bytes, where f is the fragment length, to store the past ADUs that are used to compute the current redundancy fragments.

Algorithm 5 Fragmentation and redundancy fragment encoding algorithm using MPC .

```
1: sequence ← Random(fragment#)
2: for all j ∈ sequence do
3:     redundantFragment ← LinearCombinaison(WL,RD,fragment[j]);
4: end for
5: Transmit(redundantFragment)
```

5.2.1.8 Decoding on the NS

The decoding is computed using a best effort linear resolution of the equation system. The work matrix lines are filled with all the received fragments indexes followed by their data. The linear system solving operations are determined and computed from the indexes structure. All the corresponding (XOR) operations are applied to the whole data part of the fragment in order to reconstruct the lost elements. When a new fragment comes in, diagonalization of the index matrix is advanced as much as possible using Gaussian elimination on the new fragment and then with the fragment itself and possible new pivot(s). In the end, each updated index line which only contains a single "1" has its data part delivered to the de-fragmentation procedure. Otherwise, it stays as is, waiting for the next fragment diagonalization to be applied for possible complete decoding later on.

Algorithm 6 Decoding and update algorithm of the index and data matrices.

```
1: for all newFragment do
2:     StoreData(newFragment,dataMatrix)
3:     InsertInDiagonal(newFragment,indexMatrix)
4:     DiagonalUpdates(indexMatrix,dataMatrix,DD)
5:     if LinesWithSingleOne(indexMatrix) then
6:         DeliverDataFragments(dataMatrix);
7:     end if
8: end for
```

At the NS side, from the algorithm presented in algo.6, the decoding process computation complexity is $O(WL^2 \times DD)$ for each received fragment and it requires a buffer of size $(DD \times WL)^2/8 + (DD \times WL \times f)$ bytes in memory to store the decoding matrices. With the discussed practical numbers, this stays very reasonable for a NS.

5.2.2 LoRaFFEC Simulation

We performed extensive simulations to evaluate the performance of LoRaFFEC with parameter variations. The simulation scenario decodes a LoRaFFEC stream with random i.i.d packet erasure.

5.2.2.1 Simulator Description

To evaluate the LoRaFFEC protocol and check the proposed CP-ECC, a simulator[13] was designed which executes the actual LoRaFFEC protocol on a simulated communication channel. The sim-

[13] Code is available at `https://gricad-gitlab.univ-grenoble-alpes.fr/coutaudu/LoRa_QoS`

ulator encodes the input stream with LoRaFFEC, and pushes it to the LoRaFFEC decoder engine following the pre-computed channel erasure pattern. The channel erasure pattern simulates the wireless communications using a slow Raleigh channel model. The channel parameters are set to mimic LoRa physical and LoRaWAN link layers.

5.2.2.2 Sensitivity Analysis

LoRaFFEC has various parameters that can be tuned to minimize the *DER* and latency: *WL* and *RD* at the encoding side and *DD* at the decoding side. We note LoRaFFEC (x, y, z) a LoRaFFEC experiment with $WL = x$, $RD = y$ and $DD = z$. Fig.5.18 compares LoRaFFEC (*WL*,0.6,5) performance for $WL \in \{8, 16, 32, 128\}$. Results for transmission using BSR with $Nb_{\text{Trans}} = 2$, and thus equivalent redundancy ratio, are also plotted for the sake of comparison. LoRaFFEC provides high reliability ($DER < 0.01$) over a link with $FER \leq 0.45$, $FER \leq 0.40$, $FER \leq 0.35$ and $FER \leq 0.25$ for respectively $WL = 128$, $WL = 32$, $WL = 16$, $WL = 8$.

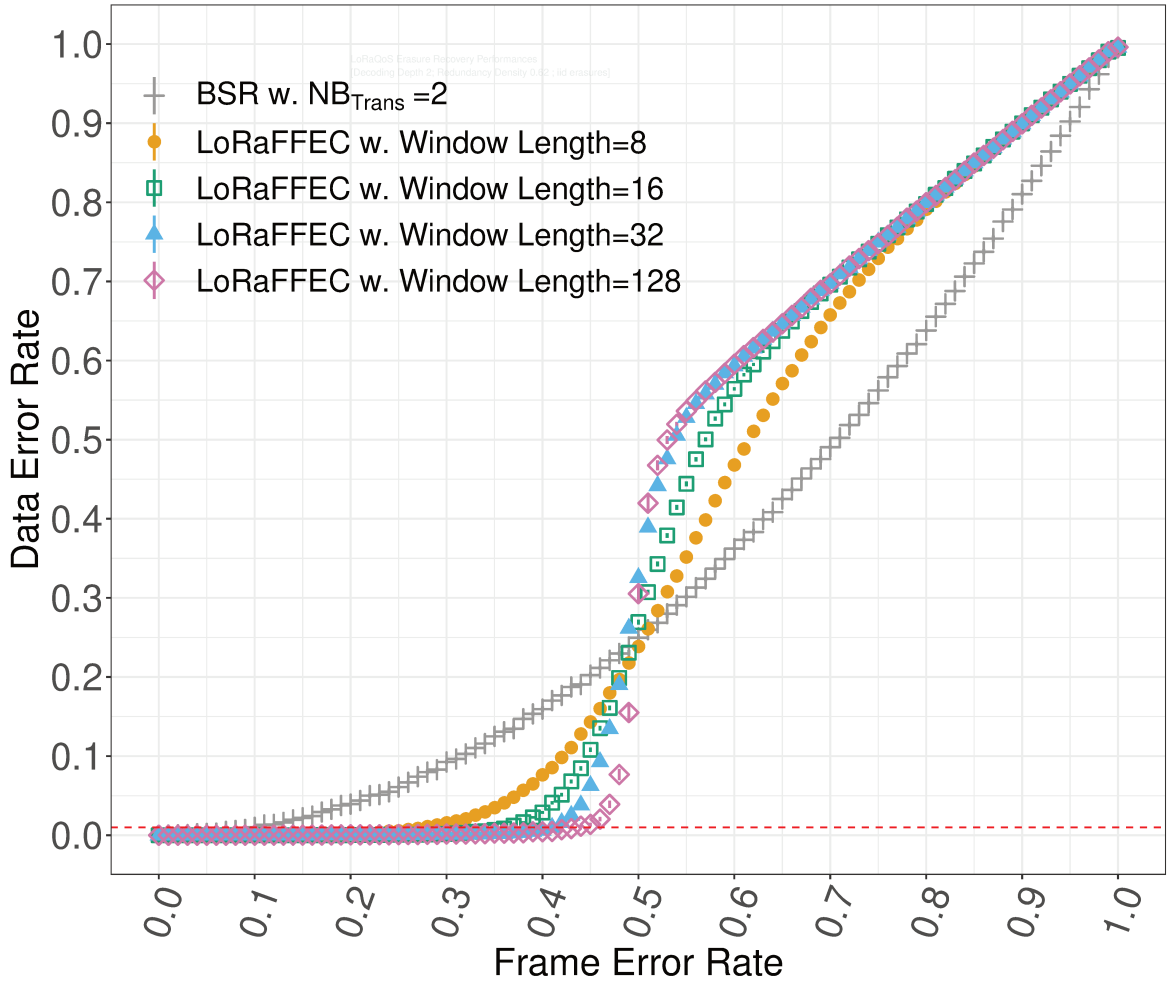

Figure 5.18: Simulated *DER* as a function of the *FER* for LoRaFFEC (*WL*;0.6;5) and LoRaWAN BSR with $Nb_{\text{Trans}} = 2$. The red dashed line marks the $DER = 0.01$ threshold.

When the *FER* increases, *DER* increases in a waterfall manner up to the raw channel erasure rate (thus the *FER* in our case), meaning that LoRaFFEC is unable to recover any lost data. LoRaFFEC with large *WL* offers more diversity and thus is less sensitive to link *FER* local variations. But the waterfall is more pronounced for longer *WL*, i.e. *DER* stays < 0.01% over higher *FER*, but then it increases at a steeper angle.

As we target to offer high reliability in practice, LoRaFFEC with $WL = 128$ should provide connection with $DER < 0.01$ over lossy channels up to $FER = 0.45$. For higher FER on the channel, others solutions like LoRaWAN BSR or ADR downlink commands to change the transmission parameters toward higher P_{Tx}, higher SF, must be considered to maintain proper functioning.

Fig. 5.19 shows LoRaFFEC DER progression for various redundancy density when transmitting on a $FER = 0.4$ erasure channel. For small WL ($WL = 8$), the RD has some significant influence, has shown on fig.5.19 but for larger WL ($WL = 128$), the DER is stable and below 0.01 as long $RD \in [12.5, 0.9]$. Hence, in our $WL = 128$ target implementation we chose $RD \approx 0.6$.

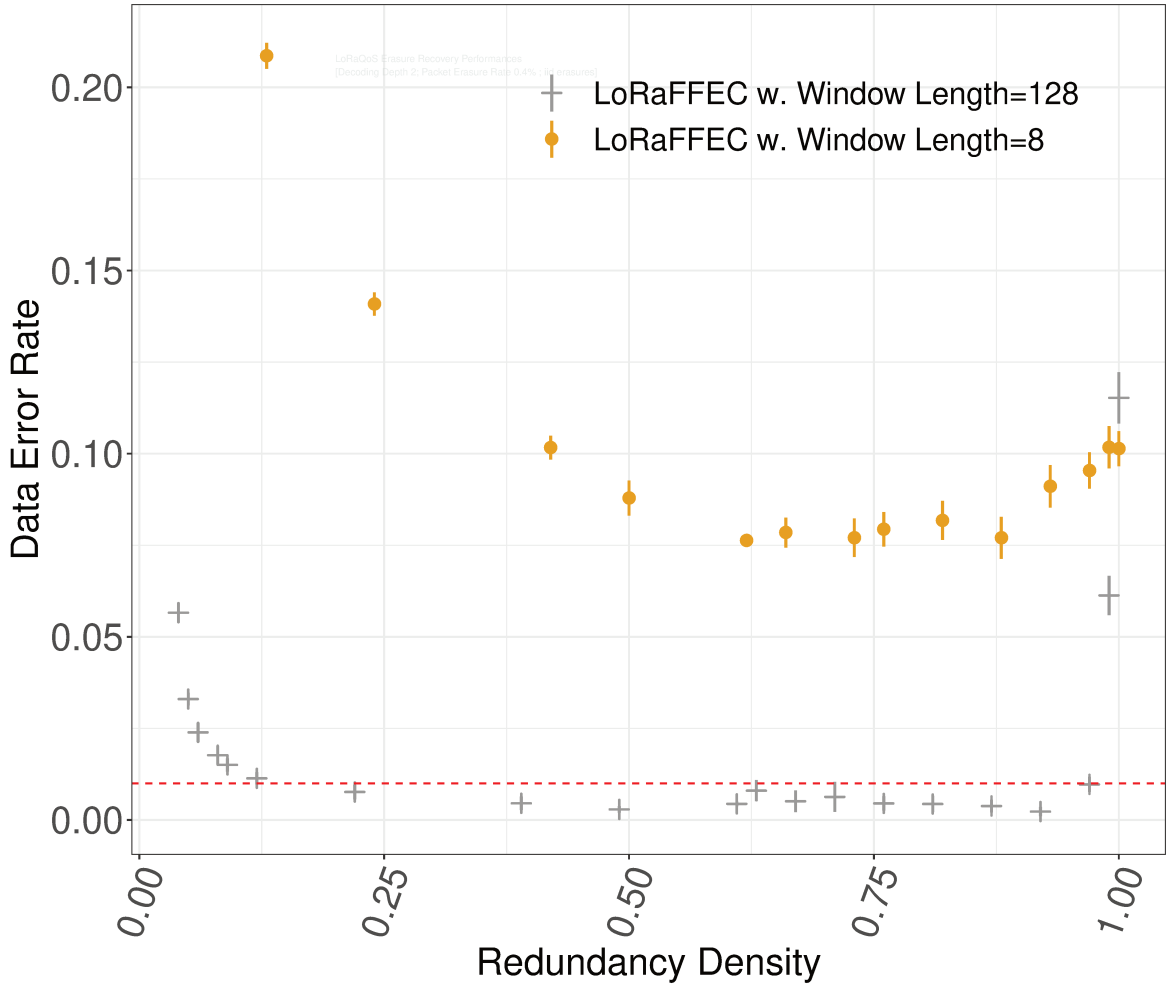

Figure 5.19: Simulated DER as a function of RD with LoRaFFEC (128; RD; 2) and LoRaFFEC (8; RD; 2) over a $FER = 40$ erasure channel. The red dashed line marks the $DER = 0.01$ threshold.

Fig. 5.20 shows LoRaFFEC (128,0.6,DD) recovery performances for $DD \in \{1,2,3,4,5\} \times WL$. The curves present a good performance flat part followed by a step waterfall-like degradation and a higher DD pushes the waterfall to the right, meaning high reliability is provided over channel with higher FER. However, in practice, the only significant variation happens with $DD = 1 \times WL$. This corresponds to the situation where the decoding matrix is barely diagonalizable, i.e. some erased data fragments are still present into redundancy fragments but could not be extracted. As $DD > 2 \times WL$, the variation is very small; in our implementation we set $DD = 2 \times WL$ to keep decoding complexity down.

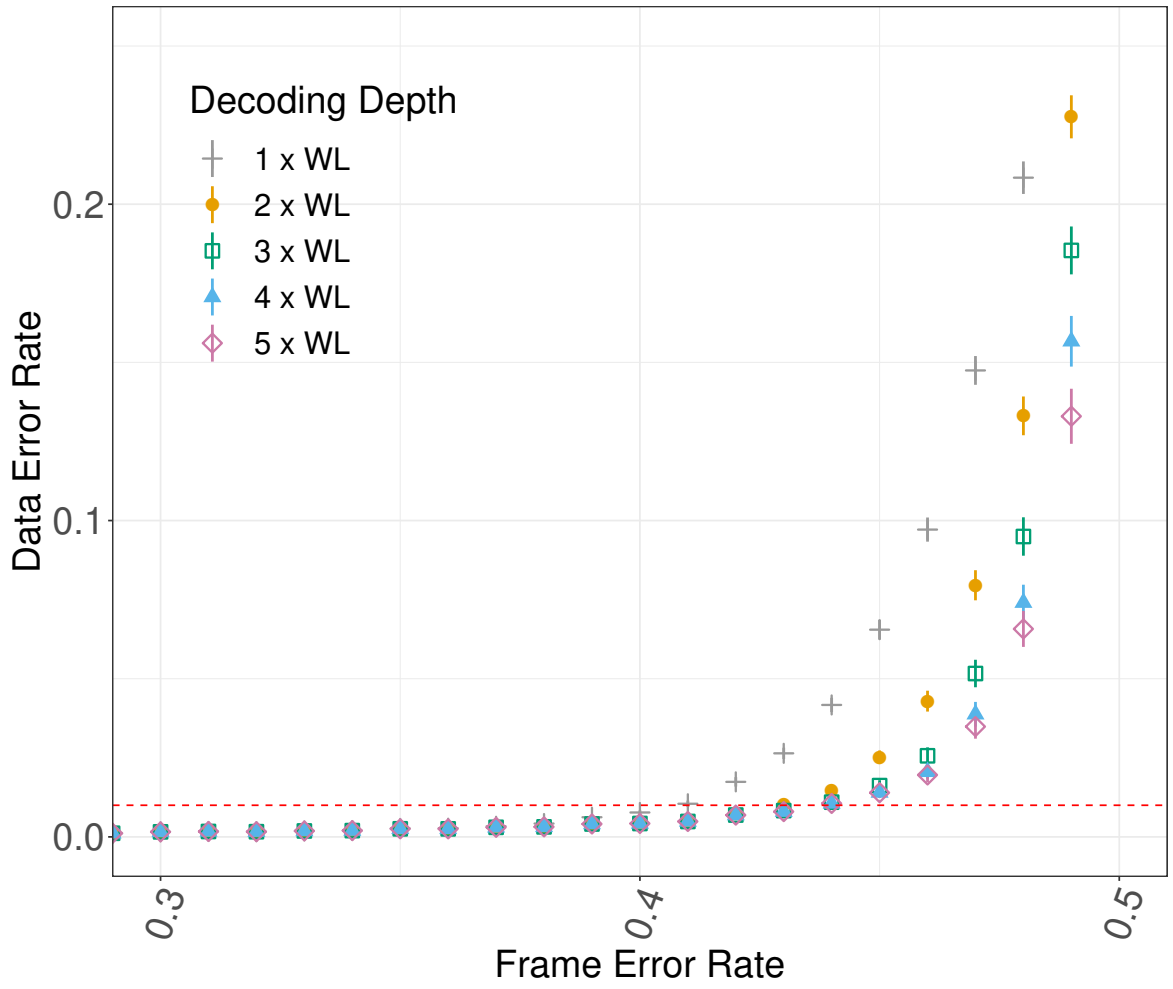

Figure 5.20: Simulated *DER* as a function of *FER* with LoRaFFEC $(128; 0.6; DD)$ for various *DD*. The red dashed line marks the $DER = 0.01$ threshold.

5.2.2.3 Impact of Fragmentation

Fragmentation negatively impacts *DER* as every data fragments of the IDU must be retrieved and delivered to the fragmentation layer in order to be able to reconstruct the ADU . I.e. $DER = 1 - (\text{FragmentDeliveryRate}^n)$ with n the number of data fragments which compose a given ADU . Fig.5.21 shows this phenomenon with the *DER* for two LoRaFFEC streams, without fragmentation and with a relatively large fragmentation ($n = 28$). As soon a small percentage of lost data fragment cannot be recovered, the *DER* of the fragmented LoRaFFEC stream increases drastically. Also, instead of increasing up to the channel *FER*, the *FER* of LoRaFFEC with this fragmentation increases up to 1 because even if a few data fragments are correctly received, they are not enough to fully recover any ADU .

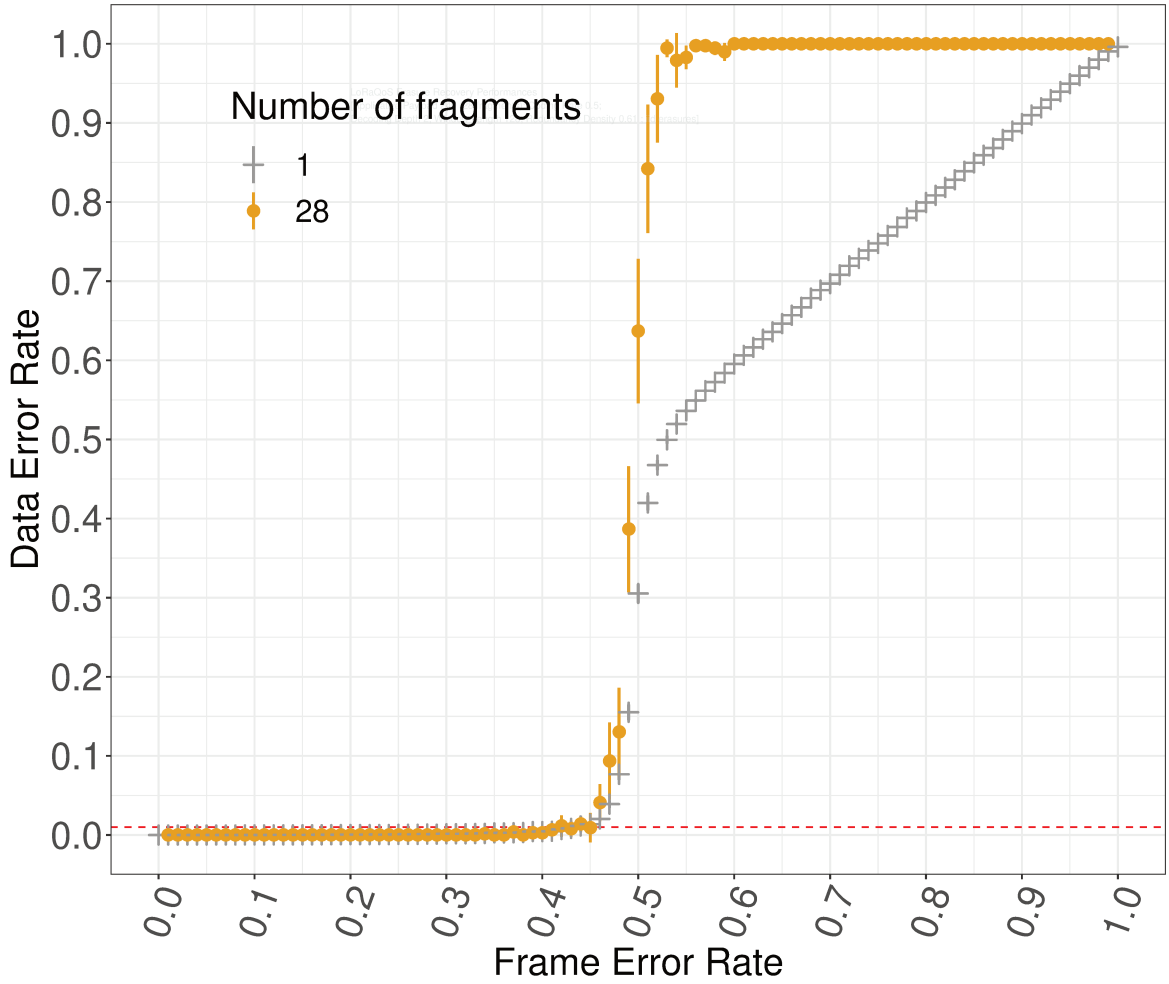

Figure 5.21: Simulated *DER* as a function of the *FER* with LoRaFFEC (128; 0.6; 5) without fragmentation and $n = 28$ fragments. The red dashed line marks the $DER = 0.01$ threshold.

5.2.2.4 Reconstruction Latency

Fig.5.22 shows the mean latency of LoRaFFEC for several *WL* as a function of the *FER*. The latency is expressed in "fragments offset", i.e. the number of received fragments between an erasure and its recovery, taking into account data and redundancy fragments. LoRaFFEC provides erasure correction with low latency for reasonable *FER*: lost fragments are recovered within 10 fragments when $FER < 0.3$ and within 20 fragments when $FER < 0.38$. In this case, the decoder is maintained in a state where a large majority of data fragments from the past are known (either correctly received or already recovered) and the required data is quickly extracted to recover new erasures.

Latency increases when the *FER* is between 0.3 and 0.5. In this case, the decoder is often in an intermediary state where so many data fragments are lost that it can barely extract lost data from redundancy fragments. For $FER > 0.5$, the latency concerns a few exceptional corrections when very short linear combination gear effect is successful.

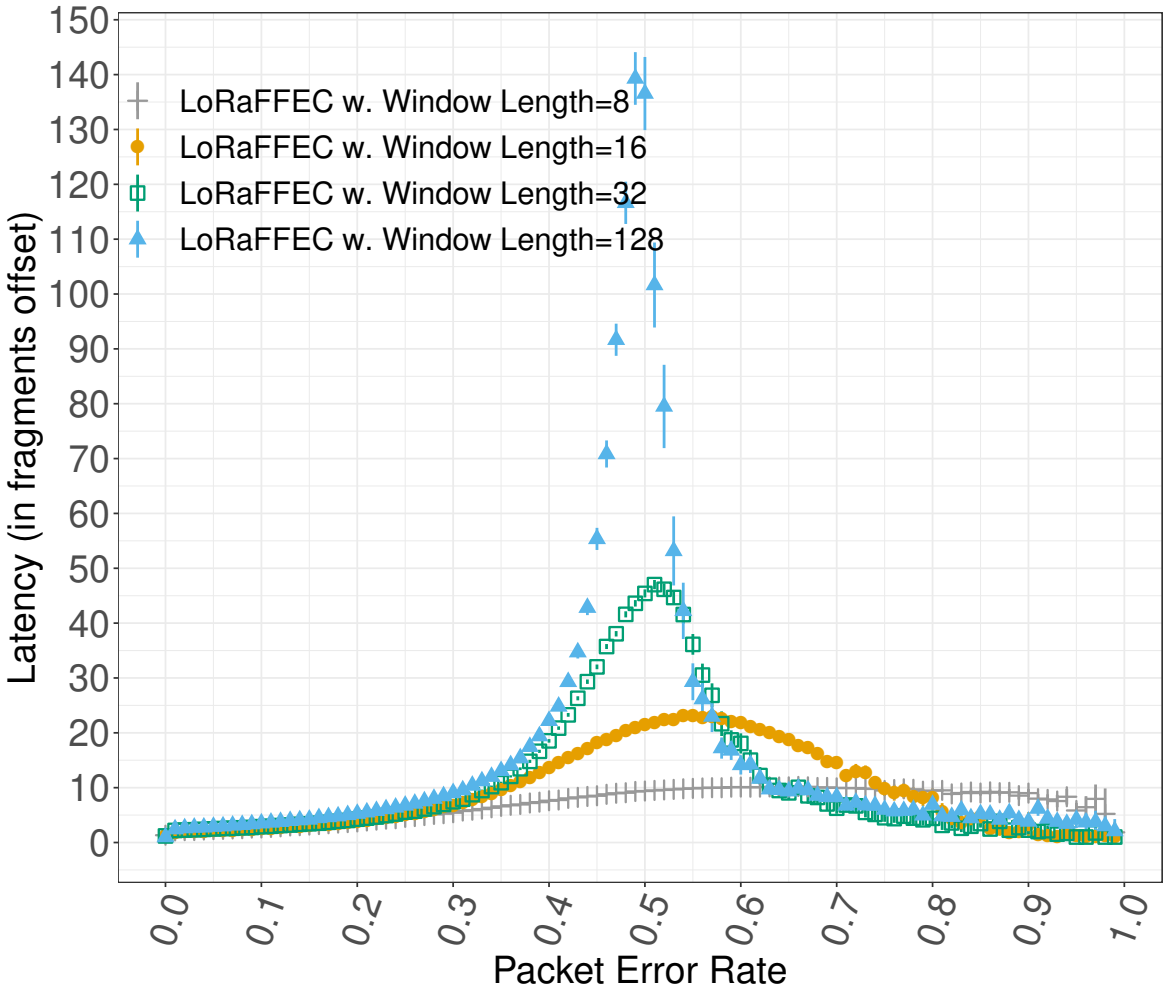

Figure 5.22: Simulated latency mean of LoRaFFEC (WL;0.6;2) as a function of *FER*.

Fig.5.23 compares the latency's cumulated frequencies of LoRaFFEC with $WL = 8$ and $WL = 128$ and over an erasure channel with $FER = 0.4$: the short window length ($WL = 8$) recovers more fragments with low latency ($latency < 35$), but at this point reaches a threshold and cannot recover more lost fragments. In the opposite, the longer window ($WL = 128$) keeps correcting lost data fragments for longer and up to full recovery (cumulated value = 1).

5.2.3 LoRaFFEC Experimental Results

LoRaFFEC is not yet deployed in the field but based on the field experiments from Chap.4 we evaluate LoRaFFEC in a real LoRaWAN traffic scenario. We replay the experimental collected stream applying LoRaFFEC on it and thus validate the potential benefit. For the sake of comparison, a simulation of LoRaWAN BSR with $Nb_{\text{Trans}} = 2$ is also computed.

Streams Replay Reconstructed Results

The first reconstructed transmission uses LoRaFFEC $(128, 0.6, 2 \times w)$, no fragmentation and no aggregation, i.e. data fragments and redundancy fragments, are sent in different frames. Fig.5.24

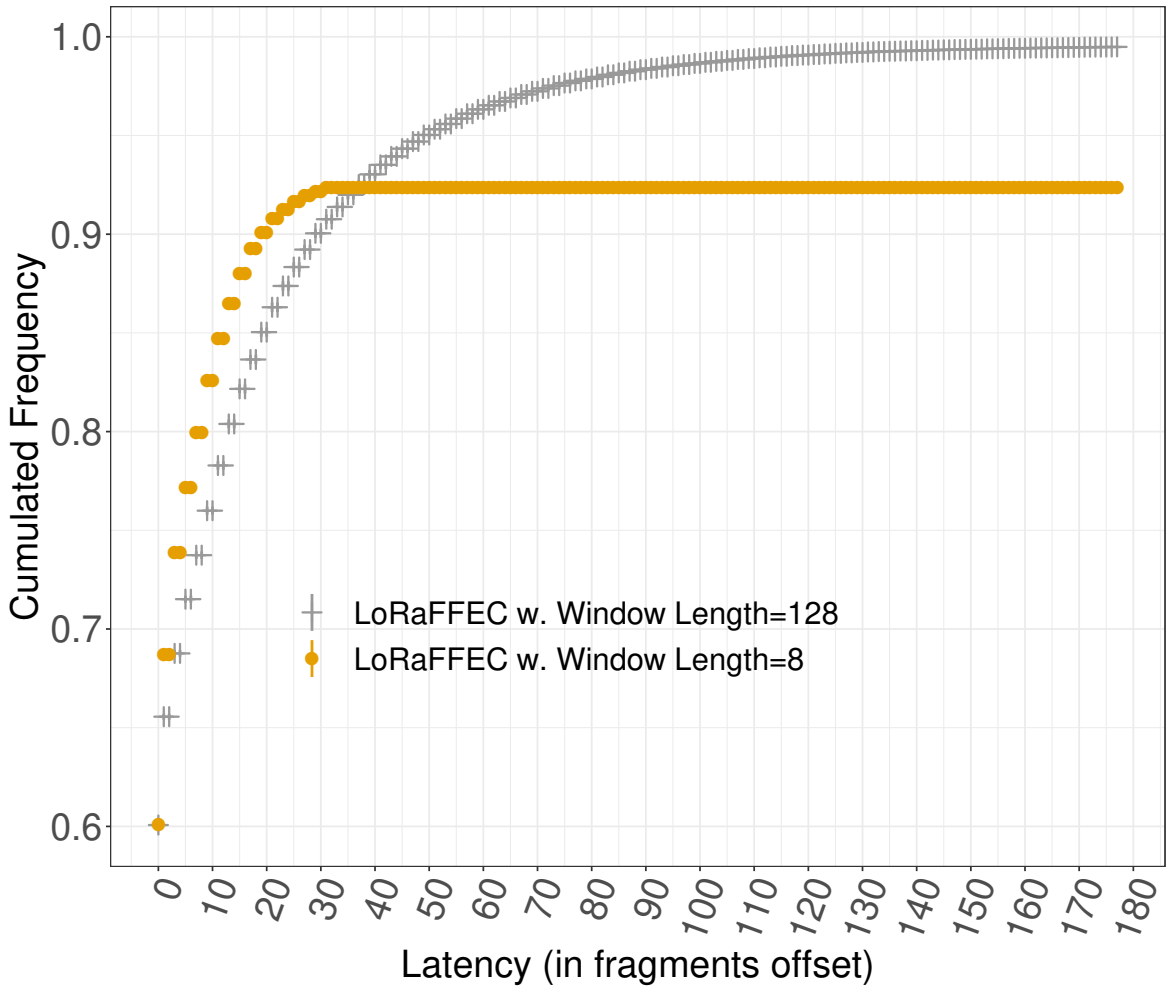

Figure 5.23: Simulated cumulative frequency of LoRaFFEC (WL;0.6;5) as a function of latency over an erasure channel with $FER = 0.4$.

plots the *DER* as a function of the *FER* for LoRaFFEC (128;0.6;256).

For comparison, the *DER* of transmission using LoRaWAN BSR with $Nb_{\text{Trans}} = 2$ is also plotted. The plots from experimental erasure patterns corroborate very closely the simulated results with i.i.d. erasure patterns discussed in Section 5.2.1. This allows to distinguish three practical scenarii that can guide LoRaFFEC usage in field deployments:

- Link $FER \in [0;0.4[$: with this link quality, LoRaFFEC is very efficient and provides $DER < 0.01$. With the same overhead, BSR with $Nb_{\text{Trans}} = 2$ is less reliable, with a *DER* difference comprised between a few percentage points up to more than 15 percentage points .
- Link $FER \in [0.4;0.6[$: in this case, LoRaFFEC *DER* increases toward the *FER*, crossing BSR with $Nb_{\text{Trans}} = 2$ *DER* for $FER \approx 0.47$ at $DER = 0.75$. With such "bad quality channel", it is difficult to ensure a high *DER* with a reasonable overhead. Other actions to reduce the *FER*, such as *SF* or P_{Tx} increase, need to be taken.
- Link $FER \in [0.6;1]$: LoRaFFEC does not provide any erasure recovery and LoRaWAN BSR is better but this very high *DER* range is already unpractical .

Overall, LoRaFFEC is very efficient in the $FER \in [0;0.4[$ range.

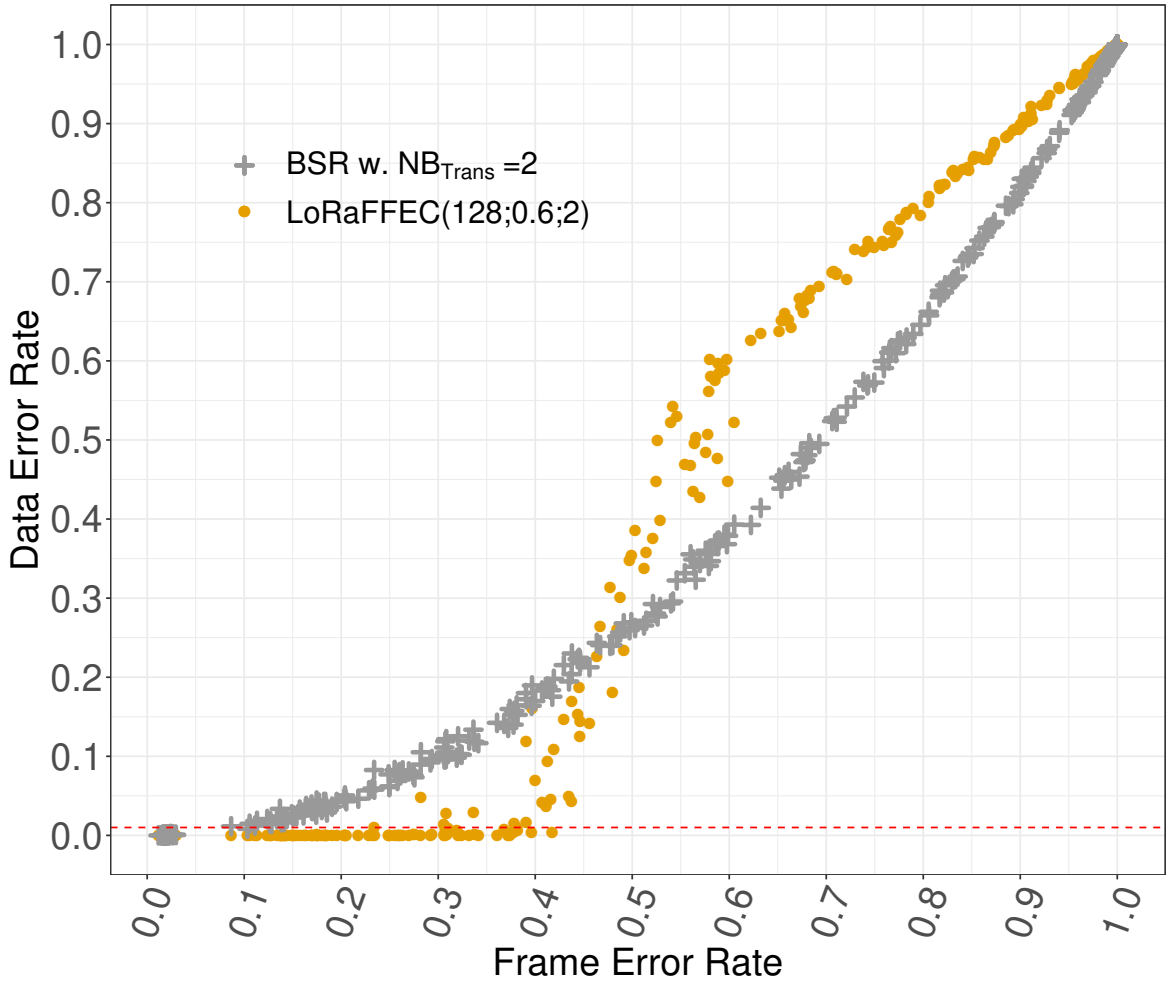

Figure 5.24: *DER* of LoRaFFEC (128;0.6;2) as a function of *FER* on experimental data streams, each dot is an independent experimental stream, with different GW, *SF*, P_{Tx} combination. The red dashed line marks the $DER = 0.01$ threshold.

Rare values are slightly out of the global trend: this may be explained by the length of the streams,

over seven days one can experiment a short period of harsh environment and *FER* will be temporally worse than its average value. The average *FER* of the stream may hide some variations of the channel over time (day and night shifts, professional occupancy, weather variations with cloudy humid days, etc.) [105]. For instance, the *FER* might be above 0.4 temporarily and for a bit too long, resulting in application level losses even if the overall *FER* if below 0.4.

Also, the comparison with the case of LoRaWAN BSR with $Nb_{\text{Trans}} = 2$, is favorable to LoRaFFEC only with $FER < 0.45$. Thus, from a reliability perspective, a mix of the two strategies(CP-ECC and BSR) would be effective.

This emphasizes the need for an appropriately tailored ADR to support LoRaFFEC: the LoRaWAN ADR should be triggered in order to increases Nb_{Trans} (along P_{Tx}, *SF*, and *CR*) and thus keep channel *FER* in a range where the LoRaFFEC protocol will ensure an almost null *DER*. We discuss this in Section 6.2.1.

5.3 Chapter Conclusion

In this chapter we proposed two novel approaches that improve LoRaWAN reliability by the means of CP-ECC.

The first proposed protocol, CCARR, uses Reed-Solomon codes and an intrinsic dynamic coding rate. The strength of CCARR is its ability to regulate itself according to the real effective channel *PER*. However, the price to pay is seldom segment-based downlink acknowledgments. Hence, CCARR provides high reliability over lossy channels with low overload on the network compared to the existing LoRaWAN strategy (BSR). As a result, for a given *PER* over the channel, the TOA is smaller with CCARR. For instance, in our experiments, CCARR (10,140) sustains $DER < 0.01$ over a $PER = 0.33$ channel with TOA increased by a factor 2.3 only due to the redundancy overload.

The second proposed protocol, LoRaFFEC, combines fragmentation and application-level error correction based on fragment pseudo-random combination. For instance, LoRaFFEC with coding rate $\frac{1}{2}$ reaches satisfactory data delivery ($DER < 0.01$) over channels with *PER* up to 0.4. However, LoRaFFEC is unable to exploit the redundancy if the *PER* is higher than this recovery threshold. Thus LoRaFFEC needs to be integrated within a tailored ADR to maintain the *PER* below the required threshold.

Both CCARR and LoRaFFEC performances are demonstrated over simulated channels and experimental deployment or reconstructed experimental erasure patterns frame streams.

CCARR and LoRaFFEC shows that using CP-ECC as a reliability layer on top of LoRaWAN stack has the ability to provide high reliability over a lossy channel. Moreover, this approach as the potential to relax the constraint on the EDs transmission parameters and thus use less conservative parameters and reduce the TOA within equivalent or even higher reliability. This opens new perspectives for ADR optimization and might lead to substantial improvement in network capacity while ensuring high reliability.

Chapter 6

LoRaWAN Adaptive Data Rate

Contents

Chapter Introduction

In this chapter, we re-invest and cross the results from chapters 4 and 5 to improve the ADR algorithm described in the section 2 in order to provide a reliable LoRaWAN connection at a large scale. That is to say that we are going to dynamically configure the network (the EDs transmissions parameters) to keep the *DER* low, while keeping the EDs TOA as low as possible as well. On the one hand we propose to optimize the "native" parameters of LoRaWAN (Nb_{Trans}, *SF*, P_{Tx}). On the other hand we propose to use the opportunity of using a CP-ECC to relax the constraints on the "native" parameters and this way achieve high reliability at lower TOA cost.

In this chapter, it is fundamental to keep in mind the precise definitions of the *FER*, the *PER* and the *DER*:

- The Frame Erasure Rate (*FER*) is the physical loss ratio between an ED and a given GW (i.e. without duplicate transmission from LoRaWAN BSR).
- The Packet Error Rate (*PER*) is the loss ratio between an ED and the NS. *PER* benefits from multiple GWs reception and frame duplicated transmissions from BSR.
- The Data Error Rate (*DER*) is the loss ratio between an ED and the AS, thus benefiting from the presence of an additional erasure recovery mechanism such as a CP-ECC.

6.1 Needs, constraints and levers for ADR optimization

As already described in Chapter 4, because of the multipath propagation, the LoRaWAN link is likely to follow a Rayleigh channel model. As a consequence, appropriate tuning of the *SF* and P_{Tx} is thus fundamental to obtain connectivity with a reasonable *FER*, but it is not sufficient to establish a highly reliable channel, as the link might be subject to an erasure floor of few percents. Hence, it is hopeless to only rely over P_{Tx} and *SF* increases to provide a high reliability with LoRaWAN.

It requires the use of an erasure recovery mechanism, either the LoRaWAN BSR with $Nb_{\text{Trans}} > 1$, or a CP-ECC algorithm. These erasure recovery mechanisms can be complementary and should be carefully used to exploit the full potential of each solutions.

See for instance in Fig.6.1 which plots the *DER*, for replayed experimental series with *SF* and Nb_{Trans} such that their TOA is roughly equivalent, with various P_{Tx} (and thus different P_{Rx} conditions). There is no best Nb_{Trans} and *SF* combination for all cases but rather locally best combination. However, when the GW is far (emulated by lower P_{Tx}), a configuration with high *SF* and low Nb_{Trans} provides better *DER* because the GW is simply out of range if using lower *SF*. When the GW is in a reasonable range (emulated by higher P_{Tx}) for lower *SF*, the tendency is quickly inverted and low *SF* with high Nb_{Trans} provides better *DER*. This shows the potential for complementary of the *SF* and Nb_{Trans} parameters to reach the best *DER* for a given TOA budget. Thus, this calls for a smart response against Rayleigh channels to avoid a counter-productive increase of *SF* or Nb_{Trans}.

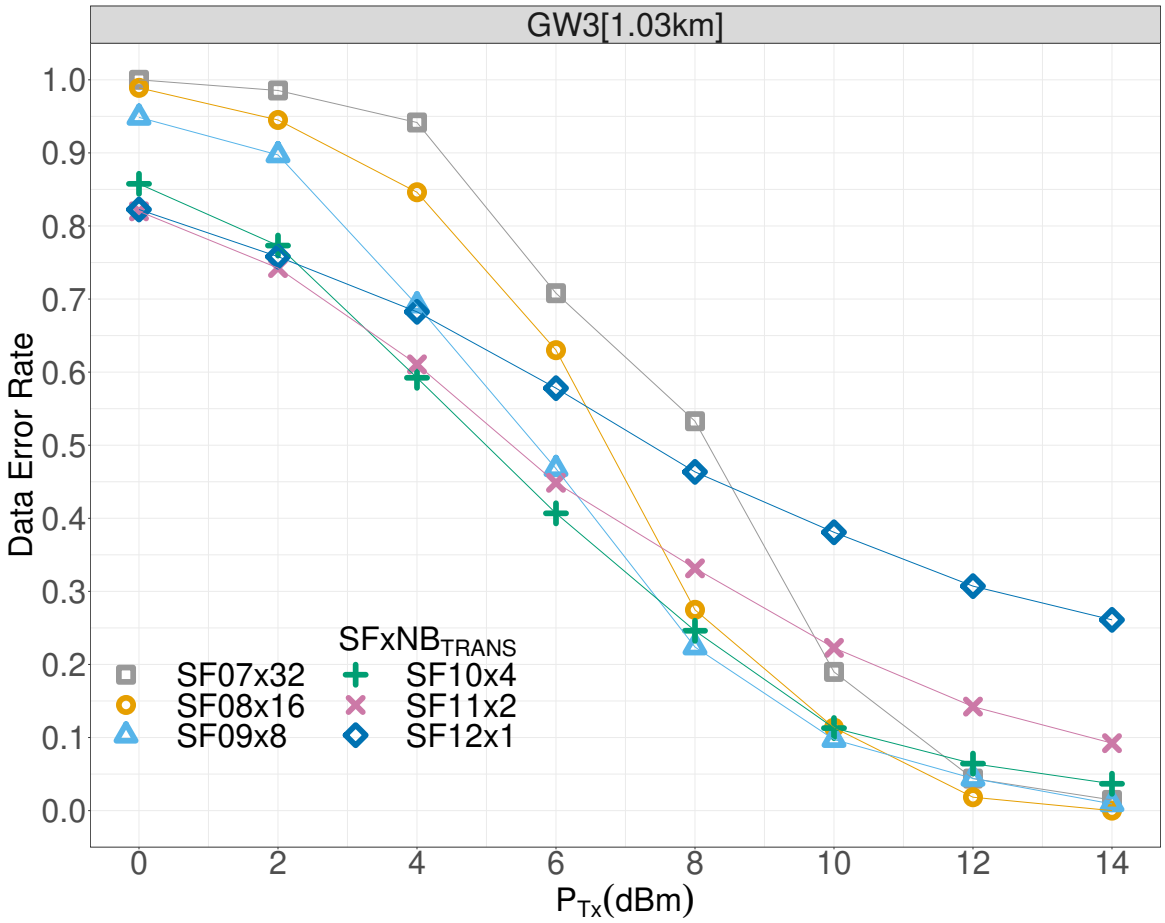

Figure 6.1: Experimental *DER* as a function of P_{Tx} using several combinations of *SF* and Nb_{Trans} with roughly equivalent TOA .

6.2 ADR for Single Gateway LoRaWAN Network

In this section we start by optimizing the ADR algorithm in the simplified context of a mono-GW LoRaWAN network.

6.2.1 Improving Adaptive Data Rate

Based on the insights gained previously, we design $ADR_{\text{opt-SG}}$, an improved version of ADR. It consists in a precise computation of the ADR algorithm's parameters (described in algorithms 1 and 2): MARGIN, PER_{High}, PER_{Med}, PER_{Low}, for LoRaMAC® using CP-ECC and LoRaWAN BSR.

We first turn our attention to evaluating the *PER* degradation due to the channel overload caused by BSR in a pure-Aloha network. Considering (unslotted) ALOHA access without capture effect [3], *DER* over the channel is defined as $P(\lambda T) = 1 - e^{-2\lambda T}$ where λ is the Poisson process intensity — the number of packets generated per second— and T is the average frame duration. The formula extends to Nb_{Trans} duplicated transmissions with:

$$P(Nb_{\text{Trans}}, \lambda T) = (1 - (e^{-2Nb_{\text{Trans}}\lambda T}))^{Nb_{\text{Trans}}}$$

This leads to $P(2, \lambda T) < P(1, \lambda T) < 0.4$ for $\lambda T \leq \frac{log(\frac{-1+\sqrt{5}}{2})}{-2} \approx 0.24$.

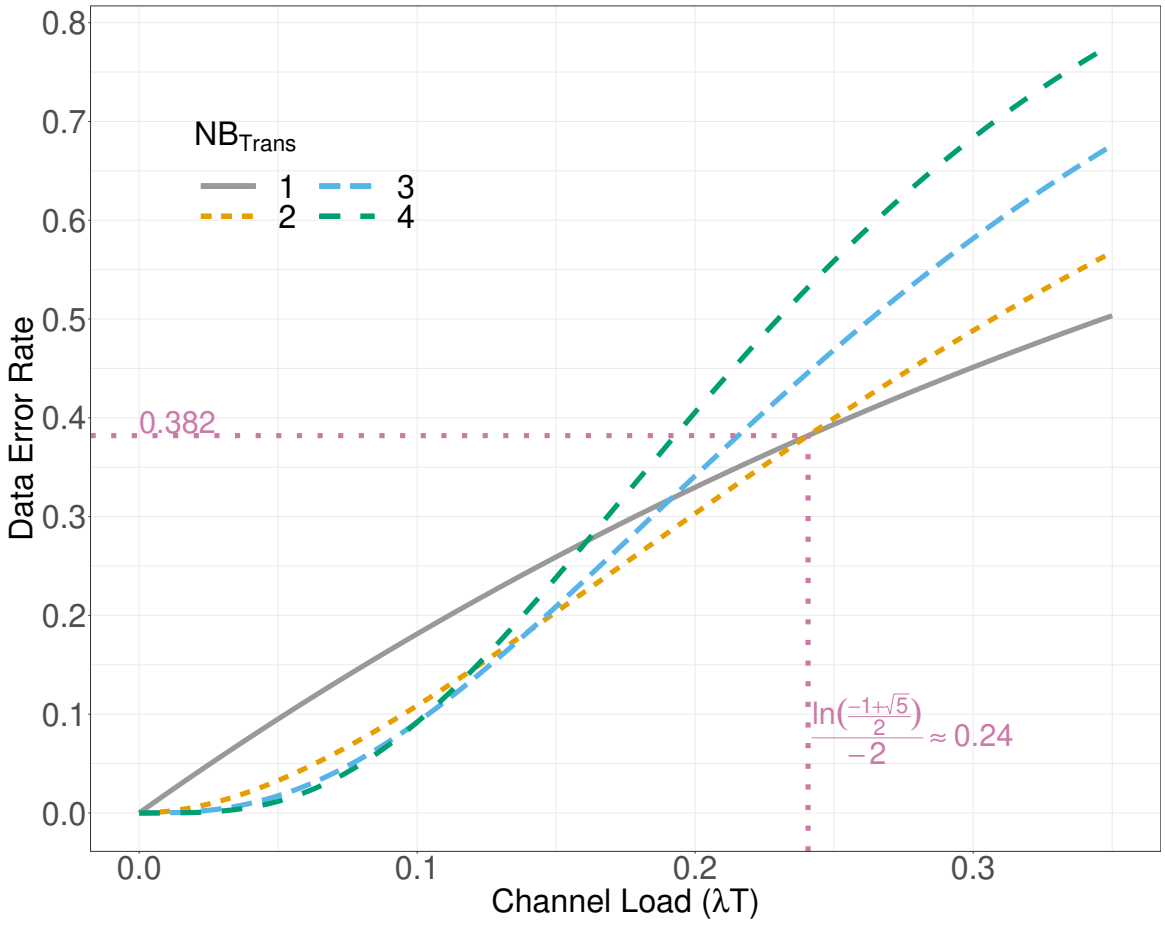

Figure 6.2: *DER* of an ALOHA network without capture effect as a function of the channel load for variousNb_{Trans} values.

We saw in Section 5.2 that LoRaFFEC (128;0.6;2) over a *PER* = 0.4 channel provides high reliabil-

ity, thus $ADR_{\text{opt-SG}}$ will be tailored to provide $PER < 0.4$ to the LoRaFFEC layer. Also, $x > 2$ only provides *DER* improvement over a low load channel and otherwise, performances quickly drop, as illustrated in Fig.6.2 with $P(x, \lambda T)$ computations. Thus, $ADR_{\text{opt-SG}}$ should operate mainly with Nb_{Trans} =2, with fluctuation up to 3 and down to 1 when the channel is either highly degraded or of high quality. Hence, LoRaFFEC will eventually operate with fitted *PER* and provide the high reliability. Thus, we set PER_{High}, PER_{Med} and PER_{Low} which are the threshold for Nb_{Trans} adaptation to respectively 10%, 30% and 70%. This way *PER* is maintained under 0.4 and this reduces the overall TOA.

Assuming a Rayleigh channel for LoRa, the *SNR* follows an exponential distribution with cumulative distribution function, $F(x) = 1 - e^{-x}$ (and its inverse $F^{-1}(x) = -log(1-x)$).

Notice that the NS estimates the link quality by taking the maximal *SNR* over the last 20 received packets without taking into account neither duplicates from BSR or losses. Hence, the effective sample's size increases with Nb_{Trans} and *FER*. Finally, 60 is an acceptable tradeoff to estimate the number of frames effectively used for the link quality estimation, as it matches the targeted functioning point Nb_{Trans} =2 and $PER \approx 0.4$.

Thus, we can compute $F^{-1}(0.9^{1/60}) = -log(1-0.9^{\frac{1}{60}}) \approx 6.3 \approx 10^{\frac{8}{10}}$, which means that there is 90% chances over the last 60 received frames, the maximal measured *SNR* is less than 8 dB over the $\overline{SNR}$.

Also, $F^{-1}((1-0.4)^{1/2}) = 1 = 0$dB, i.e, 0 dB is the *SNR* threshold such that $PER = 0.4$ with Nb_{Trans} =2. So, *MARGIN* = 8dB is a good approximation for $PER = 0.4$ with Nb_{Trans} =2, as it gives minimum TOA. Eventually, this *PER* is enough for CP-ECC to recover the remaining erasures as shown in Chapter 5.2.

Moreover we modify the initialization of the ADR: if the NS did not received enough packets, instead of introducing extra margin, it just waits for a minimum of 5 received packets before replying to the ED with an ADR command.

Without loss of generality, we disabled the power control as it only keeps P_{Tx} to its max unless *SNR* is strong enough and *SF* is already minimal which corresponds to unavailable data rate (SF=7 BW=250kHz or SF=6).

6.2.2 Performance comparison

First we show $ADR_{\text{opt-SG}}$ performances over a simulated Rayleigh channel. Then we confirm the results from simulation by emulating $ADR_{\text{opt-SG}}$ over our experimental series, i.e by replaying the real-world data-set gathered from the experiments described in chapter 4.

For simplicity, we assume a perfect downlink channel which allows to transmit all the ADR commands. We assume LoRaFFEC is used as CP-ECC and consider that payload's overhead is piggybacked into existing packets and so, the LoRa payload increases from 28 to 50 bytes[1]. Note that the frame size has little impact on the *FER* with such sizes (see Section 4.4) and so, we do not consider any *FER* penalty for longer frames.

The simulated Rayleigh channel is a serie of frames with a fixed *SNR* mean ($\overline{SNR}$), which correspond to fixed positions of the ED and the GW. For each frame f, $SNR_f = \overline{SNR} \times X$ where X is a unit mean exponential probability density function. Thus, a frame is dropped if $SNR_f < SNR_{\text{floor}}$.

[1] 13 (LoRaWAN headers) + 15 bytes to 13+1+(15+3)×2 = 37 bytes of payload respectively without and with LoRaFFEC.

We simulate it for $\overline{SNR}$ in [-30 dB, 10 dB] by steps of 0.5 dB with series of 5000 frames, each experiment is repeated 50 times.

We simulated $ADR_{\text{opt-SG}}$ and ADR_{TTN} in a single GW LoRaWAN network with Rayleigh channel and $\overline{SNR}$ ranging from -30dB to 10dB. We do not simulate congestion on the network. Figure 6.3 plots the simulated *DER* and TOA of $ADR_{\text{opt-SG}}$, ADR_{TTN}.

$ADR_{\text{opt-SG}}$ sharply adapts the transmission parameters and provides $DER < 0.01$ over a channel with $\overline{SNR} > -21.5\,dB$. This corresponds to SF =12 with LoRaFFEC (128;0.6;2) and Nb_{Trans} =3, sort of "Maximal Effort" policy result in this context. However, $ADR_{\text{opt-SG}}$'s TOA is higher than ADR_{TTN}'s for channel with $\overline{SNR} \leq -17\,dB$. This corresponds to the extra energy invested by $ADR_{\text{opt-SG}}$ to achieve a reliable communication. For channel with $\overline{SNR} > -17\,dB$, the transmissions parameters of $ADR_{\text{opt-SG}}$ are more accurate and thus reliability is obtained with lower TOA .

$ADR_{\text{opt-SG}}$ performances over real world series of transmissions are shown in figures 6.4 and 6.5. The results real-world traces results confirm the simulations: $ADR_{\text{opt-SG}}$ provides adequate tuning for the transmissions and either $DER < 0.01$ is achieved or a most robust available configuration is used. Except for GW7, $DER < 0.01$ is reach for every GW with $P_{\text{Tx}} > 6\,dBm$. However, in some rare cases (for GW 3 and 6 at P_{Tx} 2 and 4 dBm), $ADR_{\text{opt-SG}}$ slightly under-performs because the variations of the channel conditions are faster than the adaptation rate.

From experiments and models, $ADR_{\text{opt-SG}}$ proposes large optimizations of the LoRaWAN ADR using both LoRaFFEC and carefully computed parameters. $ADR_{\text{opt-SG}}$ software protocol successfully provides high reliability, with $DER < 0.01$ in LoRaWAN networks even over channel with low $\overline{SNR}$. The proposition is validated both by simulation and experimental channel transmissions replays. Moreover, $ADR_{\text{opt-SG}}$ employs no more additional downlinks than the legacy LoRaWAN ADR. $ADR_{\text{opt-SG}}$'s TOA is bounded by the maximal effort configuration which advocates for its scalability and makes it realistic for real life deployment.

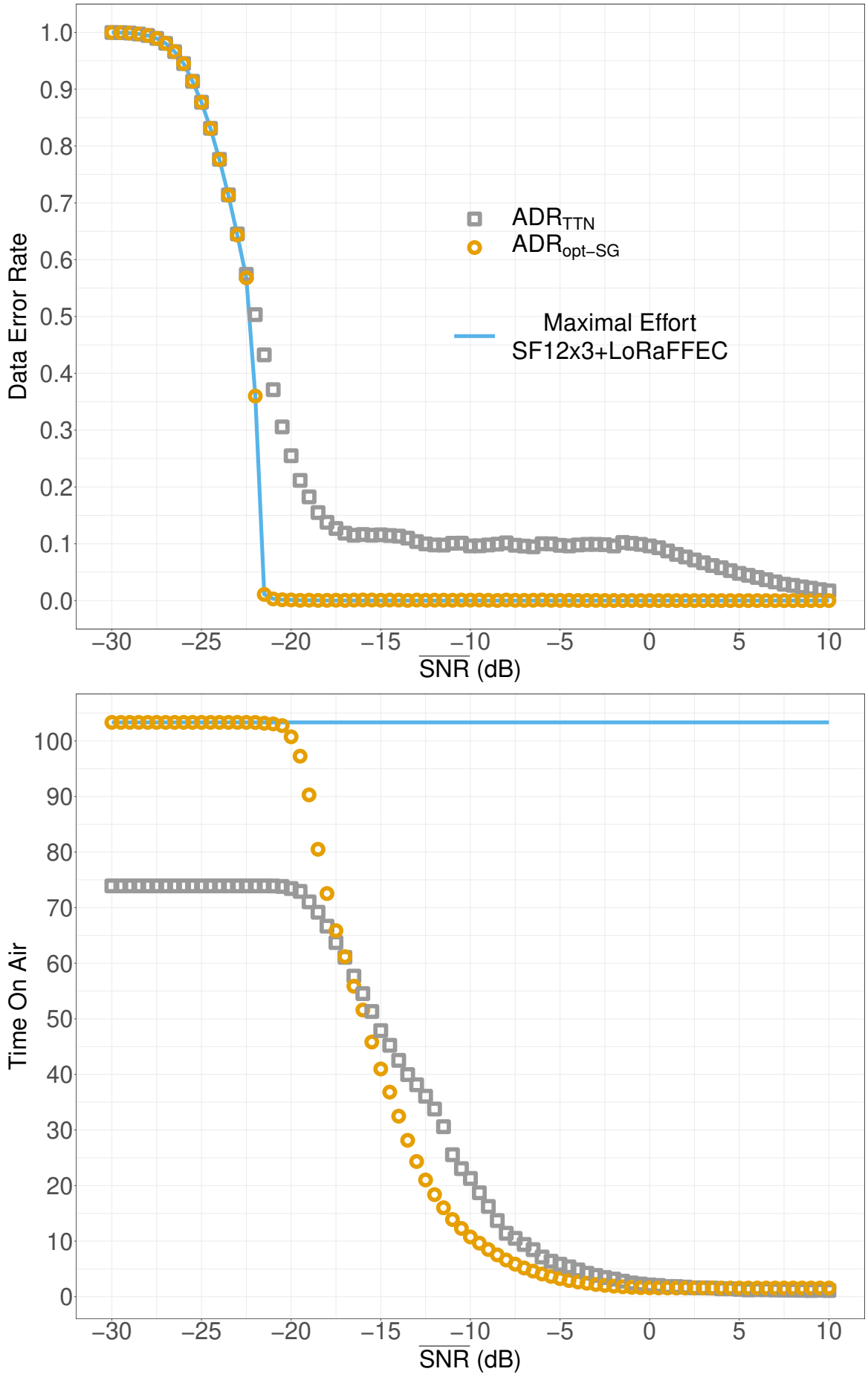

Figure 6.3: Simulation results for *DER* and TOA as a function of $\overline{SNR}$ for $ADR_{\text{opt-SG}}$ and ADR_{TTN} in a single GW LoRaWAN networks.

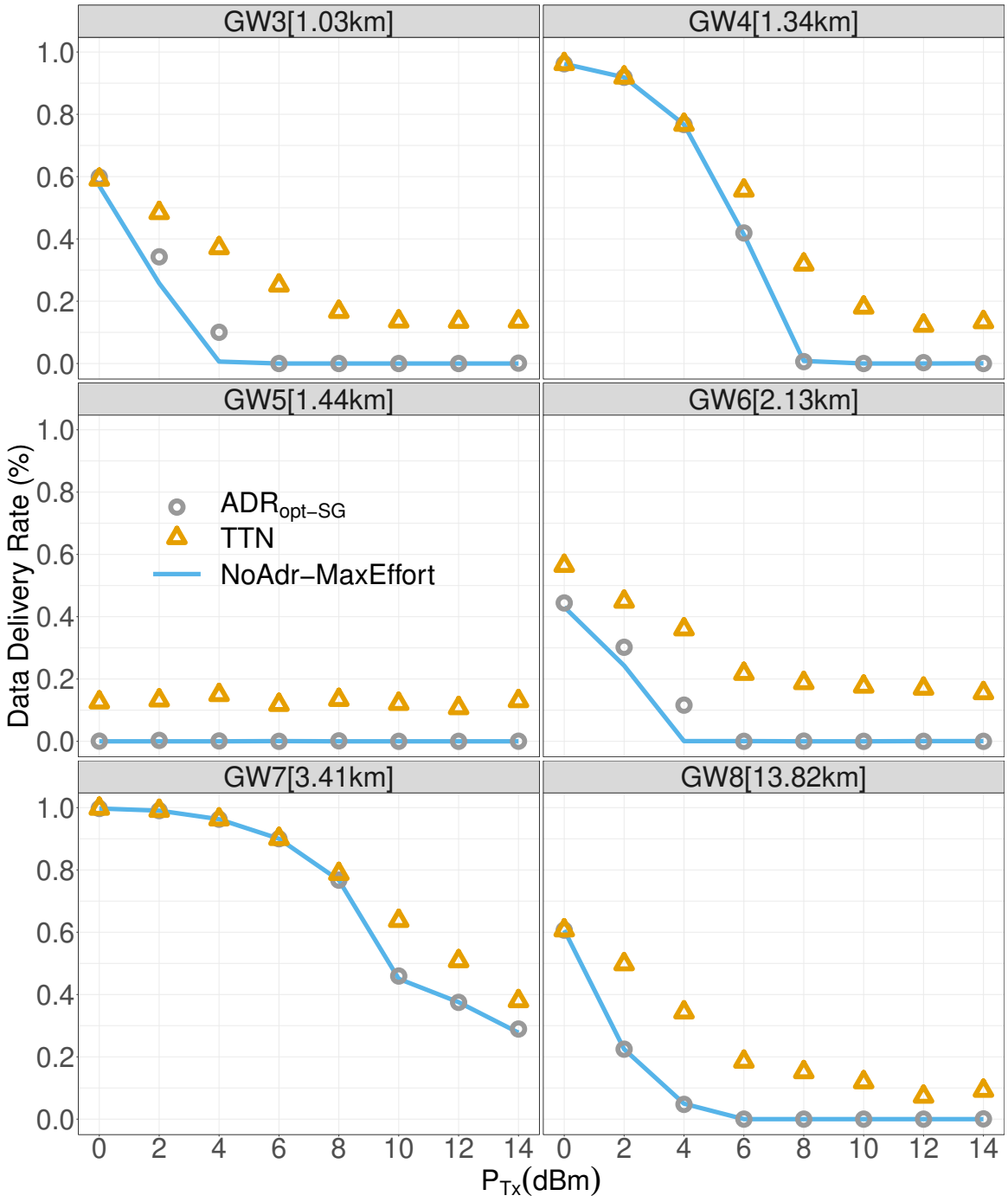

Figure 6.4: *DER* of $ADR_{\text{opt-SG}}$ over replayed real world series of packets for several GW.

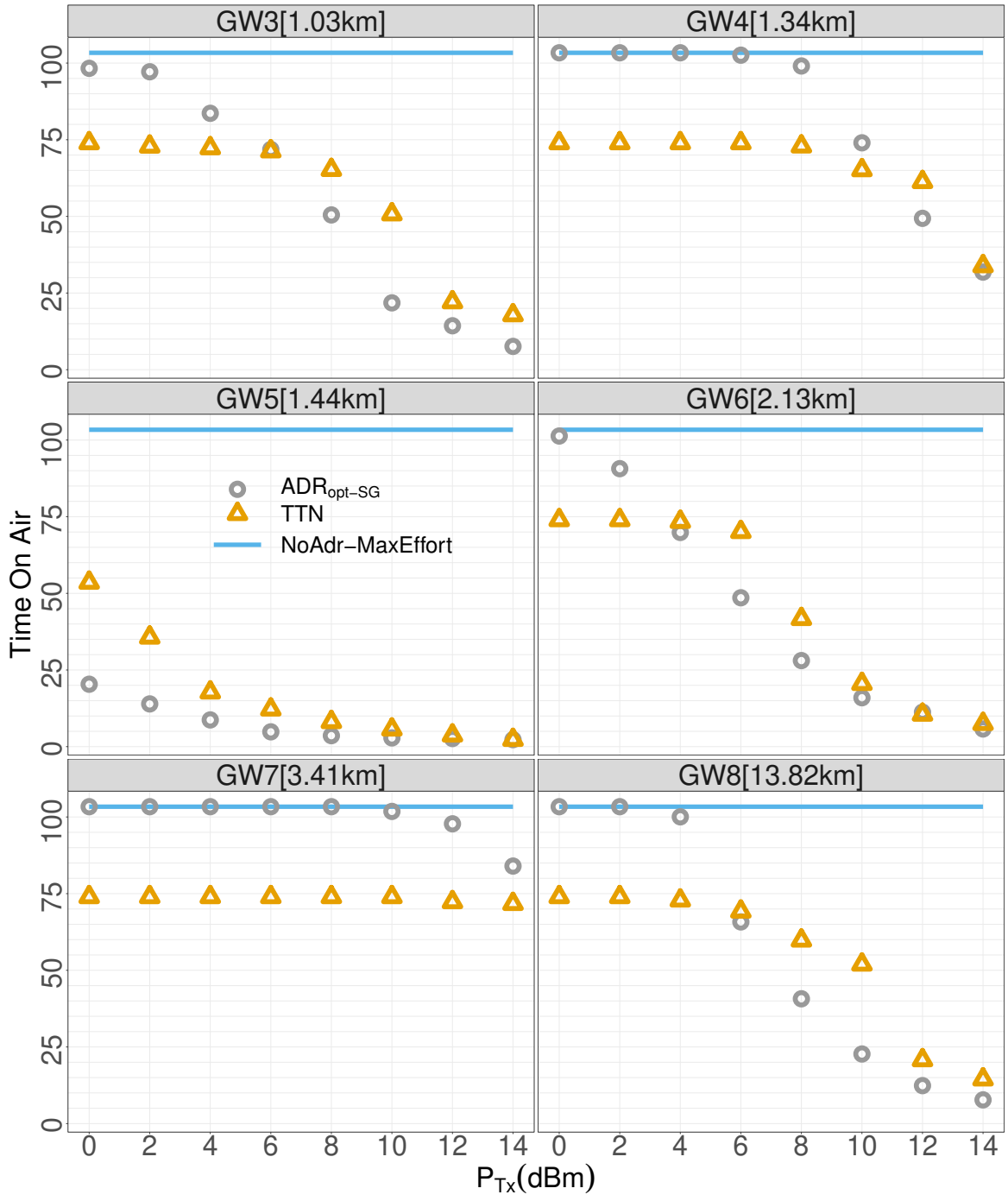

Figure 6.5: TOA of $ADR_{\text{opt-SG}}$ over replayed real world series of packets for various GW. TOA normalized against no FEC, SF7 and Nb_{Trans} =1, for several GW.

6.3 ADR for Multiple Gateways LoRaWAN Network

In this section, we deepen the $ADR_{\text{opt-SG}}$ optimization proposal from section 6.2. In particular we extend the optimization to fully take into account the case of a multi-GW LoRaWAN cells, and thus fully exploit the LoRaWAN's natural macro-diversity.

6.3.1 $ADR_{\text{opt-MG}}$ a Configurable and Optimized ADR

First, we propose $ADR_{\text{opt-MG}}$, an NS-side flexible ADR algorithm, optimized for Rayleigh channel model. $ADR_{\text{opt-MG}}$ is flexible in the sense that it is configurable to target any given *PER* (PER_{target}). The EDs transmissions parameters will be tuned to reach PER_{target} with minimized TOA. $ADR_{\text{opt-MG}}$ uses "raw" LoRaWAN, i.e. no additional CP-ECC layer is used.

6.3.1.1 $ADR_{\text{opt-MG}}$ Algorithm

For the sake of simplicity we restrain the available transmission configurations to any combinations of $SF \in \{7..12\}$, $CR = \frac{4}{5}$ and $Nb_{\text{Trans}} \in [1..3]$ with $BW = 125$kHz and $CF \in \{868.3, 868.5, 868.8\}$MHz. Finally, we consider a constant P_{Tx}, as it is reduced from its maximal value only when the signal is very strong and both *SF* and Nb_{Trans} are set to the lowest values, thus P_{Tx} has little influence on the performance of ADR in terms of *PER* and TOA.

$ADR_{\text{opt-MG}}$, detailed in 7, extrapolates a presumable *PER* for each $[SF; Nb_{\text{Trans}}]$ pair from the observation on the channel over the previous transmission period. $ADR_{\text{opt-MG}}$ then chooses the transmission parameters to maintain *PER* just below the target level PER_{target}.

The $ADR_{\text{opt-MG}}$ *FER* estimation function is based on the assumption that the channel is Rayleigh as described in section 4.2. In the following, we refer to $\widehat{SNR}$ as the computed extrapolation, therefore imperfect, of $\overline{SNR}$. For a given GW, we can compute $\widehat{SNR}$ over a period of time. Assuming that the channel does not change drastically for the next period, we can compute the expected *FER* for any transmission parameters. And eventually, with the assumption that each transmission and reception by different GWs are independent, we can extrapolate the *PER* by combining the *FER* for each of the GWs in the reception range of the transmitting ED.

Because a loaded network would distort the estimation of $\widehat{SNR}$ from the observed *FER*, we choose to rely on another characteristic of the exponential distribution that would not suffer such bias: the highest received *SNR*: SNR_{max}. As the channel history buffer keeps a limited number of received frames[2], we have to compute what would be the size of the sample ($Size_{sample}$) with its censored part, i.e. the erased frames:

$$Size_{sample} = \frac{20}{(1 - FER_{\text{current}})} \times Nb_{\text{Trans}}$$

We then estimate what would be the maximal value of such a sample following Unit Mean Exponential Distribution (UMED). We approximate the theoretical $SNR_{\text{Max}}(S_{\text{UMED}})$ by $SNR_{\approx\text{Max}}(S_{\text{UMED}})$ that we define as the middle of the interval in which there is 90% chances that this maximum *SNR* lies, with $Size_{sample}$trials:

[2]The TTN NS keeps only the last 20 frames.

$$SNR_{\approx \mathrm{Max}}(S_{\mathrm{UMED}}) = \frac{\left(10 \times \log_{10}\left(CDF_{\mathrm{exp}}^{-1}\left(0.95^{(1/Size_{sample})}\right)\right)\right)}{2} + \frac{\left(10 \times \log_{10}\left(CDF_{\mathrm{exp}}^{-1}\left(0.05^{(1/Size_{sample})}\right)\right)\right)}{2}$$

From this we estimate $\widehat{SNR}$ in dB:

$$\widehat{SNR} = ChHistory_{GW}(SNR_{\mathrm{max}}) - SNR_{\approx \mathrm{Max}}(S_{\mathrm{UMED}}).$$

We combine this $\widehat{SNR}$ with the typical *SNR* demodulation floor of LoRa [168]:

$$SNR_{\mathrm{floor}<SF>} = (-20) + ((12 - SF) * 2.5).$$

Thus $\widehat{FER_{<GW_i;SF>}}$, the estimated *FER* between the ED and GW_i using the given *SF*, is:

$$\widehat{FER_{<GW_i;SF>}} \approx CDF_{exp}(10^{\left(\frac{SNR_{\mathrm{floor}<SF>} - \widehat{SNR}}{10}\right)}).$$

Which leads to $\widehat{PER_{<Nb_{\mathrm{Trans}};SF>}}$,

$$\widehat{PER_{<Nb_{\mathrm{Trans}};SF>}} \approx \prod_{\forall GW_i} (\widehat{FER_{<GW_i;SF>}})^{Nb_{\mathrm{Trans}}}$$

These formulae compute an accurate approximation of the *FER* between the ED and a given GW and consequently the *PER* between the ED and the NS, for each available transmission parameters combination.

With $ADR_{\text{opt-MG}}$ the PER_{target} is an input parameter of the algorithm that can be fixed to an arbitrary value. Thus $ADR_{\text{opt-MG}}$ adapts to arbitrary reliability needs.

6.3.1.2 $ADR_{\text{opt-MG}}$ Simulation

We assume a perfect downlink channel which allows to transmit all the $ADR_{\text{opt-MG}}$ piggybacked commands and parameters into downlink ACKs. The Rayleigh channel describes a series of frames with a fixed *SNR* mean ($\overline{SNR}$), which corresponds to fixed positions of the ED and the GW. For each frame f, $SNR_f = \overline{SNR} \times X$ where X is a random variable following the UMED distribution function. Thus, a frame is dropped if $SNR_f < SNR_{\mathrm{floor}<SF>}$. We simulate this for $\overline{SNR}$ in $[-30..10]_{dB}$ by steps of 0.5 dB with series of 6000 frames repeated 60 times.

$ADR_{\text{opt-MG}}$ performance over the simulated Rayleigh channel appears in Fig. 6.7 and Fig. 6.6 in presence of 1, 2, 4 and 8 GWs when the $\overline{SNR}$ to all GWs are equal. Notice that in a configuration with unequal $\overline{SNR}$, GWs with relatively low $\overline{SNR}$ bring little benefits: the overall performances tend to be the performances of a network with only the best $\overline{SNR}$ GW, i.e. most of the time the closest ones.

$ADR_{\text{opt-MG}}$ sharply adapts the transmission parameters to reach PER_{target}. We distinct three cases:

- $\overline{SNR}$ is too low and PER_{target} cannot be met. In this case, $ADR_{\text{opt-MG}}$ uses the most robust and most TOA expensive transmission configuration available. The ability to meet the required PER_{target} is conditioned by the most robust available configuration. The most robust parameters combination is, in our case, SF =12 with Nb_{Trans} =3. It is also conditioned by the

Algorithm 7 $ADR_{\text{opt-MG}}$-Server algorithm.

ChHistory(20) // Initialization of the list of the last 20 frames received.
PER_{target}
while true **do**
    ACK_Req=waitRx();
    if (ACK_Req) **then**
        // Compute a prediction of the *PER* for each configuration.
        for all $GW \in$ receptionGW(*ChHistory*) **do**
            for $SF \in \{7;8;9;10;11;12\}$ **do**
                FER = estimateFer(*GW*, *SF*, *ChHistory*)
                for $Nb_{\text{Trans}} \in \{1;2;3\}$ **do**
                    $PER_{\text{predic}}[SF; Nb_{\text{Trans}}] *= FER^{Nb_{\text{Trans}}}$;
                end for
            end for
        end for
        $PER_{\text{local target}} = PER_{\text{target}}$;
        PER_{current} = getPER(*ChHistory*);
        if $PER_{\text{current}} > PER_{\text{target}}$ **then**
            // A CP-ECC layer may fail to recover all the lost frames if PER falls below the recovery threshold for too long, thus $PER_{local\ target}$ *is reduced to better compensate erasures and achieve recovery.*
            $PER_{\text{local target}}$ = max(0.01,PER_{target}-(PER_{current}-PER_{target});
        end if
        //Choose the best configuration that fits the PER requirement and minimal ToA.
        setValidLowestToAConfig(PER_{predic}, $PER_{\text{local target}}$)
    end if
end while

number of GWs in range.

- $\overline{SNR}$ is medium and PER is just above PER_{target}. In this case, $ADR_{\text{opt-MG}}$ uses the transmission configuration corresponding to the smallest TOA while meeting the reliability requirement. There are PER fluctuations due to the discrete nature of available configurations and their corresponding reliability. These fluctuations therefore also depend on the slope of the CDF_{exp} at the targeted focal point PER_{target}. These fluctuations are accentuated by the number of GWs.

- $\overline{SNR}$ is high and PER is far below PER_{target}. In this case, $ADR_{\text{opt-MG}}$ uses the least TOA intensive transmission configuration, SF =7 with Nb_{Trans} =1, and this ED will over perform in terms of reliability.

Fig. 6.6 and Fig. 6.7 also compare $ADR_{\text{opt-MG}}$ with the TTN ADR default implementation (ADR_{TTN}). ADR_{TTN} reduces the SF whenever with a default margin of 15 dB. Besides, ADR_{TTN} increases and decreases Nb_{Trans}, with a ceiling at Nb_{Trans} =3, whenever FER <0.7 and FER >0.9, respectively. ADR_{TTN} relies on the EDs loss of connectivity denoted by the lack of downlinks (96 by default) to increase the SF and thus regain connectivity. More details of the ADR_{TTN} algorithm can be found in previous works [140, 142].

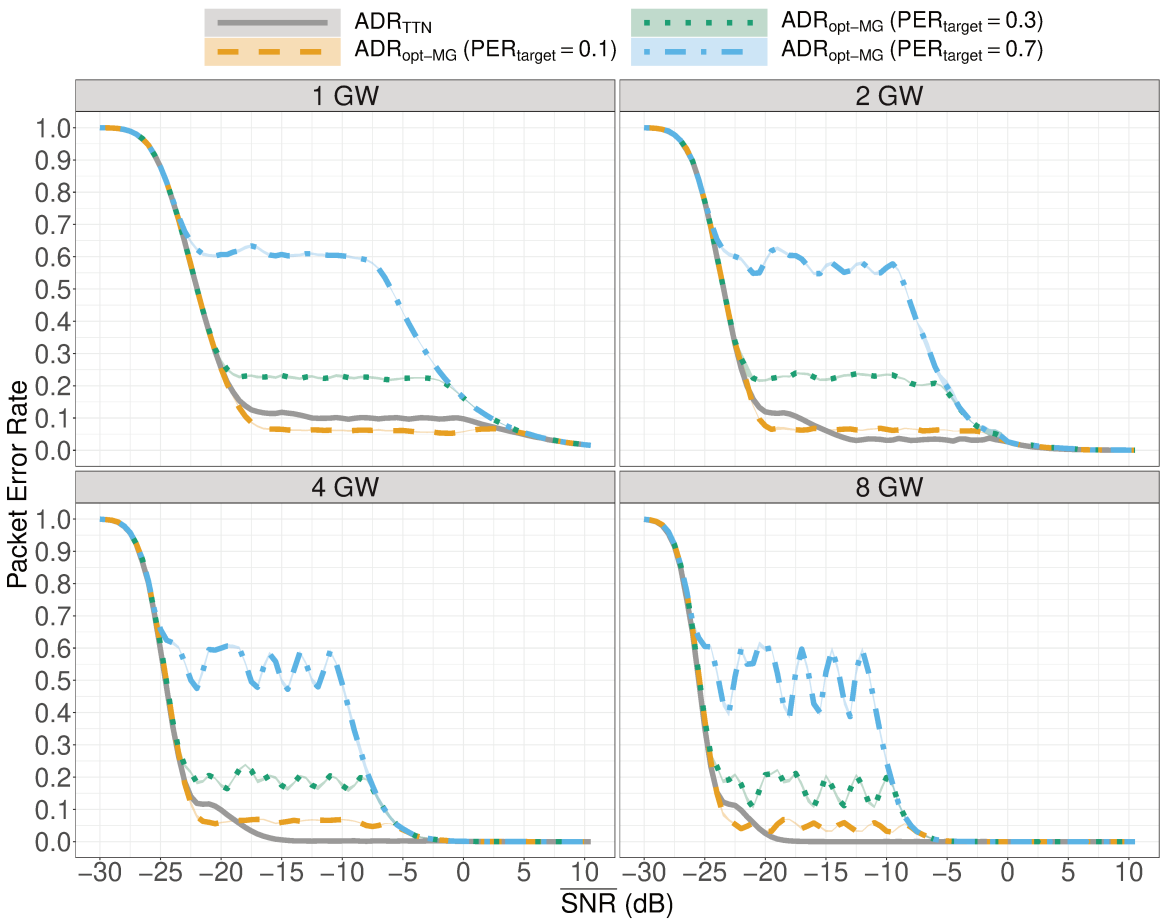

Figure 6.6: DER as a function of $\overline{SNR}$ for the simulated series of frames with multiple GWs (99% confidences interval plots).

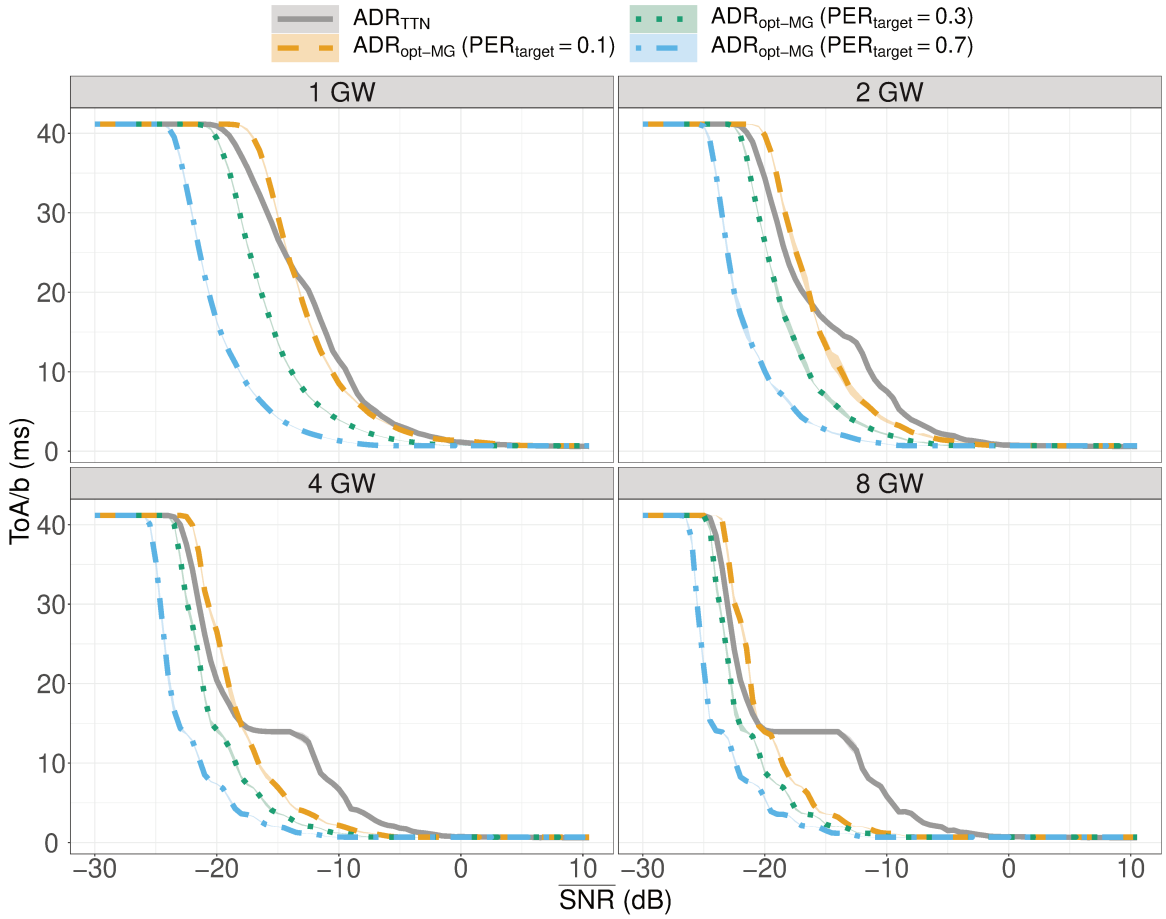

Figure 6.7: *ToA/b* as a function of $\overline{SNR}$ for the simulated series of frames with multiple GWs (99% confidences interval plots).

6.3.1.3 $ADR_{\text{opt-MG}}$ on Replayed Traces

We ran the experiments over several subsets of our real world transmission records described in chapter 4. It appears that the reachable GWs can be classified following their *SNR* range. Fig. 6.8 and Fig. 6.9 show the results for these subsets: GWs 5 and 6 that have low *SNR* (respectively $\overline{SNR} \approx -8.1$ dB and $\overline{SNR} \approx -12.1$ dB with P_{Tx} =14dBm), GWs 9 and 17 that have medium *SNR* (respectively $\overline{SNR} \approx -5.8$ dB and $\overline{SNR} \approx -6.6$ dB with P_{Tx} =14dBm), GWs 2 and 7 that have high *SNR* (respectively $\overline{SNR} \approx 4.6$ dB and $\overline{SNR} \approx -0.4$ dB with P_{Tx} =14dBm), and finally the aggregation of GWs 2, 5, 6, 7, 9 and 17.

The results derived from our real world transmission traces confirm the simulations of section 6.3.1.2. For any subset and P_{Tx} configuration, $ADR_{\text{opt-MG}}$ provides adequate tuning for the transmissions and either $PER < PER_{\text{target}}$ is achieved or the most robust available configuration is used. Notice that the performances for the subset with GWs 2, 3, 4, 5, 6 and 8 is strongly dominated by the GWs providing the best signal reception, i.e. GWs 2 and 3. As a consequence, its performances is just slightly better than the subset with GWs 2 and 3.

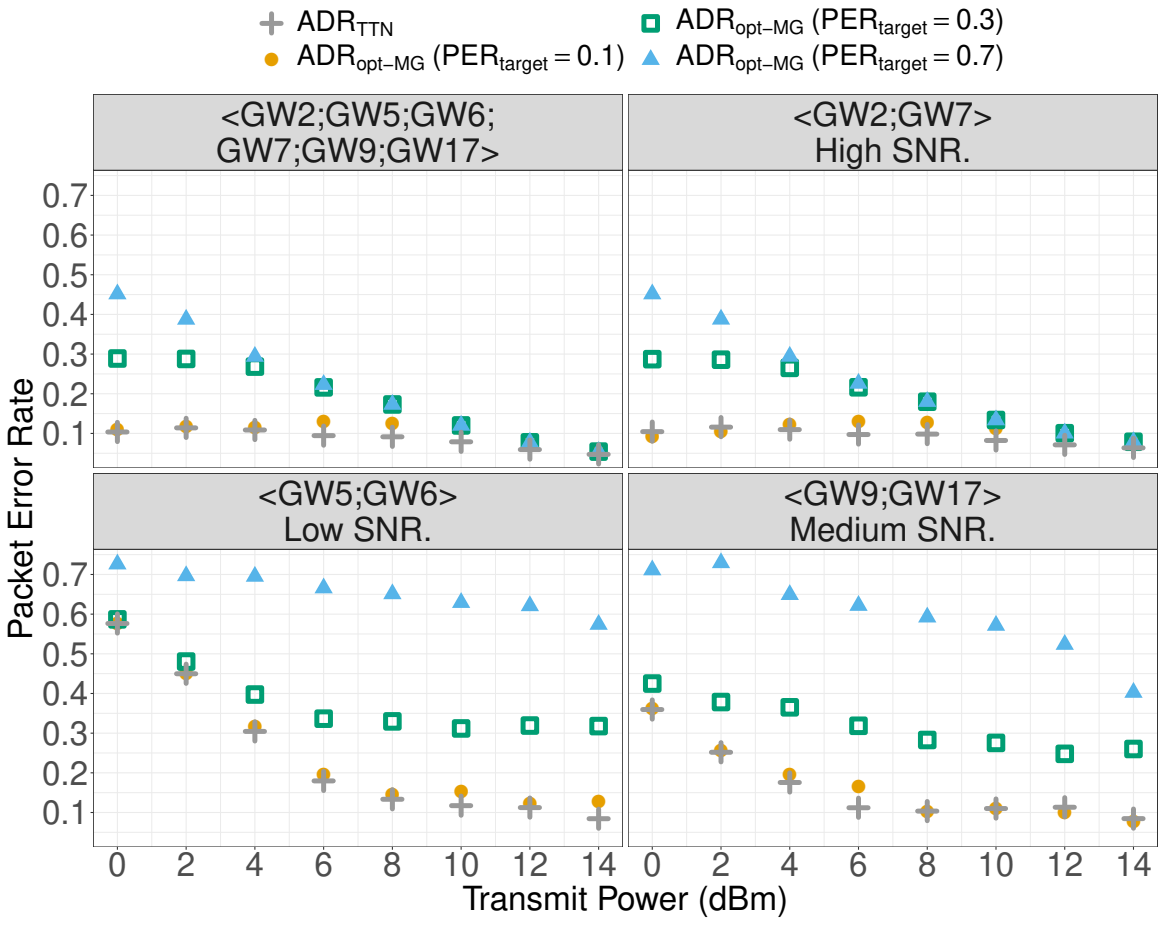

Figure 6.8: *DER* as a function of P_{Tx}, for selected real world series of frames replays.

6.3.2 ADR_{HR} for High Reliability

6.3.2.1 Cross-frame ECC for LoRaWAN

In the following, we refine $ADR_{\text{opt-MG}}$ with the additional use of a CP-ECC layer, to provide highly reliable LoRaWAN communication ($DER < 0.01$) with minimized TOA.

We choose to use CP-ECC scheme based on a linear combination of packets, LoRaFFEC described

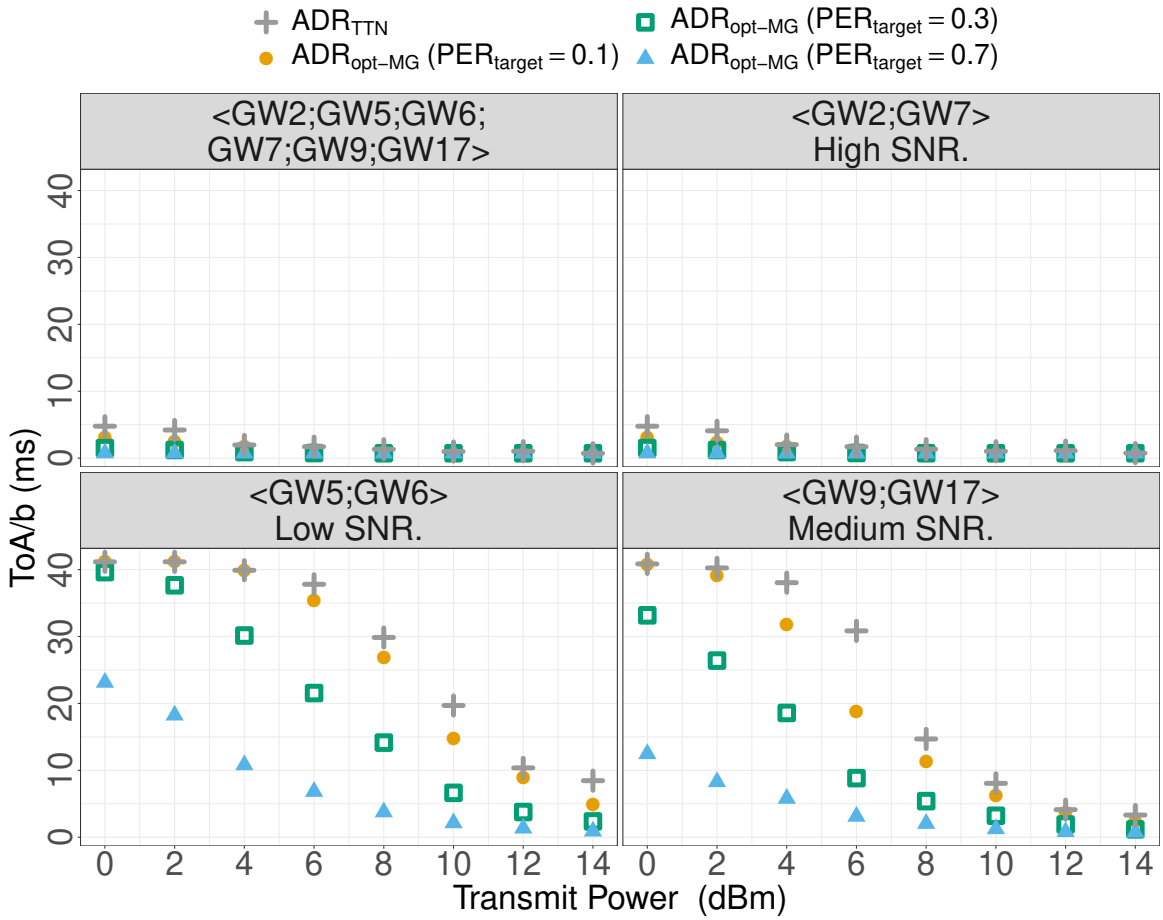

Figure 6.9: *ToA/b* as a function of P_{Tx}, for selected real world series of frames replays.

in section 5.2, which is efficient to recover the typical residual errors from a Rayleigh channel up to $PER \approx 0.3$. We use LoRaFFEC (128;0.6;2), which spreads the redundancy over 128 frames and so, introduces more time diversity. Notably, the redundancy spreading is higher than the default ADR downlink transmission period[3]. Moreover, LoRaFFEC does not require additional downlink signaling. The redundant data overhead of LoRaFFEC, can either be transmitted in separate frames or piggybacked into existing ones. Here, we choose to piggyback, as the LoRa and LoRaWAN headers overhead are then paid only once, which improves the *ToA/b*. The frame are lengthened[4] by a ratio < 2 and so, the sensitivity loss is not prohibitive as it stays less than one dB as detailed in Sec. 4.4.

$ADR_{\text{opt-MG}}$ is set to keep the *PER* above the correction threshold of LoRaFFEC (128;0.6;2), i.e. PER_{target} =0.3 in our case [5]. LoRaFFEC (128;0.6;2) recovers the remaining erasures and provides high reliability with *DER* <0.01.

We call ADR_{HR} this combination of LoRaFFEC (128;0.6;2) with $ADR_{\text{opt-MG}}$.

6.3.2.2 ADR_{HR} Simulation

We compare the performances of ADR_{HR} with ADR_{TTN} the default ADR implementation of TTN. We consider 15 bytes application payload. For the sake of simplicity we do not take into account the sensitivity impact of the varying frame length. The simulated channel is the same as in section 6.3.1.2.

ADR_{HR} performance over the simulated Rayleigh channel appears in figures 6.11 and 6.10 in presence of 1, 2, 4 and 8 GWs when the $\overline{SNR}$ to all GWs are equal. ADR_{HR} sharply adapts the transmission parameters to reaches *DER* <0.0.1. For instance, in figure 6.11 ADR_{HR} provides $DER < 0.01$ over a single GW network with $\overline{SNR} \geq -21.5$ dB. This threshold is reduced as the number of GWs increases. ADR_{HR} provides $DER < 0.01$ over an 8 GWs network with $\overline{SNR} \geq -25$ dB to all GWs.

However, as shown in figure 6.11, ADR_{HR} TOA is higher than ADR_{TTN} for channels with low $\overline{SNR}$ (-17 dB and -23 dB for respectively 1 or 8 GWs). This corresponds to the extra energy invested by ADR_{HR} to achieve a more reliable communication than ADR_{TTN}. For higher $\overline{SNR}$ values, the transmission parameters adjustments of ADR_{HR} are more fine-grained and the same reliability is obtained for lower TOA as shown in figure 6.11.

6.3.2.3 ADR_{HR} on Replayed Traces

The results from real world traces replay, with same subset as in Sec. 6.3.1.3 shown in Fig. 6.12 and Fig. 6.13 confirm the simulation results. Either the most robust transmission parameters are used or *DER* <0.01 is achieved.

[3] Limited to ACK_LIMIT+ACK_DELAY=96 frames.

[4] A 15 bytes application payload needs 53 symbols at *SF* =7. This becomes with LoRaFFEC $1 + (15 + 3) \times 2 = 37$ bytes, and 83 symbols at *SF* 7 (with $CR = \frac{4}{5}$).

[5] Notice that a slightly higher PER_{target} could be used at the expense of stability and latency.

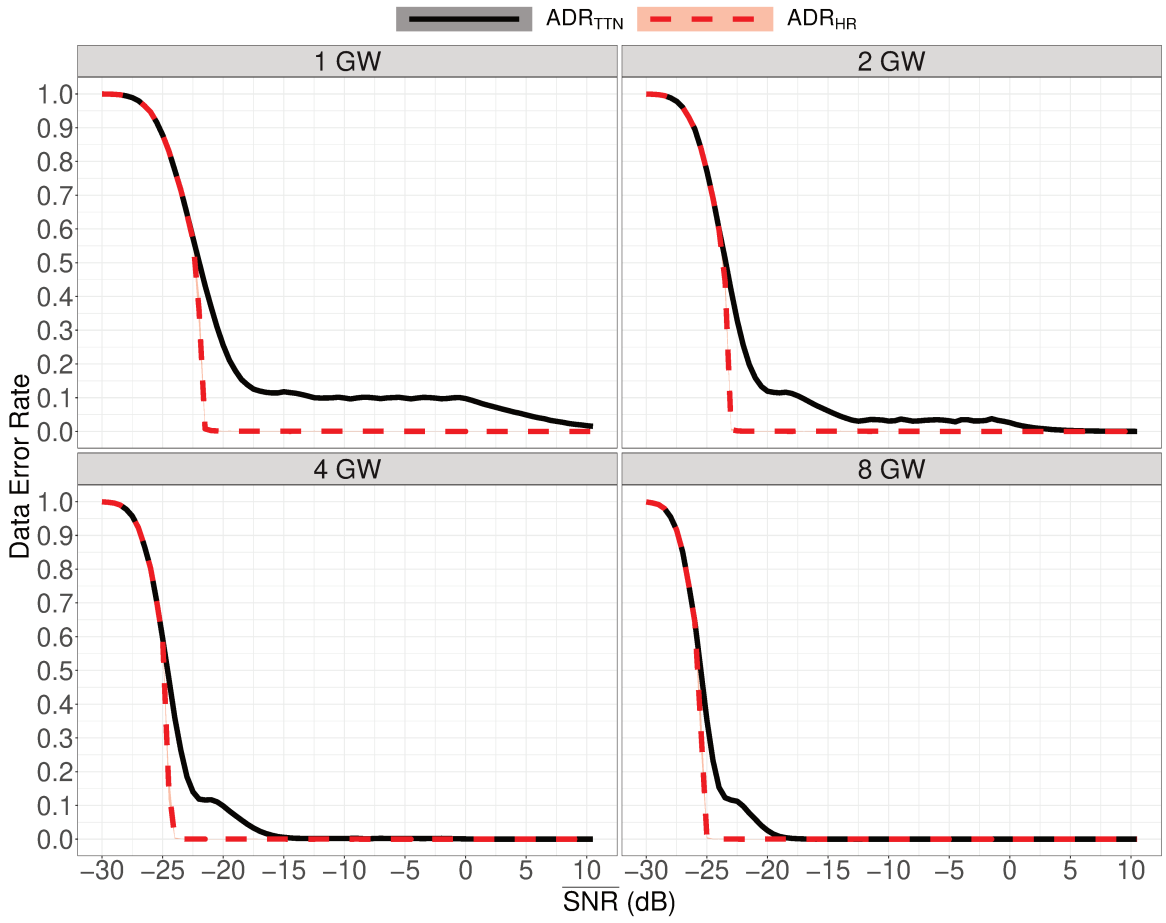

Figure 6.10: *DER* against $\overline{SNR}$ for the simulated series of frames (99% confidences interval plots).

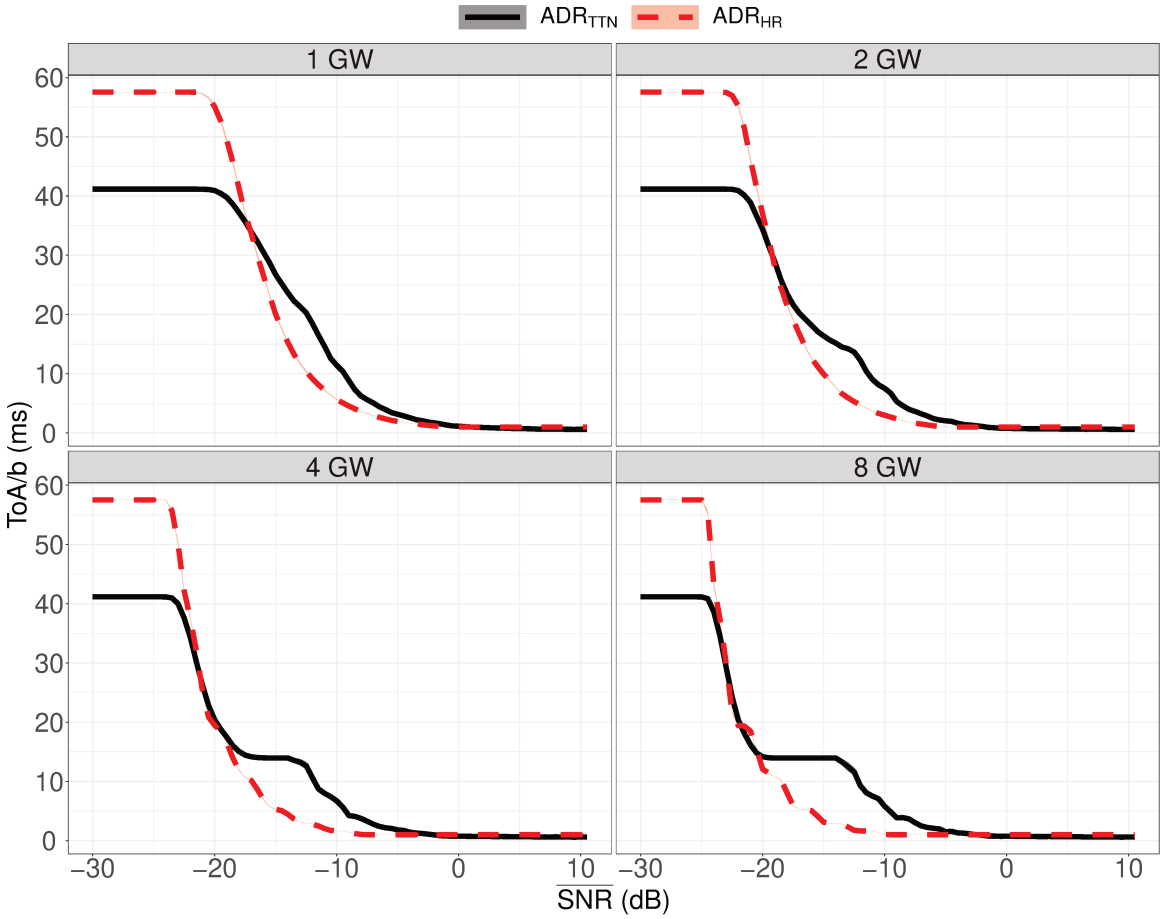

Figure 6.11: *ToA/b* as a function of $\overline{SNR}$ for the simulated series of frames with several GWs (99% confidences interval plots).

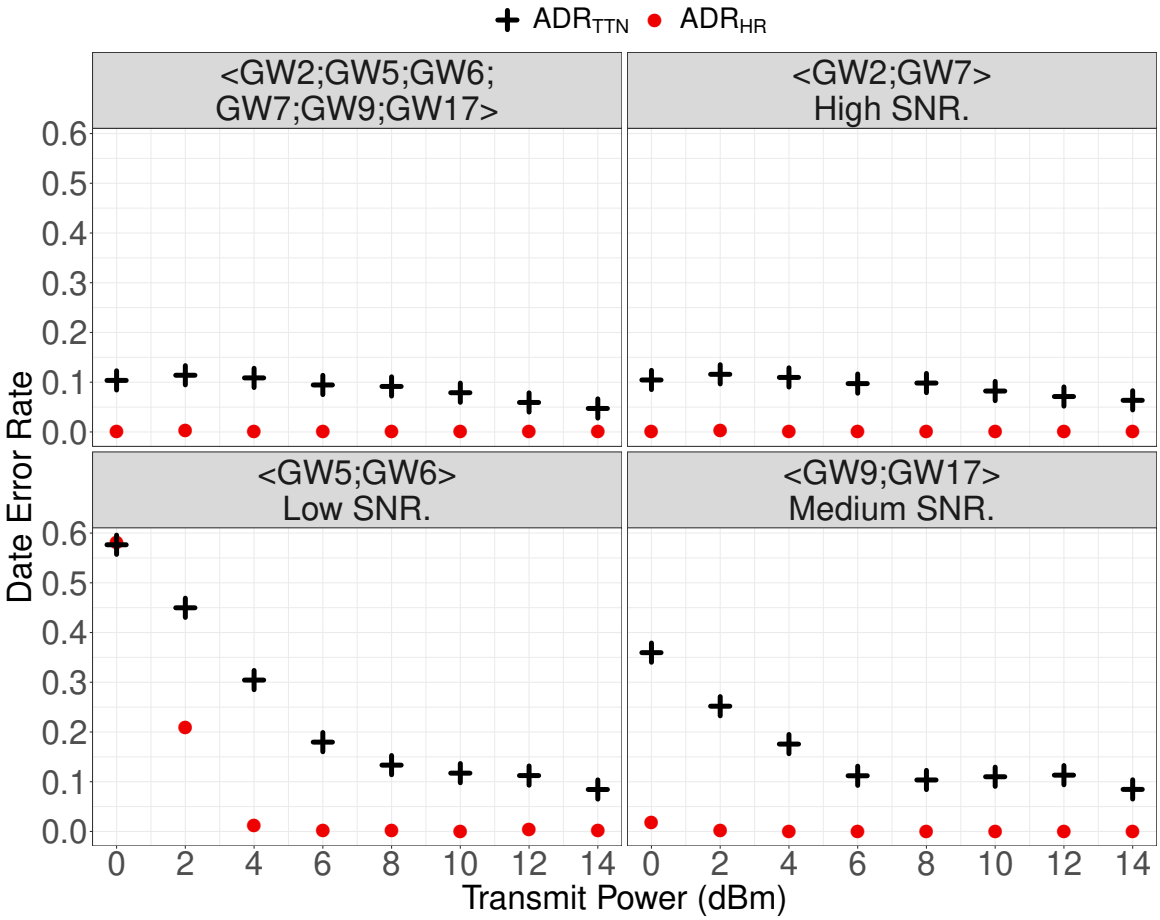

Figure 6.12: *DER* as a function of P_{Tx}, for selected real world series of frames replays.

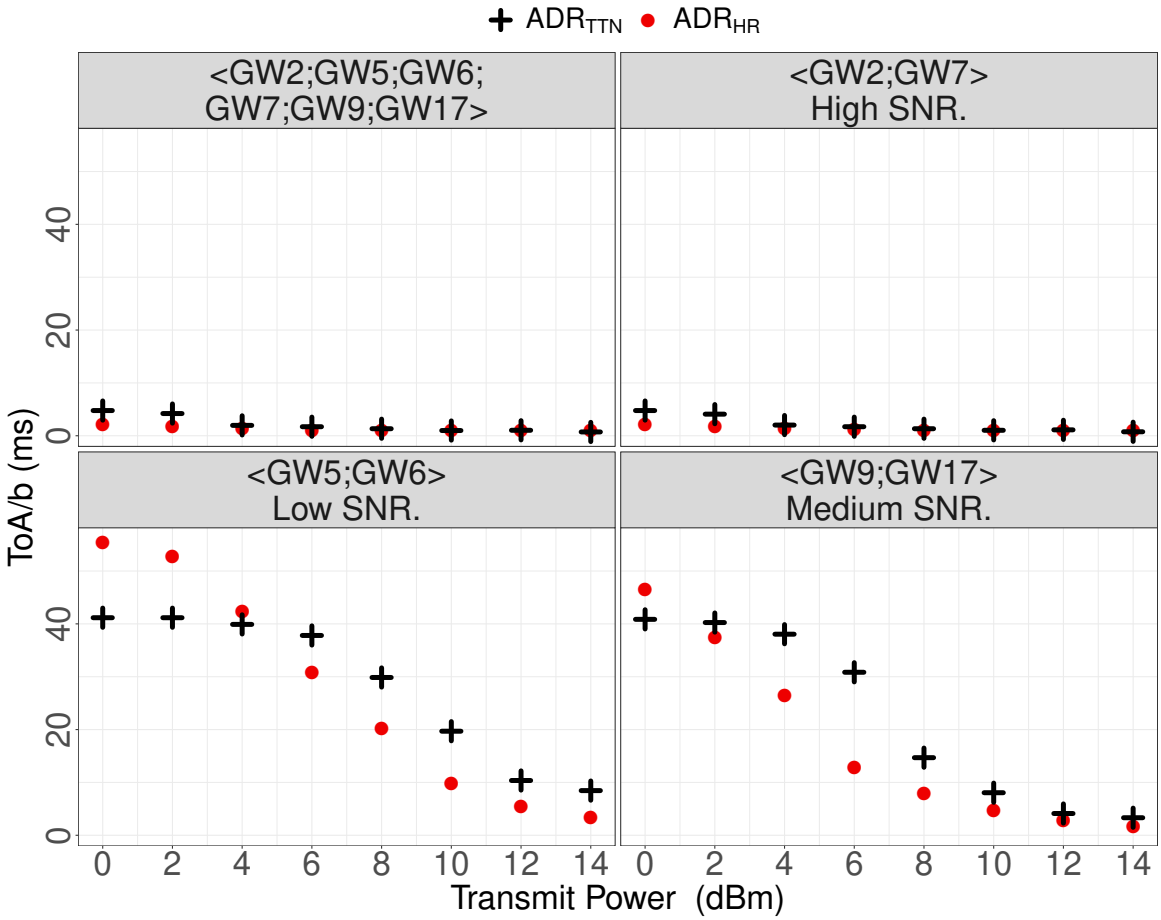

Figure 6.13: *ToA/b* as a function of P_{Tx}, for selected real world series of frames replays.

6.4 Chapter Conclusion

6.5 Conclusion

In this chapter we used the channel model draw from the traffic collected on a real-world LoRaWAN deployment to tailor optimized ADR.

First, we describe $ADR_{\text{opt-SG}}$, which statically optimizes the LoRaWAN ADR parameters in the presence of a CP-ECC-based reliability layer in the case of a mono-GW cell. This first approach demonstrates the substantial gains that can be obtained, in reliability and in TOA, by the joint use of CP-ECC and an optimized ADR. However, $ADR_{\text{opt-SG}}$ is a rough approximation and does not exploit the natural macro-diversity of LoRaWAN multi-GWs cells.

Then, we describe $ADR_{\text{opt-MG}}$ which derives the expected *PER* for any transmission parameter settings in presence of an arbitrary amount of GWs in range. This *PER* prediction is the basis allowing $ADR_{\text{opt-MG}}$ to be configured to match an arbitrary reliability goal in terms of *PER*. $ADR_{\text{opt-MG}}$ inherently takes into account macro-diversity and the observed channel variability due to SSF.

Finally we described ADR_{HR} which is the integration of CP-ECC into $ADR_{\text{opt-MG}}$. ADR_{HR} efficiently provides high reliability ($DER < 0.01$) in LoRaWAN networks, even for challenging transmission conditions. It is a significant improvement over the LoRaWAN ADR implemented by *The Things Network*. ADR_{HR} tackles the inevitable frame losses with LoRa communications by the use of CP-ECC. ADR_{HR} does not necessitate any additional downlink transmissions compared to the legacy LoRaWAN ADR.

$ADR_{\text{opt-SG}}$, $ADR_{\text{opt-MG}}$ and ADR_{HR} TOA are bounded by the maximal effort configuration, warrant scalability and are realistic options for current and future deployments. The $ADR_{\text{opt-SG}}$, $ADR_{\text{opt-MG}}$ and ADR_{HR} propositions are validated both by simulation and by replaying experimental channel transmission traces.

We adopted here the quasi-static Rayleigh channel model which corresponds to an urban LoRaWAN deployment. But as we detailed the design steps of our optimized $ADR_{\text{opt-MG}}$, we give the opportunity to adapt the same method to other channel models such as Rice or AWGN channel models.

Chapter 7

Conclusion

This concluding chapter summarizes the main contributions of this thesis and highlights their consequences for the use and future evolutions of the LoRaWAN technology.

The chapter 4 shows that the LoRaWAN link in an urban environment can be characterized as following a quasi-static Rayleigh channel model (also called slow Rayleigh channel). It means that the received signal power varies for each new transmission around its average following an exponential law. As a result, a significant fraction of frame transmission is confronted to an extremely hostile channel. Correctly decoding and receiving this small fraction of frames would require the use of the most robust modulation parameters. Such modulation parameters are therefore overkill for most transmissions which do not undergo such attenuation. Moreover, these more robust modulation parameters have a lower data rate and thus have longer transmission time. It results in higher network load and higher energy consumption for the terminals devices. For instance 5% of frames experience an attenuation 13dB above the average, which is more than the sensitivity delta between least and more robust parameters of a standard LoRaWAN network (-12.5dB from spreading factor 7 to 12). We claim it is counterproductive to seek to receive these frames only by pushing the modulation towards a better sensitivity. It is therefore necessary to either design the applications so that they are tolerant to this data loss floor, or to design an accurate reliability protocol in LoRaWAN.

Due to the strong constraints of LoRaWAN, mostly the non-slotted Aloha access method, the large amount of terminal devices to be connected and the extremely restrained downlink capacity, the design of an efficient and viable reliability protocol is challenging. Indeed, the conventional error control methods such as acknowledgments or blind systematic repetition of each frame a large number of times are inadequate because these methods congest the network. We show in chapter 5 that the use of error correcting codes applied across packets is particularly adapted and can provide high reliability in LoRaWAN. This approach introduces time diversity into the communication and therefore smooths the channel packets losses. Thus the residual packet losses, including the losses in burst, are compensated and repaired by the error correcting code, without having to resort neither to acknowledgments at a high frequency, nor to resorting to an over-calibrated frame repetition rate. The two solutions for LoRaWAN's reliability build on cross-packet error correction code can maintain the data loss rate below 1% despite packet loss rates of up to 40% and 92% respectively.

The availability of a reliability protocol based on cross-packet error correction code changes the paradigm for the use of the LoRaWAN physical layer: the LoRa modulation. Thanks to the ability to compensate for packet losses, the constraints on the LoRa modulation parameters are relaxed. In particular, in order to receive the full data, it is no longer necessary for all the frames to be received with a power above the demodulation threshold. On the contrary, as we show in chapter 6, it is possible and even relevant to configure the parameters of the physical layer in order to voluntarily obtain a packet loss rate just below the tolerance threshold of the reliability layer. The cross-packet error correction code ensures the stability and reliability of the communication, and the transmission time is optimized.

Bibliographie

Scientific Papers on Aloha MAC

[1] Lawrence G. Roberts. “ALOHA Packet System with and Without Slots and Capture”. In: *SIGCOMM Comput. Commun. Rev.* 5.2 (April 1975), pp. 28–42. ISSN: 0146-4833. DOI: 10.1145/1024916.1024920. URL: http://doi.acm.org/10.1145/1024916.1024920.

[2] Fouad Tobagi and Leonard Kleinrock. “Packet switching in radio channels: Part II-The hidden terminal problem in carrier sense multiple-access and the busy-tone solution”. In: *IEEE Transactions on communications* 23.12 (1975), pp. 1417–1433.

[3] N. Abramson. “Development of the ALOHANET”. In: *IEEE Transactions on Information Theory* 31.2 (1985), pp. 119–123.

[4] Wuyi Yue. “The effect of capture on performance of multichannel slotted ALOHA systems”. In: *IEEE Transactions on Communications* 39.6 (1991), pp. 818–822.

[5] Tien-Shin Ho and Kwang-Cheng Chen. “Performance analysis of IEEE 802.11 CSMA/CA medium access control protocol”. In: *Proceedings of PIMRC'96-7th International Symposium on Personal, Indoor, and Mobile Communications*. Vol. 2. IEEE. 1996, pp. 407–411.

[6] Sumit Roy and H-Y Wang. “Performance of CDMA slotted ALOHA multiple access with multiuser detection”. In: *WCNC. 1999 IEEE Wireless Communications and Networking Conference (Cat. No. 99TH8466)*. Vol. 2. IEEE. 1999, pp. 839–843.

[7] Y.Birk and Y.Keren. “Judicious Use of Redundant Transmissions in Multichannel ALOHA Networks with Deadlines”. In: *IEEE* (1999).

[8] Dongxu Shen and Victor OK Li. “Stabilized multi-channel ALOHA for wireless OFDM networks”. In: *Global Telecommunications Conference, 2002. GLOBECOM'02. IEEE*. Vol. 1. IEEE. 2002, pp. 701–705.

[9] Y.BIRK and Y.REVAH. “Increasing Dealine-Constrained Throughput in Multi-Channel ALOHA Networks via Non-Stationary Muliple-Power-Level Transmission”. In: *Wireless Networks 11* (2005).

[10] Sunghyun Choi, Youngkyu Choi, and Inkyu Lee. “IEEE 802.11 MAC-Level FEC scheme with retransmission combining”. In: *IEEE Transactions on Wireless Communications* 5.1 (2006), pp. 203–211. DOI: 10.1109/TWC.2006.1576544.

[11] Jeongkeun Lee et al. “An experimental study on the capture effect in 802.11 a networks”. In: *Proceedings of the second ACM international workshop on Wireless network testbeds, experimental evaluation and characterization*. 2007, pp. 19–26.

Books

[12] Andrew S Tanenbaum, David Wetherall, et al. *Computer networks*. 1996.

[13] Andrea Goldsmith. *Wireless communications*. Cambridge university press, 2005.

Scientific Papers on Error Correction Codes

[14] G. Solomon I. S. Reed. "Polynomial Codes Over Certain Finite Fields". In: *Journal of the Society for Industrial and Applied Mathematics* 8.2 (1960), pp. 300–304. ISSN: 03684245. URL: http://www.jstor.org/stable/2098968.

[15] Irving S Reed and Gustave Solomon. "Polynomial codes over certain finite fields". In: *Journal of the society for industrial and applied mathematics* 8.2 (1960), pp. 300–304.

[16] Robert Gallager. "Low-density parity-check codes". In: *IRE Transactions on information theory* 8.1 (1962), pp. 21–28.

[17] Andrew Viterbi. "Error bounds for convolutional codes and an asymptotically optimum decoding algorithm". In: *IEEE transactions on Information Theory* 13.2 (1967), pp. 260–269.

[18] David A Patterson, Garth Gibson, and Randy H Katz. "A Case for Redundant Arrays of Inexpensive Disks (RAID)". In: *PATTERSON88* (1988).

[19] Anthony J McAuley. "Reliable broadband communication using a burst erasure correcting code". In: *ACM SIGCOMM Computer Communication Review*. Vol. 20. 4. ACM. 1990, pp. 297–306.

[20] Claude Berrou, Alain Glavieux, and Punya Thitimajshima. "Near Shannon limit error-correcting coding and decoding: Turbo-codes. 1". In: *Communications, 1993. ICC'93 Geneva. Technical Program, Conference Record, IEEE International Conference on*. Vol. 2. IEEE. 1993, pp. 1064–1070.

[21] Ender Ayanoglu, Pramod Pancha, Amy R Reibman, and Shilpa Talwar. "Forward error control for MPEG-2 video transport in a wireless ATM LAN". In: *Mobile Networks and Applications* 1.3 (1996), pp. 245–257.

[22] John W Byers, Michael Luby, Michael Mitzenmacher, and Ashutosh Rege. "A digital fountain approach to reliable distribution of bulk data". In: *ACM SIGCOMM Computer Communication Review* 28.4 (1998), pp. 56–67.

[23] J-C Bolot, Sacha Fosse-Parisis, and Don Towsley. "Adaptive FEC-based error control for Internet telephony". In: *IEEE INFOCOM'99. Conference on Computer Communications. Proceedings. Eighteenth Annual Joint Conference of the IEEE Computer and Communications Societies. The Future is Now (Cat. No. 99CH36320)*. Vol. 3. IEEE. 1999, pp. 1453–1460.

[24] Michael G Luby, Michael Mitzenmacher, Mohammad Amin Shokrollahi, and Daniel A Spielman. "Efficient erasure correcting codes". In: *IEEE Transactions on Information Theory* 47.2 (2001), pp. 569–584.

[25] T Cooklev. "Dynamic bandwidth allocation and channel coding in providing QoS for wireless local area networks". In: *Telecommunications, 2003. ICT 2003. 10th International Conference on*. Vol. 2. IEEE. 2003, pp. 1388–1393.

[26] Fan Zhai, Yiftach Eisenberg, and Aggelos K Katsaggelos. "Joint source-channel coding for video communications". In: *Handbook of Image and Video Processing* (2005).

[27] Christina Fragouli, Jean-Yves Le Boudec, and Jörg Widmer. “Network Coding: An Instant Primer”. In: *SIGCOMM Comput. Commun. Rev.* 36.1 (January 2006), pp. 63–68. ISSN: 0146-4833. DOI: 10.1145/1111322.1111337. URL: http://doi.acm.org/10.1145/1111322.1111337.

[28] C. Fragouli, D. Katabi, A. Markopoulou, M. Medard, and H. Rahul. “Wireless Network Coding: Opportunities & Challenges”. In: *MILCOM 2007 - IEEE Military Communications Conference*. October 2007, pp. 1–8. DOI: 10.1109/MILCOM.2007.4454988.

[29] Andreas F Molisch, Neelesh B Mehta, Jonathan S Yedidia, and Jin Zhang. “Performance of fountain codes in collaborative relay networks”. In: *IEEE Transactions on Wireless Communications* 6.11 (2007).

[30] Gokul Sridharan, Abishek Kumarasubramanian, Andrew Thangaraj, and Srikrishna Bhashyam. “Optimizing burst erasure correction of LDPC codes by interleaving”. In: *2008 IEEE International Symposium on Information Theory*. IEEE. 2008, pp. 1143–1147.

[31] Jin Lu and José MF Moura. “Linear time encoding of LDPC codes”. In: *IEEE Transactions on Information Theory* 56.1 (2009), pp. 233–249.

[32] Enrico Paolini and Marco Chiani. “Construction of near-optimum burst erasure correcting low-density parity-check codes”. In: *IEEE Transactions on Communications* 57.5 (2009), pp. 1320–1328.

[33] Dino Sejdinovic, Dejan Vukobratovic, Angela Doufexi, Vojin Senk, and Robert J Piechocki. “Expanding window fountain codes for unequal error protection”. In: *IEEE Transactions on Communications* 57.9 (2009).

[34] A. G. Dimakis, P. B. Godfrey, Y. Wu, M. J. Wainwright, and K. Ramchandran. “Network Coding for Distributed Storage Systems”. In: *IEEE Transactions on Information Theory* 56.9 (July 2010), pp. 4539–4551. ISSN: 0018-9448. DOI: 10.1109/TIT.2010.2054295.

[35] Weiyao Xiao and David Starobinski. “Extreme value FEC for reliable broadcasting in wireless networks”. In: *IEEE Journal on Selected Areas in Communications* 28.7 (2010), pp. 1180–1189.

[36] Sian-Jheng Lin, Wei-Ho Chung, and Yunghsiang S Han. “Novel polynomial basis and its application to reed-solomon erasure codes”. In: *2014 ieee 55th annual symposium on foundations of computer science*. IEEE. 2014, pp. 316–325.

[37] Xueqing Gong and Chi Wan Sung. “Zigzag Decodable codes: Linear-time erasure codes with applications to data storage”. In: *Journal of Computer and System Sciences* (2017).

[38] Nianqi Tang and Yun Lin. “Fast Encoding and Decoding Algorithms for Arbitrary (n,k) Reed-Solomon Codes Over F2m”. In: *IEEE Communications Letters* 24.4 (2020), pp. 716–719.

[39] Henry Minsky. *https://sourceforge.net/projects/rscode/*. URL: https://sourceforge.net/projects/rscode/.

Scientific Papers on Internet of Things

[40] Jin-Shyan Lee, Yu-Wei Su, Chung-Chou Shen, et al. “A comparative study of wireless protocols: Bluetooth, UWB, ZigBee, and Wi-Fi”. In: *Industrial electronics society* 5 (2007), pp. 46–51.

[41] Leila Ben Saad and Bernard Tourancheau. “Exploiting addresses correlation to maximize lifetime of ipv6 cluster-based wsns”. In: *2011 IEEE 7th International Conference on Wireless and Mobile Computing, Networking and Communications (WiMob)*. IEEE. 2011, pp. 483–489.

[42] Jayavardhana Gubbi, Rajkumar Buyya, Slaven Marusic, and Marimuthu Palaniswami. “Internet of Things (IoT): A vision, architectural elements, and future directions”. In: *Future generation computer systems* 29.7 (2013), pp. 1645–1660.

[43] Rahim Kacimi, Riadh Dhaou, and André-Luc Beylot. “Load balancing techniques for lifetime maximizing in wireless sensor networks”. In: *Ad hoc networks* 11.8 (2013), pp. 2172–2186.

[44] Malisa Vucinic et al. “Topology Construction in RPL Networks over Beacon-Enabled 802.15.4”. In: *Computers and Communication (ISCC), 2014 IEEE Symposium on*. Madeira, Portugal, June 2014. DOI: 10.1109/ISCC.2014.6912563. URL: https://hal.inria.fr/hal-00985933.

[45] G.Margelis, R.Piechocki, D.Kaleshi, and P.Thomas. “Low Throught Networks for the IoT : Lessons Learned From Industrial Implementations.” In: *IEEE* (2015).

[46] Claire Goursaud and Jean-Marie Gorce. “Dedicated networks for IoT: PHY/MAC state of the art and challenges”. In: *EAI endorsed transactions on Internet of Things* (2015).

[47] Ramon Sanchez-Iborra and Maria-Dolores Cano. “State of the art in LP-WAN solutions for industrial IoT services”. In: *Sensors* 16.5 (2016), p. 708.

[48] Mads Lauridsen, Huan Nguyen, Benny Vejlgaard, István Z Kovács, Preben Mogensen, and Mads Sorensen. “Coverage Comparison of GPRS, NB- IoT , LoRa , and SigFox in a 7800 km^2 Area”. In: *Vehicular Technology Conference (VTC)*. IEEE. 2017.

[49] Usman Raza, Parag Kulkarni, and Mahesh Sooriyabandara. “Low power wide area networks: An overview”. In: *IEEE Communications Surveys & Tutorials* 19.2 (2017), pp. 855–873.

[50] Felix Wunsch, Kristian Maier, Holger Jäkel, and Friedrich K Jondral. “Implementation and performance evaluation of IEEE 802.15. 4 LECIM DSSS PHY at 2.4 GHz”. In: *Proceedings of the GNU Radio Conference*. Vol. 2. 1. 2017, pp. 6–6.

[51] Wael Ayoub, Fabienne Nouvel, Abed Ellatif Samhat, Jean-Christophe Prevotet, and Mohamad Mroue. “Overview and measurement of mobility in DASH7”. In: *2018 25th International Conference on Telecommunications (ICT)*. IEEE. 2018, pp. 532–536.

[52] Wael Ayoub, Abed Ellatif Samhat, Fabienne Nouvel, Mohamad Mroue, and Jean-Christophe Prévotet. “Internet of mobile things: Overview of lorawan, dash7, and nb-iot in lpwans standards and supported mobility”. In: *IEEE Communications Surveys & Tutorials* 21.2 (2018), pp. 1561–1581.

[53] Joseph Finnegan and Stephen Brown. “A comparative survey of LPWA networking”. In: *arXiv preprint arXiv:1802.04222* (2018).

[54] Nitin Naik. “LPWAN technologies for IoT systems: choice between ultra narrow band and spread spectrum”. In: *2018 IEEE International Systems Engineering Symposium (ISSE)*. IEEE. 2018, pp. 1–8.

[55] Yoann Roth, Jean-Baptiste Doré, Laurent Ros, and Vincent Berg. *The Physical Layer of Low Power Wide Area Networks: Strategies, Information Theory's Limit and Existing Solutions*. 2018.

[56] Mncedisi Bembe, Adnan Abu-Mahfouz, Moshe Masonta, and Tembisa Ngqondi. “A survey on low-power wide area networks for IoT applications”. In: *Telecommunication Systems* 71.2 (2019), pp. 249–274.

[57] Heikki Karvonen, Carlos Pomalaza-Ráez, Konstantin Mikhaylov, Matti Hämäläinen, and Jari Iinatti. “Experimental performance evaluation of ble 4 versus ble 5 in indoors and outdoors scenarios”. In: *Advances in Body Area Networks I*. Springer, 2019, pp. 235–251.

[58] Hassan Malik et al. “NB-IoT network field trial: Indoor, outdoor and underground coverage campaign”. In: *2019 15th International Wireless Communications & Mobile Computing Conference (IWCMC)*. IEEE. 2019, pp. 537–542.

[59] Kais Mekki, Eddy Bajic, Frederic Chaxel, and Fernand Meyer. “A comparative study of LPWAN technologies for large-scale IoT deployment”. In: *ICT express* 5.1 (2019), pp. 1–7.

[60] Francesca Righetti, Carlo Vallati, Daniela Comola, and Giuseppe Anastasi. “Performance measurements of IEEE 802.15. 4g wireless networks”. In: *2019 IEEE 20th International Symposium on" A World of Wireless, Mobile and Multimedia Networks"(WoWMoM)*. IEEE. 2019, pp. 1–6.

[61] Axel Sikora, Manuel Schappacher, Zubair Amjad, et al. “Test and Measurement of LPWAN and Cellular IoT Networks in a Unified Testbed”. In: *2019 IEEE 17th International Conference on Industrial Informatics (INDIN)*. Vol. 1. IEEE. 2019, pp. 1521–1527.

[62] IoT Analytics. *LPWAN Market Report 2020-2025*. Tech. rep. https://iot-analytics.com/, 2020.

[63] Romain Barbau, Vincent Deslandes, Gentian Jakllari, Jérôme Tronc, Jean-Frédéric Chouteau, and André-Luc Beylot. “NB-IoT over GEO Satellite: Performance Analysis”. In: *2020 10th Advanced Satellite Multimedia Systems Conference and the 16th Signal Processing for Space Communications Workshop (ASMS/SPSC)*. IEEE. 2020, pp. 1–8.

[64] Tobia De Koninck, Serena Santi, Jeroen Famaey, and Filip Lemic. “Experimental validation of IEEE 802.11 ah propagation models in heterogeneous smarty city environments”. In: *GLOBECOM 2020-2020 IEEE Global Communications Conference*. IEEE. 2020, pp. 1–6.

[65] Brandon Foubert and Nathalie Mitton. “Long-range wireless radio technologies: A survey”. In: *Future internet* 12.1 (2020), p. 13.

[66] Fei Gu, Jianwei Niu, Landu Jiang, Xue Liu, and Mohammed Atiquzzaman. “Survey of the low power wide area network technologies”. In: *Journal of Network and Computer Applications* 149 (2020), p. 102459.

[67] Emmanuel M Migabo, Karim D Djouani, and Anish M Kurien. “The Narrowband Internet of Things (NB-IoT) Resources Management Performance State of Art, Challenges, and Opportunities”. In: *IEEE Access* 8 (2020), pp. 97658–97675.

[68] Konstantin Mikhaylov et al. “Communication Performance of a Real-Life Wide-Area Low-Power Network Based on Sigfox Technology”. In: *ICC 2020-2020 IEEE International Conference on Communications (ICC)*. IEEE. 2020, pp. 1–6.

[69] Jakob Thrane, Krzysztof Mateusz Malarski, Henrik Lehrmann Christiansen, and Sarah Ruepp. “Experimental evaluation of empirical nb-iot propagation modelling in a deep-indoor scenario”. In: *arXiv preprint arXiv:2006.00880* (2020).

[70] Marco Centenaro, Cristina E. Costa, Fabrizio Granelli, Claudio Sacchi, and Lorenzo Vangelista. “A Survey on Technologies, Standards and Open Challenges in Satellite IoT”. In: *IEEE Communications Surveys Tutorials* (2021), pp. 1–1. DOI: 10.1109/COMST.2021.3078433.

[71] Satya N Gupta, Alice Maltseva, and Keshav Sharma. “Collaborating for Self-Reliance–Co-Creating IoT Connectivity Solutions Using NB. Fi”. In: *AKGEC INTERNATIONAL JOURNAL OF TECHNOLOGY* 11.2 ().

Scientific Papers on LoRaWAN

[72] M.Aref and A.Sikora. “Free-Space Range Measurements with Semtech LoRa Technologie”. In: *IEEE* (2014).

[73] L.Vangelista, A. Zannella, and M.Zorzi. “Long-range IoT technologies: the dawn of LoRa ”. In: *Future Access Enablers for Ubiquitous and Intelligent Infrastructures*. 2015.

[74] Juha Petajajarvi, Konstantin Mikhaylov, Antti Roivainen, Tuomo Hanninen, and Marko Pettissalo. “On the coverage of LPWANs: range evaluation and channel attenuation model for LoRa technology”. In: *ITS Telecommunications (ITST)*. IEEE. 2015.

[75] Nihesh Rathod et al. “Performance analysis of wireless devices for a campus-wide IoT network”. In: *Modeling and Optimization in Mobile, Ad Hoc, and Wireless Networks (WiOpt), 2015 13th International Symposium on*. IEEE. 2015, pp. 84–89.

[76] Aloÿs Augustin, Jiazi Yi, Thomas Clausen, and William Mark Townsley. “A study of LoRa : Long range & low power networks for the internet of things”. In: *Sensors* 16.9 (2016), p. 1466.

[77] Martin C Bor, Utz Roedig, Thiemo Voigt, and Juan M Alonso. “Do LoRa low-power wide-area networks scale?” In: *Proceedings of the 19th ACM International Conference on Modeling, Analysis and Simulation of Wireless and Mobile Systems*. 2016, pp. 59–67.

[78] Juha Petäjäjärvi, Konstantin Mikhaylov, Matti Hämäläinen, and Jari Iinatti. “Evaluation of LoRa LPWAN technology for remote health and wellbeing monitoring”. In: *Medical Information and Communication Technology (ISMICT), 2016 10th International Symposium on*. IEEE. 2016, pp. 1–5.

[79] Tara Petrić, Mathieu Goessens, Loutfi Nuaymi, Laurent Toutain, and Alexander Pelov. “Measurements, performance and analysis of LoRa FABIAN, a real-world implementation of LPWAN”. In: *2016 IEEE 27th Annual International Symposium on Personal, Indoor, and Mobile Radio Communications (PIMRC)*. IEEE. 2016, pp. 1–7.

[80] Congduc Pham. “Towards quality of service for long-range IoT in unlicensed radio spectrum”. In: *2016 Wireless Days (WD)*. IEEE. 2016, pp. 1–3.

[81] Brecht Reynders, Wannes Meert, and Sofie Pollin. “Range and coexistence analysis of long range unlicensed communication”. In: *2016 23rd International Conference on Telecommunications (ICT)*. IEEE. 2016.

[82] Thiemo Voigt, Martin Bor, Utz Roedig, and Juan Alonso. “Mitigating inter-network interference in LoRa networks”. In: *arXiv preprint arXiv:1611.00688* (2016).

[83] Ferran Adelantado, Xavier Vilajosana, Pere Tuset-Peiro, Borja Martinez, and Joan Melia. “Understanding the limits of LoRaWAN”. In: *IEEE Communications* 55.9 (2017).

[84] Said Benaissa et al. “Internet of animals: characterisation of LoRa sub-GHz off-body wireless channel in dairy barns”. In: *Electronics Letters* 53.18 (2017), pp. 1281–1283.

[85] Norbert Blenn and Fernando Kuipers. “LoRaWAN in the wild: Measurements from the things network”. In: *arXiv preprint arXiv:1706.03086* (2017).

[86] Martin Bor and Utz Roedig. “LoRa transmission parameter selection”. In: *Distributed Computing in Sensor Systems (DCOSS)*. IEEE. 2017.

[87] Marco Cattani, Carlo Alberto Boano, and Kay Römer. “An experimental evaluation of the reliability of lora long-range low-power wireless communication”. In: *Journal of Sensor and Actuator Networks* 6.2 (2017), p. 7.

[88] Johnny Gaelens, Patrick Van Torre, Jo Verhaevert, and Hendrik Rogier. “LoRa mobile-to-base-station channel characterization in the Antarctic”. In: *Sensors* 17.8 (2017), p. 1903.

[89] Orestis Georgiou and Usman Raza. “Low power wide area network analysis: Can LoRa scale?” In: *IEEE Wireless Communications Letters* 6.2 (2017), pp. 162–165.

[90] Vojtěch Hauser and Tomáš Hégr. “Proposal of adaptive data rate algorithm for LoRaWAN-based infrastructure”. In: *Future Internet of Things and Cloud (FiCloud)*. IEEE. 2017.

[91] Jetmir Haxhibeqiri, Abdulkadir Karaagac, Floris Van den Abeele, Wout Joseph, Ingrid Moerman, and Jeroen Hoebeke. “LoRa indoor coverage and performance in an industrial environment: Case study”. In: *2017 22nd IEEE international conference on emerging technologies and factory automation (ETFA)*. IEEE. 2017, pp. 1–8.

[92] Salaheddin Hosseinzadeh, Hadi Larijani, Krystyna Curtis, Andrew Wixted, and Amin Amini. “Empirical propagation performance evaluation of LoRa for indoor environment”. In: *2017 IEEE 15th international conference on industrial informatics (INDIN)*. IEEE. 2017, pp. 26–31.

[93] Oana Iova et al. “LoRa from the city to the mountains: Exploration of hardware and environmental factors”. In: *Proceedings of the 2017 international conference on embedded wireless systems and networks*. 2017.

[94] Mads Lauridsen, Benny Vejlgaard, István Z Kovács, Huan Nguyen, and Preben Mogensen. “Interference measurements in the European 868 MHz ISM band with focus on LoRa and SigFox”. In: *Wireless Communications and Networking Conference (WCNC)*. IEEE. 2017, pp. 1–6.

[95] Davide Magrin, Marco Centenaro, and Lorenzo Vangelista. “Performance evaluation of LoRa networks in a smart city scenario”. In: *2017 IEEE International Conference on communications (ICC)*. ieee. 2017, pp. 1–7.

[96] P. J. Marcelis, V. Rao, and R. V. Prasad. “DaRe: Data Recovery Through Application Layer Coding for LoRaWAN”. In: *Internet-of-Things Design and Implementation*. ACM. 2017.

[97] Moises Nunez Ochoa, Arturo Guizar, Mickael Maman, and Andrzej Duda. “Evaluating LoRa energy efficiency for adaptive networks: From star to mesh topologies”. In: *2017 IEEE 13th International Conference on Wireless and Mobile Computing, Networking and Communications (WiMob)*. IEEE. 2017, pp. 1–8.

[98] Juha Petäjäjärvi, Konstantin Mikhaylov, Marko Pettissalo, Janne Janhunen, and Jari Iinatti. “Performance of a low-power wide-area network based on LoRa technology: Doppler robustness, scalability, and coverage”. In: *International Journal of Distributed Sensor Networks* 13.3 (2017), p. 1550147717699412.

[99] Alexandru-Ioan Pop, Usman Raza, Parag Kulkarni, and Mahesh Sooriyabandara. “Does bidirectional traffic do more harm than good in LoRaWAN based LPWA networks?” In: *Global Communications (GLOBECOM)*. IEEE. 2017.

[100] Brecht Reynders, Wannes Meert, and Sofie Pollin. “Power and spreading factor control in low power wide area networks”. In: *2017 IEEE International Conference on Communications (ICC)*. IEEE. 2017.

[101] Madoune R Seye, Bamba Gueye, and Moussa Diallo. “An evaluation of LoRa coverage in Dakar Peninsula”. In: *2017 8th IEEE Annual Information Technology, Electronics and Mobile Communication Conference (IEMCON)*. IEEE. 2017, pp. 478–482.

[102] Lorenzo Vangelista. “Frequency shift chirp modulation: The LoRa modulation”. In: *IEEE Signal Processing Letters* 24.12 (2017), pp. 1818–1821.

[103] Nuttakit Vatcharatiansakul, Panwit Tuwanut, and Chotipat Pornavalai. “Experimental performance evaluation of LoRaWAN: A case study in Bangkok”. In: *2017 14th International Joint Conference on Computer Science and Software Engineering (JCSSE)*. IEEE. 2017, pp. 1–4.

[104] Khaled Q Abdelfadeel, Victor Cionca, and Dirk Pesch. “Fair adaptive data rate allocation and power control in LoRaWAN”. In: *2018 IEEE 19th International Symposium on" A World of Wireless, Mobile and Multimedia Networks"(WoWMoM)*. IEEE. 2018.

[105] Thomas Ameloot, Patrick Van Torre, and Hendrik Rogier. “A Compact Low-Power LoRa IoT Sensor Node with Extended Dynamic Range for Channel Measurements”. In: *MDPI Sensors* 18.7 (2018).

[106] Ulysse Coutaud and Bernard Tourancheau. “Channel Coding for Better QoS in LoRa Networks”. In: *Wireless and Mobile Computing, Networking and Communications (WiMob)*. IEEE. 2018.

[107] Daniele Croce, Michele Gucciardo, Stefano Mangione, Giuseppe Santaromita, and Ilenia Tinnirello. “Impact of LoRa imperfect orthogonality: Analysis of link-level performance”. In: *IEEE Communications Letters* (2018).

[108] Francesca Cuomo, Manuel Campo, Enrico Bassetti, Lorenzo Cartella, Federica Sole, and Giuseppe Bianchi. “Adaptive mitigation of the Air-Time pressure in LoRa multi-gateway architectures”. In: *European Wireless 2018; 24th European Wireless Conference*. VDE. 2018.

[109] Sungryul Kim and Younghwan Yoo. “Contention-aware adaptive data rate for throughput optimization in LoRa WAN”. In: *Sensors* 18.6 (2018).

[110] Shengyang Li, Usman Raza, and Aftab Khan. “How Agile is the Adaptive Data Rate Mechanism of LoRaWAN?” In: *2018 IEEE Global Communications Conference (GLOBECOM)*. IEEE. 2018, pp. 206–212.

[111] Qasim Lone, Andrzej Duda, Etienne Duble, Franck Rousseau, Ingrid Moerman, and Spilios Giannoulis. “WiSH-WalT: A Framework for Controllable and Reproducible LoRa Testbeds”. In: *IEEE PIMRC*. Bologna, Italy, September 2018. URL: `https://hal.archives-ouvertes.fr/hal-01835904`.

[112] Samuel Montejo-Sanchez, Cesar A Azurdia-Meza, Richard Demo Souza, Evelio Martin Garcia Fernandez, Ismael Soto, and Arliones Hoeller. “Coded redundant message transmission schemes for low-power wide area IoT applications”. In: *IEEE Wireless Communications Letters* 8.2 (2018), pp. 584–587.

[113] Andri Rahmadhani and Fernando Kuipers. “When lorawan frames collide”. In: *Proceedings of the 12th International Workshop on Wireless Network Testbeds, Experimental Evaluation & Characterization*. 2018, pp. 89–97.

[114] Mariusz Slabicki, Gopika Premsankar, and Mario Di Francesco. “Adaptive configuration of LoRa networks for dense IoT deployments”. In: *Network Operations and Management Symposium (NOMS)*. IEEE/IFIP. 2018.

[115] Thanh-Hai To and Andrzej Duda. “Simulation of LoRa in ns-3: Improving LoRa performance with csma”. In: *2018 IEEE International Conference on Communications (ICC)*. IEEE. 2018, pp. 1–7.

[116] Daeun Yim et al. “An experimental LoRa performance evaluation in tree farm”. In: *2018 IEEE sensors applications Symposium (SAS)*. IEEE. 2018, pp. 1–6.

[117] Andrea Abrardo and Alessandro Pozzebon. “A Multi-Hop LoRa Linear Sensor Network for the Monitoring of Underground Environments: The Case of the Medieval Aqueducts in Siena, Italy”. In: *Sensors* 19.2 (2019), p. 402.

[118] Ibrahim Amadou, Brandon Foubert, and Nathalie Mitton. “LoRa in a haystack: A study of the LORA signal behavior”. In: *2019 International Conference on Wireless and Mobile Computing, Networking and Communications (WiMob)*. IEEE. 2019.

[119] Thomas Ameloot, Patrick Van Torre, and Hendrik Rogier. “Indoor Body-to-Body LoRa Link Characterization”. In: *2019 IEEE-APS Topical Conference on Antennas and Propagation in Wireless Communications (APWC)*. IEEE. 2019, pp. 042–047.

[120] Thomas Ameloot, Patrick Van Torre, and Hendrik Rogier. “Periodic LoRa Signal Fluctuations in Urban and Suburban Environments”. In: *European Conference on Antennas and Propagation (EuCAP)*. IEEE. 2019.

[121] Takwa Attia, Martin Heusse, Bernard Tourancheau, and Andrzej Duda. “Experimental Characterization of LoRaWAN Link Quality”. In: *Global Communications Conference (GLOBECOM)*. IEEE. 2019.

[122] Christelle Caillouet, Martin Heusse, and Franck Rousseau. “Optimal SF allocation in LoRaWAN considering physical capture and imperfect orthogonality”. In: *2019 IEEE Global Communications Conference (GLOBECOM)*. IEEE. 2019, pp. 1–6.

[123] Gilles Callebaut and Liesbet Van der Perre. “Characterization of LoRa Point-to-Point Path-Loss: Measurement Campaigns and Modeling Considering Censored Data”. In: *IEEE Internet of Things Journal* (2019).

[124] Valentina Di Vincenzo, Martin Heusse, and Bernard Tourancheau. “Improving Downlink Scalability in LoRaWAN”. In: *International Conference on Communications (ICC)*. IEEE, 2019.

[125] Andrzej Duda and Martin Heusse. “Spatial issues in modeling lorawan capacity”. In: *Proceedings of the 22Nd International ACM Conference on Modeling, Analysis and Simulation of Wireless and Mobile Systems*. 2019, pp. 191–198.

[126] Rida El Chall, Samer Lahoud, and Melhem El Helou. “LoRaWAN network: Radio propagation models and performance evaluation in various environments in Lebanon”. In: *IEEE Internet of Things Journal* 6.2 (2019), pp. 2366–2378.

[127] Tallal Elshabrawy and Joerg Robert. “Evaluation of the BER Performance of LoRa Communication using BICM Decoding”. In: *2019 IEEE 9th International Conference on Consumer Electronics (ICCE-Berlin)*. IEEE. 2019, pp. 162–167.

[128] Jansen C Liando, Amalinda Gamage, Agustinus W Tengourtius, and Mo Li. “Known and unknown facts of LoRa : Experiences from a large-scale measurement study”. In: *ACM Transactions on Sensor Networks (TOSN)* 15.2 (2019), pp. 1–35.

[129] Wei-Shun Liao, Ou Zhao, Kentaro Ishizu, and Fumihide Kojima. “Adaptive Parameter Adjustment for Uplink Transmission for Multi-gateway LoRa Systems”. In: *2019 22nd International Symposium on Wireless Personal Multimedia Communications (WPMC)*. IEEE. 2019, pp. 1–5.

[130] Tommaso Polonelli, Davide Brunelli, Achille Marzocchi, and Luca Benini. “Slotted aloha on lorawan-design, analysis, and deployment”. In: *Sensors* 19.4 (2019), p. 838.

[131] René Brandborg Sørensen, Nasrin Razmi, Jimmy Jessen Nielsen, and Petar Popovski. “Analysis of LoRaWAN uplink with multiple demodulating paths and capture effect”. In: *arXiv preprint arXiv:1902.02866* (2019).

[132] J Tapparel. *Complete reverse engineering of LoRa PHY*. 2019.

[133] Patrick Van Torre, Thomas Ameloot, and Hendrik Rogier. “Long-range body-to-body LoRa link at 868 MHz”. In: *2019 13th European Conference on Antennas and Propagation (EuCAP)*. IEEE. 2019, pp. 1–5.

[134] Weitao Xu, Jun Young Kim, Walter Huang, Salil Kanhere, Sanjay Jha, and Wen Hu. “Measurement, Characterization and Modeling of LoRa Technology in Multi-floor Buildings”. In: *IEEE Internet of Things Journal* 7.1 (2019), pp. 298–310.

[135] O. Afisiadis, A. Burg, and A. Balatsoukas-Stimming. “Coded LoRa Frame Error Rate Analysis”. In: *International Conference on Communications (ICC)*. IEEE, 2020.

[136] Jaber Babaki, Mehdi Rasti, and Rojin Aslani. “Dynamic Spreading Factor and Power Allocation of LoRa Networks for Dense IoT Deployments”. In: *2020 IEEE 31st Annual International Symposium on Personal, Indoor and Mobile Radio Communications*. IEEE. 2020, pp. 1–6.

[137] Carolynn Bernier, François Dehmas, and Nicolas Deparis. “Low complexity LoRa frame synchronization for ultra-low power software-defined radios”. In: *IEEE Transactions on Communications* 68.5 (2020), pp. 3140–3152.

[138] Siddhartha S Borkotoky, Udo Schilcher, and Christian Raffelsberger. “Application-Layer Coding with Intermittent Feedback Under Delay and Duty-Cycle Constraints”. In: *ICC 2020-2020 IEEE International Conference on Communications (ICC)*. IEEE. 2020, pp. 1–6.

[139] Gonglong Chen, Jiamei Lv, and Wei Dong. “Exploiting rateless codes and cross-layer optimization for low-power wide-area networks”. In: *2020 IEEE/ACM 28th International Symposium on Quality of Service (IWQoS)*. IEEE. 2020, pp. 1–9.

[140] U. Coutaud, M. Heusse, and B. Tourancheau. “Adaptive Data Rate for Multiple Gateways LoRaWAN Networks”. In: *2020 16th International Conference on Wireless and Mobile Computing, Networking and Communications (WiMob)(50308)*. IEEE. 2020.

[141] Ulysse Coutaud, Martin Heusse, and Bernard Tourancheau. “Fragmentation and Forward Error Correction for LoRaWAN small MTU networks”. In: *Embedded Wireless Systems and Networks (EWSN)*. ACM. 2020, pp. 289–294.

[142] Ulysse Coutaud, Martin Heusse, and Bernard Tourancheau. “High Reliability in LoRaWAN”. In: *Symposium on Personal, Indoor and Mobile Radio Communications (PIMRC)*. IEEE, 2020.

[143] Ousmane Dieng, Congduc Pham, and Ousmane Thiare. “Comparing and Adapting Propagation Models for LoRa Networks”. In: *2020 16th International Conference on Wireless and Mobile Computing, Networking and Communications (WiMob)(50308)*. IEEE. 2020, pp. 1–7.

[144] Ana Elisa Ferreira, Fernando M Ortiz, Luis Henrique MK Costa, Brandon Foubert, Ibrahim Amadou, and Nathalie Mitton. “A study of the LoRa signal propagation in forest, urban, and suburban environments”. In: *Annals of Telecommunications* (2020).

[145] J. Finnegan, R. Farrell, and S. Brown. “Analysis and Enhancement of the LoRaWAN Adaptive Data Rate Scheme”. In: *IEEE Internet of Things Journal* (2020).

[146] Weifeng Gao, Zhiwei Zhao, and Geyong Min. “AdapLoRa: Resource Adaptation for Maximizing Network Lifetime in LoRa networks”. In: *2020 IEEE 28th International Conference on Network Protocols (ICNP)*. IEEE. 2020.

[147] Martin Heusse, Takwa Attia, Christelle Caillouet, Franck Rousseau, and Andrzej Duda. “Capacity of a LoRaWAN Cell”. In: *Proceedings of the 23rd International ACM Conference on Modeling, Analysis and Simulation of Wireless and Mobile Systems*. 2020, pp. 131–140.

[148] Nikolaos Kouvelas, Vijay S Rao, R Venkatesha Prasad, Gauri Tawde, and Koen Langendoen. “p-CARMA: Politely Scaling LoRaWAN.” In: *EWSN*. 2020, pp. 25–36.

[149] Junhyun Park, Kunho Park, Hyeongho Bae, and Chong-Kwon Kim. “EARN: Enhanced ADR with coding rate adaptation in LoRaWAN”. In: *IEEE Internet of Things Journal* 7.12 (2020), pp. 11873–11883.

[150] Gopika Premsankar, Bissan Ghaddar, Mariusz Slabicki, and Mario Di Francesco. “Optimal configuration of lora networks in smart cities”. In: *IEEE Transactions on Industrial Informatics* (2020).

[151] Jean Michel de Souza Sant’Ana, Arliones Hoeller, Richard Demo Souza, Samuel Montejo-Sanchez, Hirley Alves, and Mario de Noronha-Neto. “Hybrid coded replication in LoRa networks”. In: *IEEE Transactions on Industrial Informatics* 16.8 (2020), pp. 5577–5585.

[152] J. Tapparel, O. Afisiadis, P. Mayoraz, A. Balatsoukas-Stimming, and A. Burg. “An Open-Source LoRa Physical Layer Prototype on GNU Radio”. In: *21st International Workshop on Signal Processing Advances in Wireless Communications (SPAWC)*. IEEE. 2020.

[153] Ulysse Coutaud, Martin Heusse, and Bernard Tourancheau. “LoRa Channel Characterization for Flexible and High Reliability Adaptive Data Rate in Multiple Gateways Networks”. In: *Computers* 10.4 (2021), p. 44.

[154] https://www.thethingsnetwork.org. URL: `https://www.thethingsnetwork.org`.

[155] Semtech and Stackforce. URL: `https://github.com/Lora-net/LoRaMac-node/releases/tag/v4.4.3`.

Miscellaneous Scientific Papers

[156] J. Bernoulli and L.G.F. Vastel. *L’art de conjecturer*. G. Le Roy, 1801. URL: `https://books.google.fr/books?id=vHIAAAAAMAAJ`.

[157] Claude Elwood Shannon. “Communication in the presence of noise”. In: *Proceedings of the IRE* 37.1 (1949), pp. 10–21.

[158] C. E. Luna, Y. Eisenberg, R. Berry, T. N. Pappas, and A. K. Katsaggelos. “Joint source coding and data rate adaptation for energy efficient wireless video streaming”. In: *IEEE Journal on Selected Areas in Communications* 21.10 (2003), pp. 1710–1720. ISSN: 0733-8716. DOI: `10.1109/JSAC.2003.815394`.

[159] Daniel Marco and David L. Neuhoff. “Reliability vs. Efficiency in Distributed Source Coding for Field-gathering Sensor Networks”. In: *Proceedings of the 3rd International Symposium on Information Processing in Sensor Networks*. IPSN ’04. Berkeley, California, USA: ACM, 2004, pp. 161–168. ISBN: 1-58113-846-6. DOI: 10.1145/984622.984647. URL: http://doi.acm.org/10.1145/984622.984647.

[160] Diba Mirza, Maryam Owrang, and Curt Schurgers. “Energy-efficient wakeup scheduling for maximizing lifetime of IEEE 802.15. 4 networks”. In: *First International Conference on Wireless Internet (WICON’05)*. IEEE. 2005, pp. 130–137.

[161] Najib Ahmed Mohammed, Ali Mohammed Mansoor, and Rodina Binti Ahmad. “Mission-critical machine-type communication: An overview and perspectives towards 5G”. In: *IEEE Access* 7 (2019), pp. 127198–127216.

[162] Jorge Navarro-Ortiz, Pablo Romero-Diaz, Sandra Sendra, Pablo Ameigeiras, Juan J Ramos-Munoz, and Juan M Lopez-Soler. “A survey on 5G usage scenarios and traffic models”. In: *IEEE Communications Surveys & Tutorials* 22.2 (2020), pp. 905–929.

Technical documentation

[163] Francois Sforza. “Communications system”. In: *US Patent US8406275B2* 26 (2013).

[164] Semtech. *LoRaMote User Guide*. 2014.

[165] LoRa Alliance. *A technical overview of LoRa and LoRaWAN*. Tech. rep. LoRa Alliance, 2015.

[166] LoRa Alliance. *What is LoRa*. "https://lora-alliance.org/lorawan-for-developers". https://www.lora-alliance.org/What-Is-LoRa/Technology. 2015.

[167] Semtech. *SX1272 73 datasheet*. 2015.

[168] Semtech Corporation. *LoRa® Modulation Basics*. Tech. rep. AN1200.22. Semtech Corporation, 2015.

[169] Kerlink. *Wirnet Station 868*. https://www.thethingsnetwork.org/forum/uploads/default/original/1X/1be8efc0 2016.

[170] European Telecommunications Standards Institute. *EN 300.220 Electromagnetic compatibility and Radio spectrum Matters (ERM); Short Range Devices (SRD)*. 2017.

[171] Semtech. *SX1301 Datasheet*. 2017.

[172] LoRa Alliance. *LoRaWAN® 1.0.3 revision A Regional Parameters*. Tech. rep. LoRa Alliance, 2018.

[173] N.Sornin and A.Yegin. *LoRaWAN® 1.0.3*. Tech. rep. LoRa Alliance, 2018.

List of figures

List of Tables

Glossary & list of acronyms

ACK acknowledgement. 36, 38, 39, 41

ADR LoRaWAN algoritm for dynamic over-the-air adaptation of the EDs transmissions parameters. vi, 29, 38, 40, 41, 43, 45, 56, 57, 59, 60, 62, 97, 103, 105, 106, 108–110, 114, 121, 126

ADU Application Data Unit. 91–95, 99, 143

AES Advanced Encryption Standard. 38

ALOHA *Aloha multiple access algorithm* - each node can transmit at any time without coordination either with the other nodes or with the base station.. 12, 14

AM Amplitude Modulation. 4

ARQ Automatic Repeat reQuest. 39, 58, 78, 79, 85

AS *Application Server*. 30–32, 36, 39, 40, 106, 142

AWGN *Additive White Gaussian Noise* - A noise model which add uniformely across the frequency band an independant and identically distributed random variable following the zero-mean normal distribution to the received power. 7, 18, 141

BEC *Binary Erasure Channel*. 17–19, 141

BER *Bit Error Rate*. 22, 23, 25, 35, 47, 48, 145

BFSK *Binary Frequency Shift Keying*. 22, 145

BPSK *Binary Phase Shift Keying*. 18, 22, 141, 145

BSR Blind Systematic Repetition. v, 39, 42, 43, 55, 63, 64, 73, 75, 77, 78, 80–89, 96, 97, 100, 102, 103, 106, 108, 109, 142, 143

BW *Bandwidth* - The difference between the lowest and highest frequency used by the carrier. 6–9, 14, 15, 22–26, 32–37, 40, 43, 50–52, 69, 83, 114, 141, 142

CCARR Channel Coding Adaptive Redundancy Rate. vi, 60, 77–90, 103, 143, 145

CDMA *Code Division Multiple Access* - A multiplexing technique based on spread spectrum orthogonality. 8, 12

CF carrier frequency. 32, 33, 35–37, 39, 57, 64, 88, 114, 142

chirp compressed high intensity radar pulse. 32–34, 142, 148

CMAC cypher-based message authentification code. 38

***Cnt*$_{\mathbf{App}}$** *LoRaFFEC Applicative Data Unit Counter*. 91

CP-ECC Cross-Packet ECC. 16, 18, 46, 60, 73, 78, 88, 90–92, 94, 95, 103, 106, 108, 109, 114, 116, 119, 126

CR coding rate. 16, 19, 34, 35, 40, 43, 47, 48, 50–52, 64, 66–69, 75, 78, 83, 103, 114, 121, 141, 142

CRC cycling redundancy check. 18, 34, 35

CSMA *Carrier Sense Multiple Access* - Also refered to as Listen-Before-Talk (LBT). 11, 12

CSMA/CD *Carrier Sense Multiple Access with Collision Detection.* 11

CSS chirp Spread Spectrum. 32, 34

D *Distance between the transmitter and the receiver*. 9, 10, 149, 151

***d*$_{\mathbf{0}}$** Reference distance for the log-distance model. 10, 150

***D*$_{\mathbf{frame}}$** *Frame duration.* 12, 13, 67, 141

DAB Digital Audio Broadcasting. 4

DD *LoRaFFEC Decoding Depth parameter*. 77, 91, 94–98, 143

DER *Data Error Rate.* 25, 38, 40, 56, 60, 78, 85–91, 96–99, 102, 103, 106–112, 117, 119, 121, 122, 124, 126, 143, 144

Df demodulation floor. 65–69, 142, 145

dPMR446 Digital Private Mobile Radio 446. 4

DR Data Rate. 90

***DR*$_{app}$** *Applicative Data Rate* - The data rate available and usable by the application layer. 25, 40

***DR*$_{mod}$** *Modulation Data Rate* - The data rate of the physical modulation (sometimes refered to as “gross bit rate” or “raw bit rate”), i.e. the symbol rate of the modulation mutiplied by the signal valence. 6, 7, 34, 36, 39, 148

***DR*$_{net}$** *Physical net Data Rate* - The data rate provided by the physical layer i.e. the number of bits -transmitted to the upper layer thus excluding protocols overhead and potential erasure correction code overhead- transmitted per seconds. 7, 23–25, 141

***DR*$_{phy}$** *Physical Data Rate* - The data rate of the physical layer i.e. the modulation data rate (DR_{mod}) multiplied by the coding rate of the potential erasure correction code redundancy. 7, 34–36, 38–41, 145

DSSS Direct Sequence Spread Spectrum. 26

DTT Digital Terrestrial Television. 4

DVB-S Digital Video Broadcasting - Satellite. 4

***E*$_{\mathbf{b}}$** *Energy per bit*, i.e. the P_{Rx} divided by the number of bits in the packet. 22–25, 46, 48, 141, 151

ECC *Error Correction Code* - Also known as Forward Error Correction (FEC). v, 3, 4, 11, 15–19, 26, 34, 35, 45, 47, 48, 59, 60, 63, 64, 66, 75, 78, 79, 105, 119, 141, 148

ED *End Device*. 30–32, 35–42, 51, 53, 55–59, 61, 62, 64, 65, 74, 77–80, 85, 87, 88, 91, 93–95, 103, 106, 109, 114, 115, 117, 142, 147

$\boldsymbol{\eta}$ Spectral efficiency - Number of bits transmitted per second and per hertz. 7

FDMA *Frequency Division Multiple Access*. 12

FER *Frame Error Rate*. 35, 39, 40, 47, 56–58, 65–70, 73–75, 80, 85–89, 96–103, 106, 109, 114–117, 142–144

FM Frequency Modulation. 4

FSPL *Free Space Path Loss*. 10

$\boldsymbol{G}$ *Channel load*. 12–14, 141

$\boldsymbol{G_{Rx}}$ *Antenna gain in reception*. 10

$\boldsymbol{G_{Tx}}$ *Antenna gain in transmission*. 9, 10

γ *Path loss exponent*. 9, 10, 50–52, 149

GSM Global System for Mobile Communications. 4

GW gateway. 30–32, 34–37, 39, 40, 42, 51, 53, 55–59, 64, 65, 73, 74, 87, 102, 106, 108–115, 117–119, 121, 126, 142, 144

Hz Hertz: Unit of frequency - 1Hz is 1 cycle per second. 6, 7

IDU Integrity Data Unit. 91, 92, 99, 143

IoT Internet Of Things. v, 1–5, 19–22, 27, 31

ISM License-free, even though regulated, radio bands reserved initially for industrial, scientific and medical usage. 25, 26, 29, 35, 90, 145

$\boldsymbol{\lambda}$ *Wavelength*. 10

LBT *Listen-Befor-Talk* - Also refered to as Carrier Sense Multiple Access (CSMA). 12

LDPC *Low Density Parity Check*. 11, 18, 19, 26, 92, 141

LMPL *Lossy Medium Path Loss*. 10

log-distance model Statistical model for Large Scale Fading (LSF)- $PL(D) = PL_0 + 10\gamma \log_{10} \frac{D}{d_0}$ Where PL_0 is the Path Loss (PL) at the reference distance d_0 . 10, 148, 150

log-normal shadowing Common Shadow Fading (ShF) model - shadowing is computed as a random variable X following a log-normal distribution: $X \sim log\text{-}\mathcal{N}(\mu, \sigma^2)$ with parameters μ and σ^2 respectively the average and variance of the variable's natural logarithm. 11

LoRaFFEC LoRaWAN Fragmentation and Forward Error Correction. vi, 77, 90, 91, 94–103, 108–110, 119, 121, 143, 144, 148, 151

LoS Line-of-Sight. 65

LPWAN Low Power Area Networks. v, 1–5, 12, 13, 22–25, 27, 30, 53, 60, 79

LSB Least Significants Bytes. 91

LSF *Large Scale Fading*. 9, 10, 53, 75, 149

LTE Long-Term Evolution. 4

MAC Medium Access Control. 5, 11, 14, 30, 64

MIC message integrity code. 38

MPC Multiple Parity Check. 92, 95

MPSK *Multiple Phase Shift Keying*. 22, 145

MSB Most Significants Bytes. 91

$\boldsymbol{\mu}$ Means of the natural logarithm of random variable following the log-normal distribution. 11, 12, 149

$\boldsymbol{N_0}$ *Noise Spectral Density*, i.e. the noise power per unit of bandwidth. 7, 8, 22–25, 46, 48, 141, 151

$\boldsymbol{N_s}$ number of symbols per frame. 64, 67–69, 142, 145

$\boldsymbol{Nb_{\text{Trans}}}$ LoRaWAN number of frame transmission: $NB_{\text{Trans}} = 2$ each frame is emitted twice. 39–43, 73, 80, 82–89, 96, 100, 102, 103, 106–110, 113–117, 142–144

NS *Network Server*. 30–32, 38, 39, 41, 42, 55, 58, 59, 77–80, 82, 85, 87, 88, 91, 93–95, 106, 109, 114, 115, 142

OLS Ordinary Least Square. 67–69, 145

OSI *Open Systems Interconnection*. 5, 30, 141

$\boldsymbol{P_e}$ *Probability of error*. 12–14, 18, 81, 82, 141, 143

$\boldsymbol{P_g}$ *Processing gain* of a spread spectrum modulation: $P_g = \frac{BW_{\text{narrow}}}{BW_{\text{wide}}}$. 8

$\boldsymbol{P_{\text{N}}}$ *Noise floor power*, i.e. the strengh of the sum of all noise sources. 7

$\boldsymbol{P_{\text{Rx}}}$ *Received signal power*, i.e. the strengh of the received signal. 3, 7–10, 23–25, 51–53, 55–59, 74, 106, 141, 148, 151

$\boldsymbol{P_{\text{Tx}}}$ *Transmitted signal power*, i.e. the strengh of the transmitted signal. 9, 10, 23, 34, 35, 40–42, 50–52, 59, 64–67, 72–74, 88, 97, 102, 103, 106, 107, 109, 110, 114, 119, 120, 124, 125, 142, 144, 151

PA *Power Amplifier*. 23

PER *Packet Error Rate*. 25, 38–40, 42, 53, 56, 58, 60, 73, 78–85, 103, 106, 108, 109, 114–117, 119, 121, 126, 142, 143

$\boldsymbol{\pi}$ 3.1415. 9, 10, 22

PL *Path Loss* - The attenuation of the signal between the transmitter and the receiver: $PL = \frac{P_{\text{Tx}}}{P_{\text{Rx}}}$. 9–11, 23, 40, 55, 56, 58, 59, 64, 85, 149, 150

$\boldsymbol{PL_0}$ PL at the reference distance d_0 for the log-distance model. 10

PMR446 Private Mobile Radio 446. 4

QAM *Quadrature Amplitude Modulation.* 22, 145

RD *LoRaFFEC Redundancy Density parameter*. 77, 91, 94–97, 143

RS *Reed-Solomon.* 18, 19, 141

RSSI Received Signal Strength Indication. 55

S *Surface power density emitted by an isotropic antenna* - $S = \frac{P_{\text{Tx}}}{4 \times \pi \times D^2}$. 9, 10

sensitivity Minimal required received power for correct demodulation, it can either be in absolute value P_{Rx} or relative to the noise power with a minimal *SNR* or a minimal $\frac{E_b}{N_0}$. 7, 24

SF spreading factor. 32–34, 36, 37, 39–43, 46–48, 50–52, 56–61, 64, 66–69, 73, 74, 83, 88, 97, 102, 103, 106, 107, 109, 110, 114, 115, 117, 121, 142, 144

ShF *Shadow Fading*. 9–11, 53, 56, 57, 75, 149

$\boldsymbol{\sigma^2}$ Variance of the natural logarithm of random variable following the log-normal distribution. 11

SNR Signal-to-Noise Ratio. 7, 8, 22–24, 40–42, 46, 47, 53, 58, 59, 65–68, 73, 74, 78, 109–111, 114, 115, 117–119, 121–123, 142–145, 151

spectral efficiency *Spectral efficiency* - Number of bits transmitted per second and per hertz (noted η). 7, 24, 25, 141

SSF *Small Scale Fading*. 9, 11, 53, 56, 57, 59, 75, 126

$\boldsymbol{T_{\text{symbol}}}$ *Symbol duration.* 32

TDMA *Time Division Multiple Access.* 12

TOA Time-On-Air. 29, 39–41, 55, 56, 58–60, 69, 74, 77–79, 81–84, 86–89, 103, 106, 107, 109–111, 113–115, 117, 119, 121, 126, 143–145

TTN The Things Network. 55, 64

UMED Unit Mean Exponential Distribution. 114, 115

UMTS Universal Mobile Telecommunications System. 4

V Valence of a signal - Number of possible differents states of a transmitted signal. 6, 7, 141

W *Watt* - Power unit: $1W = 1kg \times m^2 \times s^{-3}$. 9, 10

WL *LoRaFFEC Windows Length parameter*. 77, 91–97, 99–101, 143

WLAN Wireless Local Area Network. 4, 20

WPAN Wireless Personal Area Network. 4, 21

WWAN Wireless Wide Area Network. 20, 21